The University of Hull

Fault Tolerant Control for Nonlinear Aircraft based on Feedback Linearization

Being a thesis submitted for the degree of PhD

in the University of Hull

by

YIMENG TANG

MSc Control Theory and Engineering (China)

July 2013

Acknowledgements

To my supervisor Professor Ron J Patton;

to my parents;

to the China Scholarship Council (CSC) and the University of Hull for full financial support;

to my friends and colleagues at the University of Hull, especially the past and present members of the Control and Intelligent Systems Engineering (Control Group), the Department of Engineering.

Yimeng Tang

29th July 2013

Abstract

The thesis concerns the fault tolerant flight control (FTFC) problem for nonlinear aircraft by making use of analytical redundancy. Considering initially fault-free flight, the feedback linearization theory plays an important role to provide a baseline control approach for de-coupling and stabilizing a non-linear statically unstable aircraft system. Then several reconfigurable control strategies are studied to provide further robust control performance:

- A neural network (NN)-based adaption mechanism is used to develop reconfigurable FTFC performance through the combination of a concurrent updated learning law.
- The combined feedback linearization and NN adaptor FTFC system is further improved through the use of a sliding mode control (SMC) strategy to enhance the convergence of the NN learning adaptor.
- An approach to simultaneous estimation of both state and fault signals is incorporated within an active FTFC system. The faults acting independently on the three primary actuators of the nonlinear aircraft are compensated in the control system.

The theoretical ideas developed in the thesis have been applied to the nonlinear Machan Unmanned Aerial Vehicle (UAV) system. The simulation results obtained from a tracking control system demonstrate the improved fault tolerant performance for all the presented control schemes, validated under various faults and disturbance scenarios.

A Boeing 747 nonlinear benchmark model, developed within the framework of the GARTEUR FM-AG 16 project “fault tolerant flight control systems”, is used for the purpose of further simulation study and testing of the FTFC scheme developed by making the combined use of concurrent learning NN and SMC theory. The simulation results under the given fault scenario show a promising reconfiguration performance.

Table of Contents

List of Figures

List of Tables

List of Symbols and Abbreviations

Symbols

$\|\cdot\|$	Euclidean norm (vector) or induced spectral norm (matrices)
$\|\cdot\|_F$	Frobenius norm
$\|\cdot\|_\infty$	Infinity norm
$\|\cdot\|$	The absolute value
$tr(\cdot)$	The trace operator
$\mathcal{R}, \mathcal{R}^+$	Field of real numbers and the set of strictly positive real numbers
$G(s)$	Transfer function via Laplace transformation

Abbreviations

6DoF	Six Degree of Freedom
BP	Back-Propagation
FD	Fault Diagnosis
FDD	Fault Detection and Diagnosis
FDI	Fault Detection and Isolation
FDIR	Fault Detection, Isolation and Reconfiguration
FL	Fuzzy Logic
FTC	Fault Tolerant Control
FTFC	Fault Tolerant Flight Control
GA	Genetic Algorithms
I-O	Input-Output
I-S	Input-State

LMI	Linear Matrix Inequality
LQG	Linear Quadratic Gaussian
LTI	Linear Time Invariant
MIMO	Multi-Input and Multi-Output
MRAC	Model Reference Adaptive Control
NDI	Nonlinear Dynamic Inversion
NN	Neural Network
PD	Proportional and Derivative
PID	Proportional Integral Derivative
SHL	Single Hidden Layer
SISO	Single-Input and Single-Output
SMC	Sliding Mode Control
UAV	Unmanned Aerial Vehicle

List of Publications

Within the period of this research the following works were submitted and accepted for publication:

- Tang, Y., & Patton, R. J. (2013, October 9-11). "Reconfigurable Flight Control using Feedback Linearization with online Neural Network Adaption", to be presented at the IEEE *SysTol 2013* Conference (2nd International Conference on Control and Fault-Tolerant Systems) at Nice.
- Tang, Y., & Patton, R. J. (2012, September 3-5). "Phase modulation of robust variable structure control for nonlinear aircraft". *2012 UKACC* International Conference on Control, (pp. 172-177), Cardiff.
- Tang, Y., & Patton, R. J. (2012, August 28-30). "Active FTC for Non-Linear Aircraft Based on Feedback Linearization and Robust Estimation". Presented at the IFAC Symposium *Safeprocess 2012*, Vol. 8, No. 1, pp. 210-215, Mexico City.
- Tang, Y., & Patton, R. J. (2012, July 3-6). "Fault-Tolerant flight control for nonlinear-UAV". 20th IEEE Mediterranean Conference on Control & Automation, *MED 2012*, (pp. 512-517), Barcelona.

Chapter 1 Introduction

1.1 Historical Overview

As modern technological systems become increasingly complex for the developed practical requirements, their corresponding control systems also increase in complexity to meet increased safety and performance requirements. Consequently, conventional feedback control methodologies have evolved and indeed simple mechanical feedback structures may result in an unsatisfactory performance, or even instability when applied to modern systems (Patton, 1993, 1997). Therefore, advanced electronic devices involved with optimized control strategies are expected to support high performance computation, especially for highly unstable or nonlinear systems. These challenges have attracted both researchers and industrial application studies focussed on the implementation of reliable approaches for advanced control methods (Zhang & Jiang, 2008).

The subject of "Reconfigurable Control" developed in the field of flight control as a way of using available repeated hardware or software to change the control system and actuators/sensors when it is determined that a fault has occurred (Patton, 1997; Steffen, 2005). In the early 1990s some authors referred to a new subject of "Failure tolerant control" (Stengel, 1991) or the preferred title of "Fault tolerant control" (FTC) (Srichander & Walker, 1993; Patton, 1993, 1997). There is a subtle difference between reconfigurable control and FTC in that the former is concerned primarily with reconfiguration issues, whilst the latter covers a wider field that includes reliable control and even robust control in which the system can be made insensitive to faults by the design of a fixed control system. Due to historical reasons, mainly concerned with the development of advanced flight control, most of the research on reconfigurable control and FTC has been carried out as separate entities.

A Fault Tolerant Control (FTC) System is known as a control system designed to automatically handle wide changes in system operation, focusing mainly on tolerating component malfunctions or external disturbances whilst maintaining desirable reliability, dependability and integrity in terms of stability, robustness and performance. These requirements are particularly important for safety-critical applications, such as aircraft, spacecraft, nuclear power and chemical process plants processing hazardous materials. Minor, although often benign faults could potentially develop into catastrophic events if not

managed correctly by the control system and/or the system operation (Stengel, 1991; Patton, 1993, 1997; Blanke, Frei, Kraus, Patton & Staroswiecki, 2000; Staroswiecki & Gehin, 2001; Steffen, 2005; Steinberg, 2005; Blanke, Kinnaert, Lunze, Staroswiecki & Schröder, 2006; Zhang & Jiang, 2008; Ducard, 2009).

During the last three decades the study of FTC systems for achieving various fault tolerant performances has given rise to several different but sometimes combined topics for dealing with the fault tolerant control problem for practical use. On a parallel path, research on reconfigurable control systems has increased progressively since the initial research on restructurable control and self-repairing flight control systems began in the early 1980s (Montoya, Howell, Bundick, Ostroff, Hueschen & Belcastro, 1983; Chandler, 1984; Eterno, Weiss, Looze & Willsky, 1985; Gao & Antsaklis, 1991; Beard, 1994; Rauch, 1995; Boskovic, Bergström & Mehra, 2005; Boskovic, Prasanth & Mehra, 2007).

As a development of advanced control methodology, FTC is studied and used by the combination of robust control, adaptive control, reconfigurable control, nonlinear control, fault diagnosis and predictive control systems (Patton, 1993, 1997; Chen & Patton, 1999; Maciejowski & Jones, 2003; Zolghadri, 2012).

Zhang and Jiang (2008) describe milestones on both subjects of restructurable/reconfigurable control and FTC of the important 2-day workshop on Restructurable Controls was held at NASA Langley Research Center, Hampton, Virginia, in September 1982 (Montoya, Howell, Bundick, Ostroff, Hueschen & Belcastro, 1983). The first triennial IFAC Symposium on Fault Detection, Supervision and Safety for Technical Process (SAFEPROCESS) was held in 1991 in Baden-Baden, Germany, followed by an IEE Colloquium on Fault Diagnosis and Control System Reconfiguration in 1993 in London, England and an International Conference on Fault Diagnosis (TOOLDIAG) in April 1993 in Toulouse, France. Another triennial series of IFAC Workshop on On-Line Fault Detection and Supervision in Chemical Process Industries was first held in 1992 in Newark, USA. More recently, invited tutorial sessions, workshops and plenary talks on these topics have frequently appeared at several major conferences such as AIAA Guidance, Navigation and Control Conference, American Control Conference, the biennial European Control Conference series, IEEE Conference on Decision and Control, IFAC World Congress, the IFAC SAFEPROCESS series and the new IEEE Conference on Control and Fault-Tolerant Systems (SysTol) in 2010 and 2013. Two special issues on reconfigurable flight control system designs appeared in 1999 (Banda, 1999) and 2005 (Hess, 2005), respectively.

Apart from reconfigurable control within the domain of FTC, systematic concepts, design methods, and even terminology are still not yet standardized, despite almost three decades of extensive publications. Although, some efforts have been made to give terminology on FTC (Patton, 1997; Blanke, Frei, Kraus, Patton & Staroswiecki, 2000; Blanke, Kinnaert, Lunze & Staroswiecki, 2006), a significant disparity exists in the literature between the ways in which the terminology is used.

Historically, from the point of view of practical application, a significant amount of research on FTC systems was motivated by aircraft flight control system designs, which is usually presented as Fault Tolerant Flight Control (FTFC) (Steinberg, 2005, Ducard, 2009). As stated above there is a significant overlap between the two fields of FTC and reconfigurable control. The original goal for FTFC control was to provide a ‘‘self-repairing’’ capability in order to ensure a safe landing in the event of severe faults in the aircraft and this was defined within the reconfigurable/restructurable control domain (Chandler, 1984; Eterno, Weiss, Looze & Willsky, 1985; Rauch, 1995; Patton, 1997). The motivation for work on reconfigurable/restructurable was enhanced by two commercial aircraft accidents in the late 1970s as shown in Figure 1-1. In the case of Delta Flight 1080 (April 12, 1977) (McMahan, 1978; Montoya, Howell, Bundick, Ostroff, Hueschen & Belcastro, 1983), the elevator became jammed at 19 degrees up and the pilot had been given no indication on this malfunction. Fortunately, the pilot successfully reconfigured the remaining control elements and landed the aircraft safely, based on his experience and knowledge about the actuation redundancy in the L-1011 airplane (Patton, 1997). In another accident involving American Airlines DC-10 crash in Chicago (Flight 191, May 25, 1979), the pilot had only 15 seconds to react before the plane crashed. Subsequent investigation showed that the crash could have been avoided (Montoya, Howell, Bundick, Ostroff, Hueschen & Belcastro, 1983).

(a) Delta Airlines Flight 1080, 1977 (b) America Airlines Flight 191, 1979

Figure 1-1 Two commercial aircraft accidents in the 1970s

The Delta Flight 1080 case in 1977 indicates that in many cases even the damaged aircraft can still be controlled and safely landed, which suggests that a successful FTFC system can help to achieve a higher reliability and sustainable flight through the use of redundancy methods. Since all aircraft have redundancy, in terms of repeated or functionally similar actuators, sensors, computers, etc., flight control has become an interesting subject for the development of FTC and reconfigurable control concepts (Patton, 1997; Steinberg, 2005, Ducard, 2009).

Unexpected flight scenarios or unusual system events during flight missions can mean that the performance and even the stability of the designed closed-loop system can be degraded easily in complex flight circumstances related to uncertain aerodynamics and aircraft asymmetry and low controllability. It has been become increasingly apparent that classical control design techniques e.g. optimal control, Linear Quadratic Gaussian (LQG) control, frequency response–Bode, Nichols, Nyquist may not be entirely appropriate for flight control designs for modern and advanced aircraft.

Advanced high-performance aircraft with highly nonlinear dynamic characteristics and with Multi-Input and Multi-Output (MIMO) control structure, require high manoeuvrability with static instability (Zemlyakov, Rutkovskii & Silaev, 1996; Gross, Hansford, Phillips, Waldie & Perhinschi, 2008). These characteristics provide very significant challenges for the design of FTFC systems involving Fault Detection and Isolation (FDI), or Fault Detection and Diagnosis (FDD) and various robustness concepts of robust FDI/FDD, robust fault estimation, robust control, and Fault Detection, Isolation and Reconfiguration (FDIR), etc. (Maybeck, 1999; Steinberg, 2005; Cook, 2012; Zolghadri, 2012). The FDD role is usually reserved for cases when a more complete diagnosis of a fault is carried out (than would be the case for FDI). Since fault estimation gives rise to more complete information about a fault, it is assumed in this work that the terminology FDD can be used whenever fault estimation is involved.

This thesis addresses the subject of FTFC, focusing on approaches that are appropriate for aircraft with unstable nonlinear dynamics subject to in flight actuator faults, modelling uncertainty and wind gust disturbance. The work is demonstrated using two nonlinear aircraft examples of (a) an Unmanned Aerial Vehicle (UAV) – the Machan and (b) a benchmark model of a Boeing 747 aircraft used for international research studies.

1.2 Concepts and Terminology

To enable the concept of FTC to be specified in later chapters, some basic concepts and terminology must be introduced. The definition provided in this thesis is in compliance with the definitions given by the IFAC SAFEPROCESS technical committee [Definitions established by the Technical Committee for IFAC (International Federation of Automatic Control) Symposium SAFEPROCESS (Fault Detection Supervision and Safety for Technical Processes), Isermann & Ballé, 1997] which were developed to set a standard in this area in order to avoid confusion among researchers. In addition to the terminology, different control methods should be clearly distinguished. First some basic definitions are given as follows.

Fault: this is an unpermitted deviation of at least one characteristic property or parameter of the system from the acceptable/usual/standard condition.

Failure: this is a permanent interruption of a system's ability to perform a required function under specified operating conditions.

Faults in the components of controlled systems may lead to total system failure, depending on the precise conditions, the criticality of the fault, etc., and if appropriate action is not taken. On the other hand, "failure" describes the condition when the system is no longer performing the required function i.e. the system function involving the faulty component may have failed.

Controlled system: this is a physical plant under consideration with sensors and actuators used for control.

Fault-tolerance: this represents the ability of a controlled system to maintain control objectives, despite the occurrence of a fault. A degradation of control performance may be accepted. Fault-tolerance can be obtained through fault accommodation or through system and/or controller reconfiguration.

Reconfiguration: this represents certain change in input-output between the controller and plant through change of controller structure and parameters. The original control objective is achieved although performance may degrade.

Supervision: this represents the ability to monitor whether control objectives are met. If not, obtain/calculate a revised control objective and a new control structure and parameters that make a faulty closed loop system meet the new modified objective.

Supervision should take effect if faults occur and it is not possible to meet the original control objective within the fault-tolerant scheme.

Fault detection: determination of the presence and the time of detection of a fault.

Fault isolation: determination of the kind, location and time of detection of a fault.

Fault identification: determination of the size-variant and time-variant behaviour of a fault.

Fault diagnosis: determination of the presence and characteristics of a fault.

Redundancy: this is the duplication of critical components or functions of a system with the intention of increasing reliability of the system, usually in the case of a system with fault-tolerance properties, by involving repeated or functionally similar actuators, sensors, computers, etc., can be categorized according to whether the redundancy is similar or dissimilar.

The redundancy can be in an analytical form e.g. using estimators, state observers, or FDI/FDD, etc. The analytical redundancy (sometimes known as functional redundancy) arises from the concept of estimation of measured quantities, providing redundant analytical signals. The most familiar form of redundancy is the dissimilar repetition of actuators or sensor function or computers in a fly-by-wire system in which the hydraulic systems or some elements of the control system may be triplicated in triplex redundancy (Patton, 1991).

The use of redundancy is very important in flight control systems and has become a very significant aspect of pilotless aircraft, e.g. a UAV to ensure a high degree of mission sustainability. Analytical redundancy is important for such vehicles to significantly alleviate the requirements for extra hardware, reducing weight and cost (Ducard, 2009).

1.3 Motivation

As mentioned in Section 1.1, historically research into FTC has been largely motivated by the control problems encountered in aircraft flight control system design. As air traffic activities and fly-by-wire technologies continue to grow around the world, the safety and reliability of modern aircraft as well as fuel economy have presented challenges for aircraft design as well as the development and design of avionics and flight control systems to meet these challenges and to minimize the potential risk of accidents, whilst also satisfying the manoeuvrability requirement.

As introduced in Section 1.2, some form of redundancy (repeated, dissimilar, hardware or analytical) is an important function for developing an FTC. For example the required control system to be selected, subsequent to detecting and isolating that a fault has occurred can be computed off-line and then a special approach to FTC makes use of a so-called "projection" approach to activate the new control system based on a redundant actuation structure (Gao & Antsaklis, 1991).

For military aircraft, redundancy is already available in abundance. Even though it is not meant for the purpose of FTFC, the use of these extra control surfaces provides the possibility of using dissimilar flight surfaces to obtain the same effect as the original control surface. This is the concept of the so-called "control configured vehicle" (Weingarten & Rynaski, 1972). The secondary control surfaces can be used in an emergency in an unconventional way to achieve the same effect as the primary control surfaces (Patton, 1997). Transport aircraft are subjected to less challenging flight scenarios and tend to have a very conventional form of redundancy based on repeated actuation systems e.g. for an aileron will have two actuators, one being active and the second in stand-by mode.

A recent view of the aerospace industry is the need to reduce the 'carbon footprint' left by aircraft with many manufacturers trying to reduce fuel consumption by designing high efficiency engines, by reducing weight and eliminating some hardware redundancy, favouring the use of analytical redundancy. This has been the focus topic of the recent EU FP7 ADDSAFE project ("Advanced Fault Diagnosis for Sustainable Flight Control") (ADDSAFE, 2009) which developed from the ACARE European initiative "Horizon 2020" (Advisory Council Aviation Research and Innovation in Europe) (ACARE, 2012).

In other words, FTFC is not only a safety-critical issue; but it is of interest in the sustainability of flight as well as to ensure higher dependability and reliability. This is particularly for UAV that reliable and sustainable flight is essential. The UAV must be inexpensive to develop and maintain and have robust operation even when some faults occur. So for the case of UAV systems analytical redundancy must be used instead of repeated hardware (Ducard, 2009).

The research described in this thesis is motivated by the subject of FTFC, together with concepts of feedback linearization to handle the design of MIMO open-loop unstable nonlinear aircraft subject to in flight actuator faults, modelling uncertainty and wind gust disturbance, without a requirement for using hardware redundancy.

1.4 Practical Requirements of FTFC

For the aircraft flight systems, modern pilots have limited authority surrounded by complex avionics systems with quadruplex fly-by-wire redundancy. The dissimilar redundancy flight computer hardware and software systems are able to maintain the safety and integrity of the flight for many fault scenarios.

However, there is a real danger when the controllability and stability of the aircraft are lost and an accident will then occur owing to the malfunctions caused by faults in the control system. Many factors result in aviation accidents and sometimes multiple causes contribute to a single accident.

In the past 25 years, crews of many aircraft types, including B-747, L-1011, DC-10, B-52, and C-5A, have experienced major flight control system failures, and have had to use system redundancy for emergency flight control. In most cases, a crash has resulted; the B-747, DC-10, and C-5A crashes claimed more than 1200 lives (Burcham, Burken, Maine & Fullerton, 1997).

The **Air Crash Record Office (ACRO)**, a non-government organization based in Geneva, compiled statistics between 1918-2009 on aviation accidents carrying more than six passengers, excluding helicopters, balloons, or combat aircraft, which is shown in Figure 1-2.

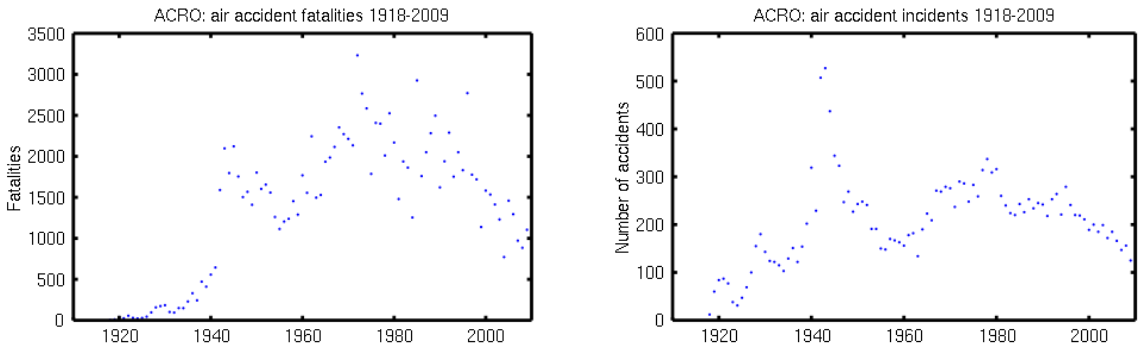

Figure 1-2 Statistics of air accident fatalities and incidents 1918-2009, from ACRO records
(https://en.wikipedia.org/wiki/Aviation_accidents_and_incidents)

A review of recent aviation accident and related statistical results is outlined below to identify the effects of pilot errors and other contributing factors and to help to gain an idea of the potential use of FTC methods for prompt flight control performance (Steinberg, 2005; Joosten & Maciejowski, 2009).

Table 1-1 is compiled from the **PlaneCrashInfo.com** accident database and represents 1,085 fatal accidents involving commercial aircraft, world-wide, from 1950 to 2010 for which a specific cause is known. This does not include aircraft with 18 or fewer people aboard, military aircraft, private aircraft or helicopters.

Table 1-1 ICAO/CAST fatal accident taxonomical distribution

(ICAO: International Civil Aviation Organization; CAST: Commercial Aviation Safety Team)

Cause (%)	1950s	1960s	1970s	1980s	1990s	2000s	All
Pilot Error	41	34	24	26	27	30	29
Pilot Error (weather related)	10	17	14	18	19	19	16
Pilot Error (mechanical related)	6	5	5	2	5	5	5
Total Pilot Error	57	56	43	46	51	54	50
Other Human Error	2	9	9	6	9	5	7
Weather	16	9	14	14	10	8	12
Mechanical Failure	21	19	20	20	18	24	22
Sabotage	5	5	13	13	11	9	9
Other Cause	0	2	1	1	1	0	1

In addition to the results in Table 1-1, Smaili, Breeman, Lombaerts & Joosten (2006) summarize some accident statistics showing that there are two major categories of accidents. These can be attributed to a single primary cause, namely ‘‘collision with ground’’ (controlled flight into terrain) where a fully functional aircraft hits the terrain due to the loss of situational awareness of the pilot, which accounts for as many as 26% of the accidents. This percentage has been decreasing in recent years thanks to the development of cockpit display technology. The second major category is ‘‘loss of control in flight’’, which can be attributed to a technical malfunctioning. This category accounts for 17% of all aircraft accident cases and is a persistent cause of accidents, with a few examples given in Table 1-2.

The NASA (National Aeronautics and Space Administration) 1997 report (Burcham, Burken, Maine & Fullerton, 1997) indicates that many accidents and incidents have resulted from major flight control failures in which the crew either did or could have used the available redundancy in a better way for emergency flight control.

Table 1-2 Aircraft accidents caused by loss of flight control

Date	**Flight No.**	Delta Airlines 1080	**Aircraft Type**	Lockneed L-1011 Trijet
Apr 12, 1977	**Cause**	One of the horizontal stabilizers jammed in the full trailing edge-up position before an instrument flight rules departure out of San Diego. This failure resulted in a large nose-up pitching and rolling moment that almost exceeded the capability of the flight controls.		
	Result	Safe landing in San Diego International Airport in California by using throttle control. All 41 passengers and 8 crew on board were saved.		
Date	**Flight No.**	American Airlines AA191	**Aircraft Type**	McDonnell Douglas DC10
May 25, 1979	**Cause**	Lost its left engine at the moment of take-off rotation, and crashed after a few minutes due to partial loss of hydraulics leading to asymmetric slat retraction and local wing stall.		
	Result	Crashed moments after take-off from Chicago. All 258 passengers and 13 crew on board were killed, along with two people on the ground.		
Date	**Flight No.**	Japan Airlines JL123	**Aircraft Type**	Boeing 747
Aug 12, 1985	**Cause**	Lost its fin and hydraulics became directionally unstable and crashed while trying to return to the airport, steered by the engines only.		
	Result	Crashed on Mount Osutaka. All 15 crew members and 505 out of 509 passengers died, resulting in a total of 520 deaths and four survivors.		
Date	**Flight No.**	American Airlines AA232	**Aircraft Type**	McDonnell Douglas DC10
Jul 19, 1989	**Cause**	Catastrophic failure of its tail-mounted engine and lost its hydraulics.		
	Result	Successfully landing at Sioux City using only thrust control, Iowa, saved 181 of 296 persons on board.		
Date	**Flight No.**	United Airlines 585	**Aircraft Type**	Boeing 737
Mar 3, 1991	**Cause**	Suffered a rudder hard-over, lost control and crashed immediately.		
	Result	Carrying 20 passengers plus a flight crew of 5, crashed while on final approach to runway 35 at the Colorado Springs airport, no survivors.		
Date	**Flight No.**	EL AL Flight 1862	**Aircraft Type**	Boeing 747 (cargo plane)
Oct 4, 1992	**Cause**	Freighter lost two engines and partially its hydraulics, it crashed while trying to make an emergency landing.		
	Result	Crashed in the suburbs of Amsterdam. A total of 43 people were killed, including the plane's crew of three, a non-revenue passenger in a jump seat, and 39 people on the ground. Many more were injured. The disaster was made worse by the fact that the plane exploded and started a large fire after the crash.		
Date	**Flight No.**	US Air Flight 427	**Aircraft Type**	Boeing 737
Sep 8, 1994	**Cause**	Experienced a sudden loss of control and slammed into the ground in an 80 degree nose down position, while banked 60 degrees to the left, crashed immediately.		
	Result	Crashed at West Palm Beach, Florida, killing all 127 passengers and 5 crew members on board.		
Date	**Flight No.**	DHL Cargo Flight	**Aircraft Type**	Airbus A300 cargo plane
Nov 22, 2003	**Cause**	It was struck on the left wing suffered a surface-to-air missile impact. Severe wing damage resulted in a fire and complete loss of hydraulic flight control systems.		
	Result	Returning to Baghdad, the three-man crew made an injury-free landing of the crippled aircraft, using differential engine thrust as the only pilot input.		

Concerning the case of El Al Flight 1862 Bijlmermeer Incident, on 4 October 1992 (see Figure 1-3), NASB indicated that: "…the plane had only managed to maintain level flight at first due to its high air speed (280 knots). The damage to the right wing, resulting in reduced lift, had made it much more difficult to keep the plane level. At 280 knots (520 km/h), there was nevertheless sufficient lift on the right wing to keep the plane aloft. Once the plane had to reduce speed for landing, however, it was doomed; there was too little lift on the right wing to enable stable flight, and the plane banked sharply to the right without any chance of recovery…" [Netherland Aviation Safety Board: (NASB)].

Figure 1-3 El Al flight 1862: the aircraft and the Bijlmermeer apartment building

There have been many other similar accidents in this category. Although current civil airliners have a lot of hardware redundancy on the level of flight control computers, hydraulics and actuators, these failures were very improbable to survive with the current autopilot systems.

However, many experiments, take the two cases Delta Airlines Flight 1080 (1977) and American Airlines Flight 232 (1989) in Table 1-2 for example, show that a damaged aircraft is still flyable, controllable and some level of performance can still be achieved (Burcham, Fullerto & Maine, 2004), to allow the pilot to safely land the aircraft. The presence of an automatic adaptive control strategy would have increased the chances for survivability.

All these situations have led to a common conclusion: from an aeronautical-technical point of view, given the technology and computing power available on this moment, it might have been possible to recover the aircraft in the situations above on the condition that non-conventional control strategies such as fault tolerant and adaptive control would have been available.

An independent investigation by Smaili and Mulder (2000) on the El Al flight 1862, suggested that there was still some control and flying capability associated with the crippled aircraft, where pilots may successfully land the crippled aircraft. Maciejowski and Jones (2003) demonstrated in simulation, using a model-based predictive control approach that the

El Al 1862 disaster could have been avoided and it may have been possible to control the crippled aircraft using a form of FTC in the flight control system to maintain the required controllability for the purpose of a quick landing back at Schiphol airport, Amsterdam.

In 2004, the Group for Aeronautical Research and Technology in Europe (GARTEUR) organization initiated the FM-AG (Flight Mechanics Action Group) 16 to study this accident further. The FM-AG 16 group developed further research on "Fault Tolerant Flight Control" and demonstrated the value of using FTFC methods to reduce the probability of accident for cases such as the El Al 1862 Amsterdam flight disaster. The goal was to apply a number of FDI/FDD and FTC algorithms within a realistic failure scenario, based on the earlier study provided by Smaili and Mulder (2000).

Although the aircraft of the El Al 1862 flight was a Boeing 747, modern aircraft (e.g. Boeing 777; Airbus 320, 330, 340, 350, 360, 370 and 380) are equipped with fly-by-wire flight control computers which can increase the safety of aircraft operations by guarding the safe flight envelope and easing manual flight control. With a forward looking interest the FM-AG 16 study developed and tested several types of FTFC systems that could be used not only for systems such as the Boeing 747 but mainly for modern fly-by-wire aircraft systems. The controllers employed techniques ranging from H_∞ (Cieslak, Henry, Zolghadri & Goupil, 2008), Sliding Mode Control (SMC) allocation (Alwi & Edwards, 2010), Model Predictive Control (MPC) (Joosten & Maciejowski, 2009) and adaptive flight control based on Nonlinear Dynamic Inversion (NDI) theory (Lombaerts, Huisman, Chu, Mulder & Joosten, 2009). The use of these FTC algorithms in a high fidelity flight simulator can further increase safety in the case of actuator, aerodynamic or even structural failures in the aircraft.

In conclusion, the requirement of robustness and integrity of the flight control system which are of high importance but are also of a very large percentage of the cost of the development of a modern aircraft reflects the cost of the high integrity avionics and flight systems (Ganguli, Marcos & Balas, 2002; Boskovic, Bergström & Mehra, 2005; Boskovic, Prasanth & Mehra, 2007; Alwi & Edwards, 2010). The quadruplex level of redundancy of a fly-by-wire aircraft can, under certain circumstances, be reduced to a triplex level of redundancy by using FTC systems, by replacing the hardware redundancy by analytical redundancy using system model information (Patton, 1991). The detection, isolation and diagnosis of faults in a FTC system can be used in several ways to enhance the system integrity. Once the faults are detected and isolated, the unhealthy parts of the system can be replaced by using either

analytical estimation methods or by using control system reconfiguration. Alternatively, the fault can be estimated on-line and compensated by an adaptive control scheme.

Since technical solutions involve FTC strategies are getting more widely available to prevent accidents, the following chapters of this thesis will research into methods to deal with undesirable but clearly bounded fault effects and disturbances acting on aircraft during flight missions so that safe, reliable and green system operation can be maintained. There is a focus on automatic correction of certain faults enabling pilots to take suitable commanding action of the aircraft to avoid disaster and land the aircraft safely.

1.5 Thesis Structure and Contributions

The remainder of the thesis is arranged in the following manner:

Chapter 2 following definitions of the terms fault and failure, Chapter 2 briefly discusses the different types of faults and failures which can occur on actuators and sensors with specific aircraft examples. Chapter 2 also introduces the concept of FTC and gives a general overview of the different FDI/FDD and FTC methods as used in various application-driven research fields. Some general classifications on the FDI/FDD and FTC strategies provide a suitable focus towards the requirements for FTFC for use in the remaining chapters of the thesis.

Chapter 3 provides the relevant background and preliminary knowledge for establishing the aircraft mathematical model of flight control. The main three primary control surfaces, including aileron, rudder and elevator, are described as these are of relevance for the aircraft physical structure study. This chapter introduces several important aircraft reference frames required for further understanding of the aerodynamics. The main aerodynamic forces and moments are explained and some necessary mathematical equations have also been derived and discussed briefly as a background to the use of the modelling in subsequent chapters. The nonlinear Machan UAV model is described in Chapter 3 with the comparison and analysis of its linear and nonlinear performance simulation results in Section 3.5.

Chapter 4 gives the main concepts of the feedback linearization approach for the nonlinear system to develop the baseline control structures in FTC scheme. The appropriate properties of linear and nonlinear systems are outlined and summarized via a short review of current analysis and control strategies for nonlinear system design. The preliminary mathematical concepts required for the development of exact feedback linearization are presented and the construction method of the feedback linearization transformations is presented. Chapter 4

ends with a focus on the application of the feedback linearization strategy to nonlinear flight control issue in Section 4.4. The nonlinear aerodynamic model of the Machan UAV introduced in Chapter 3 is used to analyze the feasibility and validity for applying feedback linearization to the highly nonlinear and MIMO aircraft system, aimed towards the derivation of a special cascade control scheme to satisfy the feedback linearization requirement.

Chapter 5 presents a new approach to FTFC with a reconfigurable control scheme making use of a simplified concurrent learning Neural Network (NN) adaptor for application to the nonlinear Machan UAV system. The controller is based on Nonlinear Dynamic Inversion (NDI) theory and incorporates an adaptive NN element using standard back-propagation learning for compensating the output tracking errors caused by bounded faults, disturbance and system uncertainty. A recently proposed concurrent learning approach (Chowdhary & Johnson, 2008) is used to improve the training of the online NN weight adaption. This concurrent learning NN scheme is analyzed and further simplified in Section 5.4.4 for the nonlinear aircraft application in this work. With the results provided in Section 5.5.2, the modified concurrent learning NN adaptor is shown to achieve improved FTFC performance validated through simulations on the nonlinear Machan UAV system under various faults and disturbance scenarios, and shows a remarkable learning capability to control complex dynamical systems while assuring system stability.

Chapter 6 gives a brief introduction to the concept of Sliding Mode Control (SMC) and its benefits when applied in the fields of nonlinear system control. An approach to SMC that is particularly suitable for application to certain nonlinear systems is outlined. Chapter 6 also highlights the combination of SMC design with computational intelligence. A considerable improvement is made in this chapter to the reconfigurable FTFC scheme using NDI and an NN learning adaptor described in Chapter 5. In Section 6.3 the concurrent NN learning adaptor is considered as a nonlinear dynamical system to which the SMC is applied to enhance the stability and convergence of the learning scheme. The proposed control strategy is evaluated in Section 6.4 using the nonlinear Machan UAV in order to evaluate its performance and practical feasibility. The simulation tracking control results demonstrate that the SMC-NN based FTFC strategies have adequate and stable performance. Hence, the inclusion of the SMC is viewed as a suitable development of the work in Chapter 5 for realistic application of fault-tolerant and adaptive control purposes since considerable performance improvements are realized.

Chapter 7 considers the development of reconfigurable active FTFC strategies for nonlinear flight control based on robust fault estimation. As stated in Chapters 5 & 6, the NDI approach based on feedback linearization transformation theory is used to achieve a base-line controller for stabilizing the nonlinear aircraft system and invoking a decoupled structure. A simultaneous state/fault estimator due to Gao & Ding (2007) is outlined and a novel approach is developed through combing the Gao and Ding approach with the NDI controller. This is a form of active FTFC since the feedback is dependent on a bounded estimate of the fault. Good FTFC performance is achieved using the scheme proposed in this chapter, demonstrating the power of this fault reconfiguration method with the compensation of the faults acting within the control system. The simulation results on the Machan UAV aircraft model demonstrate the robustness of the FTC with the fault estimation, corresponding to simultaneously acting faults occurring on each of the three primary flight actuators (aileron, elevator and rudder) and wind disturbance. The feedback linearization and NDI strategy has enabled the three faults to be compensated simultaneously, through the strategy of decoupling the dynamics into three separate systems as a model for the control development.

Chapter 8 presents the El Al flight 1862 (Bijlmermeer incident) scenario which is one of the case studies of the GARTEUR FM-AG 16 project. A Boeing 747 benchmark model for the integrated evaluation of new fault detection, isolation and reconfigurable control techniques, developed within the framework of the GARTEUR FM-AG 16 on "Fault Tolerant Flight Control", is introduced for simulation study in this chapter. The concurrent SMC-NN based reconfigurable control presented in Chapter 6 is tested for on-line compensation of the system tracking error using the Boeing 747 benchmark under certain model simplification and taking into account a lack of knowledge of information of on-line aerodynamic parameters. The simulation results in Section 8.3, which under the actual El Al flight 1862 failure scenario, show promising reconfiguration performance and future study for a complete flight control scheme based on the use of this compensator system in pursuit of good reconfigurability and stability performance is encouraged.

Chapter 9 summarizes and concludes the work described by the thesis and makes suggestions and recommendations as to how the research can be further developed in the future.

Chapter 2 Fault Tolerant Flight Control Methodology

This chapter provides a classification and review of FTC schemes that are applicable to highly nonlinear, high performance aircraft with an emphasis on adaptive systems and the combination of methods that are capable of achieving flight control reconfiguration. An outline of relevant model-based methods for FDI/FDD and FTC are outlined and their robustness properties are discussed. A further discussion of advantages and drawbacks of various approaches to FTFC is given as a basis for outlining the control strategy chosen for the work in Chapters 5, 6, 7 and 8.

2.1 Fault Classification

As introduced in Section 1.2, the definition of a fault is an unpermitted deviation of at least one characteristic property or parameter of the system from the standard condition. It can also be known as an unexpected change in the system function and is actually a state that may lead to a malfunction or failure of the system which normally depends on precise conditions and criticality of the fault. Malfunctions are usually caused by design errors, implementation errors, human operator errors, environmental aggressions, etc. A fault in a dynamic system can take on many forms, such as actuator faults, sensor faults, unexpected abrupt changes of some parameters or even unexpected structural changes. Despite the component faults, sensor faults are effective on the outputs, while actuator faults are effective on the inputs and states.

On the other hand, a disturbance is defined as an unknown and uncontrolled input acting on the system which results in a departure from the current state. For example, for an aircraft turbulence acts as a disturbance that can mask the effect of a fault in the system so that the fault cannot be promptly detected and isolated. Disturbances (and uncertain effects, such as modelling errors) compete against the effects of faults in the system, imposing a considerable robustness challenge to the FDI/FDD roles (Patton, Frank & Clarke, 1989; Blanke, Frei, Kraus, Patton & Staroswiecki, 2000). Since robust and reliable fault information is required for active FTC, this robustness problem also has an important bearing on the reconfigurability of the system subsequent to fault occurrence.

2.1.1 Basic characterization of faults

According to the fault model representation adopted faults can be classified as either additive or multiplicative, as depicted in Figure 2-1. Additive faults are suitable for representing actuator or sensor faults in the system, whilst parametric changes act in a multiplicative way in the system (Chen & Patton, 1999).

Figure 2-1 Additive and multiplicative faults

Faults can also be categorized according to their time characteristics as abrupt, incipient and intermittent, shown in Figure 2-2.

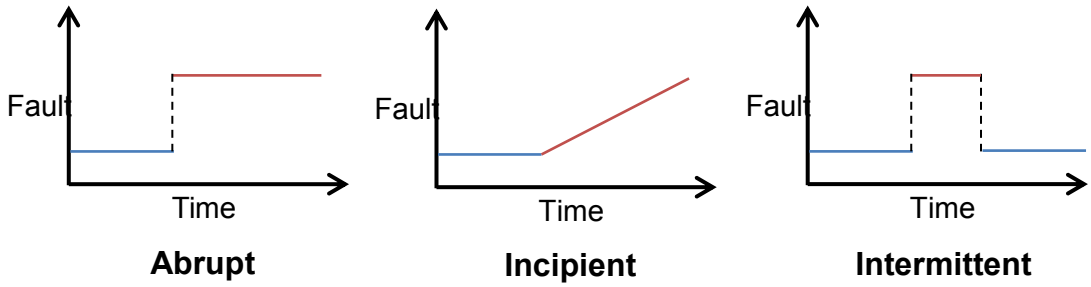

Figure 2-2 Faults classification in term of time

Abrupt faults exhibit sudden and unexpected changes and are usually easily noticed by the operator. For example, an abrupt failure of actuator jam (known as hard-over) is a kind of fault that occurs instantaneously often as a result of hardware damage. This can be very severe when affecting the performance and/or the stability of the controlled system, thus prompt reaction from the FTC system is required (Isermann, 2006).

Incipient faults, for example a slow drift in a sensor, are more subtle and their effects are not so obvious so that these faults are difficult to detect. The slowly developing parametric changes represented by incipient faults often represent a result of ageing or operational wear and tear. Over a short time-scale incipient faults appear to be unimportant or less severe compared with other fault types. However, if left undetected incipient faults may develop gradually into more serious fault conditions which can severely affect the system performance and even lead to catastrophic failures (Chen & Patton, 1999).

Finally, intermittent faults appear and disappear repeatedly, for instance due to partially damaged wiring (Patton, 1997).

2.1.2 Requirements for fault isolation

In general, faults may be found to arise in the input/output from actuators and sensors or within the system itself. Each part of the system can also be corrupted by faults and thus faults have to be classified according to the location of occurrences and their characteristics. For the purpose of the research, focusing on the types of faults is relatively important. In general, faults in the controlled system may be seen to take place in three different parts: (i) actuators, (ii) sensors, or (iii) in the controller or within the system being controlled, as shown in Figure 2-3 (Patton, 1993; Isermann, 2006; Henry, Simani & Patton, 2010).

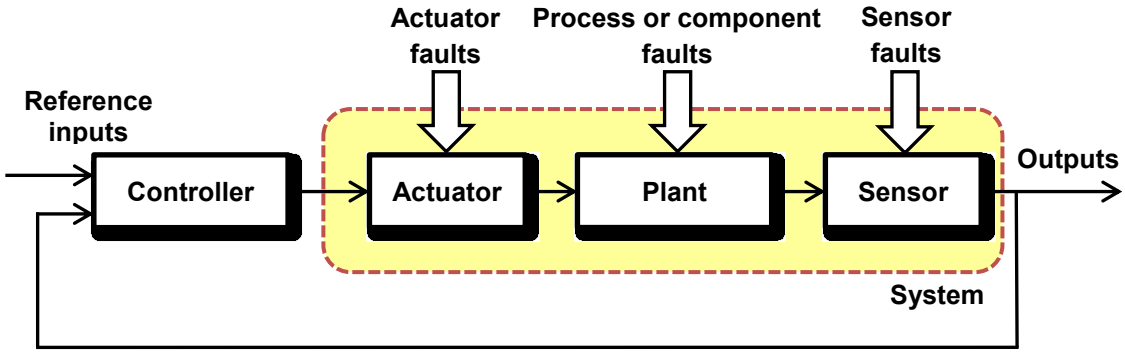

Figure 2-3 Classification of faults in a controlled system

Actuator faults: An actuator fault represents a partial loss of control action or represents only a part of the normal actuation. This may occur due to increased resistance through friction and, as actuators usually require a separate power source, a fall in a supply voltage or current. Due to the fact that the actuator is the part of the system which takes part in delivering power into the system, actuator faults must be detected and isolated or compensated very quickly. Generally, actuator faults in an aircraft might correspond to engine fuel loss or lack of fuel flow, a sticking or stuck aileron, a stuck rudder or elevator, all of which will cause the aircraft flight regime to become limited (Isermann, 2006; Ducard, 2009).

Sensor faults: The sensors are any equipment that takes a measurement or observation from the system, and faults are often due to poor calibration or bias, scaling errors or a change in the sensors dynamic characteristics. A sensor fault provides a reading which is erroneous, although some useful information could still be retrieved. Sensors need to be operated efficiently and accurately in aircraft systems to make sure that the aircraft flight is sustainable (Isermann, 2006; Ducard, 2009).

Component faults: Faults within the system itself are often termed component faults, e.g. a malfunction in a motor, valve, pump, etc. Component faults are arising as variations from the structure or parameters used during system modelling. They mainly result in changes of the dynamical behaviour of the controlled system. Generally, component faults cover a very wide class of situations and thus they are considered the most difficult ones to deal with because this type of fault may be simple to detect but can be difficult or expensive to isolate, estimate and compensate through an active FTC system (Isermann, 2006; Ducard, 2009).

2.1.3 Aircraft actuator/sensor fault/failure characteristics

As introduced in Section 1.2, a failure is clearly a condition which is much more severe than a fault. When a fault occurs in an actuator for example, the actuator is still usable but may have a slower response or become less effective. But when a failure occurs, a totally different actuator is needed to be able to produce the desired effect. To provide a more complete understanding of the meaning of the fault effect, this Section introduces the faults that typically occur on many control system actuators and sensors (Alwi, Edwards & Tan, 2011) and are typical of some of the fault scenarios that can be considered for flight control systems (Ducard, 2007, 2009).

(1) Actuator fault/failure types

In aircraft systems, there are some distinct types of actuator failure, the four most common are shown in Figure 2-4 (Ducard, 2007).

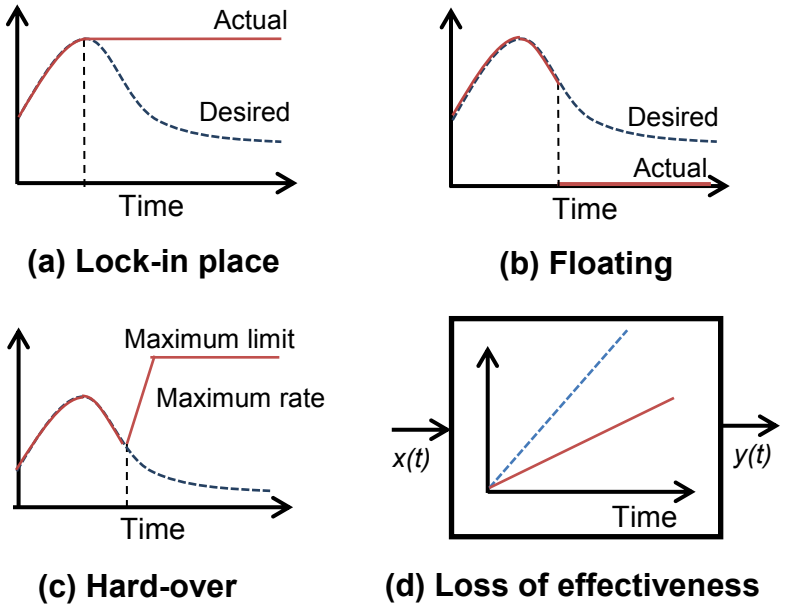

Figure 2-4 Type of fault and failure on aircraft actuator

A **lock-in failure** is a failure condition when an actuator becomes stuck and immovable. This might be caused by a mechanical jam, due to lack of lubrication for example. This type of failure is considered to have occurred according to reports that followed accidents such as flight 1080 (Lockheed L-1011, San Diego, 1977), outlined in Table 1-2, as one of the horizontal stabilizers of the aircraft jammed in the full trailing edge-up position.

A **floating failure** is a failure condition whereby the control surface moves freely without providing any moment to the aircraft. This type of failure can occur following loss of hydraulic fluid. Examples of research considering floating type failures can be found in the accident reports of Flight 123 (B-747, Japan, 1985) and DHL A300B4 (A300, Baghdad, 2003). Both of these accident cases involved a total loss of hydraulics (Burcham, Burken, Maine, & Fullerton, 1997).

One of the most catastrophic types of failure is **hard-over** (or called runaway). In a **hard-over** situation the control surface will move at its maximum rate limit until it reaches its maximum position limit or its blow-down limit. For example, a rudder hard-over can occur when there is an electronic component failure which causes an un-commanded large signal to be sent to the actuators causing the rudder to be deflected at its maximum rate to its maximum deflection at low speed (or its blow-down limit at high speed). This type of failure is known to have occurred in accidents such as flight 427 (B-737, Aliquippa, Pennsylvania, 1994) and Flight 85 (B-747, Anchorage, Alaska, 2002) (Lombaerts, Huisman, Chu, Mulder & Joosten, 2009). Note that the above failures are related to the aircraft's control surfaces.

Whilst some failure scenarios occur without warning, faults if left undetected and uncompensated can eventually lead to failure scenarios. An example of this can be considered to occur when part of the aircraft structure becomes damaged e.g. because of excessive loading on the airframe or as a result of battle damage (in the case of a UAV or military vehicle). The *structural damage* will tend to change the operating conditions of the aircraft due to changes in the aerodynamic coefficients (e.g. main wing or tail surface lift, etc.) or a change in the centre of gravity, causing a change to the aerodynamics. Examples of failures caused by serious structural damage are, rudder structural failure (flight 961, A310, Varadero, 2005) or detachment of one engine on a wing causing the detachment of the second engine (flight 1862, B-747, Amsterdam, 1992). Other examples are detachments of some body parts of the aircraft e.g., the vertical fin/stabiliser (Flight 123, B-747, Japan, 1985) and (flight 587, A300, New York, 2001), loss of wing (DHL, A300, Baghdad, 2003), breakdown in fuselage skin integrity caused by detachment of cargo doors (flight 981, DC-10, Paris, 1974)

(Burcham, Burken, Maine & Fullerton, 1997; Smaili & Mulder, 2000; Lombaerts, Huisman, Chu, Mulder & Joosten, 2009).

(2) Sensor fault/failure types

Figure 2-5 (Ducard, 2007) describes some typical sensor faults in aircraft. **Bias** is a constant offset/error between the actual and measured signals. **Freezing** of sensor signals results in the sensor providing a constant value instead of the true value. **Sensor drift** is a condition whereby the measurement errors increase over time (and might be due to loss of sensitivity of the sensor). **Loss of accuracy** occurs when the measurements never reflect the true values of the quantities being measured. Similar as actuator mentioned above, *structural damage* also could cause sensor faults result in **calibration error** (Ducard, 2007, 2009; Alwi, Edwards & Tan, 2011).

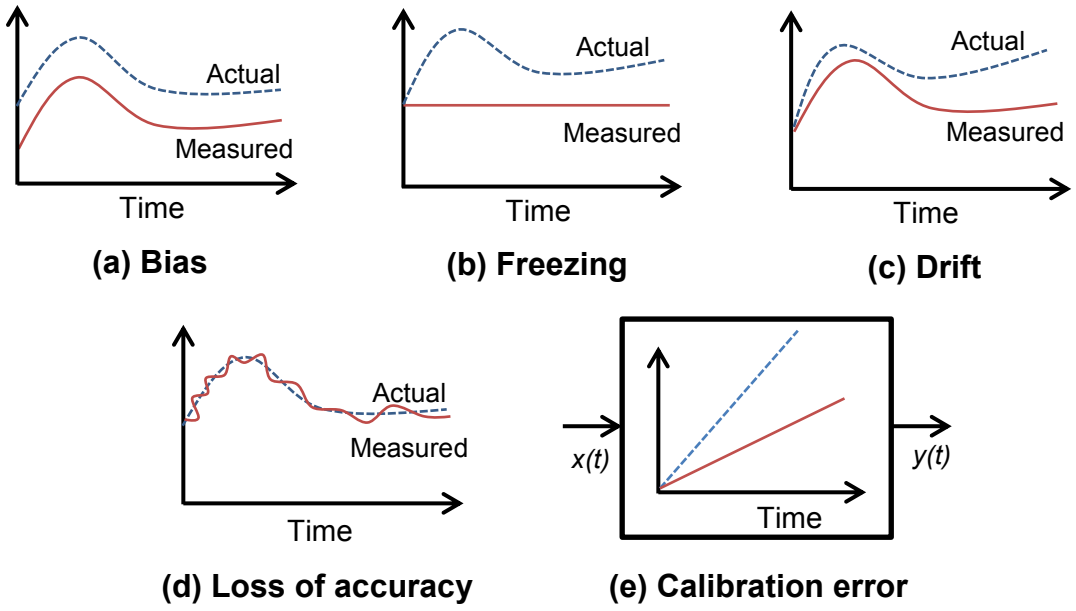

Figure 2-5 Type of fault and failure on aircraft sensor

A **calibration error** is a wrong representation of the actual physical meaning of the quantity being processed via the electronic signals that emerge from a sensor unit. Sensor faults can occur due to malfunctions in the components in the sensor unit, loose mounting of the sensors or loss of accuracy due to component ageing or power supply faults, etc. An example of an incident resulting from multiple accelerometer sensor faults (flight 124, B-777, Perth, 2005) caused a flight control upset and contributed to violent behaviour of the aircraft which led to the autopilot and navigation unit being switched off. Luckily, the aircraft was stabilized and it landed safely back at Perth airport (Ducard, 2007).

2.2 Classification and Review of FTC Methods

Generally speaking, FTC methods can be classified into two types: (a) passive FTC systems and (b) active FTC systems (Eterno, Weiss, Looze & Willsky, 1985; Stengel, 1991; Patton, 1993; Chen & Patton, 1999).

In passive FTC system, controllers are fixed and are designed to be robust against a class of presumed faults (Eterno, Weiss, Looze & Willsky, 1985). This approach needs neither FDI/FDD schemes nor controller reconfiguration, but it has limited fault-tolerant capabilities. Discussions on passive FTC can be found in the following (Siljak, 1980; Veillette, Medanic & Perkins, 1992; Veillette, 1995; Zhao & Jiang, 1998; Liang, Liaw & Lee, 2000; Yang, Wang & Soh, 2000; Hsieh, 2002). In the literature, passive FTC is also known as reliable control systems or control systems with integrity (Patton, 1997).

In contrast to passive FTC, active FTC reacts to the system component failures actively by reconfiguring control actions so that the stability and acceptable performance of the entire system can be maintained (Stengel, 1991; Patton, 1997). In certain circumstances, degraded performance may have to be accepted (Blanke, Staroswiecki &Wu, 2001; Stengel, 1991; Patton, 1997). Active FTC systems are also referred to as self-repairing (Chandler, 1984; Eterno, Weiss, Looze & Willsky, 1985), or reconfigurable (Moerder, Halyo, Broussard & Caglayan, 1989), or restructurable (Montoya, 1983), or self-designing (Monaco, Ward, Barron & Bird, 1997) control systems by various researchers. From the viewpoint of functionality in handling faults, active FTC makes use of fault detection, identification (diagnosis), fault estimation and accommodation schemes by other researchers (Napolitano, Neppach, Casdorph & Naylor, 1995; Polycarpou & Vemuri, 1995; Belcastro & Belcastro, 2001; Theilliol, Noura & Ponsart, 2002). In such control systems, the controller compensates for the impacts of the faults either by selecting a pre-computed control law (Maybeck & Stevens, 1991; Moerder, Halyo, Broussard & Caglayan, 1989; Rauch, 1995; Zhang & Jiang, 2001a, 2001b) or by synthesizing a new one on-line reconfiguration scheme (Patton, 1997; Zhang & Jiang, 2002; Benosman, 2009).

In summary, the main goal of an FTC system (passive or active) is to design a controller with a suitable structure to achieve stability and satisfactory performance, not only when all control components are functioning normally, but also in cases when there are malfunctions in sensors, actuators, or other system components (e.g. the system itself, control computer hardware or software).

2.2.1 Passive and active FTC schemes

In the *passive* approach, robust control techniques are used to make sure that the control-loop system remains insensitive to faults. Hence, the passive solution consists of using a unique robust controller to handle the system robustness with all the expected faults. The effectiveness of this strategy, that usually must be limited to a very restrictive repertory of faults, depends upon the robustness of the nominal closed-loop system to each of the faults (as if they are acting as uncertainty). Thus the passive FTC approach has the drawback of being reliable only for the class of faults expected and taken into account in the design. However, it has the advantage of avoiding the inevitable time-delay that is a characteristic of an active FTC scheme. Passive FTC methods have been proposed, mainly based on robust control theory, using multi-objective optimization; Linear Matrix Inequalities (LMI), H_∞ optimization, SMC theory, passivity-based FTC, etc. (Patton, 1997; Yang, Zhang, Lam & Wang, 1998; Zhang & Jiang, 2008).

In the *active* approach, a new control system is re-designed according to the estimation of the fault performed by the FDI/FDD unit and according to the specification to be met for the faulty system. The control law(s) is/are reconfigured/restructured to achieve performance requirements, subsequent to faults. Therefore most active FTC requires FDI/FDD to provide the fault or failure information so that reconfiguration can be achieved. Active approaches are divided into two main types of methods: (1) projection-based methods and (2) on-line automatic controller redesign methods. In projection-based methods, a new pre-computed control law is selected according to the required controller structure (i.e. depending upon the type of malfunction which has been isolated). The latter calculates new controller parameters in response to control impairment. This is referred to as reconfigurable control. The literature on active FTC research includes the following categories: pseudo-inverse modelling, adaptive control systems, eigen-structure assignment, multiple-model methods, reliable control, H_∞ control, model-matching, compensation via additive input design, NN and SMC (Zhang & Jiang, 2008; Benosman, 2009). Figure 2-6 shows the generally accepted taxonomy of active and passive FTC methods.

In active FTC, FDI/FDD plays a vital role in providing information about faults/failures in the system to enable appropriate reconfiguration to take place. The main function of FDI/FDD is to detect that a fault has occurred and to find its location so that corrective action can be made to eliminate or minimize its effect on the overall system performance. Figure 2-7 presents the architecture of active FDI/FDD-based FTC consisting of two blocks: (1) fault

diagnosis and (2) controller re-design, these tasks are carried out in the two steps of FTC (Blanke, Staroswiecki &Wu, 2001; Blanke, Kinnaert, Lunze & Staroswiecki, 2006):

(1) The diagnosis block uses the measured inputs and outputs and tests their consistency with the plant model. Its result is a characterisation of the fault with sufficient accuracy for the controller re-designs.

(2) The re-design block uses the fault information and adjusts the controller to the faulty situation.

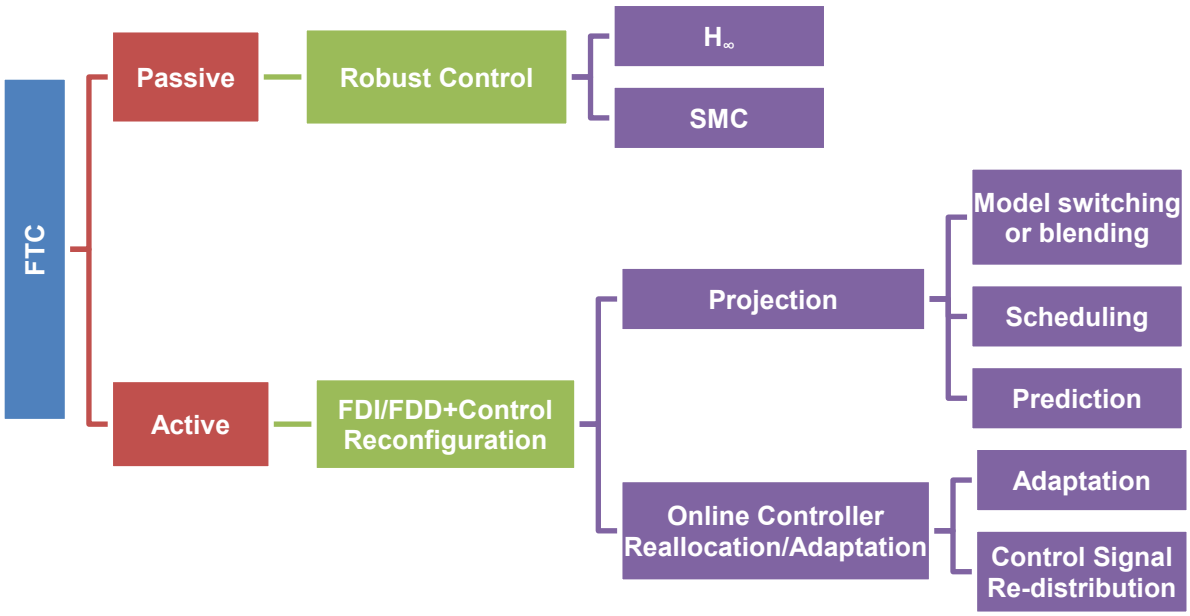

Figure 2-6 Active and passive FTC methods

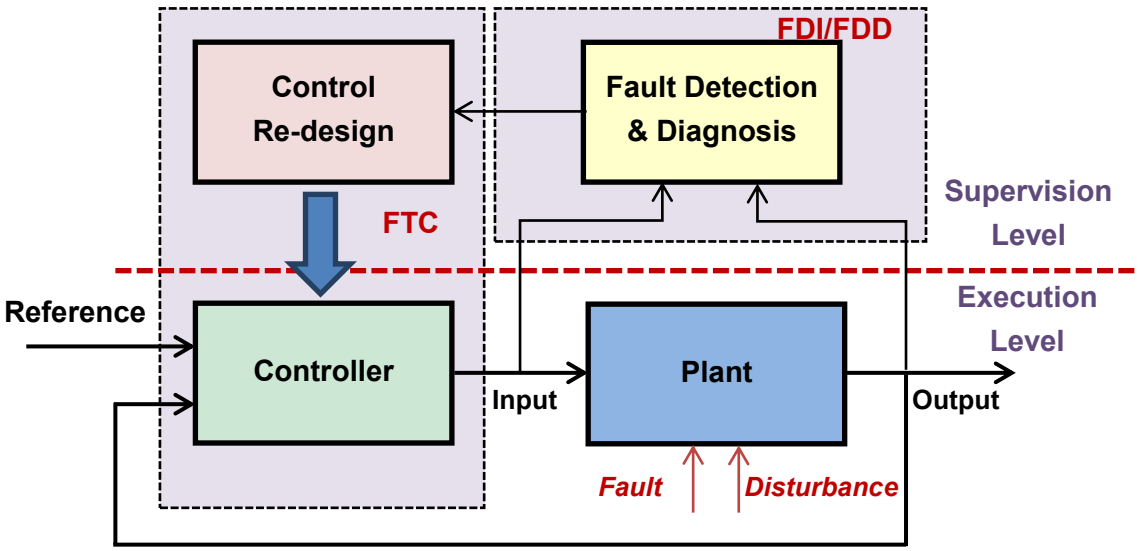

Figure 2-7 Active FTC system architecture

Figure 2-7 (Blanke, Kinnaert, Lunze & Staroswiecki, 2006) illustrates that active FTC extends the usual feedback controller by a supervisor, which includes the diagnostic function and the controller re-design blocks. In the absence of a fault, the system works as before, i.e. on the execution level. The nominal controller (sometimes referred to as the "baseline" controller, see Patton, 1997), which is designed for the fault-free system, attenuates the disturbance and ensures good set-point/reference following and other requirements on the closed-loop system. In this situation, the diagnostic block recognizes that the closed-loop system is faultless (fault-free) and no change of the control law is necessary. If a fault occurs, the supervision level makes the control loop fault-tolerant. The diagnostic block identifies the fault and the controller re-design block adjusts the controller to the new situation. Following this, the execution level alone continues to satisfy the control target.

The combination of both FDI/FDD and reconfigurable controllers within the overall system structure is the main feature distinguishing active from passive FTC. Therefore the main issues in active FTC are how to design; (i) a controller which can be easily reconfigured, (ii) a FDI/FDD unit with high sensitivity to faults and robustness to model uncertainties and external disturbances, and (iii) a reconfiguration mechanism which leads as much as possible to recover the pre-fault system performance in the presence of uncertainties and time-delays in FDD within the constraints of control inputs and system states.

In the FDI/FDD module, any fault in the system should be detected and isolated as quickly as possible (either using FDI residual signals or using FDD fault estimates), and the fault parameters, system state/output variables, and post-fault system models need to be estimated on-line in real-time. The FDI/FDD unit is responsible for providing the supervision system with information about the onset, location and severity of any faults. Based on the system inputs and outputs together with fault decision information from the FDI/FDD unit, the supervision system will reconfigure the sensor set and/or actuators to isolate the faults, and tune or adapt the controller to accommodate the fault effects.

Based on the on-line information on the post-fault system model, the reconfigurable controller should be designed automatically to maintain stability, desired dynamic performance and steady-state performance. In addition, the design must ensure that the closed-loop system tracks a command input trajectory in the event of faults. For this purpose a reconfigurable feed-forward controller often needs to be synthesized. To avoid potential actuator saturation and to take into consideration the degraded performance after the fault occurrence, in addition to a reconfigurable controller, a command/reference governor may

also need to be designed to adjust the command input or reference trajectory automatically (Patton, 1997; Hess, 2005).

Note that fault-tolerance can also be achieved without the structure given in Figure 2-7 by means of well-established control methods. As this is possible only for a restricted class of faults, they require brief outline as follows (Patton, 1997):

(i) *Robust control*: a fixed controller is designed that tolerates changes of the plant dynamics. The controlled system satisfies its goals under all faulty conditions. Fault tolerance is obtained without changing the controller parameters. It is, therefore related closely to passive fault tolerance. However, the theory of robust control has shown that robust controllers exist only for a restricted class of changes that may be caused by faults. The controller is not adjusted to the nominal process behaviour but is chosen to satisfy the performance specifications for the plant subject to all faults.

(ii) *Adaptive control*: the controller parameters are adapted to changes of the plant parameters. If these changes are caused by some fault, the adaptive control may provide active fault tolerance. However, the theory of adaptive control shows that this principle is particularly efficient only for plants that are described by linear models with slowly varying parameters. These restrictions are usually not met by systems under the influence of faults, which typically have a nonlinear behaviour with sudden parameter changes. The faults cause nonlinear effects as the system moves away from its known equilibrium point.

(iii) *Control reallocation*: one approach to manage the actuator redundancy for different control strategies handling actuator faults. This is usually achieved by finding the "best solution" to a system of linear equations. The benefits of control reallocation is that the controller structure does not have to be reconfigured in the case of faults and it can deal directly with total actuator failures through automatically redistributing the control signal without requiring reconfiguration/accommodation of the controller.

2.2.2 FDI/FDD approaches for active FTC

On-line monitoring tools not only provide early warning of plant malfunction (including loss of safety, environmental degradation, poor economy, etc.) but also information as to how to minimize maintenance schedule costs. Precise diagnostic information must be generated quickly to protect the plant/system from shut down and provide human operators with appropriate process status information to help them take correct decisive actions not only

when faults become serious but also when faults are developing and difficult to detect (also called incipient faults in Section 2.1.1). It is clear that the application of supervised on-line diagnosis schemes can be profitable in terms of a decrease in service costs (Patton, 1997; Chen & Patton, 1999, Isermann, 2006).

In view of the overall fault tolerant strategy, model-based Fault Diagnosis (FD) schemes are grouped based on their capabilities into two major categories; (i) FD using residual schemes (residual generation) and, (ii) FD which has the capability to estimate the faults (fault estimation) [see Figure 2-8] (Chen & Patton, 1999).

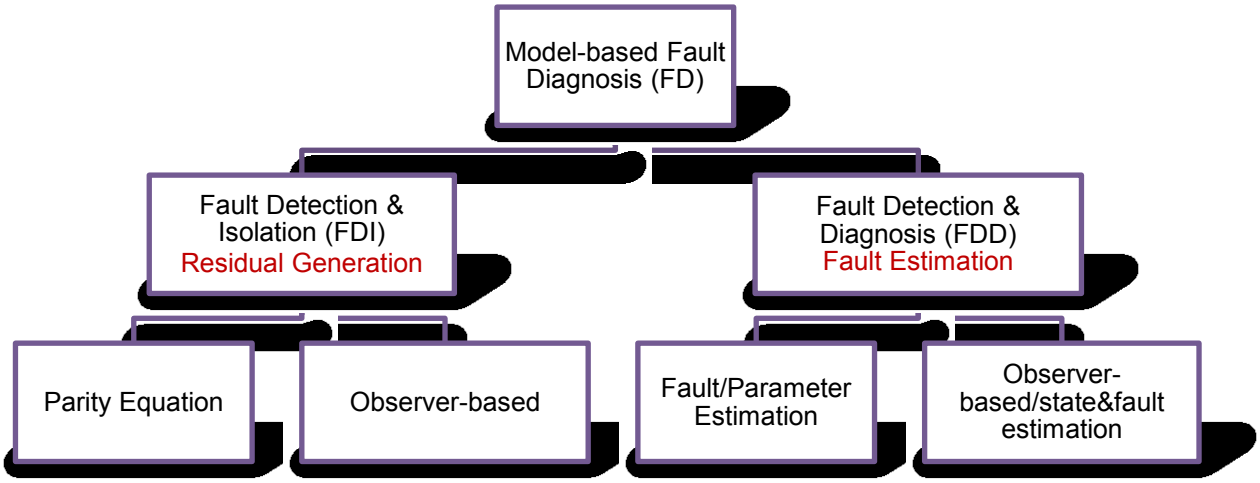

Figure 2-8 Fault diagnosis classification

The main idea behind model-based FDI/FDD is to compare the system's available measurements, with *a priori* information represented by the system's mathematical model as illustrated in Figure 2-9 (Chen & Patton, 1999). The signals that reflect inconsistencies between nominal and faulty system operation, termed "residuals", are usually generated using analytical approaches, such as observers (Chen & Patton, 1999; Patton, Frank & Clark, 2000), parameter estimation (Isermann, 1993) or parity equations (Gertler, 1998) based on analytical (or functional) redundancy (Gertler, 1988; Beard, 1994; Patton, Frank & Clark, 1989, 2000; Simani, Fantuzzi & Patton, 2003; Blanke, Kinnaert, Lunze & Staroswiecki, 2006; Isermann, 2006; Ding, 2008).

Figure 2-9 shows the conceptual structure model-based fault diagnosis comprising residual generation and decision making: (i) the residual generation provides a residual signal that carries information on the time and location of the faults. The residual signal should be close to zero in the fault-free case and deviate from zero when a fault has occurred, whereas (ii) the decision-making evaluates the residuals and monitors if and where a fault has occurred. This

two-stage structure was first suggested by Willsky and Chow (1980) and is now widely accepted by the fault diagnosis community.

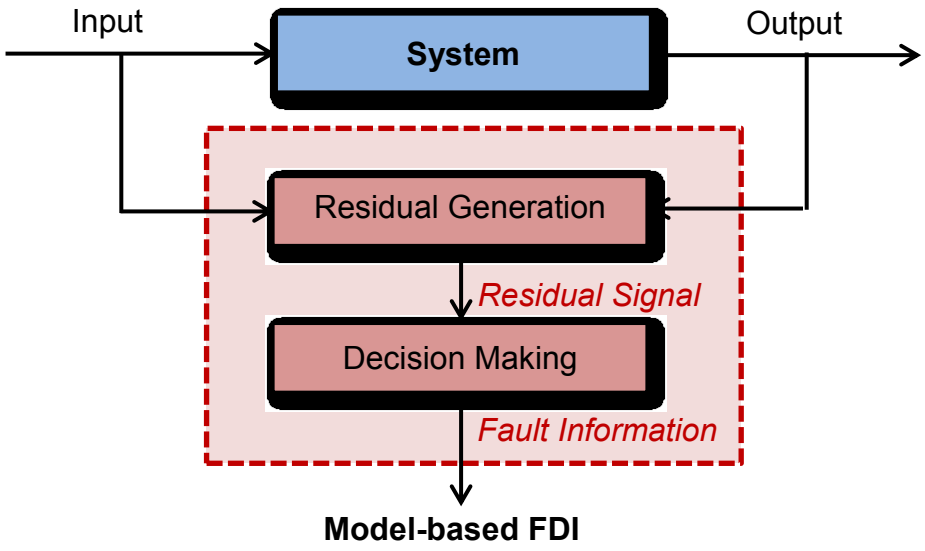

Figure 2-9 Residual generation structure of model-based FDI

The main advantage of the model-based approach is that no redundant hardware components are required to implement FDI/FDD scheme. The model-based information is used to create a form of analytical or functional redundancy, rather than hardware redundancy. A model-based FDI/FDD algorithm can be achieved in software on the process control computer and in many cases the measurements needed for control are sufficient for the FDI/FDD algorithm so that no additional hardware is required.

The most important issue for the design of a model-based FDI/FDD scheme is to ensure satisfactory robustness against modelling uncertainty arising from incomplete or inaccurate modelling of the monitored process. Robust fault diagnosis has become an interesting research issue over recent years (Patton, 1997; Chen & Patton, 1999), making the "early detection and isolation" of faults difficult to achieve in the presence of significant modelling uncertainty and disturbance.

In the field of flight control systems, model-based FDI/FDD methods are very suitable since for most flight regimes the dynamical structure of the aircraft is well understood in terms of the appropriate non-linear differential equations (Chandler, 1984; Patton, 1991; Smaili & Mulder, 2000; Alwi & Edwards, 2010; Cieslak, Henry, Zolghadri & Goupil, 2008). Linear or linearized FDI/FDD methods can thus be used as long as modelling uncertainty is correctly accounted for.

An additional issue is that the complexity of advanced aircraft systems may require time-varying methods of FDI/FDD to be used. This subject is becoming an important issue, keeping in mind the need for real-time methods that can be verified and certified for flight application.

2.2.3 Other issues in FTC design

There are a number of other significant issues that can arise when designing FTC systems (Patton, 1997; Zhang & Jiang, 2008; Benosman, 2009). For the active approach to FTC a suitable *integration* between the FDI/FDD and reconfiguration mechanism must be made. The majority of approaches in the literature are focused on either the FDI/FDD or the FTC problem but very few studies consider the integration of both. In other words the majority of the literature considers either the FDI/FDD or FTC by considering that the second function operates perfectly (Patton, 1997; Cieslak, Henry, Zolghadri & Goupil, 2008; Ding, 2009).

However, the interconnection of such methods may be infeasible and there can be no guarantees that a satisfactory post-fault performance, or even stability, can be maintained by such a scheme. It is therefore very important that the FDI or FDD designs and FTC, when carried out separately, are each performed bearing in mind the presence and imperfections of the other, i.e. what is necessary is integrated design. For making the interconnection possible, one should first investigate what information from the FDI/FDD unit is needed by the FTC, as well as what information can actually be provided by the FDI/FDD scheme. Imprecise information from the FDI/FDD that is incorrectly interpreted by the FTC scheme might lead to a complete loss of stability of the system.

During reconfiguration the control system has a time-delay effect due to the time taken for the fault to be correctly detected and isolated. An unsolved issue in active FTC is how to include the effect of this time-delay at the design stage, most probably by using an integrated design procedure. The idea would be to combine the FDI/FDD designs with the control system design whilst also taking account of the detection/isolation time window (Cieslak, Henry, Zolghadri & Goupil, 2008).

Another very important issue is that every real-life controlled system has *control action saturation*, i.e. the input and/or output signals cannot exceed certain values. In the design phase of a control system usually the effect of the saturation is accommodated by making sure that the control action will not get overly active and will remain inside the saturation limits under normal operating conditions. Faults, however, can have the effect that the control

action stays at the saturation limit. For instance, when a partial 50% loss of effectiveness in an actuator has been diagnosed, a standard and easy way to accommodate the fault is to re-scale the control action by two so that the resulting actuation approximates the fault-free actuation. As a result the control action becomes twice as big and may go to the saturation limits. Clearly, in such situations one should not try to completely accommodate the fault but one should be willing to accept certain performance degradation imposed by the saturation (Zhang & Jiang, 2003).

When dealing with FTC for aircraft, an important issue for the FTFC system design is that the dynamics of the aerodynamic system cannot be represented accurately enough by linear dynamical models. Hence, *nonlinear models* have to be used. This necessities the development of techniques for FTC system design that can explicitly deal with nonlinearities in the mathematical representation of the system. Nonlinearities are very often encountered in the representations of complex systems like aircraft and spacecraft. To reduce the inherent complexity of the control design, it is usual that the aircraft lateral and longitudinal dynamics are decoupled so that they have no effect on each other. This significantly simplifies the model of the aircraft and makes it possible to design the corresponding controllers independently. This decoupling condition can be achieved approximately for a healthy aircraft, but certain faults can easily destroy the de-coupling, so that more powerful control strategies could be considered alternatively (Brian & Frank, 2003; Stengel, 2005).

2.3 Fault Tolerant Flight Control Strategy

In this section an overview of the existing work in the area of FTFC is given focusing on reconfigurable flight control strategies. Due to the improved performance and the ability of dealing with a wider class of faults, active FTC methods have gained much more attention in the literature than the passive FTC methods. The current active FTC methods are given in the following review, of which several have been evaluated within the GARTEUR FM-AG 16 subject “Fault tolerant flight control” (mentioned in Section 1.4).

2.3.1 Classification of FTFC schemes

As discussed in Section 2.2 and shown in Figure 2-6, most FTC methods have active properties involving some form of control reconfiguration triggered either by fault-decision form an FDI unit or by fault estimation from an FDD unit. Many methods have been proposed to solve the FTFC problem, including reconfiguration issues. The term

reconfigurable flight control is used to refer to software algorithms designed specifically to compensate for faults e.g. in flight surface actuators or inertial/air data sensors by generating compensating forces and moments through using "reconfigured" control action based on healthy but similar or dissimilar actuator/sensor redundancy. Figure 2-10 shows the main classification of FTFC strategies that may or may not include active reconfiguration.

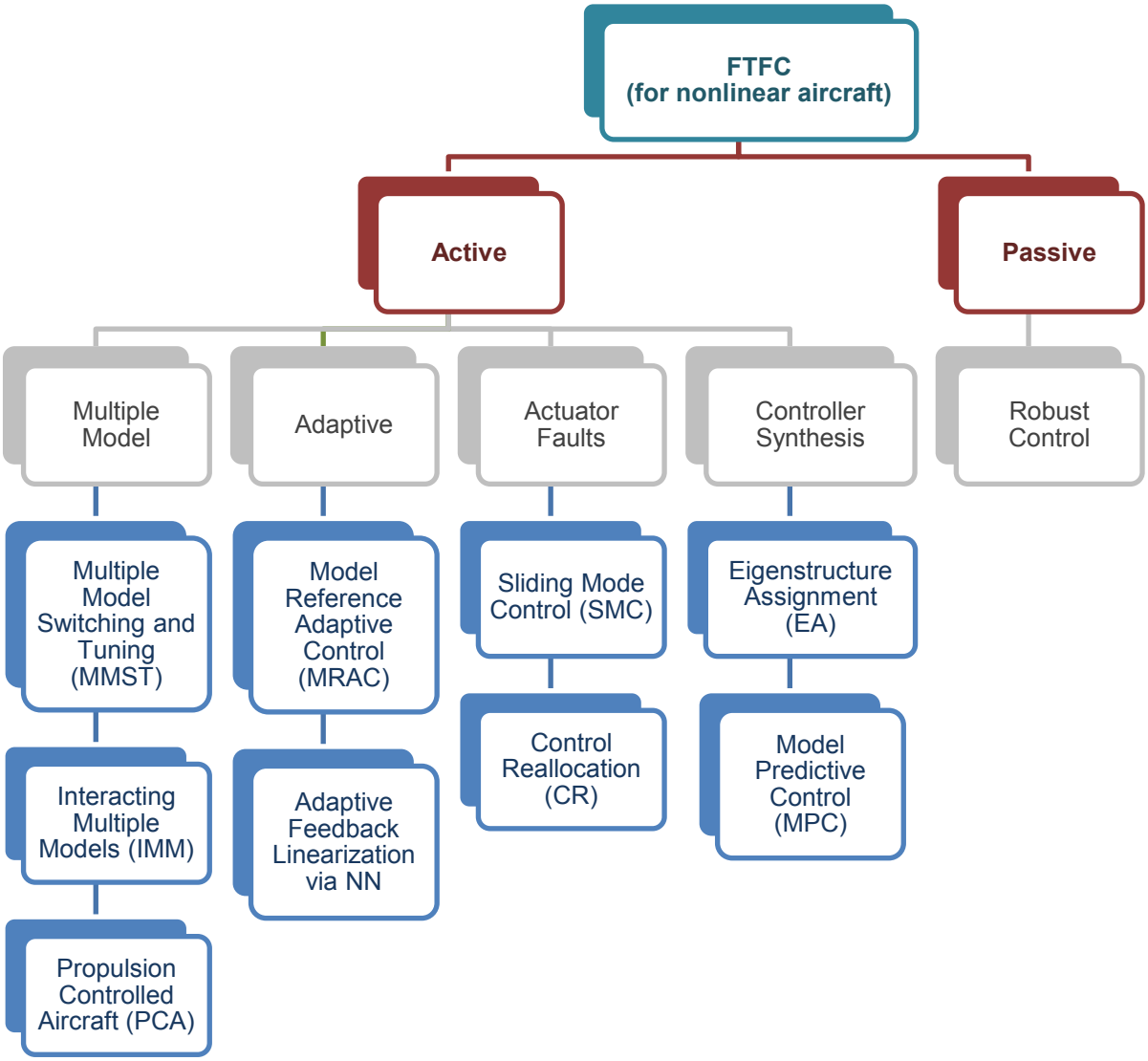

Figure 2-10 Classification of FTFC methods

Many FTFC control design methods rely on those ideas in Figure 2-10 (Zhang & Jiang, 2008) that had been investigated in the past for other control purposes rather than for aircraft. Even though well-known control design methods have been used, it poses new problems and challenges that may not appear in the conventional controller designs. An important criterion for judging the suitability of a control method for FTFC system is its ability to be implemented to maintain an acceptable (nominal or degraded) performance in the impaired

flight control system in an online setting. In addition, methods based on combination of different approaches may be more appropriate to achieve the best overall FTFC system.

2.3.2 Comparison of reconfigurable FTFC methods

Table 2-1 presents a comparison of the FTFC methods mentioned in Figure 2-10. The dots denote methods that have a specific property whilst empty circles imply that a suggested approach or modification that could be used to incorporate the property. The columns are explained as follows:

- Failures: Types of failures that the method can handle.
- Robust: The method uses robust control techniques.
- Adaptive: The method uses adaptive control techniques.
- FDI/FDD: An FDI/FDD algorithm is incorporated into the method.
- Assumed: An FDI/FDD algorithm is assumed to be used to provide fault information.
- Constraints: The method can handle actuator constraints.
- Model Type: The type of internal model used.

As can be seen from Table 2-1 (Zhang & Jiang, 2008), many methods have been suggested for FTFC, but most of these are chosen to deal with some but not all of the important issues. Hence, the designer should select the most appropriate approach according to various performance requirements, based on various scenarios.

Table 2-1 Comparison of reconfigurable control methods

Method	Failures		Robust	Adaptive	Fault Model		Constraint	Model Type	
	Actuator	Structural			FDI/FDD	Assumed		Linear	Nonlinear
MMST		•		•	•			•	
IMM		•		•	•		○	•	
PCA	•		○			•		•	•
CR	•					•	○	•	
Feedback Linearization	•	•		•	•				•
SMC	○	•	•				•		•
EA		•				•		•	
MRAC		•		•	•			•	○
MPC	•	•	○	○	•	•	•	•	○

2.3.3 The choice of reconfigurable FTFC

The FTFC approach described in this thesis uses a transparent physical modular approach, allowing the designers and engineers to interpret the data in each step, based on the assumption that the physical model information will facilitate certification for eventual flight airworthiness. Hence, focus is placed on the use of mathematical representations based on the known flight dynamics. All quantities and variables which appear in the model have a physical meaning and should thus be interpreted as such. The details of the nonlinear mathematical model used and the aerodynamic parameters of an Unmanned Aerial Vehicle (UAV), the Machan are introduced in Chapter 3.

The air accident survey and statistics presented in Section 1.4 make a clear case for reconfigurable FTFC. As outlined in Section 2.3.2, there are several possible control approaches available to achieve reconfigurable FTFC for aircraft. In this research an adaptive control approach has been chosen based on feedback linearization theory. The starting point is a nonlinear system structure and a requirement to develop a baseline controller structure for the fault-free aircraft providing a good de-coupling of the nonlinear aircraft into approximately linear subsystems to which suitable outer-loop FTC control designs can be applied.

The feedback linearization procedure described in Chapter 4 inevitably results in a robustness issue, since the nonlinear dynamics are not completely cancelled. The approach then turns to suitable approaches to handle the resulting modelling uncertainty, bearing in mind that a realistic aircraft system is perturbed by wind gust disturbance. The approach to be used must also take into account the effects of bounded actuator or sensor faults either by making the closed-loop system insensitive to these faults or be estimating the faults and compensating their effects on-line in FTFC system.

The action of either reducing the sensitivity of the faults in the control (with or without fault estimation) is the “reconfigurable” part of the FTFC system. The main strategy is to make use of an adaptive NN, described in Chapter 5, which is updated on-line to provide adaptive performance to minimise the combined effects of faults, disturbances and modelling uncertainty. The use of the adaptive NN means that the FTFC incorporates adaptive control and it is argued that this has a powerful capability of causing the flight system to adapt flexibly to dynamic changes.

It should be noted that adaptive control systems are dynamical systems which usually require online parameter estimation and can be classified according to whether or not they are "integrated" or "direct" or alternatively as to whether or not they are "modular" or "indirect". The individual approaches in this classification all have their specific advantages and drawbacks. The advantage of the integrated approach is that it is possible to prove stability of the controller structure, subject to certain bounding conditions. On the other hand, the modular approach allows the control problem to be partitioned according to either an identification approach or a direct model-based control step. This helps to reduce the overall controller complexity, although no formal proof of stability can be given.

In the identification approach all the controller performance depends primarily on the convergence of the estimated model parameters to their true but unknown values. However, in this research, all the parameters are assumed to be already known or estimated. Thus, the basic modularity of this adaptive control setup has been exploited to enable a physical control technique to be selected. This selection is made using NDI in combination with on-line adaptive or active aerodynamic model compensation. A more elaborate discussion of the properties of the proposed approach for reconfigurable FTFC and some description of improvements about different reconfiguring control techniques based on this scheme can be found in Chapters 5, 6, 7 and 8.

2.4 Conclusion

In this chapter, the classification of general fault types and popular FTC methods are reviewed with a focus on the FTFC problem for flight control. The methods applicable for active FTFC are outlined with an emphasis on approaches combining model-based FDI/FDD and controller reconfiguration. The main principles and most relevant techniques of model-based FDI/FDD and FTFC are discussed with an emphasis on robustness requirements, considering modelling uncertainty, exogenous disturbance the FTC requirement. Several important issues of FTC that remain unsolved are outlined. In this chapter, the basic schemes of controller reconfiguration based on the use of FDI/FDD fault information are also summarized. The issue of FDI/FDD residual design/fault estimation for closed-loop systems has also been stated. The main concepts of the thesis are summarized including the starting point of the nonlinear aircraft modelling, feedback linearization and adaptive on-line NN compensation of faults, disturbance and modelling uncertainty.

Chapter 3 Nonlinear Aircraft Model

This chapter provides the relevant background and preliminary knowledge for establishing an aircraft mathematical model of flight control. The nonlinear aerodynamic equations of typical fixed-wing aircraft valid at sub-sonic speeds are introduced and simplified for the purposes of simulation studies. The simplifications are indicated and some brief justifications are given. The derivations of the aerodynamics reference frames for aircraft are derived as they are used in Chapter 4 and later in the thesis in order to develop the strategy for feedback linearization as a key step in developing the FTC schemes.

The aircraft chosen in this thesis as a simulation example is a UAV (Unmanned Aerial Vehicle), the Machan, used as a development vehicle by Marconi Avionics, Chatham UK for research on high incidence flight and nonlinear control laws, with RAE Farnborough UK and NASA Dryden in the 1980's (Aslin, 1985).

3.1 Main Control Surface

Aircraft control systems are a combination of mechanical and electronic equipment that are carefully designed to allow adequate responsiveness to control inputs and also allow an aircraft to be flown with exceptional precision and reliability. The purpose of the control systems is to transfer motion input from a pilot or autopilot to a control surface. A conventional aircraft is equipped with certain fixed and movable surfaces which provide stability and control manoeuvre during flight (Etkin & Reid, 1996).

For an aircraft to fly, the lift forces must be sufficient to counteract the drag forces and the weight of the aircraft. The effective force at the centre of gravity is considered as the major force required maintaining stable flight. In general, all control surfaces utilize the principle of lift forces in different directions. The forces generated from the motions of these control surfaces act either independently or in conjunction with one another on the aircraft to produce various manoeuvres (Aslin, 1985; Etkin & Reid, 1996).

In an aircraft system, the main control surfaces that perform movement include aileron, rudder and elevator as shown in Figure 3-1.

Aileron: The ailerons are a pair of movable roll-control surfaces attached to the trailing edge of the wings and move in the opposite direction from each other. They are used to roll the aircraft by creating unequal lifting forces on opposite sides of the aircraft. Movement of the ailerons changes the shape of the wing, creates more curvature on one side and drag force on the opposite wing. Aileron deflections are necessary for smooth coordinated turns. The combination of roll and yaw will cause the aircraft to lean into turns.

Rudder: The rudder is a movable yaw-control surface hinged to a fixed surface - vertical stabilizer on the tail used to turn the aircraft right or left. Airflow causes a force to be applied to the rudder which helps in turning the aircraft in the direction of the force. Therefore, the rudder is used for directional control by changing the yaw of the aircraft and works in the correct sense, for example, moving the rudder to the left causes the aircraft to turn left. The effectiveness of rudder increases with speed, hence large deflections at low speeds and small deflections at high speeds may be required to provide the desired reaction.

Elevator: The elevators consist of a pair of movable pitch-control control surfaces attached on the hinged section of the tail - horizontal stabilizer. They are designed to impress a pitching movement on the aircraft, in the other words, moving the elevators either up or down simultaneously will cause the nose of the aircraft to go up or down that actually allows the aircraft to climb or dive. Pulling the control stick back causes the elevators to be defected up and also causes the airflow to force the tail down and the nose up thereby increasing the pitch-angle, making the aircraft climb.

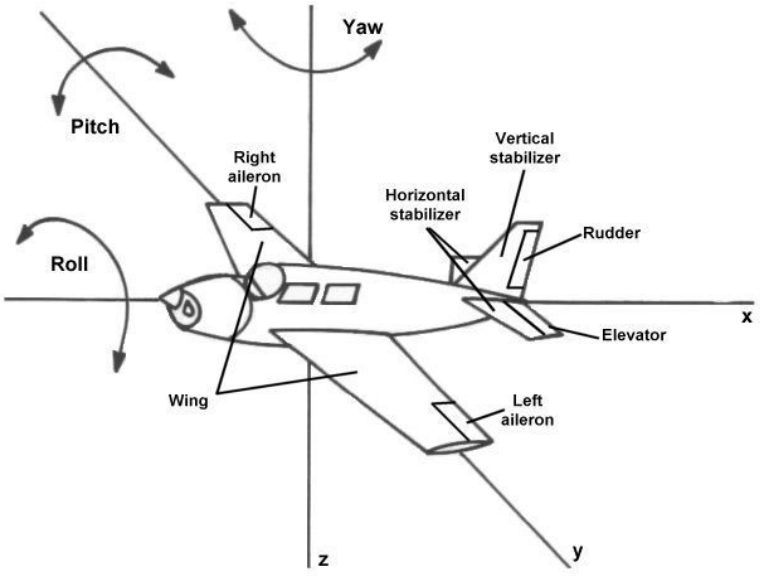

Figure 3-1 Aircraft control surfaces (rudder, elevator and aileron)

http://www.aerospaceweb.org/question/aerodynamics/q0208.html

The main aircraft motions including roll, pitch and yaw according to the three different control surfaces are shown as Table 3-1.

Table 3-1 Aircraft motions according to control surfaces

Control Surfaces	Control Motions	Control Description
Ailerons	Roll	rotation around the longitudinal axis
Rudder	Yaw	movement of the nose to left or right
Elevators	Pitch	movement of the nose up or down

In summary, any movement of these three main control surfaces would change the airflow and pressure of distribution over and around the control surface and thus directly affect the lift and drag produced by the control surface combination, which make the aircraft to be controllable about its three axes of rotation.

3.2 Nonlinear Aircraft Dynamics Modelling

An aircraft in flight could be considered as a rigid body immersed in a fluid medium, in this case, the air. The forces acting on the airframe are due to the motion of the aircraft through the air and due to the inherent properties of the framework i.e. mass, etc. The major force required to maintain steady flight is the lift force which is generated by the airflow over the wings. The lift force must counteract the weight of the aircraft, any excess of lift acting so as to increase the vertical speed of the aircraft. The aircraft's forward speed is provided by a thrust force from one or more engines of the jet or propeller type. The thrust force must balance, or be in excess of, the induced drag force on the airframe due to its forward motion (Hauser, Sastry & Meyer, 1992; Goman & Khramtsovsky, 1997). In simple terms then, when an aircraft is flying straight and level, these forces must be in equilibrium as shown in Figure 3-2 (McRuer, Graham & Ashkenas, 1972).

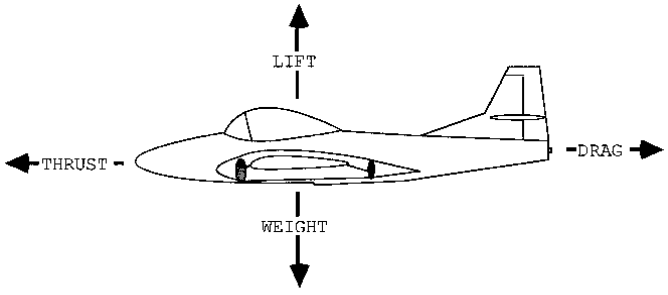

Figure 3-2 Aircraft forces in steady flight

http://www.globalsecurity.org/military/systems/aircraft/intro-performance.html

In practice an aircraft contains a three axis system and forces and moments will, in general, act in all three axes. This is a so-called 6 Degree of Freedom (6DoF) system, which specifically refers to the body freedom of moving forward/backward, up/down, left/right combined with rotation about these three perpendicular axes, often termed as pitch, yaw, and roll movement. For a realistic simulation, a model with full force and 6DoF which accommodates most of the nonlinearities of the basic aerodynamics must be derived (McRuer, Graham & Ashkenas, 1972).

Since the first successful study of control and dynamics of an aircraft was credited (Lanchester, 1907; Bryan, 1911; Cook, 1997), the equations of motion have changed little in 100 years, and the original formulations are still used. Considering the aerodynamics of an airframe are complex and inherently nonlinear, it was found necessary to simplify some of these dynamics but retain sufficient nonlinear properties to provide a realistic simulation study.

The following sections give an overview of the various reference frames used to describe an aircraft's state, provide the general mathematical model of the nonlinear Machan UAV, which could be used to represent almost all the aircrafts and used as the simulation model in this thesis. Furthermore, the basic concepts of linearization during small disturbance circumstances for aircraft are introduced.

3.2.1 Definitions of the frames

To derive a more complete picture of the aircraft in flight it is initially important to define a set of axes which will act as a reference frame around which equations of motion may be developed. Since the aircraft is a free body in space its position may be defined with respect to a set of earth or gravity fixed axes which remain fixed with respect to the earth. However, this axes system is inconvenient for analysis, a better choice being a set of axes which remain fixed relative to the airframe and form the principal axes of inertia of the aircraft. This axes set, often called the body frame, is shown diagrammatically in Figure 3-3 and clearly remains fixed relative to the geometrical distribution of the airframe. Then the forces and moments could be defined to act about this frame of reference.

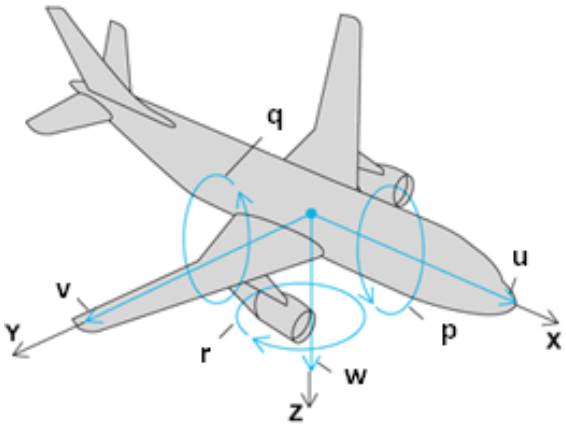

Figure 3-3 Aircraft axes system (body frame)

http://www.accessscience.com/overflow.aspx?SearchInputText=Flight&ContentTypeSelect=10&topic=ENG:AERO:AENAUT&term=Flight

In the variety of reference frames (or axes systems) used to describe the aircraft movement and orientation, the "Earth" frame F_E is suited to navigation, while F_B; F_S; F_W represent the "body", "stability" and "wind" axes, respectively which are well suited to control and are also popular in simulation and application. The relevant frames are described as following (Brian & Frank, 2003; Stengel, 2005; Sadraey & Colgren, 2009).

Body Frame F_B: This is a right-handed orthogonal reference system which has its origin O at the centre of gravity of the aircraft. The X_BOZ_B plane coincides with the aircraft's plane of symmetry if it is symmetric, or it is located in a plane, approximating what would be the plane of symmetry if it is not. It is conventional to define the nomenclature associated with the body fixed axes system according to an agreed standard as summarized in Table 3-2 with reference to Figure 3-3.

Table 3-2 Aircraft standard in body frame

	Velocities	Applied forces and moments	Distances
Forward	u	X	x
Side	v	Y	y
Vertical	w	Z	z
Roll	p	L	
Pitch	q	M	
Yaw	r	N	

In the body-fixed reference axes:

- OX_B is directed towards the nose of the aircraft and termed the longitudinal axis. Linear displacements from the steady state about this axis are defined as x (m) for an aircraft having a steady state velocity along OX_B of u (m·s^{-1}). Force components along OX_B are taken as forward positive and termed X (N). The roll component of aircraft motion is about OX_B and has velocity p (rad · s^{-1}), the resulting angle displacement being ϕ (rad) under the action of a rolling moment L (N·m) taken positive in the clockwise sense looking along OX_B from O.
- OY_B is the transverse or lateral axis pointing to the right wing. A steady state sideslip velocity v (m·s^{-1}) produces a sideslip displacement y (m) under the action of a sideslip force Y (N). Pitching moments are generated about OY_B having angular velocities q (rad·s^{-1}), angular displacements of θ (rad) and pitching moment M (N·m). The positive sense is defined as nose up or clockwise rotation about OY_B looking along OY_B from O.
- OZ_B is the normal axis pointing towards the bottom of the aircraft. An incremental change in downwards velocity of w (m·s^{-1}) gives rise to a downward displacement of z (m) with a downward force component Z (N), downwards being positive. Yawing moments take place around OZ_B producing yawing velocities of R (rad · s^{-1}), an angular displacement of ψ (rad) and a yawing moment of N (N·m). All taken positive in the clockwise sense looking down.

Earth Frame F_E: This reference frame (also called navigation frame) is a right-handed orthogonal system which is considered to be fixed in space and is attached to the earth's local tangent plane. This frame is a convenient reference set which origin can be placed at an arbitrary position, but will be chosen to coincide with the centre of gravity O of the aircraft at the start of a flight test manoeuvre. The earth frame is usually considered as a local inertial frame where *Newton's Laws* apply. In this frame**,** OZ_E axis points downwards, parallel to the local direction of gravity towards the centre of the earth. OX_E and OY_E axes lie in a plane tangential to the earth's surface with OX_E oriented eastwards (or sometimes northwards) and OY_E oriented southwards (or sometimes eastwards). The velocities along OX_E, OY_E and OZ_E are defined as u_E, v_E and w_E (m·s^{-1}), respectively, note that $w_E = -dh/dt$ where h (m) is the aircraft's height, downward velocity being positive.

Stability Frame F_S: This is a special body-fixed reference frame, used in the study of small deviations from a nominal flight condition. The reference frames F_B and F_S differ in the orientation of their respective OX axes. OX_S is chosen parallel to the projection of the true airspeed vector V on the X_BOZ_B plane (if the aircraft is symmetric and this is the plane of symmetry), or parallel to V itself in case of a symmetrical nominal flight condition. The OY_S coincides with the OY_B.

Wind Frame F_W: This reference frame, also called the wind reference frame, has its origin in the centre of gravity O of the aircraft. OX_W is aligned velocity vector of the aircraft and the OZ_W coincides with the OZ_S.

Figure 3-5, 3-6 & 3-7 show various Frames and their coordination.

3.2.2 Coordinate transformation

To translate between body frame and earth frame, a transformation matrix related to the corresponding displacement angles: ψ, θ, ϕ, also called *Euler Angles* formulating the *Euler Equations*, may be used. The rotational relationships between OX_B, OY_B and OZ_B and OX_E, OY_E and OZ_E are best understood by considering an intermediate axis set, OX_i, OY_i and OZ_i, initially coincident with OX_E, OY_E and OZ_E. The orientation of body fixed axes with respect to earth fixed axes can then be built up as follows (Byushgens & Studnev, 1988; Möckli, 2006):

1) Rotate OX_i, OY_i and OZ_i about the OZ_i axis by an angle ψ (the yaw angle).
2) Rotate OX_i, OY_i and OZ_i about the OY_i axis by an angle θ (the pitch angle).
3) Rotate OX_i, OY_i and OZ_i about the OX_i axis by an angle ϕ (the roll angle).

Three *Euler Angle* rotations continuously relate the orientation of the aircraft's body-fixed frame to the earth frame. As shown in Figure 3-4 and Figure 3-5, the earth coordinate frame is first transformed into the intermediate frame 1 via a rotation about the OZ_E axis by the angle ψ, which defines the aircraft's heading. This is followed by a rotation about the new OY_1 axis by an angle θ, which defines the aircraft's elevation. Finally, the aircraft bank angle ϕ, defines the rotation about the new OX_2 axis. Then the orientation of the body frame with respect to the earth frame described by *Euler Angles* is achieved (Durham, 1997; Ducard, 2007, 2009).

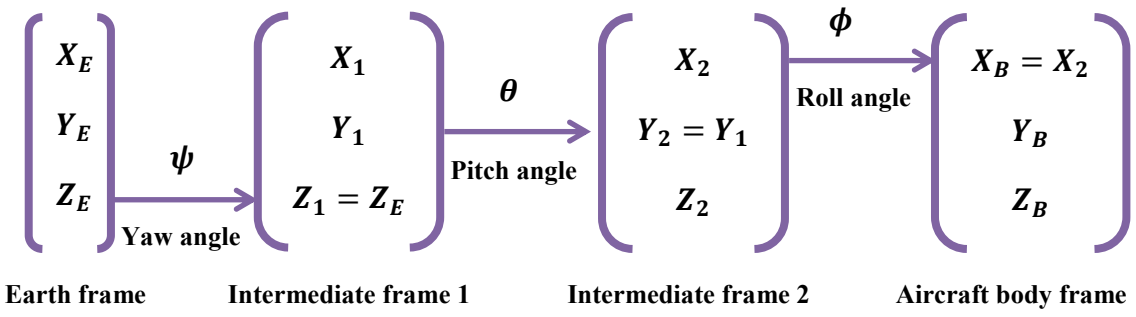

Figure 3-4 Transformation steps from earth frame to aircraft body frame

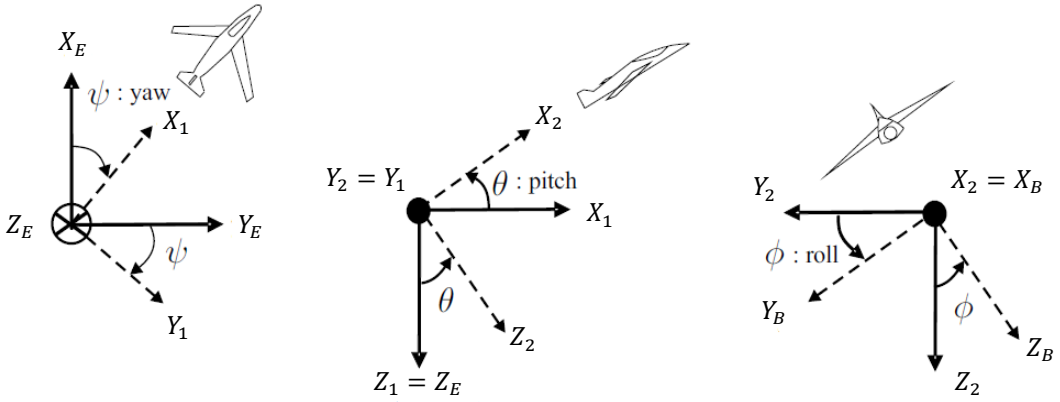

Figure 3-5 Euler angles and frame transformation

The attitude transformation matrix (also called direction cosine matrix) is necessary to transform vectors and point coordinates from the earth frame F_E to the aircraft body frame F_B. By considering each of the rotations separately as above, the direct cosine transformation matrix T_E^B can be expressed as:

$$F_B = T_E^B F_E, F_E = (T_E^B)^{-1} F_B = (T_E^B)^T F_B \tag{3-1}$$

where

$$T_E^B = \begin{bmatrix} cos\psi & sin\psi & 0 \\ -sin\psi & cos\psi & 0 \\ 0 & 0 & 1 \end{bmatrix} \begin{bmatrix} cos\theta & 0 & -sin\theta \\ 0 & 1 & 0 \\ sin\theta & 0 & cos\theta \end{bmatrix} \begin{bmatrix} 1 & 0 & 0 \\ 0 & cos\phi & sin\phi \\ 0 & -sin\phi & cos\phi \end{bmatrix} \tag{3-2}$$

Leading to

$$T_E^B = \begin{bmatrix} cos\psi cos\theta & sin\psi cos\phi + cos\psi sin\theta sin\phi & sin\psi sin\phi - cos\psi sin\theta cos\phi \\ -sin\psi cos\theta & cos\psi cos\phi - sin\psi sin\theta sin\phi & cos\psi sin\phi + sin\psi sin\theta cos\phi \\ sin\theta & -cos\theta sin\phi & cos\theta cos\phi \end{bmatrix} \tag{3-3}$$

The angular rates p, q and r are related to the rate change of the *Euler Angles* $\dot{\phi}$, $\dot{\theta}$, $\dot{\psi}$ along OX_B, $OY_B$and $OZ_B$by the following coordinate transformations:

$$\begin{bmatrix} p \\ q \\ r \end{bmatrix} = \begin{bmatrix} 1 & 0 & -sin\theta \\ 0 & cos\phi & sin\phi cos\theta \\ 0 & -sin\phi & cos\phi cos\theta \end{bmatrix} \begin{bmatrix} \dot{\phi} \\ \dot{\theta} \\ \dot{\psi} \end{bmatrix} \tag{3-4}$$

The inverse of the equation above being

$$\begin{bmatrix} \dot{\phi} \\ \dot{\theta} \\ \dot{\psi} \end{bmatrix} = \begin{bmatrix} 1 & 0 & -sin\theta \\ 0 & cos\phi & sin\phi cos\theta \\ 0 & -sin\phi & cos\phi cos\theta \end{bmatrix}^{-1} \begin{bmatrix} p \\ q \\ r \end{bmatrix} \Leftrightarrow \begin{bmatrix} \dot{\phi} \\ \dot{\theta} \\ \dot{\psi} \end{bmatrix} = \begin{bmatrix} 1 & sin\phi tan\theta & cos\phi tan\theta \\ 0 & cos\phi & -sin\phi \\ 0 & sin\phi sec\theta & cos\phi sec\theta \end{bmatrix} \begin{bmatrix} p \\ q \\ r \end{bmatrix} \tag{3-5}$$

Equations (3-2)-(3-5) break down for $\theta = +90^{\circ}$ and this may be considered a disadvantage in simulation studies but this may be tolerated providing manoeuvres requiring only relatively small pitch angles are to be modelled. The following ranges are defined:

$$\begin{gathered} -\pi \leq \psi < \pi \quad or \quad 0 \leq \psi < 2\pi \\ -\frac{\pi}{2} \leq \theta < \frac{\pi}{2} \\ -\pi \leq \phi < \pi \quad or \quad 0 \leq \phi < 2\pi \end{gathered} \tag{3-6}$$

Specially, when perturbations are small, such that ψ, θ, ϕ may be treated as small angles as $\psi, \theta, \phi \approx 0$, (3-4) may be approximated as:

$$\begin{bmatrix} p \\ q \\ r \end{bmatrix} = \begin{bmatrix} \dot{\phi} \\ \dot{\theta} \\ \dot{\psi} \end{bmatrix} \tag{3-7}$$

The air flow acting on the wind frame F_W is also responsible for the aerodynamic forces. The air flow is described by the airspeed vector V_T. Its direction relative to the wind frame defined by the attack angle α and sideslip angle β.

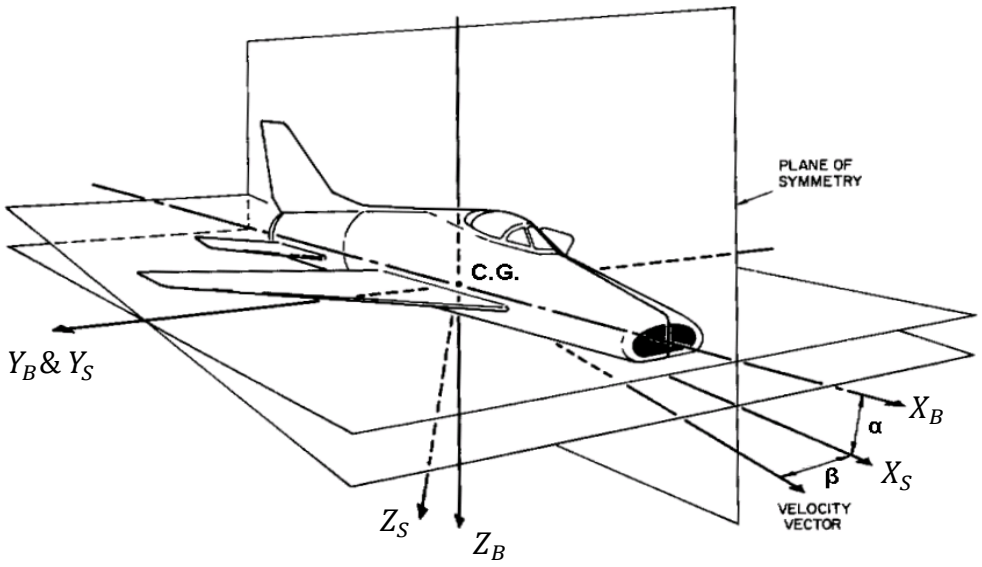

Figure 3-6 Definition of attack angle and sideslip angle

As shown in Figure 3-6, α is the angle between the projection of the airspeed vector V_T onto the (X_B, Z_B) plane and the X_B axis; β is the angle between the projection of the airspeed vector V_T onto the (X_B, Y_B) plane and the airspeed vector itself. The wind axes coordinate system is such that the X_W axis points along the airspeed vector V_T .

The rotation matrix T_B^W is necessary to transform vectors and point coordinates from the aircraft body frame F_B to the wind frame F_W according to the following formulae as:

$$F_W = T_B^W F_B \text{ or } F_B = T_W^B F_W = (T_B^W)^T F_W \tag{3-8}$$

where

$$T_B^W = \begin{bmatrix} cos\beta & sin\beta & 0 \\ -sin\beta & cos\beta & 0 \\ 0 & 0 & 1 \end{bmatrix} \begin{bmatrix} cos\alpha & 0 & sin\alpha \\ 0 & 1 & 0 \\ -sin\alpha & 0 & cos\alpha \end{bmatrix}$$

$$= \begin{bmatrix} cos\alpha cos\beta & sin\beta & sin\alpha cos\beta \\ -sin\beta cos\alpha & cos\beta & -sin\alpha sin\beta \\ -sin\alpha & 0 & cos\alpha \end{bmatrix} \tag{3-9}$$

As an example, the airspeed vector is expressed in the body frame as follow:

$$(V_T)_B = T_W^B (V_T)_W \tag{3-10}$$

$$\begin{bmatrix} u_T \\ v_T \\ w_T \end{bmatrix} = T_W^B \begin{bmatrix} V_T \\ 0 \\ 0 \end{bmatrix} \tag{3-11}$$

where $(V_T)_B$ is body axis so-called total velocity of the aircraft, $V_B = [u \quad v \quad w]^T$ is the inertial velocity vector defined by the magnitude, with the so-called angle of attack α and side-slip angles β, respectively as:

$$V_T = \sqrt{u^2 + v^2 + w^2} \tag{3-12}$$

$$\left.\begin{array}{l} u = V_T cos\alpha cos\beta \\ v = V_T sin\beta \\ w = V_T sin\alpha cos\beta \end{array}\right\} \tag{3-13}$$

with α and β defined as:

$$\alpha = tan^{-1}\left(\frac{w}{u}\right), \beta = sin^{-1}\left(\frac{v}{\sqrt{u^2+v^2+w^2}}\right) \tag{3-14}$$

The relationships between the various frames of reference related to attack angle α and sideslip angle β are shown in Figure 3-7.

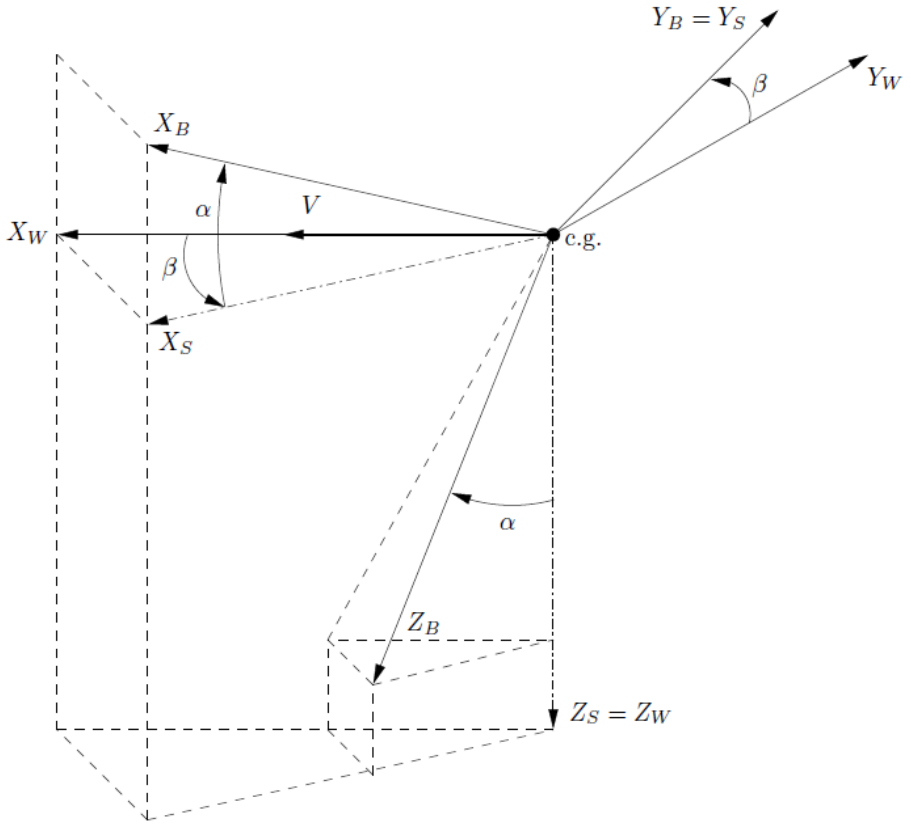

Figure 3-7 Relationship between the different reference axes F_B, F_W, F_S

Then two further important relationships between the various reference frames can now be defined as shown in Figure 3-7 since α is the angle between the body frame and the stability axis while β is the angle between the wind axis and the stability axis. To proceed further with the development of the dynamics of the aircraft the aerodynamic forces and moments acting on the aircraft must be considered. These forces and moments will produce changes in the aircraft body velocities and accelerations which may be translated to velocities relative to earth frame using (3-1) to (3-14), while the resulting dynamic behaviour of the aircraft can then be deduced (McRuer, Graham & Ashkenas, 1972; Ducard, 2007, 2009).

3.2.3 Euler equations

The Euler equations derived from a consideration of *Newton's Second Law* of motion are necessarily used for accomplishing the mathematical model of aircraft dynamics. Two basic assumptions should be given firstly (McRuer, Graham & Ashkenas, 1972):

(1) The airframe may be considered as a rigid body i.e. that the distance between any specified points within the body does not change. All aircraft exhibit some structural flexibility but for the present analysis this will be ignored.

(2) The earth may be considered as a body fixed in space so that the motion may be viewed as relative to the fixed earth. It should to be noted that for most terrestrial application this is a valid assumption but for long term navigation and extra-terrestrial flight its validity is questionable.

Given that the above assumptions are made then *Newton's Second Law* is applicable within the given reference frame. This states that the time rate of change of the linear momentum is the sum of all externally applied forces and that the time rate of change of angular momentum is the sum of all applied torques. Then the dynamic equations of the aircraft can be built from basic *Newtonian* dynamics as given by the general force and moment equations:

$$F = m\left(\frac{\partial V}{\partial t} + \Omega \times V\right), M = \frac{\partial (I\Omega)}{\partial t} + \Omega \times (I\Omega) \tag{3-15}$$

where V represents a linear velocity vector, Ω is an angular velocity vector and I is a moment of inertia tensor as $I = \begin{bmatrix} I_{xx} & -I_{xy} & -I_{xz} \\ -I_{yx} & I_{yy} & -I_{yz} \\ -I_{zx} & -I_{zy} & I_{zz} \end{bmatrix}$, then $\times$ denotes the vector product operation. The derivation of the Euler equation also assumes that the aircraft may be considered to be moving in a vacuum and is acted upon only by external forces.

By assuming that the mass of the aircraft m is unchangeable and the origin of the inertial axis system is at the aircraft centre of gravity, and that the aircraft is symmetric i.e. the OX_B, OY_B, OZ_B axes are principal axes, the complete *Euler equations* relate the forces X, Y, Z and moments L, M, N in the aircraft body frame to the angular and linear velocities in the inertial axes are shown as:

$$\begin{aligned} &\left[\dot{u} + qw - rv - a_x(r^2 + q^2) + a_y(pq - \dot{r}) + a_z(pr + \dot{q})\right]m = X \\ &\left[\dot{v} + ur - pw - a_x(pq + \dot{r}) - a_y(p^2 + r^2) + a_z(rq - \dot{p})\right]m = Y \\ &\left[\dot{w} + vp - qu + a_x(rp - \dot{q}) + a_y(rq + \dot{p}) - a_z(p^2 + q^2)\right]m = Z \end{aligned} \tag{3-16}$$

$$\begin{aligned} &I_x\dot{p} + (I_z - I_y)rq - I_{yz}(q^2 - r^2) - I_{xz}(\dot{r} + pq) - I_{xy}(\dot{q} - pr) = L + Ya_z - Za_y \\ &I_y\dot{q} + (I_x - I_z)pr - I_{yz}(\dot{r} - pq) - I_{xz}(r^2 - p^2) - I_{xy}(\dot{p} + qr) = M + Za_x - Xa_z \\ &I_z\dot{r} + (I_y - I_x)qr - I_{yz}(\dot{q} + pr) - I_{xz}(\dot{p} - rq) - I_{xy}(p^2 - q^2) = N + Xa_y - Ya_x \end{aligned} \tag{3-17}$$

where, m is the mass of the aircraft; I_x, I_y, I_z, I_{xy}, I_{yz}, I_{xz} are the moments of inertia about the axes through the centre of gravity but parallel to the aircraft body axes OX_B, OY_B, OZ_B; a_x, a_y, a_z are the co-ordinates of the centre of gravity with respect to the origin of the axes OX_B, OY_B, OZ_B, u, v and w are the forward, side and vertical velocity of the aircraft respectively; p, q and r are the roll, pitch and yaw rates, respectively.

By assuming that the origin of the inertial axis system, O, is at the vehicle's centre of gravity, which leads to $a_x = a_y = a_z = 0$ and that the vehicle is symmetric i.e. the OX_B, OY_B, OZ_B axes are principal axes, which leads to $I_{xy} = I_{yz} = I_{xz} = 0$, then (3-16) and (3-17) can be reduced to:

$$\begin{aligned} m(\dot{u} + qw - rv) &= X \\ m(\dot{v} + ur - pw) &= Y \\ m(\dot{w} + vp - qu) &= Z \end{aligned} \tag{3-18}$$

$$\begin{aligned} I_x\dot{p} + (I_z - I_y)rq &= L \\ I_y\dot{q} + (I_x - I_z)pr &= M \\ I_z\dot{r} + (I_y - I_x)pq &= N \end{aligned} \tag{3-19}$$

The *Euler equations* thus allow the definition of the body velocities in terms of forces and moments acting on the aircraft. Then the expression of these forces and moments as a function of the aircraft aerodynamics will be discussed in the following Section (McRuer, Graham & Ashkenas, 1972; Ducard, 2007, 2009).

3.2.4 Forces and moments

These forces and moments in this section are functions of the six linear and angular velocities (u, v, w, p, q, r) and the actuator (control surfaces) positions usually given by the aileron, elevator, rudder and throttle (McRuer, Graham & Ashkenas, 1972; Etkin & Reid, 1996; Bodson, 2003). The four basic forces acting on the aircraft all the time during flight include: gravity, lift, drag and thrust. In all these forces, only gravity is constant, the remaining three forces can be controlled through the designed system. All forces should be in equilibrium when an aircraft is flying straight and level at a constant speed.

Gravity: Weight is a natural (uncontrollable) force that is present because of gravity. The gravity affects all objects within the earth gravitational field and the weight acts vertically downward from the centre of gravity of the aircraft. The magnitude of the weight depends on the mass of the aircraft. In general, the aircraft will be subject to gravitational forces since it will be oriented relative to the local vertical. However, the moments perpendicular to the principal axes of gravity would not affect aircraft motion. Thus only the gravitational components of the forces G acting on the aircraft are as:

$$G = \begin{bmatrix} X_g \\ Y_g \\ Z_g \end{bmatrix} = \begin{bmatrix} -mgsin\theta \\ mgcos\theta sin\phi \\ mgcos\theta cos\phi \end{bmatrix} \tag{3-20}$$

Aerodynamic forces and moments:

- **Lift:** It is produced by a lower pressure created on the upper surfaces of the wings compared to the pressure on the lower surfaces and then achieved through the cross-sectional shape of the wing. The magnitude of the lift depends on several factors, such as the shape, size and velocity of the aircraft. The theoretical concept that summarizes the direction and force of lift is the centre of pressure which is defined just like the centre of gravity, but using the pressure distribution instead of the weight distribution.
- **Drag:** When an aircraft moves through the air, the air will resist the motion of an aircraft and this natural resistance force is called drag that works against thrust to slow the aircraft. It can also be known as retarding force acting upon a body in motion through the air, parallel to the direction of motion of a body.

When a solid body moves through a fluid medium it experiences a force due to the relative motion of the solid and fluid. The major steady aerodynamic forces acting on the airframe are lift and drag forces. These forces necessarily arise in sustained flight. The lift and drag components act along and normal to the direction of the aircraft total velocity since they are generated by the relative wind, which can be calculated in wind frame as:

$$\begin{bmatrix} X_a \\ Y_a \\ Z_a \end{bmatrix} = \begin{bmatrix} (L_w + L_T)sin\alpha - Dcos\alpha cos\beta \\ Dsin\beta \\ -(L_W + L_T)cos\alpha - Dsin\alpha cos\beta \end{bmatrix} \tag{3-21}$$

$$\begin{bmatrix} L_a \\ M_a \\ N_a \end{bmatrix} = \begin{bmatrix} \frac{1}{2} C_l \rho {V_T}^2 Sb \\ \frac{1}{2} C_m \rho {V_T}^2 S\bar{c} \\ \frac{1}{2} C_n \rho {V_T}^2 Sb \end{bmatrix} \tag{3-22}$$

where D (N) is the drag force acting on the airframe; L_w and L_T (N) represent the lift on wing and total tail respectively; M_a, N_a and L_a ($N \cdot m^{-1}$) are the pitching, yawing and rolling moment components respectively; C_l, C_m, C_n are the aerodynamic coefficients, respectively; the constants $S, b, \bar{c}, \rho$ are the wing area, wing span, mean aerodynamic chord and the density of the air fluid, respectively and clearly depend on the aircraft geometry.

Thrust force: All powered aircraft are required to have at least one propulsion unit for providing a thrust force to overcome or equal the drag force incurred due to the aircraft's motion through the air. It is an artificial force generated through engines that acts horizontally. It gives the aircraft forward momentum and creates lift on the lifting surfaces. The type of propulsion unit used varies from aircraft to aircraft (e.g. the piston engine

propeller, turboprop and jet type).The direction of this force also depends on how the engines are attached to the aircraft.

3.3 The Machan UAV Dynamics

The aircraft model that has been chosen for this study is an UAV, the Machan [see Figure 3-8], used in the Control and Intelligent Systems Engineering research group at Hull (and earlier at York and Cranfield) since 1981. The nonlinear Machan model was developed at Marconi Avionics UK during 1980 to 1982 through collaboration with RAE Farnborough and NASA Dryden involving high incidence flight research based on nonlinear flight control laws.

Although the Machan system is not representative of a large commercial aircraft it is nevertheless a good example of an open-loop unstable nonlinear flight system which is very appropriate for testing the potential use of model-based fault diagnosis methods (Aslin, 1985).

Machan was really a remotely-piloted vehicle and hence not strictly a UAV, nevertheless from an aerodynamic standpoint its size and performance may be similar to a modern UAV. It should to be noticed that since the open-loop Machan UAV is unstable, for achieving a stable FTC system, a closed-loop "base-line" control system must be configured before the further fault tolerant performance can be developed.

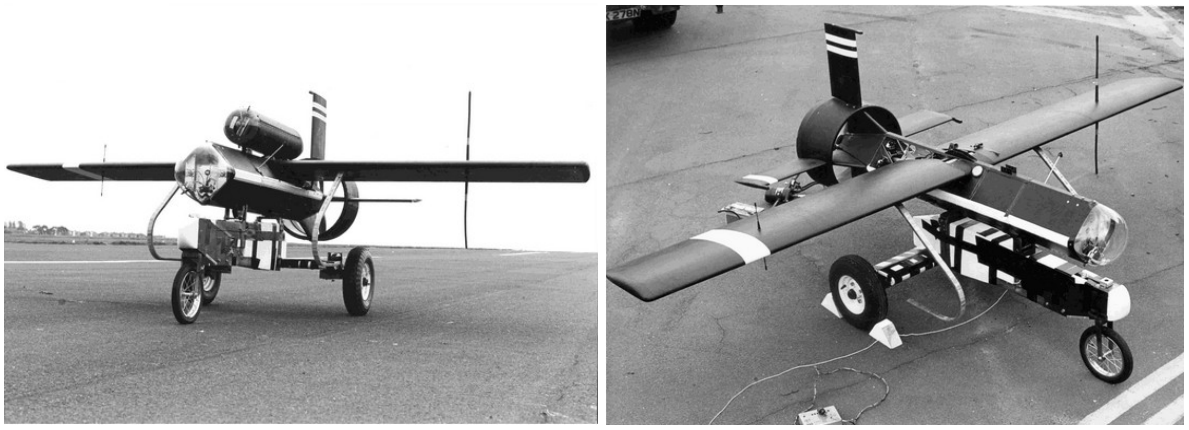

Figure 3-8 The Machan UAV at Cranfield University about 1980

http://public.cranfield.ac.uk/eh3081/uav_gallery.html

As the aerodynamic background introduced in Section 3.2.4, for the Machan case, the completed aerodynamic force and moment equations could now be written as follows. These equations include the gravitational components as given by (3-20) and the lift and drag

components of (3-21), (3-22). The value of the sideslip angle β, is taken to be zero since, in general, the sideslip angle is small compared with the incidence α. Thus the following equations can be obtained as:

$$\begin{aligned} X &= X_E - Dcos\alpha + (L_w + L_T)sin\alpha - mgsin\theta \\ Y &= Y_a + mgcos\theta sin\varphi \\ Z &= -(L_W + L_T)cos\alpha - Dsin\alpha + mgcos\theta cos\varphi \end{aligned} \tag{3-23}$$

$$\begin{aligned} L &= L_a + L_E \\ M &= M_a + L_w(cg - 0.25)\bar{c} - L_q(l_t + 0.25 - cg) \\ N &= N_a \end{aligned} \tag{3-24}$$

where the forces and moments are as defined above and cg (m) is the position of the aircraft centre of gravity; X_E (N) is the thrust force due to the engine whilst; l_t (m·s^{-1}) is the tail moment; $\bar{c}$ (m) is the mean aerodynamic chord and L_E (m·s^{-1}) is the rolling moment due to the engine; L_w is the tail lift due to the pitch rate L_q and the appropriate moment arms. The more details of these components derived from wind tunnel tests are in Aslin (1985).

3.3.1 Specific thrust model

As explained before, the aircraft use a propulsion system to generate thrust force for maintaining flight. However, it is difficult to devise a set of equations relating thrust presenting the pilot throttle demand (or angle) and a generalized model is not possible due to the various types and configurations of engines used.

For the Machan UAV in this study, the propulsion unit is a small piston engine driving a four bladed propeller. The propeller is housed in a nacel mounted at the rear of the aircraft and forming part of the tailplane assembly. Airflow is directed over the propeller through a duct, slightly forward of the nacel. The thrust force provided by this arrangement is thus along the plane of asymmetry in Figure 3-6. The engine also develops a torque, due to the airscrew rotation, about the body axis OX_B and this contributes to the rolling moment equation. The engine power demand is controlled by the setting of the throttle control T_H (Aslin, 1985).

The nominal power P_{nom} generated by the engine is given as:

$$P_{nom} = P_{max}T_H \tag{3-25}$$

where P_{max} is the maximum engine power and T_H is the throttle demand with the range of 0-100%. The actual power P_{act} generated by the airscrew is given as:

$$P_{act} = P_{max}\delta_p \tag{3-26}$$

where δ_p is the propeller efficiency.

The power generated to the airscrew is related to the resulting thrust force X_E, expressed as a first order nonlinear engine dynamic as:

$$\dot{X}_E = (P_{act} - X_E U_2)/K_e \tag{3-27}$$

where U_2(m·s^{-1}) is the air flow rate over the propeller and K_e is the engine rise rate in metres, $X_E U_2$ then being the power supplied.

The thrust power is also supplied by the rate of increase in energy of the working fluid which leads to:

$$\dot{E} = \frac{1}{2}\rho A_D U_2\left({U_3}^2 - u^2\right) = X_E U_2 \tag{3-28}$$

where A_D is the duct area, U_3 is the flow rate in the propeller wake; ρ is the density of the air fluid and u is forward velocity as defined previously. Re-arranging (3-28) and making U_3 the subject of the equation as:

$$U_3 = \sqrt{\frac{2X_E}{\rho A_D} + u^2} \tag{3-29}$$

The flow rate through the duct U_2 can be derived by considering the thrust equation as:

$$X_E = \rho A_D U_2 (U_3 - u) \tag{3-30}$$

which leads to:

$$U_2 = \frac{X_E}{\rho A_D (U_3 - u)} \tag{3-31}$$

Additionally, the engine speed rpm (revs·min^{-1}) is given as:

$$rpm = \frac{U_2}{P_p} \times 60 \tag{3-32}$$

where P_p is the propeller pitch. The torque due to the airscrew can be derived by relating this to the nominal engine power as:

$$2\pi L_E \cdot \frac{rpm}{60} = P_{nom} \Leftrightarrow L_E = \frac{P_{nom} \cdot 60}{2\pi \cdot rpm} \tag{3-33}$$

where L_E is the rolling moment due to the engine defined as previously in (3-24). The further parameter details are given in Aslin 1985.

3.3.2 System variables and control vectors

As shown in Figure 3-3 and Figure 3-6, the XZ plane lift is required to maintain steady flight and a corresponding drag force is incurred. In the XY plane side lift is normally undesirable whilst manoeuvres requiring constant angles of sideslip to be set up are not normally required. It is thus convenient to separate the two planes of motion into longitudinal (XZ plane) and lateral (XY plane) motions according to the asymmetric plane.

The coordinate system in state space for the Machan aircraft for subsequent analysis includes 10 state variables x and 4 control states u as (Aslin, 1985):

$$\begin{gathered} x = [u \quad v \quad w \quad p \quad q \quad r \quad \theta \quad \phi \quad \psi \quad h] \\ u = [\delta_e \quad \delta_t \quad \delta_r \quad \delta_a] \end{gathered} \tag{3-34}$$

which can be partitioned into lateral and longitudinal sets of equations. These state variables are affected by the control vectors formed by the control surface deflections with the change in thrust setting from the power plant as shown in Table 3-3.

Table 3-3 The system variables and control vectors according to different modes

	Longitudinal modes	Lateral modes
States variables	$x_{long} = [u \quad w \quad q \quad \theta \quad h]$	$x_{lat} = [v \quad p \quad r \quad \phi \quad \psi]$
Control variables	$u_{long} = [\delta_e \quad \delta_t]$	$u_{lat} = [\delta_r \quad \delta_a]$

For Machan, the transfer functions $G(s)$ for describing the actuators dynamic (control surfaces δ_e, δ_r and δ_a) are modelled by the first-order linear systems as:

$$G_{\delta_e}(s) = \frac{20}{s+20}, G_{\delta_r}(s) = \frac{10}{s+10}, G_{\delta_a}(s) = \frac{20}{s+20} \tag{3-35}$$

where s is the Laplace variable.

3.3.3 Linearized equations of motion

As presented in Section 3.2, the complete aerodynamic equations developed are very cumbersome to employ directly or use for control system design. To be useful, a most popular strategy is to develop a set of linear equations which preserve the essential dynamics of the nonlinear equations but are analytically tractable. It is inevitable that in determining such a model some gross simplifications must be made since the aircraft is inherently a very difficult system to model accurately. Indeed, some basic assumptions have already been made in

determining the equations above which are not necessarily true in certain flight configurations. The particular linear model which is obtained will largely be determined by the assumptions which are made in its derivation and for this reason some care is necessary when making these assumptions. Ideally, for a complete linear model it may be found that some model parameters change little over the flight envelope or are sufficiently small so as to be negligible.

Conventionally, however, a set of assumptions are first formulated, these allowing certain gross simplifications to be made in deriving a linear time invariant model. This method is perfectly valid for a *small perturbations* situation when, for example, the stability of the aircraft is of interest. The interest in this study is whether or not and how the aircraft returns to its undisturbed equilibrium position after a small perturbation in a control surface position (Sadraey & Colgren, 2005; Ozdemir & Kavsaoglu, 2008).

By assuming that the motion of the aircraft consists of small deviations from a reference condition of steady flight as one of the following:

- steady wings-level flight: $\boldsymbol{\phi}, \dot{\boldsymbol{\phi}}, \dot{\boldsymbol{\theta}}, \dot{\boldsymbol{\psi}} = \mathbf{0}$
- steady turning flight: $\dot{\boldsymbol{\phi}}, \dot{\boldsymbol{\theta}} = \mathbf{0}$
- steady pitch: $\boldsymbol{\phi}, \dot{\boldsymbol{\phi}}, \dot{\boldsymbol{\psi}} = \mathbf{0}$
- steady roll: $\dot{\boldsymbol{\theta}}, \dot{\boldsymbol{\psi}} = \mathbf{0}$

where $\dot{p}, \dot{q}, \dot{r}, \dot{V}, \dot{\alpha} = 0$ and all control surface inputs are zero.

Then a linearized model around the trim condition can be obtained in state space form as:

$$\begin{aligned} \dot{x} &= Ax + Bu \\ y &= Cx \end{aligned} \tag{3-36}$$

The complete state-space equations of the system include both longitudinal and lateral modes with the cross-coupling matrices A_1, A_2 and can be expressed as:

$$\dot{x} = \begin{bmatrix} A_{long} & A_1 \\ A_2 & A_{lat} \end{bmatrix} x + \begin{bmatrix} B_{long} \\ B_{lat} \end{bmatrix} u \tag{3-37}$$

As shown in Table 3-3, the longitudinal model of the Machan UAV involves five state variables including the forward velocity u, the vertical velocity w, the pitch rate q, the pitch angle θ, the height h, and two control variables: the elevator angle δ_e and the engine thrust δ_t, which can be expressed as:

$$\dot{x}_{long} = A_{long} x_{long} + B_{long} u_{long} \tag{3-38}$$

The lateral model of the Machan UAV involves five state variables including the side velocity v, the roll rate p, the yaw rate r, the roll angle ϕ, the yaw angle ψ, and two control variables: the rudder angle δ_r and the aileron angle δ_a, which can be expressed as in state-space equations as:

$$\dot{x}_{lat} = A_{lat}x_{lat} + B_{lat}u_{lat} \tag{3-39}$$

By evaluating the first partial derivatives for each of the state variables and using the nonlinear equations in Section 3.2, the state matrices A_{long}, A_{lat} and B_{long}, B_{lat} can be formed into the appropriate system. Then the system may be locally linearized about a specifically trimmed flight condition. For the linear Machan system, the state dynamics of both the longitudinal and lateral modes are constant in a trim condition. It is assumed that all the states are measurable (a reasonable assumption for a modern aircraft flight control system) and thus the matrix C is always an identity matrix.

It should to be noticed that, as shown in (3-37), there are certain state space elements providing the functional cross-coupling matrices A_1, A_2 between longitudinal and lateral motions of the aircraft model. Although the cross-coupling elements between lateral and longitudinal motions are usually neglected for *small perturbations* about trim flight conditions during linearization at equilibrium point, for large incidence flight or manoeuvring motions, some of the cross-coupling dynamics terms become significant. It is then a task of the flight control system design to provide good de-coupling (McRuer, Graham & Ashkenas, 1972).

In Chapter 4 it will be shown that by using a procedure known as feedback linearization all the nonlinearity of the aircraft is taken into account implicitly proving a suitable structure for control design according to three important subsystems centred on three body angles ψ, θ, ϕ, thus obviating the need for the linear lateral-longitudinal state space interactions in the flight control system design.

3.4 Fault Models

The goal of this section is to describe the types of failures that could occur on an aircraft during simulation study, which may be relatively limited when compared to a general aircraft.

3.4.1 Aircraft failures

As discussed in Section 2.1.2, aircraft failures can be grouped into three categories: sensor, actuator and structure failures, or some combination of the three. Table 3-4 describes the general failures that could occur with classification into the three categories (Stengel, 2005).

It should to be noticed that large aircraft, for example large commercial jets in particular, have triply redundant sensor systems and so the likelihood of a fault is extremely small (Stengel, 2005; Shearer & Cesnik, 2007). A sensor failure by itself does not necessarily pose a threat to a large aircraft, as there is always a pilot on board with his own set of backup sensors. Sensor failures can become significant in autonomous craft. However, as many authors have shown (Shore & Bodson, 2005), any single failed sensor can be recreated from the remaining working ones, assuming the aerodynamics of the craft have not changed.

On the contrary, actuator failures are critical as they change the aircraft structure of aircrafts that the controller was designed for. Structural or aerodynamic failures caused by physical damage also affect the equations of motion. Actually, the structure of the model remains the same during such a failure, as the equations of motion are completely general. However, the constants governing the behaviour may change a lot. Thus the controller design for achieving tolerant or reconfigurable performance from actuator and structural failures is always getting more attention than the sensor one.

Table 3-4 Aircraft failure modes

Sensor	*Actuator*	*Structural*	Failure	Effect
√			Sensor loss	Minor if it is the only failure
	√		Partial hydraulics loss	Maximum rate decrease on several control surfaces
	√		Full hydraulics	One or more control surfaces become stuck at last position for hydraulic driven aircraft, or oat on light aircraft
	√		Control loss on one or more actuators due to internal fault	One or more control surfaces become stuck at last position
	√	√	Loss of part/all of control surface	Effectiveness of control surface is reduced, but rate is not; minor change in the aerodynamics
	√	√	Loss of engine	Large change in possible operating region; significant change in the aerodynamics
		√	Damage to aircraft surface	Possible change in operating region; Significant change in aerodynamics

3.4.2 Simulation model of actuator and sensor faults

In the mathematical model of the control system, the symbol u is used to present the control input to the actuator. As described in Section 2.1.3, the four typical types of **actuator faults** are chosen in the simulation modelled as:

- Lock-in place

$$\begin{gathered} u_{iout}(t) = a_i \\ u_{imin} \le u_{iout}(t) \le u_{imax} \\ u_{imin} \le a_i \le u_{imax} \end{gathered} \tag{3-40}$$

- Floating

$$u_{iout}(t) = 0 \tag{3-41}$$

- Hardover

$$u_{iout}(t) = u_{imin} \text{ or } u_{iout}(t) = u_{imax} \tag{3-42}$$

- Loss of effectiveness

$$u_{iout}(t) = \beta_i u_{iin}(t) \tag{3-43}$$

where a_i is an optional constant, u_{iout} is the real output of the i^{th} actuator (when fault occur), u_{iin} is the output of the actuator during normally work, u_{imin} and u_{imax} are the minimum and maximum rate limit of the actuator, respectively, β_i is effective parameter: $0 \le \beta_i \le 1$. Note that $\beta_i = 0$ means the i^{th} actuator is locked in the place; when $\beta_i = 1$, means the i^{th} actuator normally works.

Also according to Section 2.1.3, the three types of sensor faults are chosen in the simulation modelled as:

- Bias

$$y_{iout}(t) = y_{iin}(t) + \Delta_i \tag{3-44}$$

- Frozen measurement

$$y_{iout}(t) = a_i \tag{3-45}$$

- Calibration error

$$y_{iout}(t) = \beta_i y_{iin}(t) \tag{3-46}$$

where: Δ_i and a_i are optional constants, u_{iout} is the real output of the i^{th} actuator when a fault occurs, y_{iout} is the real output of the i^{th} sensor when a fault occurs, y_{iin} is the output of the sensor during normal work and β_i an effective parameter caused by damage, $0 \leq \beta_i \leq 1$.

3.4.3 Dryden spectrum model of wind turbulence

Despite the parametric faults corresponding to aircraft damage mentioned above, the effects of disturbance acting on the aircraft should also be taken into account. Naturally the disturbance is unpredictable so the filtering of disturbance signals will be necessary. Wind turbulence is considered as the principal component of disturbance on the aircraft, various wind turbulence is normally considered as kind of external disturbance.

For this study, the well-known Dryden Spectrum (Etkin & Reid, 1996) procedure is used to model the effect of lift disturbances acting on a body passing through an air flow.

As a simple representation the wind turbulence is considered as the output of a band-limited filter with uniform random noise signal acting as input. It is assumed that the wind turbulence has the main effect to the normal velocity and hence its effect can be modelled by adding a band-limited disturbance signal to the normal velocity w_B of the aircraft body frame.

The transfer function denoting the wind disturbance of the turbulence filter model $G_d(s)$ is chosen to have the following structure as:

$$G_d(s) = \frac{5s}{(s+0.1)(s+5)} \tag{3-47}$$

3.5 Comparison of Linear & Nonlinear Machan System

To get an overall idea of the differences between the nonlinear system and the linear one, the characteristics of the Machan UAV system are analyzed and simulated in this section.

It is known that eigenvalues of the state matrix A in (3-36) play an important role in directing the open-loop response of the system, which is determined by inspection and comparison with the standard description of a linear system in state space form. The stability of an open-loop system is tested by the sign of the real parts of the eigenvalues of the state matrix A, which are usually complex numbers and it is known that negative real parts indicate the system's stability.

Since the characteristic equation for the open-loop system is given as:

$$\det(sI - A) = 0 \tag{3-48}$$

where s is the Laplace variable. The eigenvalues λ of the state matrixes in system (3-38) and (3-39) are calculated as:

$$\begin{cases} (\lambda_{long})_1 = 0 \\ (\lambda_{long})_{2,3} = -1.8110 \pm 3.4692i \\ (\lambda_{long})_{4,5} = -0.0596 \pm 0.6755i \\ (\lambda_{long})_6 = -2.1677 \end{cases} \tag{3-49}$$

$$\begin{cases} (\lambda_{lat})_1 = 0 \\ (\lambda_{lat})_2 = -8.5573 \\ (\lambda_{lat})_3 = 0.1190 \\ (\lambda_{lat})_{4,5} = -0.5013 \pm 3.5067i \end{cases} \tag{3-50}$$

(3-49) and (3-50) show that the longitudinal motion is stable for all λ with negative real part while the lateral motion dynamics are initially open-loop unstable since one of the eigenvalues has a positive real part, which is demonstrated in the open-loop simulation.

The ideal design objective is to achieve a control system with good performance for the typical linear system that could be satisfactorily applied on the fully nonlinear aircraft model. Besides, the validity of the trim setting linearization and the robustness of the control system design, means the insensitivity to parameter changes and disturbances in the time-varying or nonlinear model, is highly required. After making sure that both lateral and longitudinal models are stable, an integration model is then created by combining them together. The integration of both models is important because the lateral and longitudinal motions usually rely on each other to achieve balanced flight and various aircraft flight actions such as climbs, descents, turns, etc.

By assuming all the states are measurable, a controller based on the LPV strategy accomplished by Lejun Chen (Chen & Patton, 2011) in the Control Lab of University of Hull. As the control states are: $[\delta_e \quad \delta_t \quad \delta_r \quad \delta_a] = [0.8 \quad 0.11 \quad 0 \quad 0]$, the system longitudinal responses with this LPV controller are shown in Figure 3-9.

Note that the closed-loop responses for the linear representation of the Machan system are derived from the simulation data using the time-varying dynamics according to longitudinal and lateral motion, which are more realistic than the completely linearized system. However, Figure 3-9 shows the LPV controller designed for the time-varying dynamics and validated against the original nonlinear system, which has slowly developing unstable longitudinal dynamics. Moreover, this strategy leads to a constant feedback control matrix, which may not be suitable for the nonlinear Machan system. In fact, the simulation cannot accommodate

lateral system disturbances (e.g. non-zero initial angles or angular rates). For this reason only the longitudinal responses are shown below.

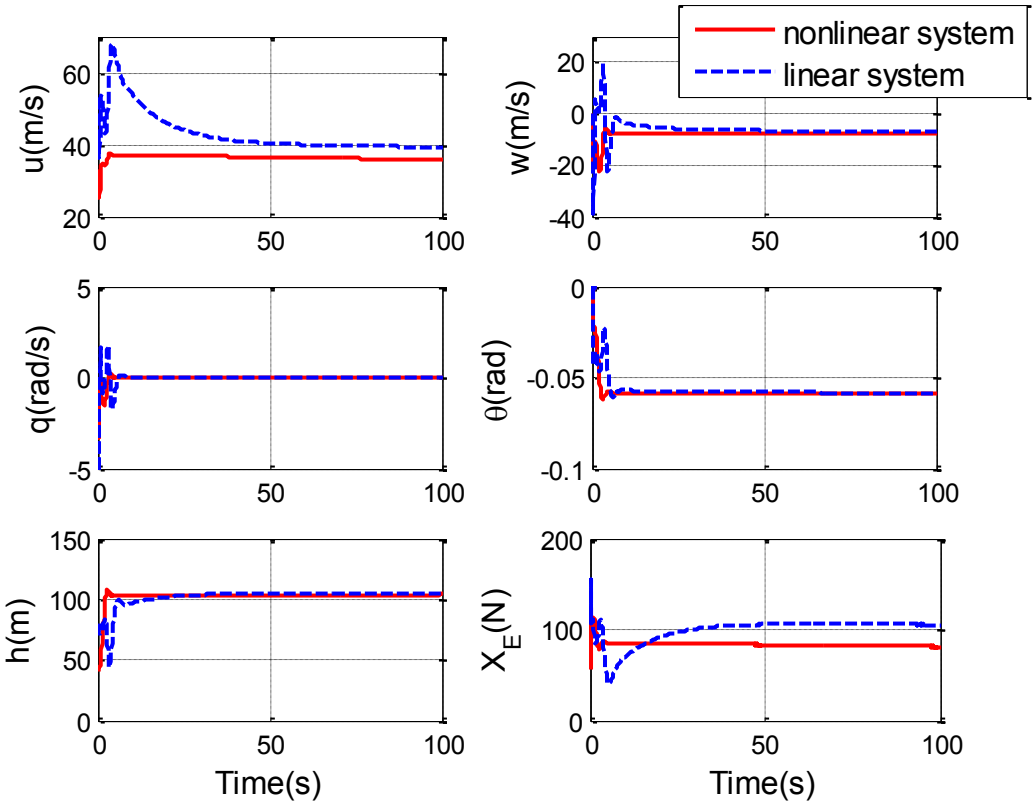

Figure 3-9 Comparison of close-loop longitudinal responses for nonlinear and linear Machan using LPV controller

Figure 3-9 demonstrate that the linearized system analysis is generally restricted to small perturbations about the specified trim condition which may not provide satisfactory performance over certain flight circumstances for this nonlinear system. Thus, the study of a strategy for nonlinear FTFC has significant importance for this nonlinear flight system.

3.6 Conclusion

This chapter deals with the development of the equations of motion of a nonlinear aircraft system with a special focus on the Machan UAV aircraft which is used in this thesis. The fundamental definitions required for flight control are given, involving control surfaces, the motions involved, the forces and moments acting on the aircraft. Additionally, the chapter introduces several important aircraft reference frames required for further understanding of the aircraft dynamics. The main three primary control surfaces, including aileron, rudder and elevator, are described as these are of relevance for the Machan study. The main aerodynamic

forces and moments have been explained and some necessary mathematical equations have also been derived and briefly discussed. This chapter has also given the open-loop lateral & longitudinal eigenvalues analysis of the aircraft system and the close-loop longitudinal states simulation for comparing and analyzing the difference between the linearized and nonlinear system.

The nonlinear Machan model described in this chapter provides a basis for the simulation study of the aircraft to be investigated in Chapters 5, 6, 7. Chapter 4 presents the main concepts of the feedback linearization approach for a nonlinear system, focusing towards the end of the chapter on the application to flight control.

Chapter 4 Nonlinear System Control based on Differential Geometry

Among various control strategies and applications results to achieve design and implementation issues for nonlinear control systems, feedback linearizing controllers are studied and developed in the past three decades, resulting in a variety of nonlinear controller design techniques based on differential geometry (Brockett, Millman & Sussmann, 1983; Fliess, 1990; Byrnes & Isidori, 2000; Agrachev & Sachkov, 2004). Many of these studies focus on approaches to robust control and adaptive control. An extension of this approach has been considered for the development of base-line control structures for use in FTC (Napolitano, An & Seanor, 2000; Calise, Hovakimyan & Idan, 2001; Ducard, 2009; Lombaerts, Chu, Mulder & Stroosma, 2010).

According to the problem analyzed in Chapter 3, the aircraft model and thus its flight control system are formulated as collections of input-parameterized differential equations. These ordinary differential equations are assumed to be described on smooth manifolds as required by geometric control theory. As a background to the application of feedback linearization theory to nonlinear flight control given in Chapters 5, 6, 7 & 8, the fundamental concepts involving linearizing transformations and geometric control are introduced in this chapter.

4.1 Introduction

The control systems described by linear, time-invariant dynamics can now be developed using very powerful design tools involving well known computer-aided design and the mathematical tools exist to make use of the latest theoretical developments in linear system analysis and design. In contrast, the development of methodologies for nonlinear control system design has lagged behind their linear counterparts. As most practical systems behave in a nonlinear fashion, there exists a strong incentive to carry out further investigations into the use of nonlinear controller design methods.

The most popular approach to control a nonlinear system is to linearize the nonlinear dynamics about an operating point and apply proven linear control design approaches. The design is then verified and validated by exhaustive computer simulations of the response of

the combination of the nonlinear dynamics with the linear controller over a variety of initial conditions and disturbances. Since linearized systems are only valid for small perturbations around an assumed operating point in state space this approach may only be practical for only a small range of operating conditions. Indeed, there are instances where the nonlinear terms in a state space system cannot be ignored. In high performance applications, a wide range of operating conditions are typically encountered and linear control design methods based on local approximation may be inadequate, and in the worst case fail. These types of conditions may be encountered for example in a 6DoF underwater vehicle control, in satellite attitude control problems, high incidence aircraft control, and magnetic field applications (Slotine & Li, 1991; Henson, 1992; Henson & Seborg, 1997; Agrachev & Sachkov, 2004).

Another case when linearized analysis is inadequate is when discontinuous nonlinearities are present. Examples are saturating actuators, on-off actuators such as reaction or thruster control systems for spacecraft, unidirectional thrusters where the thrust can only be applied in one direction, backlash in geared systems caused by gaps, dry friction where the friction force is dependent on the velocity direction etc. For most of these application systems linearized analysis cannot be applied due to the discontinuous nature of the dynamics or thruster systems, etc. The discontinuous nonlinearities cannot be approximated using linear theory (Fliess, Lévine, Martin & Rouchon, 1995; Henson & Seborg, 1997).

On the other hand continuous (i.e. smooth) nonlinearities, usually occur when a system is described in a non-inertial frame. The rotational notion of a rigid body is commonly expressed in terms of the equations of motion relative to a rotational body frame, as introduced in Section 3.2. The equations of motion within the body-fixed coordinates result in the *Euler Equations* which have quadratic dependence on velocity components. Other examples of non-inertial frame induced nonlinearities are the centrifugal and coriolis effects present in rotating systems such as robotic manipulators, planar linkage mechanisms like four-bar, planetary gear-trains etc. Such nonlinearities may be referred to as kinematic nonlinearities since they originate or are induced by the kinematical structure of the system (Henson & Seborg, 1997; Vincent & Grantham, 1999).

Nonlinearities can be either static or dynamic in terms of their input-output relations, for example as follows including their typical range or type of input signal dependence (Henson & Seborg, 1997; Sastry, 1999):

- Saturation (with large signals)
- Dead space or backlash (affecting small signals)
- Power-law dependence (e.g., damping force via velocity)
- Frequency-dependent dampers (linear at low frequencies, nonlinear at high frequencies)

The characteristic curves for the first three (static) nonlinearities above are as in Figure 4-1.

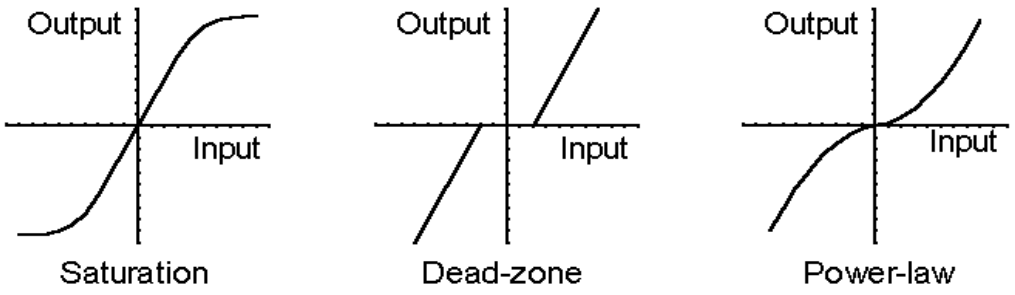

Figure 4-1 Characteristics curves for various nonlinearities

A further complication arises when the nonlinear system to be controller is under-actuated, which means there are fewer actuators than degrees of motion freedom. A common occurrence is when a fully actuated system experiences a malfunction in one or more actuators. For this type of system a general control design methodology is more challenging to accomplish since most established nonlinear control design methods require square or fully actuated systems, which means the number of control actuators equals the number of system degrees of freedom. Examples of square design methodologies are SMC and Lyapunov based adaptive control (Henson & Seborg, 1997; Sastry, 1999).

The Machan UAV simulation results in Chapter 3 illustrate that ignored nonlinear properties can severely affect system performance. In such cases the designed linear systems-based flight controller may not achieve the desired performance when applied on the truly nonlinear aircraft system. Moreover, when considering system FTC properties the nonlinearities not only relate to model properties, but also to various faults (e.g. actuator or sensor faults) and disturbances (e.g. turbulence) acting on the system. Thus for better preparation for FDI/FDD or FTC system design, the nonlinearity derived from the aerodynamics should be considered for verifying the validity of the flight control system. The general approach applicable to continuous nonlinear system control problems is to use transformation techniques based on differential geometry that simplify the nonlinear equations such that existing results in linear control theory can then be applied.

4.1.1 Properties of linear time-invariant and nonlinear system

In this section, a brief overview of the main properties of linear and nonlinear systems is presented. The objective is to highlight and contrast the complicated behaviour that nonlinear systems can exhibit as opposed to the responses of linear systems (LaSalle, 1968; Bedrossian, 1991; Byrnes, Isidori & Willems, 1991; Isidori, 1995).

The linear time-invariant dynamics are defined in the state-space form as:

$$\dot{x} = Ax + Bu \tag{4-1}$$

and the nonlinear time-variant dynamics are in the non-affine form as:

$$\dot{x} = f(x, u) \tag{4-2}$$

For linear systems, the main features to be considered are equilibrium points, stability, and free or forced response behaviour, summarized as follows.

- **Equilibrium**: for the unforced system (i.e. $u = 0$) the equilibrium point is unique if the state matrix A is nonsingular. Then $x_e = 0$ is the only equilibrium point. If A is singular there exists an infinite number of equilibrium points.
- **Stability**: stability about the equilibrium point is solely defined by the spectrum or eigenvalues of A. The system is stable if all eigenvalues of A have negative real parts. The definition of stability is independent of the initial conditions, forcing functions, and the concepts of local or global behaviour.
- **Forced Response**: linear systems satisfy the property of superposition and homogeneity as:

$$x\big(u_1(t) + u_2(t)\big) = x\big(u_1(t)\big) + x\big(u_2(t)\big) \tag{4-3}$$

$$x\big(au(t)\big) = ax\big(u(t)\big) \tag{4-4}$$

In contrast, for nonlinear systems, no general statements like the above can be made. Their behaviour is much more complicated and cannot be captured by a few simple characteristics.

- **Equilibrium**: for the unforced system (i.e. $u = 0$) there may exist none, one, or multiple equilibrium points.
- **Stability**: stability about an equilibrium point is dependent on initial conditions and forcing functions as well as having a local or global property. Furthermore, nonlinear systems may exhibit limit cycles which are closed, unique trajectories or orbits or

bifurcations between equilibria (e.g. chaos). These equilibrium manifolds may be attractive or repulsive and may even change their characteristics dynamically.

- **Forced Response**: Nonlinear systems do not satisfy the principles of superposition and homogeneity. The responses are not unique, producing different trajectories according to initial conditions and may even exhibit chaotic or oscillatory behaviour without being forced.

In conclusion, nonlinear systems exhibit behavioural complexity which makes their analysis a very difficult task. As a consequence, each system is usually studied separately as there are very few properties that are shared by all nonlinear systems and their response is difficult to analyze or predict. This situation has forced the development of particular nonlinear control design techniques that are applicable to certain systems (Isidori, 1995).

4.1.2 Nonlinear control synthesis methods

In this section, a brief summary of available and popular nonlinear control design methods is presented. All of the nonlinear control design approaches can essentially be thought of providing in one form or another way to generate the control action as a function of the system states. This mapping may be linear or nonlinear, static or dynamic, according to the following classification (Charlet, Lévine & Marino, 1989; Isidori, 1995).

(1) Analysis techniques for nonlinear systems

***Describing function method*:** This approach is an approximate procedure for analysis of certain nonlinear control problems. It is based on quasi-linearization, which is the approximation of the nonlinear system under investigation by a Linear Time Invariant (LTI) system transfer function that depends on the amplitude and frequency of an assumed sinusoidal test input waveform. By definition, a transfer function of a true LTI system cannot depend on the amplitude and frequency of this input test function. Thus, this dependence on amplitude and frequency generates a family of linear systems that can be combined in an attempt to capture salient features of the nonlinear system behaviour. This approach is mainly suitable for systems with simple nonlinear structures and that have mainly oscillatory (limit cycle) behaviour (Isidori, 1995).

Phase plane method: This method refers to graphically determining the existence of limit cycle or other solution features of a second order nonlinear differential equation. The solutions to the differential equation form a manifold of system behaviour around a known

equilibrium. The approach is limited to second order systems so that the trajectories can be plotted or examined as a two-dimensional vector field. Higher order systems can be de-coupled (even if only approximately) into several second order and first order systems, thus allowing a series of phase-plane analysis steps to be made on each second order subsystem (White & Zinober, 1990).

Central manifold theorem: In mathematics, if a linearized dynamical system has eigenvalues whose real part is zero, then these give rise to the so-called *central manifold* as a second order subsystem in n dimensional nonlinear space. The behaviour on the central manifold is generally only determined by local linearization (i.e. at each solution point) and is thus more difficult to study. Central manifolds play an important role in bifurcation theory because interesting behaviour takes place on the central manifold. As the stability of the equilibrium correlates with the stability of its manifolds, the existence of a central manifold brings up the question about the dynamics on the central manifold, relating to existence or otherwise of system bifurcations from one form of behaviour to another (Guckenheimer & Holmes, 1983).

Small-gain theorem: For nonlinear systems, the formalism of so-called "input-output stability" is an important and efficient approach in studying the stability of interconnected systems since the gain of a system directly relates to how the norm of a signal increases or decreases as it passes through the system. The small-gain theorem, which gives a sufficient condition for finite-gain stability of the feedback connection, can be seen as a generalization of the *Nyquist criterion* to nonlinear time-varying MIMO systems (Isidori, 1995).

(2) Controller design based on linear methods:

Linear control: This is an approach that the nonlinear system is linearized about an equilibrium point, and a linear controller using a variety of techniques is designed. Using recently developed synthesis tools, robustly stable compensators can be designed to account for norm bounded model uncertainty. However, such designs are limited to the operating region surrounding a known equilibrium (e.g. trim point) where the linear approximation is valid (Isidori, 1995).

Gain-scheduled linear control: This approach attempts to expand the region of linear control operation by linearizing the dynamics about different operating points and designing linear controllers for each point. In between operating points, the control action or the gains are interpolated or scheduled. Some of the drawbacks of this approach are that there is no

stability guarantee during transition between operating points, and it is computationally intensive if many operating points are considered as well as when the dimension of the nonlinear system is high. Despite these drawbacks this is the most frequently used control strategy for real flight control application (Isidori, 1995).

(3) Controller design based on Lyapunov stability criteria:

Back-stepping: This is a technique developed for designing stabilizing controls for a special class of nonlinear dynamical systems. These systems are built from subsystems that radiate out from an irreducible subsystem that can be stabilized using some other method. The approach results in a recursive structure so that the designer can start the design process at a known-stable system and "back out" new controllers that progressively stabilize the remaining "outer" subsystems. The process terminates when the final "external control" is reached. Hence, this process is known as back-stepping (Lee & Kim, 2001).

Sliding Mode Control (SMC): This is an example of a robust nonlinear tracking control design method applied to systems that can be put in a controllable canonical form. This is a powerful method that provides robust stability and robust performance to parametric modelling uncertainty and unmodelled dynamics that satisfy a so-called "matching" condition. The approach is to define a so called "sliding surface" in state space that represents the tracking error. The control action is then chosen such that the system remains on the "sliding surface" in the presence of modelling uncertainty. The main feature is that the undesirable nonlinear dynamics are robustly cancelled and desirable linear dynamics inserted (Zinober, 1990, 1994; Chang, 2009; Alwi, Edwards & Hamayun, 2011).

Adaptive control: This is a control methodology applicable to linear or nonlinear systems with unknown or uncertain parameters. One approach known as *indirect active control*, is to estimate on-line the unknown system parameters using measurements. In another approach the controller parameters are adjusted on-line to achieve a desired closed-loop behaviour (see for example in Chapters 5, 6 & 8). Note that the uncertain parameters are treated as time-varying. This may cause degradation in performance if the actual parameters are state dependent. The crucial problem of such an approach is the stability issue in the presence of disturbances, measurement noise and unmodelled dynamics, the latest research is mainly focused on handling this subject (Bodson & Groszkiewicz, 1997; Ioannou & Sun, 2012).

(4) Compensator design using transformation methods:

Input-Output feedback linearization: This approach utilizes state and control transformations coupled with feedback to realize an equivalent linear representation of the nonlinear system from the inputs to the outputs. The main concept in this and the following methods is the use of transformations in the state and control variables to alter the nonlinear dynamics to a nearly linear form such that the remaining nonlinearities can be cancelled by feedback. The state and control transformations must be constructed in such a manner that the remaining terms appear in the path of the control action in order to be cancelled. Once the linear input-output relationship is obtained, linear theory can be used to design a controller. The drawbacks of this approach are the sensitivity to modelling uncertainty and the requirement of full state measurement and can only be applied to certain nonlinear systems (Byrnes, Priscoli & Isidori, 1997).

Input-State or exact feedback linearization: This is a similar approach to the *Input-Output linearization* except that the linear equivalence is established between the inputs and the complete state. The dimension of the linear equivalent system is identical to the nonlinear one, whereas for the Input-Output approach it is less than or equal to the number of states. The existence conditions for this approach are fairly restrictive, and evaluating them is computationally intensive requiring symbolic mathematics software. Even when the existence conditions are satisfied, finding a solution requires solving a nontrivial set of partial differential equations. This approach also requires full state information for real implementation (Bullo & Lewis, 2004).

Approximate feedback linearization: This approach attempts to construct a linear approximation about an equilibrium point that is accurate to second or higher order as opposed to all orders for *Input-State linearization*. The existence conditions for this approach are similar to those for Input-State linearization, but are much less stringent. The computation of the requisite transformations requires a solution to a set of algebraic equations instead of solving partial differential equations. However, it does require full state information and is sensitive to modelling errors (Byrnes & Isidori, 2000).

It should be noted that most of the above approaches based on feedback linearization require the system to be fully actuated. For the MIMO nonlinear aircraft system, one method dealing with this situation is carefully choosing system states, referring to their performance characteristics, as new states for multiple control loops (see the cascade feedback control scheme for the Machan UAV given in Section 4.4). The work on feedback linearization for FTFC described in Chapters 5, 6, 7 & 8 is based on this approach.

4.2 Geometric Control Theory

The central idea of feedback linearization is to algebraically transform nonlinear system dynamics to an equivalent controllable linear system, or partly linear one. This is accomplished via a nonlinear state and control transformation. Subsequently, linear control techniques or modern advanced computer intelligence can be easily applied to the equivalent linear system for designing appropriate control and compensation (Slotine & Li, 1991; Henson & Seborg, 1997).

Consider a MIMO nonlinear system in continuous-time with affine expression as:

$$\begin{aligned} \dot{x} &= f(x) + g(x)u \\ y &= h(x) \end{aligned} \tag{4-5}$$

where state vector $x \in \mathcal{R}^n$, control input vector $u \in \mathcal{R}^m$; controlled output vector $y \in \mathcal{R}^m$; nonlinear functions vector $f(x) \in \mathcal{R}^n$; nonlinear functions matrix $g(x) \in \mathcal{R}^{n \times m}$; and nonlinear functions vector $h(x) \in \mathcal{R}^m$.

Consider the *Jacobian linearization* of the nonlinear model (4-5) about an equilibrium point (x_e, y_e, u_e) as:

$$\begin{aligned} \dot{x} &= \left[\frac{\partial f(x_e)}{\partial x} + \frac{\partial g(x_e)}{\partial x} u_e\right](x - x_e) + g(x_e)(u - u_e) \\ y - y_e &= \frac{\partial h(x_e)}{\partial x}(x - x_e) \end{aligned} \tag{4-6}$$

By using partial derivatives the Jacobian model can be written as a general linear state-space system (corresponding to the various equilibrium state vectors) as:

$$\begin{aligned} \dot{x} &= Ax + Bu \\ y &= Cx \end{aligned} \tag{4-7}$$

where the dimensions of (4-7) are as for the original nonlinear system of (4-5) with compatible dimensions for the matrices A, B and C. It is important to note that the Jacobian model is an exact representation of the nonlinear model only at the point (x_e, y_e, u_e). As a result, a control strategy based on a linearized model may yield unsatisfactory performance and robustness at other operating points.

Thus another nonlinear control technique to produce a linear model that is an exact representation of the original nonlinear model over a large set of operating conditions is developed, typically called feedback linearization, which as a general approach is based on two operations: (i) nonlinear change of coordinates; and (ii) nonlinear state feedback.

Thus, feedback linearization is a way of transforming the original nonlinear system structure into an equivalent model or models of simpler form. This strategy is completely different from conventional Jacobian linearization, because feedback linearization is achieved by exact state transformation and feedback, rather than by linear approximations of the dynamics.

4.2.1 Feedback equivalence

Before proceeding to the subject of feedback linearization, the notion of *feedback equivalence* is introduced (Charlet, Lévine & Marino, 1989; Byrnes, Isidori & Willems, 1991). Feedback equivalence is intrinsically connected with linearization of nonlinear systems in that the concept is central to feedback linearization as an approach to the generation of solutions to the nonlinear system via the solution to an equivalent linear system. The most general application of feedback equivalence involves nonlinear transformations of the state and control variables (Krener, 1984; Marino & Tomei, 1993; Khalil, 1996). In the following firstly feedback equivalence for linear systems is reviewed, and then extended to nonlinear systems.

For a linear system in (4-7), it is known that any controllable linear system can be transformed into a controller canonical form via a linear coordinate change of the system state. Further, if a linear coordinate change in the input variable is coupled with linear state feedback, any controllable linear system can be transformed to a special form where all poles of the transformed system are at the origin (Henson & Seborg, 1997; Sastry, 1999). Such a representation is usually referred to as a *Brunovsky Canonical form* (Brunovský, 1970; Hunt, Su & Meyer, 1983) where the state and input transformations and feedback are defined as:

$$\begin{aligned} z &= T \cdot x \\ \nu &= \alpha \cdot x + \beta \cdot u \end{aligned} \tag{4-8}$$

where new states vector $z \in \mathcal{R}^n$, and new control vector $\nu \in \mathcal{R}^n$, nonsingular constant matrix $T \in \mathcal{R}^{n \times n}$, row constant vector $\alpha \in \mathcal{R}^n$ and β is a nonzero real constant.

Consider a single input, time-invariant controllable linear system as (Bedrossian, 1991):

$$\dot{x} = Ax + Bu \tag{4-9}$$

by using the transformation and feedback, this linear system can be transformed to:

$$\dot{z} = \begin{bmatrix} 0 & 1 & 0 & 0 & \dots & 0 & 0 \\ 0 & 0 & 1 & 0 & \dots & 0 & 0 \\ \vdots & \vdots & \vdots & \vdots & \vdots & \vdots & \vdots \\ 0 & 0 & 0 & 0 & \dots & 0 & 1 \\ 0 & 0 & 0 & 0 & \dots & 0 & 0 \end{bmatrix} z + \begin{bmatrix} 0 \\ 0 \\ \vdots \\ 0 \\ 1 \end{bmatrix} \nu = A_c z + B_c \nu \tag{4-10}$$

where the matrices A_c and B_c in (4-10) are in the *Brunovsky Canonical form*. Note that the characteristic polynomial of A_c is $det(sI - A_c) = s^n$, i.e. all the poles of the transformed system are at the origin and there are no system zeros. This resulting decoupled set of integrators is by no means restricted to single input linear systems.

This notion of feedback equivalence can naturally be extended to nonlinear systems. The objective is to characterize all nonlinear systems that are *feedback equivalent* to a controllable linear system (Isidori, 1995).

Now consider the following nonlinear system as introduced in (4-5):

$$\dot{x} = f(x) + g(x)u \tag{4-11}$$

Then, (4-11) is feedback equivalent to a controllable linear system if there exists a region $\Omega \in \mathcal{R}^n$ containing the origin, state and input transformations and the feedback defined as:

$$\begin{aligned} z &= T(x) \\ v &= \alpha(x) + \beta(x)u \end{aligned} \tag{4-12}$$

where $T(x)$ is a diffeomorphism and $\beta(x) \neq 0$ for $x \in \Omega$, such that the transformed coordinates satisfy (4-10). If such a transformation exists, (4-11) is said to be feedback linearizable. In practice it is required for $T(x)$ to be a differentiable mapping with nonsingular Jacobian matrix (Bedrossian, 1991).

The transformation $T(x)$ can be thought of as a nonlinear coordinate transformation where the remaining nonlinearities after the transformation are shifted such that they only appear in the derivative of the last transformed variable. Note that the nonlinearities remaining after the state transformation have been placed in the path of the control action and thus can be cancelled. Another property of the state transformation is that the control variable does not appear except in the derivative of the last transformed variable. Once this has been accomplished, the original control action can cancel these nonlinearities and inject the transformed control variable for compensator design in the transformed linear domain.

4.2.2 Preliminary mathematical concepts

Since the later operations of feedback linearization in Chapters 5, 6, 7 and 8 are based on differential geometric control theory, a few preliminary mathematical concepts of the differential geometric language will be introduced firstly for better illustration of the specific linearization process for nonlinear system (Sussmann, 1983; Bedrossian, 1991).

In the following, various operations on scalar (e.g. $h(x)\colon \mathcal{R}^n \to \mathcal{R}$) and vector functions (e.g. $f(x)\colon \mathcal{R}^n \to \mathcal{R}^n$) will be defined. Such functions are also referred to as *fields* in that a scalar or vector assignment (or map) has continuous partial derivatives of arbitrary higher order (Bedrossian, 1991; Jakubczyk, 2001).

(1) Lie derivative

For a smooth scalar field $h(x)\colon \mathcal{R}^n \to \mathcal{R}$ and a smooth vector field $f(x)\colon \mathcal{R}^n \to \mathcal{R}^n$, the Lie derivative of h with respect to f, denote by $L_f h$, is a new scalar field defined by:

$$L_f h = \nabla h(x)\, f(x) = \sum_{i=1}^{n} \frac{\partial h(x)}{\partial x_i}\, f_i(x) \tag{4-13}$$

The notation $\nabla h(x)$ indicates the gradient of $h(x)$ with respect to x. It is evident that the Lie derivative is just the directional derivative of the scalar function $h(x)$ in the direction $f(x)$.

Repeated Lie derivatives are defined recursively by (Bedrossian, 1991):

$$\begin{aligned} L_f^0 h &= h \\ L_f^\gamma h &= L_f\left(L_f^{\gamma-1} h\right) \end{aligned} \tag{4-14}$$

(2) Relative degree

For two vector fields $f(x)\colon \mathcal{R}^n \to \mathcal{R}^n$ and $g(x)\colon \mathcal{R}^n \to \mathcal{R}^n$, the concept of relative degree γ_i is with respect to the output y_i as an integer since:

$$L_{g_j} L_f^k h_i = 0 \tag{4-15}$$

for all $1 \le j \le m$, for all $k < \gamma_i - 1$, for all $1 \le i \le m$, for all x in the region $\Omega \in \mathcal{R}^n$, and

$$L_{g_j} L_f^{\gamma_i - 1} h_i \neq 0 \tag{4-16}$$

for the Lie derivative of h_i with respect to f along f, the relative degree γ_i is exactly the number of times one has to differentiate the i^{th} output y_i, in order to have at least one component of the input vector u appear explicitly (Jakubczyk, 2001).

(3) Lie bracket

For a large class of problems a control system can be represented by dynamic systems as a family of vector fields. The qualitative properties of the control system depend on the properties of the dynamic systems in terms of vector fields as well as the interactions between different vector fields. This interaction is defined in terms of the so-called Lie bracket. This is an operator on two or more vector fields, for example for two vector fields $f(x)\colon \mathcal{R}^n \to \mathcal{R}^n$

and $g(x)$: $\mathcal{R}^n \rightarrow \mathcal{R}^n$, the Lie bracket of f and g, denoted by $[f, g]$, defines a new vector field according to:

$$[f, g] = \frac{\partial g(x)}{\partial x} f - \frac{\partial f(x)}{\partial x} g \tag{4-17}$$

The Lie bracket satisfies the skew-symmetric property and Jacobi identity as:

$$[f, g] = -[g, f] \tag{4-18}$$

$$L_{ad_f g} h = L_f L_g h - L_g L_f h \tag{4-19}$$

The bracket operations are also defined in terms of the notation $ad_f g = [f, g]$ as:

$$\begin{aligned} ad_f^0 g &= g \\ ad_f^i g &= \left[f, ad_f^{i-1} g\right] \end{aligned} \tag{4-20}$$

A geometric interpretation of the Lie bracket is presented in Section 4.2.3 (Jakubczyk, 2001).

4.2.3 Geometrical interpretation of the Lie Bracket

In this Section a geometrical interpretation of the Lie bracket is presented with the purpose of providing an intuitive understanding. In the context of differential equations, it will be shown that the Lie bracket represents a direction in state space that defines the trajectory through which the solution space can move. To give a geometrical interpretation of the Lie bracket, consider the following two input dynamical system (Bedrossian, 1991):

$$\dot{x} = u_1(t) f_1(x) + u_2(t) f_2(x) \tag{4-21}$$

It is evident that starting from any point $x(0) = x_0$, the system can move in any direction spanned by the continuous differentiable vector fields $f_1(x)$ and $f_2(x)$, denoted $F(x_0) = span\{f_1(x_0), f_2(x_0)\}$. For example, suppose that starting from $x(0)$ the system moves along $f_1(x)$ for t units of time, then along $f_2(x)$ for t units, then along $-f_1(x)$ for t units of time and finally along $-f_2(x)$ for t units of time. This path is shown in Figure 4-2.

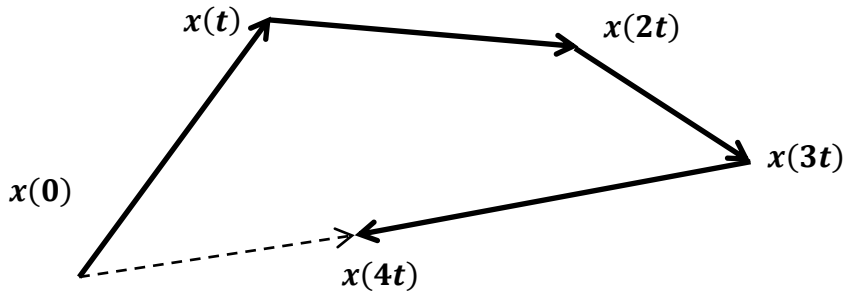

Figure 4-2 Solution trajectory for Lie bracket interpretation

To compute the terminal point of this trajectory, first set $u_1 = 1, u_2 = 0$ for t units of time. Using a Taylor series expansion, the solution to (4-21) can be written as:

$$x(t) = x(0) + \dot{x}(0)t + \frac{1}{2}\ddot{x}(0)t^2 + O^3(t)$$

$$= x(0) + f_1\big(x(0)\big)t + \frac{1}{2}\frac{\partial f_1(x(0))}{\partial x} f_1\big(x(0)\big)t^2 + O^3(t) \tag{4-22}$$

where $O^3(t)$ represents the order of the error of the series. To reduce the notational complexity, in the following all functions are evaluated at $x(0)$ unless stated otherwise. Then set $u_1 = 0, u_2 = 1$ for t further units of time to obtain by using a Taylor series expansion as:

$$x(2t) = x(t) + f_2\big(x(t)\big)t + \frac{1}{2}\frac{\partial f_2(x(t))}{\partial x} f_2\big(x(t)\big)t^2 + O^3(t) \tag{4-23}$$

It is desired to express $x(2t)$ in terms of the starting point. To accomplish this expand the vector fields evaluated at t in a series using the previous series expression for $x(t)$:

$$f_2\big(x(t)\big) = f_2\big(x(0)\big) + \frac{\partial f_2(x(0))}{\partial x}\big(x(t) - x(0)\big) + O^2\big(x(t) - x(0)\big)$$

$$= f_2 + \frac{\partial f_2}{\partial x} f_1 t + O^2(t) \tag{4-24}$$

$$\frac{\partial f_2(x(2t))}{\partial x} = \frac{\partial f_2}{\partial x} + O(t) \tag{4-25}$$

Substituting (4-24) and (4-25) into (4-23) and using the series expansion for $\tau(t)$ obtained previously:

$$x(2t) = x(t) + \left[f_2 + \frac{\partial f_2}{\partial x} f_1 t\right] t + \frac{1}{2}\frac{\partial f_2}{\partial x} f_2 t^2 + O^3(t)$$

$$= x(0) + f_1 t + \frac{1}{2}\frac{\partial f_1}{\partial x} f_1 t^2 + \left[f_2 + \frac{\partial f_2}{\partial x} f_1 t\right] t + \frac{1}{2}\frac{\partial f_2}{\partial x} f_2 t^2 + O^3(t)$$

$$= x(0) + [f_1 + f_2]t + \left[\frac{1}{2}\frac{\partial f_1}{\partial x} f_1 + \frac{\partial f_2}{\partial x} f_1 + \frac{1}{2}\frac{\partial f_2}{\partial x} f_2\right] t^2 + O^3(t) \tag{4-26}$$

Next, set $u_1 = -1, u_2 = 0$ for t further units of time and using the expansion for $x(2t)$ obtained previously:

$$x(3t) = x(2t) - f_1\big(x(2t)\big)t + \frac{1}{2}\frac{\partial f_1(x(2t))}{\partial x} f_1\big(x(2t)\big)t^2 + O^3(t)$$

$$= x(2t) - \left[f_1 + \frac{\partial f_1}{\partial x}(f_1 + f_2)t\right] t + \frac{1}{2}\frac{\partial f_1}{\partial x} f_1 t^2 + O^3(t)$$

$$= x(0) + f_2 t + \left[\frac{\partial f_2}{\partial x} f_1 - \frac{\partial f_1}{\partial x} f_2 + \frac{1}{2}\frac{\partial f_2}{\partial x} f_2\right] t^2 + O^3(t) \tag{4-27}$$

Finally, set $u_1 = 0, u_2 = -1$ for t further units of time and using the same approach:

$$x(4t) = x(3t) - f_2\big(x(3t)\big)t + \frac{1}{2}\frac{\partial f_2\big(x(3t)\big)}{\partial x} f_2\big(x(3t)\big)t^2 + O^3(t)$$

$$= x(3t) - \left[f_2 + \frac{\partial f_2}{\partial x} f_2 t\right] t + \frac{1}{2}\frac{\partial f_2}{\partial x} f_2 t^2 + O^3(t)$$

$$= x(0) + \left[\frac{\partial f_2}{\partial x} f_1 - \frac{\partial f_1}{\partial x} f_2\right] t^2 + O^3(t) \tag{4-28}$$

$$x(4t) = x(0) + [f_1, f_2](x_0)t^2 + O^3(t) \tag{4-29}$$

It is seen that the difference between the initial and terminal points to second order is:

$$x(4t) - x(0) = [f_1, f_2](x_0)t^2 \tag{4-30}$$

Note that the Lie bracket is evaluated at the starting point $x(0)$. Thus, for this example the Lie bracket $[f_1, f_2]$ moves the state space solution from $x(0)$ to the new point $x(4t)$ and hence represents a new directed solution trajectory. It is evident that higher order brackets can also be defined as Lie brackets. Furthermore, the Lie brackets enable relationships to be defined between the various vector fields via providing a measure of commutativity of these vector fields (Bedrossian, 1991).

The relevance of the Lie bracket in nonlinear control theory is apparent when one considers such issue as controllability and integrability of vector fields. For controllability analysis, the bracket represents a direction that the solution may move along even though it may not be in the linear span of the vector fields. By a given set of arbitrary vector fields it is possible to find an integral curve such that at each point its tangent space is spanned by the given vector fields (Slotine & Li, 1991).

4.3 Exact Feedback Linearization

4.3.1 Input-Output and Input-State linearization

Most feedback linearization approaches are based on Input-Output (I-O) linearization or Input-State (I-S) linearization. The choice of feedback linearization approach for different nonlinear system types depends on the relationship between the relative degree γ and the order n of the system.

The I-O linearization is used when $\gamma < n$, then there will be a so-called *internal dynamics* and an additional $n - \gamma$ state variables must be introduced to complete the coordinate transformation. When the I-S linearization is appropriate (i.e. for $\gamma = n$) for this case, the I-O linearization and the I-S linearization are the same. Then some new output $y_{new} = h_{new}(x)$ is

chosen so that with respect to y_{new}, the relative degree of the system is n. Following this the design procedure using this new output y_{new} is the same as for I-O linearization. The Venn diagram of Figure 4-3 shows the two approaches in a more clear way.

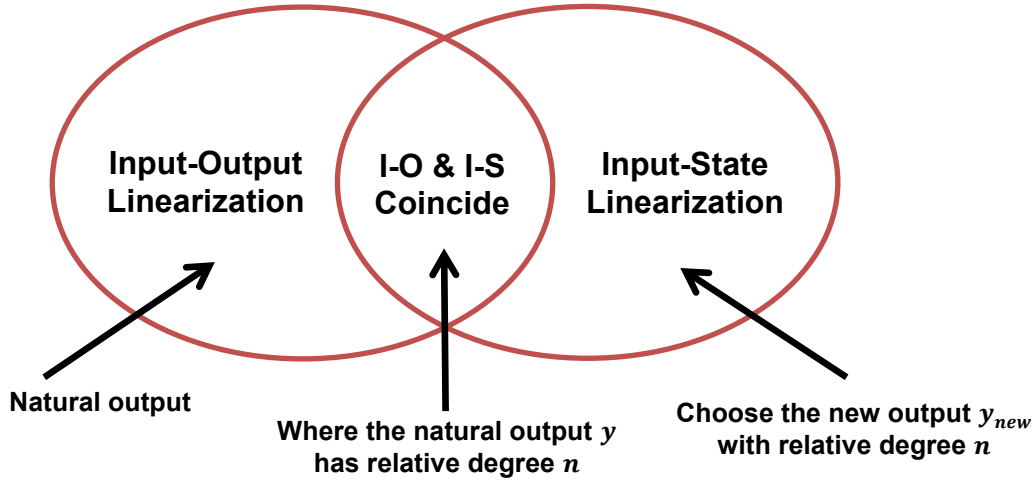

Figure 4-3 Input-Output and Input-State linearization approaches

In the I-O linearization approach, the objective is to linearize the map between the transformed inputs and the actual outputs. A linear controller is then designed for the linearized I-O model with a $n-\gamma$ dimensional subsystem that typically is not linearized. Thus I-O linearization techniques are usually restricted to processes in which these so called *zero dynamics* (the *internal dynamics* of the $n-\gamma$ dimensional subsystem when all the state variables converge to zero) are stable (Hedrick & Girard 2005).

In the state-space linearization approach, the goal is to linearize the map between the transformed inputs and the entire vector of transformed state variables. This objective is achieved by deriving artificial outputs that lead to a feedback linearized model with state dimension $\gamma = n$. A linear controller is then synthesized for the linear I-S model. For some processes, it is possible to simultaneously linearize the I-O and I-S maps for the original outputs, resulting in a linear model with dimension $\gamma = n$ (Henson & Seborg, 1997; Hedrick & Girard 2005).

4.3.2 Feedback linearization process

For a nonlinear MIMO system, if the sum of the components relative degree γ is exactly the system dimension n, which means every state of the feedback linearized system can be directly controlled by the input signal, then the MIMO system can be expressed as a general nonlinear affine form as:

$$\begin{aligned} \dot{x} &= f(x) + g(x)u \\ y &= h(x) \end{aligned} \tag{4-31}$$

According to the analysis in Section 4.2.1, assume there exists a coordinate and control transformation as:

$$\begin{aligned} z &= T(x) \\ v &= \alpha(x) + \beta(x)u \end{aligned} \tag{4-32}$$

where

$$T(x) = \begin{bmatrix} T_1(x) \\ T_2(x) \\ \vdots \\ T_n(x) \end{bmatrix} = \begin{bmatrix} h_1(x) \\ L_f h_2(x) \\ \vdots \\ L_f^{\gamma_n - 1} h_n(x) \end{bmatrix} \tag{4-33}$$

with the following properties:

(1) $T(x)$ is invertible; i.e. there exists a function $T^{-1}(z)$ such that $T^{-1}\big(T(x)\big) = x$, $T\big(T^{-1}(z)\big) = z$ for all $x \in R^n$ and all $z \in R^n$.

(2) $T(x)$ and $T^{-1}(z)$ are both smooth mappings.

A transformation of this type (4-33) is called a *global diffeomorphism*. The first property is needed to guarantee the invertibility of the transformation to yield the original state vector as:

$$x = T^{-1}(z) \tag{4-34}$$

while the second one guarantees that the description of the system in the new coordinates is still a smooth one. However, a transformation satisfying both of these properties and defined for all x is sometimes hard to find and the properties in question are difficult to check. Thus, in most cases, transformations defined only in the neighborhood of a given point are of interest. Such a transformation of this type is called *local diffeomorphism* (Bedrossian, 1991).

The objective is to transform (4-31) by using (4-32) to a linear and controllable system as:

$$\begin{aligned} \dot{z}_1 &= z_2 \\ \dot{z}_2 &= z_3 \\ &\vdots \\ \dot{z}_{n-1} &= z_n \\ \dot{z}_n &= v \end{aligned} \tag{4-35}$$

which results in a linear *Brunovsky Canonical form* in (4-10):

$$\begin{aligned} \dot{z} &= A_c z + B_c v \\ y &= C_c z \end{aligned} \tag{4-36}$$

4.4 Feedback Linearization Application for Nonlinear Aircraft Dynamics

Considering the nonlinear aircraft model derived in Chapter 3, the Machan UAV, it is clearly shown in Table 3-3 that this 6DoF model only involves 4 actuators, which is introduced in Section 4.1.1 as an *under-actuated* system since there are fewer actuators than the degrees of the system freedom.

The Euler equations (3-18), (3-19) can be transposed into the following 10 state system that includes the altitude state h as follows:

$$\left.\begin{aligned} \dot{p} &= \frac{I_y - I_z}{I_x} rq + \frac{L}{I_x} \\ \dot{q} &= \frac{I_z - I_x}{I_y} pr + \frac{M}{I_y} \\ \dot{r} &= \frac{I_x - I_y}{I_z} pq + \frac{N}{I_z} \end{aligned}\right\} \tag{4-37}$$

$$\left.\begin{aligned} \dot{u} &= rv - qw + \frac{X}{m} \\ \dot{v} &= pw - ur + \frac{Y}{m} \\ \dot{w} &= qu - vp + \frac{Z}{m} \end{aligned}\right\} \tag{4-38}$$

$$\left.\begin{aligned} \dot{\phi} &= p + qsin\phi tan\theta + rcos\phi tan\theta \\ \dot{\theta} &= qcos\phi - rsin\phi \\ \dot{\psi} &= qsin\phi sec\theta + rcos\phi sec\theta \end{aligned}\right\} \tag{4-39}$$

$$\dot{h} = V_T sin\theta \tag{4-40}$$

This choice of state variables above is appropriate for the Machan system by combining the lateral and longitudinal systems summarized in Table 3-3. In (4-37), the moment inertia $\{I_x, I_y, I_z\}$ are constant, and the moments $\{M, L, N\}$ are directly dependent on the three control actuators inputs $\{\delta_a, \delta_e, \delta_r\}$, thus the total relative degree defined in Section 4.2.2 of the angle rate states $\{p, q, r\}$ will be:

$$\gamma_p + \gamma_q + \gamma_r = n_{rates} = 3 \tag{4-41}$$

which satisfies the requirement for exact feedback linearization.

It is shown in (4-37) and (4-40) that the remaining state variables, the coordinate velocities $\{u, v, w\}$, and Euler angles $\{\phi, \theta, \psi\}$ and the altitude h have inappropriate relative degree for feedback linearization based on the control inputs $\{\delta_a, \delta_e, \delta_r\}$. However, their differentials are dependent to states $\{p, q, r\}$ with desirable relative degree (Wigdorowitz, 1992; Snell, Enns & Garrard, 1992).

Furthermore, these states also can be separated by so-called "time scale separation" according to various aerodynamic response speed. The expression of this phenomenon is that when a moment acts on an object, then primarily the angular rates change, whereas the Euler angles remain approximately the same for small time steps. This concept is commonly used in aircraft control, (Calise, Lee & Sharma, 2000; Lombaerts, Chu, Mulder & Joosten, 2011).

Thus, for achieving the controller design for the Machan UAV using feedback linearization, the aircraft states can be divided into different control loops according to their response speed, for example, the fast-response states $\{p, q, r\}$, the slow-responses states $\{\phi, \theta, \psi\}$ and even the much slower state h. As a consequence of the time scale separation property, it is sufficient for each control loop to consider the first order Lie derivative to find the relevant control input, and the local *relative degree* is unity. Theoretically, this kind of separation arrangement involves some stability issues. However, practice has shown that the bandwidths of the angular rates and attitude angles are sufficiently separated to prevent the risk for instabilities due to interactions (Lane & Stengel, 1988; Snell, Enns & Garrard, 1992).

As a result, the proposed controller is setup in a multiple-loop cascade configuration, with the ultimate goal of tracking a trajectory given by roll, pitch and yaw angle set points. The outer-loop takes the roll, pitch and yaw set points and provides the angular rate commands to the inner-loop, which is assumed to track the commands using the inputs to the actuators. In this way, control input of outer loop can be substituted by the inner loop states. The thrust input δ_t is chosen to be as reasonably constant as possible whilst providing sufficient thrust for the aircraft. The angular rate dynamics $\{p, q, r\}$ are usually chosen to denote the inner-loop system whilst the angular dynamics $\{\phi, \theta, \psi\}$ comprise the outer-loop as shown in Figure 4-4.

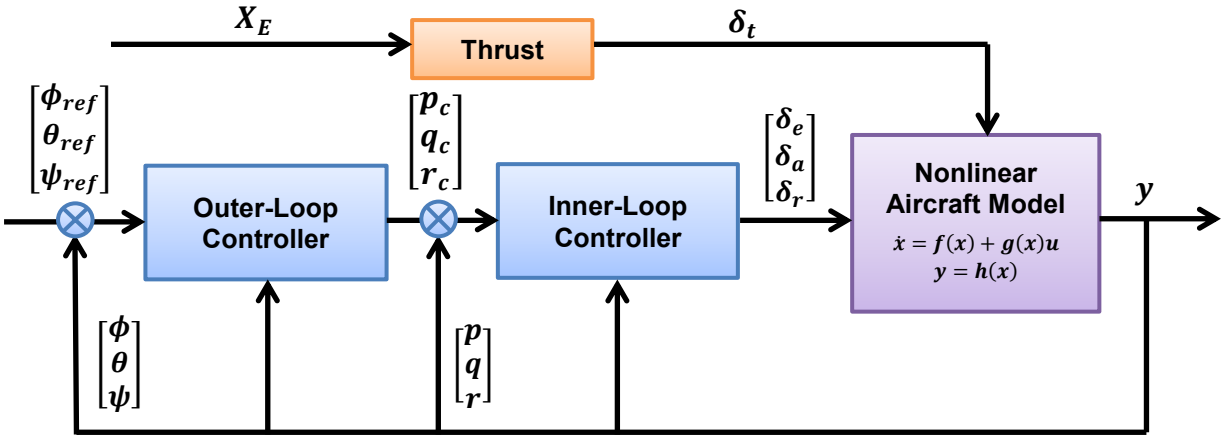

Figure 4-4 Multiple control loop scheme for aircraft feedback linearization

Note that $[\phi_{ref} \quad \theta_{ref} \quad \psi_{ref}]^T$ represents the reference signal and $[p_c \quad q_c \quad r_c]^T$ represents the commend signal for the internal control system derived from the external controller output.

It can be shown in Figure 4-4, the aircraft system is decomposed into a cascade coupling with internal and outer control loops (Snell, Enns & Garrard, 1992; Jankovic, Sepulchre & Kokotovic, 1996; Boskovic & Mehra, 2001; Buonanno & Cook, 2005). By choosing suitable output functions for each control loop, the system with the corresponding relative degree is full state linearizable and exact feedback linearization can be used as control strategy. The detailed scheme may change according to the different control strategies chosen. This issue is discussed and illustrated in Chapters 5, 6, 7 & 8 for various outer-loop design using NN adaptor, SMC-NN training adaptor and simultaneous states/faults estimator to achieve FTC performance.

4.5 Conclusion

In this chapter the essential comparison between the characteristics of linear and nonlinear systems is outlined in order to highlight the main challenges for research into the control of nonlinear systems. A short review of current analysis and control strategies for nonlinear system design is outlined. The concept of feedback equivalence is introduced as a precursor to exact feedback linearization. The operations of state and control transformations are used to define an equivalence class of linearizable nonlinear systems. The preliminary mathematical concepts required to gain an understanding of the requirements for exact feedback linearization are presented. In particular the conditions for the existence of such transformation are examined and the construction of the transformations is presented. Section 4.4 summarizes and analyzes the feasibility and validity for applying feedback linearization to an example of a highly nonlinear and MIMO aircraft system model, the Machan UAV, which is introduced in Chapter 3. The special control scheme that is required for this feedback linearization example is provided as a background for the work described in Chapters 5, 6, 7 & 8. Chapter 5 deals with the development of a reconfigurable flight control system for the Machan aircraft based on both dynamic inversion theory and making use of an on-line adaptive NN.

Chapter 5 Reconfigurable FTFC for Nonlinear Aircraft Based on Adaptive NN

This chapter focuses on an improved reconfigurable FTFC strategy based on adaptive Neural Networks (NN) for highly nonlinear flight systems which have severe parametric uncertainties and disturbances. The traditional model reference adaptive FTFC architectures were presented by Calise, Lee, & Sharma (1998a). A recently developed adaptive learning algorithm (Chowdhary & Johnson, 2008) employs the current (online) as well as stored (background) information *concurrently* for training the NN weights. Test results in Chowdhary and Johnson's work (2008, 2009, 2010, 2011a, 2011b, 2012) show that simultaneous use of current and background data confirm expected improvements in performance and practical stability properties of the traditional Model Reference Adaptive Control (MRAC) architectures.

This chapter proposes a new design approach based on recent advances in the combination of output feedback and NN adaptation algorithms, comprising approximate feedback linearization with the synthesis of fixed-gain dynamic compensator design. An improved NN using concurrent update information to compensate for model inversion error is described to compensate for the full dynamic characteristics of the aircraft system. The view held in this thesis is that the concurrent learning network control law approach of Chowdhary and Johnson (2008, 2012) is complex in terms of on-line computer implementation requirements. With a motivation for facilitating efficient on-line application this approach is simplified and validated through simulation performances using the nonlinear Machan UAV (with model provided in Chapter 3), operated under various fault scenarios and turbulence and control input induced uncertainties.

5.1 Introduction

Recent advances in aircraft technology enable flight envelopes to be significantly extended over traditional regimes, typically through the use of unconventionally configured vehicles. These developments have led to a need for substantially higher adaptive control performance and reliable reconfigurable control ability against faults and disturbances. These flight conditions give rise to unmodelled parameter variations and unmodelled vehicle dynamics

such as unsteady aerodynamic effects, saturation of aerodynamic effectors and highly coupled vehicle dynamics that may cause instability or lack of controllability during flight missions (Etkin & Reid, 1996; Stengel, 2005). Even more active controls may be required to compensate for the effects of the unmodelled dynamic phenomena that may actually arise from the unusual configurations themselves.

Aircraft with unconventional flight control configurations can potentially benefit from having adaptive control elements. Other potential beneficiaries of these advanced control designs are UAV systems which are now rapidly having extended mission capability beyond target drone and air reconnaissance toward air combat and air-to-ground combat roles. These vehicles usually contain simpler and cheaper systems with substantially smaller mass compared with manned vehicles, and in addition the UAV control designs may use minimal or no aerodynamic data. Hence, adaptive flight control systems should be designed to achieve required performance by dealing with uncertainties in the flight systems environment (Banda, 1999; Belkharraz & Sobel, 2000; Aström & Wittenmark, 2008).

As introduced in Section 2.2, control reconfiguration is an active approach in control theory to achieve FTC for dynamic systems. In addition to loop-restructuring, the controller parameters must be adjusted to accommodate changing plant dynamics. To achieve this, controller designs using adaptive NN and dynamic inversion based on geometric control theory are investigated where NN plays a key role as the principal element of adaptation to approximately cancel the effect of the inversion error, system uncertainty and even certain faults and disturbances acting on the system. This form of active FTC dealing with faults as well as uncertainty could provide robustness in nonlinear dynamic regimes (Steinberg, 2005; Ioannou & Sun, 2012).

As introduced in Chapter 4, feedback linearization which depends on nonlinear transformation techniques and differential geometry is a well-accepted approach for nonlinear control design. For NN-based adaptive control of nonlinear systems, especially for statically unstable aircraft such as the Machan UAV, a base-line control loop should be included in the nominal system design to stabilize and optimize the system performance prior to the development and implementation of further control functions, FDI/FDD or FTC, etc. The base-line control function can be developed using Nonlinear Dynamic Inversion (NDI) theory.

Artificial NN are computing architectures that comprise massively parallel interconnections of simple computing elements made from so-called “neurons” inter-connected by weights, activation functions and a layered structure. NN have been implemented in various fields such as system identification and control, image processing, speech recognition, etc. Thus, in recent decades, there have been significant research efforts to implement NN algorithms as universal approximators in nonlinear adaptive control designs, to achieve desired system performance. The on-line potential of NNs for adaptively updating and compensating for system uncertainty offers promising advantages over most other conventional linear parameter adaptive controllers (Lee & Kim, 2001; Shin, 2005; Kim & Calise, 2008).

Usually adaptive control methodologies are classified as either direct or indirect (Calise, Lee & Sharma, 1998a). In direct adaptive control, the parameters define the controller (rather than describing the system itself) without the use of estimation or on-line identification. Whilst for indirect adaptive control on-line identification of plant parameters is required with an assumption that a suitable controller is implemented (Shin, 2005).

Consequently, a direct adaptive output feedback control procedure does not rely on state estimation. This is an advantage for highly uncertain nonlinear systems and is also applicable to systems of unknown, but bounded dimension. The desirable control performance is achieved by extending the universal function approximation property of linearly parameterized NN to model unknown system dynamics from input/output data. The network weight adaptation rule is derived from Lyapunov stability analysis, which guarantees that the adapted weight errors and the tracking errors are bounded. This methodology of reconfigurable FTFC has more flexibility and thus greater potential than conventional FTFC strategies for nonlinear flight control (Johnson & Calise, 2001; Lavretsky & Wise, 2005; Shin, 2005; Kim & Calise, 2008).

The most popular NN-based reconfigurable FTFC is primarily developed by Calise, Lee & Sharma (1998a) and has been successfully utilized for a variety of aerospace applications (Calise & Rysdyk, 1998b; Calise, Lee & Sharma, 2000; Calise, Hovakimyan & Idan, 2001; Idan, Johnson, Calise & Kaneshige, 2001; Idan, Johnson & Calise, 2002; Shin, Johnson, & Calise, 2003; Shin & Kim, 2004; Johnson & Kannan, 2005; Kim & Calise, 1997, 2007, 2008; Smaili, Breeman, Lombaerts & Joosten, 2006) involving an MRAC scheme. This approach has been successfully demonstrated via simulation on the Tailless Advanced Fighter Aircraft (Calise, Lee & Sharma, 1998a) and the X-36 aircraft (Calise, Lee & Sharma, 2000).

NASA performed a series of adaptive flight control studies since the 70's, studied the verification and validation of NN for aerospace systems (Mackall, Nelson & Schumann, 2002), and has performed several research projects on intelligent adaptive FTFC implementations which incorporate innovative real-time NN technologies to demonstrate the NN capability to enhance aircraft performance under nominal conditions and to stabilize the aircraft under various critical flight conditions (Steinberg, 2005).

In recent years, a *Long-Term Learning Adaptive Flight Controller* is presented by (Chowdhary, 2010; Chowdhary & Johnson, 2008, 2009, 2010, 2011a, 2011b, 2012) for further improving continuous performance of the FTFC system based on adaptive NN learning algorithms. In their work the baseline adaptive control architecture is always used to accomplish a proven MRAC scheme by using the NN as an adaptive element. Furthermore, this method also employs the current (online) as well as stored (background) information *concurrently* for training the NN weights to achieve better adaptation. This ability allows the adaptive element to simulate long-term memory by retaining specifically stored input-output data pairs and using them for concurrent adaptation. The structure of the adaptive law ensures that concurrent training on past data does not affect the responsiveness of the adaptive element to current data. Conceptually, the baseline adaptive law attempts to minimize a quadratic cost applied to the instantaneous tracking error. This is one reason why the baseline adaptive law must be persistently provided with information in order to guarantee exponential stability. A concurrent learning adaptive law on the other hand, uses recorded and current data concurrently for adaptation. This ensures that if the recorded data are sufficiently rich, then the exponential stability of the zero solution of the tracking error and weight error dynamics can be guaranteed without requiring persistency of excitation. A proof can be found in (Chowdhary, 2010). An equivalent theorem for a different class of plants is proved in (Chowdhary & Johnson, 2010).

The study in this chapter is motivated by a challenge to investigate and improve the control performance of the concurrent learning NN adaptive laws. Instead of the need for a complicated strategy for data selection and complicated information from a stack circle, a simpler concurrent learning scheme is proposed for maintaining control efficiency whilst achieving improved reconfigurable FTFC dynamics in a much easier application adaption strategy.

5.2 Preliminaries of Adaptive Control System

5.2.1 Approximate model inversion based on feedback linearization

Conventional flight control strategies assume that the aircraft dynamics are linear and time-invariant about some nominal flight condition, and they feature stability and command augmentation systems to meet required flying/handling qualities, with feedback gains scheduled as functions of nominal flight conditions. In certain flight conditions the performance of these systems begins to deteriorate due to the unmodelled effects arising from strong nonlinearities inherent in the flight dynamics. To deal with these issues, a Nonlinear Dynamic Inversion (NDI) based on feedback linearization has been developed (Snell, Enns & Garrard, 1992; Calise, Lee & Sharma, 1998, 2000; Johnson, 2000; Lavretsky & Wise, 2005; Ducard, 2007, 2009), as an advanced flight control approach.

As outlined in Section 4.4, the rigid body dynamics of an aircraft can be described globally over the full flight envelope by a set of nonlinear differential equations in the control affine expression introduced in Section 4.2 as [refer to (4-31)]:

$$\begin{aligned} \dot{x} &= f(x) + g(x)u \\ y &= h(x) \end{aligned} \tag{5-1}$$

where state vector $x \in \mathcal{R}^n$, control input vector $u \in \mathcal{R}^m$; controlled output vector $y \in \mathcal{R}^m$; nonlinear vector fields $f(x) \in \mathcal{R}^n$; $g(x) \in \mathcal{R}^{n\times m}$; and $h(x) \in \mathcal{R}^m$.

Recall that (see Section 4.4) by assuming that the nonlinear dynamic system of (5-1) satisfies the conditions for output feedback linearization with well-defined vector relative degree γ, the principle of dynamic inversion is to realize a linear input-output behaviour of the system where the output y and its successive derivatives are directly controllable by the control input u.

As defined in Section 4.2.2, the relative degree γ_i is the smallest integer such that at least one of the inputs appears in ${y_i}^{(\gamma_i)}$ using Lie derivatives as:

$${y_i}^{(\gamma_i)} = L_f^{\gamma_i} h_i + \sum_{j=1}^{m} \left(L_{g_i} L_f^{\gamma_i - 1} h_i u_j \right) \tag{5-2}$$

In general, for all $1 \le j \le m$, for all $k < \gamma_i - 1$, for all $1 \le i \le m$, and for all x in a neighborhood of the equilibrium point with at least one of the $L_{g_i} L_f^{\gamma_i - 1} h_i \neq 0 \forall x$, and u_j is the j^{th} row of u, then the MIMO system of (5-1) with m outputs can be written in the transformed form by means of the *Lie Derivatives* as:

$$\begin{bmatrix} y_1^{(\gamma_1)} \\ \vdots \\ y_m^{(\gamma_m)} \end{bmatrix} = \alpha(x) + \beta(x)u \tag{5-3}$$

with

$$\alpha(x) = \begin{bmatrix} L_f^{\gamma_1} h_1(x) \\ \vdots \\ L_f^{\gamma_m} h_m(x) \end{bmatrix}, \beta(x) = \begin{bmatrix} L_{g_1} L_f^{\gamma_1 - 1} h_1 & \cdots & L_{g_m} L_f^{\gamma_1 - 1} h_1 \\ \vdots & \ddots & \vdots \\ L_{g_1} L_f^{\gamma_m - 1} h_m & \cdots & L_{g_m} L_f^{\gamma_m - 1} h_m \end{bmatrix} \tag{5-4}$$

If $\beta(x)$ is invertible, then a linear input-output map can be achieved by using a state transformation and a state feedback as:

$$u = \beta^{-1}(x)[-\alpha(x) + \nu] \tag{5-5}$$

which is equivalent to the inverted system dynamics control. The new input or control signal of the inverted system is referred to as a pseudo-control ν, which is generated to calculate the necessary input signal u to assure a desired system output y.

Applying the feedback control law (5-5) into the transformed system (5-3), the system dynamics may then be re-organised and the closed-loop system outputs are given by the solution to an integrator chain with the following linear system form:

$$\begin{bmatrix} y_1^{(\gamma_1)} \\ \vdots \\ y_m^{(\gamma_m)} \end{bmatrix} = \begin{bmatrix} \nu_1 \\ \vdots \\ \nu_m \end{bmatrix} \tag{5-6}$$

The linear controlled system by the dynamic inversion law in (5-5) is as shown in Figure 5-1.

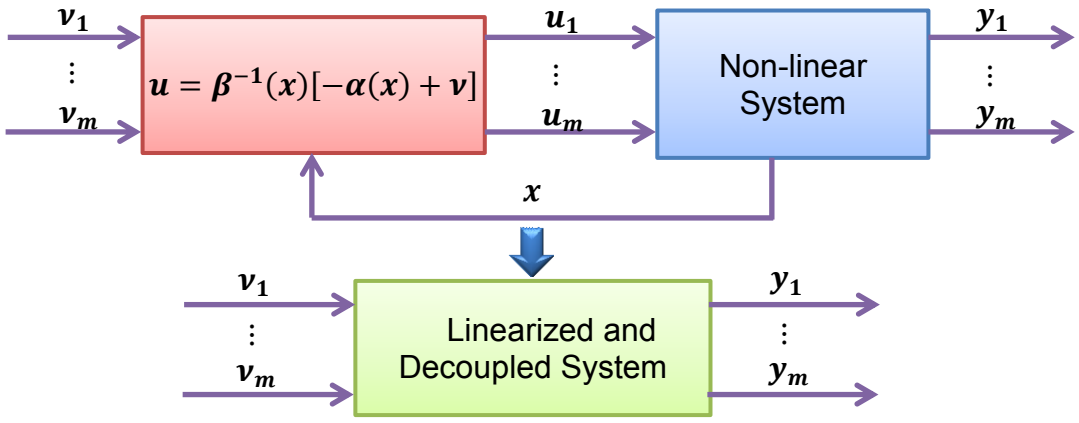

Figure 5-1 Sketch of the dynamic inversion linearization principle

Once the linearization has been achieved, any further control objectives may be easily met. If the system dynamics are not completely available in a closed algebraic form, which is the

case for many aerodynamic data sets, an approximate dynamic inversion has to be performed (Slotine & Li, 1991; Khalil & Grizzle, 2002).

The chief advantage of the NDI methodology is that it avoids the time-consuming, costly, iterative, and labour intensive gain-scheduling process of other methods. The NDI technique offers greater reusability across different airframes, greater flexibility for handling changed models as an airframe evolves during its design cycle, and greater power to address non-standard flight regimes such as super manoeuvres. Control laws based on NDI offer the potential for providing improved levels of performance over conventional flight control designs in these extreme flight conditions. This is due to the NDI controller's more accurate representation of forces and moments that arise in response to large state and control perturbations. Many studies mentioned in Section 5.1 demonstrate that NDI is an effective method for highly manoeuvrable air vehicles. However, as noted by Brinker and Wise (Brinker & Wise, 1996), NDI can be vulnerable to inaccurate modelling and inevitable inversion errors. Thus the NN-based adaptive control design is introduced to compensate for the inversion errors, unmodelled dynamics and parametric uncertainty which are quite common in highly nonlinear regimes (Isidori, 1995; Sastry, 1999; Calise, Hovakimyan & Idan, 2001).

5.2.2 Adaptive neural network

It is assumed that $\Delta(x,u)$ is a time-varying signal representing the combination of all uncertainties of modelling the real system i.e. subsequent to the application of NDI. $\Delta(x,u)$ is completely unknown but assumed to be bounded. For the purpose of adaptive control, there exists a set of NN weights such that the NN output $\nu_{ad}(x)$ approximates $\Delta(x,u)$. In other words, the NN performs the role of online identification of the uncertainties.

In this Section, the mechanisms and structures of the feed-forward Single Hidden Layer (SHL) NN are introduced and discussed and used later in Chapter 5 and further in Chapters 6 & 8.

An SHL Perceptron NN is a universal approximator (Hornik, Stinchcombe & White, 1989) in that it can approximate any smooth nonlinear function to within arbitrary accuracy, given a sufficient number of *hidden layer* neurons and sufficient input information. Figure 5-2 shows the structure of a generic SHL NN (Shin, 2005).

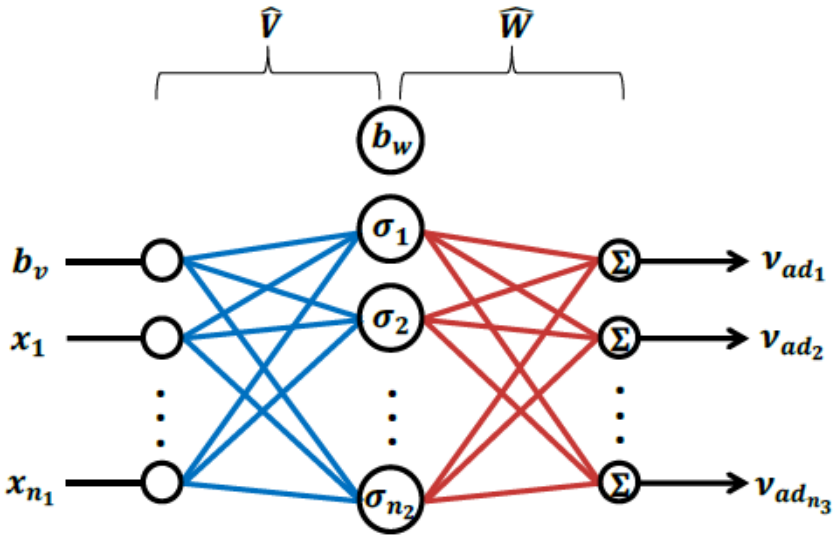

Figure 5-2 The structure of SHL NN

where W, V are the updated weights of the input-hidden and hidden-output layers, respectively; θ acts as an activation threshold for each neuron, which also allows the bias term b, to be weighted in each output channel.

It is assumed that the uncertainty $\Delta(x,u)$ is uniformly approximated by an SHL NN with bounded monotonically increasing continuous activation function and on a compact domain $D_x \in \mathcal{R}^n$. Hence, for all $\varepsilon > 0$ and $x \in D_x$, then there exists W, V and θ such that:

$$\|\Delta(x,u) - \nu_{ad}\|_\infty \triangleq \|\Delta(x,u) - \{W^T\bar{\sigma}(V^T x + \theta)\}\|_\infty \leq \varepsilon \tag{5-7}$$

The input-output map of the SHL NN can be expressed as:

$$\nu_{ad_k} = b_w\theta_{w,k} + \sum_{j=1}^{n_2} w_{j,k}\,\sigma_j \tag{5-8}$$

where $k = 1, \ldots, n_3$ and

$$\sigma_j = \sigma\left(b_w\theta_{v,j} + \sum_{i=1}^{n_2} v_{i,j}x_i\right) \tag{5-9}$$

Here n_1, n_2, and n_3 are the number of input nodes, hidden layer nodes, and outputs respectively. The scalar function $\sigma(\cdot)$ is a sigmoidal activation function that represents the "firing" characteristics of the neuron.

If the input to the hidden layer neuron is set as:

$$z = V^T x = \begin{bmatrix} z_1 \\ \vdots \\ z_{n_2} \end{bmatrix} \in \mathcal{R}^{n_2 \times 1} \tag{5-10}$$

then the basis functions can then be selected as functions of the form:

$$\sigma(z) = \frac{1}{1+e^{-az}} \tag{5-11}$$

The factor a is known as the activation potential, and can be a distinct value for each neuron.

The input-output map of the SHL NN in the controller architecture can be conveniently written in matrix form as:

$$\nu_{ad} = W^{*T}\hat{\sigma}\left(V^{*T}x\right) \tag{5-12}$$

where the two NN weight matrices V^*, W^* are estimates of the ideal weights V, W defined as follows.

The inner-layer synaptic weight matrix V is written as:

$$V^* = \begin{bmatrix} \theta_{v,1} & \cdots & \theta_{v,n_2} \\ v_{1,1} & \cdots & v_{1,n_2} \\ \vdots & \ddots & \vdots \\ v_{n_1,1} & \cdots & v_{n_1,n_2} \end{bmatrix} \in \mathcal{R}^{(n_1+1)\times n_2} \tag{5-13}$$

with a sigmoid vector defined as:

$$\bar{\sigma}(z) = \begin{bmatrix} b_w & \sigma(z_1) & \sigma(z_2) & \cdots & \sigma\left(z_{n_2}\right) \end{bmatrix}^T \in \mathcal{R}^{n_2+1} \tag{5-14}$$

where b_w is a bias term. The outer-layer weight matrix W is then defined as:

$$W^* = \begin{bmatrix} \theta_{w,1} & \cdots & \theta_{w,n_3} \\ w_{1,1} & \cdots & w_{1,n_3} \\ \vdots & \ddots & \vdots \\ w_{n_2,1} & \cdots & w_{n_2,n_3} \end{bmatrix} \in \mathcal{R}^{(n_2+1)\times n_3} \tag{5-15}$$

The input vector is now defined as:

$$\bar{x} = [b_v \quad x_1 \quad x_2 \quad \cdots \quad x_{n_1}]^T \in \mathcal{R}^{n_1+1} \tag{5-16}$$

where $b_v \geq 0$ is an input bias. The weight matrices V, W are updated online according to the following adaptation laws:

$$\begin{aligned} \dot{V}^* &= -\Gamma_v \cdot \left[\bar{x}e^T PBW^{*T}\bar{\sigma}^T + \kappa_v \cdot (V^* - V_0)\right] \\ \dot{W}^* &= -\Gamma_w \cdot \left[\left(\bar{\sigma} - \bar{\sigma}' V^{*T}\bar{x}\right)e^T PB + \kappa_w \cdot (W^* - W_0)\right] \end{aligned} \tag{5-17}$$

where e is the output tracking error; $\bar{\sigma} = \sigma\left(W^{*T}\bar{x}\right)$; W_0 and V_0 are initial or random guesses for the NN training. The Γ_v, Γ_w, κ_v $\kappa_w > 0$ are the adaption gains, and P is a positive defined solution of the Lyapunov equation:

$$A^T P + PA + Q = 0 \tag{5-18}$$

where $Q > 0$, and the properties of the linearized system matrix A are described in model tracking error form in Section 5.3.3.

The approximation error of the SHL NN is described as:

$$\begin{aligned} \Delta(x,u) - \nu_{ad}(x) &= W^T \bar{\sigma}(V^T \bar{x}) - W^{*T} \bar{\sigma}\left(V^{*T} \bar{x}\right) + \varepsilon(x) \\ &= \widetilde{W}^T \left(\bar{\sigma} - \bar{\sigma}' V^{*T} \bar{x}\right) + W^{*T} \bar{\sigma}' \tilde{V}^T \bar{x} + \varepsilon(x) \end{aligned} \tag{5-19}$$

where $\widetilde{W} \triangleq W - W^*$, $\tilde{V} \triangleq V - V^*$ are the NN estimation update law error.

It is assumed that the nonlinear function $\Delta(x,u)$ in (5-19) is linearly parameterized by the SHL NN which is described as:

$$\Delta(x,u) = W^T \bar{\sigma}(V^T \bar{x}) = W^{*T} \bar{\sigma}\left(V^{*T} \bar{x}\right) + \varepsilon(x) \tag{5-20}$$

It has been shown that the forms of the weight adaption laws in (5-17) for the SHL NN guarantee that all error signals, including the tracking error and the NN weight errors are uniformly bounded (Lewis, 1999; Calise, Hovakimyan & Idan, 2001) by using the Lyapunov direct method.

5.3 Reconfigurable FTFC Scheme based on Adaptive Compensator

As analyzed in Section 4.4, the states and outputs of the aircraft should be chosen carefully and reorganized for satisfying the required feedback linearization properties. Hence, in this section, the aircraft cascade loop control scheme is set up and the reformulated dynamics of the adaptive NN based reconfigurable control system is provided. As a result, the adaptive NDI output feedback formulation is applied to compensate for the full dynamic characteristics of the nonlinear aircraft system.

5.3.1 Two-stage dynamic inversion of nonlinear aircraft

The basic Machan UAV dynamic model used for this research is obtained from Chapter 3. In Section 4.4 a multiple-loop cascade configuration of the dynamic linearization method has been suggested considering the relative degree theorem in differential geometry control. Here a two-stage approach is used for designing a reconfigurable FTFC system by regulating fast- and slow-response states separately.

It is assumed that the state dynamics of the nonlinear aircraft can be decomposed in two stages as:

- Stage 1: dynamics, $x_1 = [p \quad q \quad r]^T$
- Stage 2: dynamics, $x_2 = [\phi \quad \theta \quad \psi]^T$

It should be noted that the references use the terminology ***slow*** and ***fast***, which are not strictly appropriate as the dynamics are not separable according to the definitions given above. However, the inverting solution does not rely on the validity of the de-coupling in the subsystem dynamics. Therefore it is more appropriate to say that the inversion is done in two stages, and this is the terminology used in most studies and references (Calise, Hovakimyan & Idan, 2001; Shin, 2005).

The structure of the inverting law and its implementation is displayed in Figure 5-3.

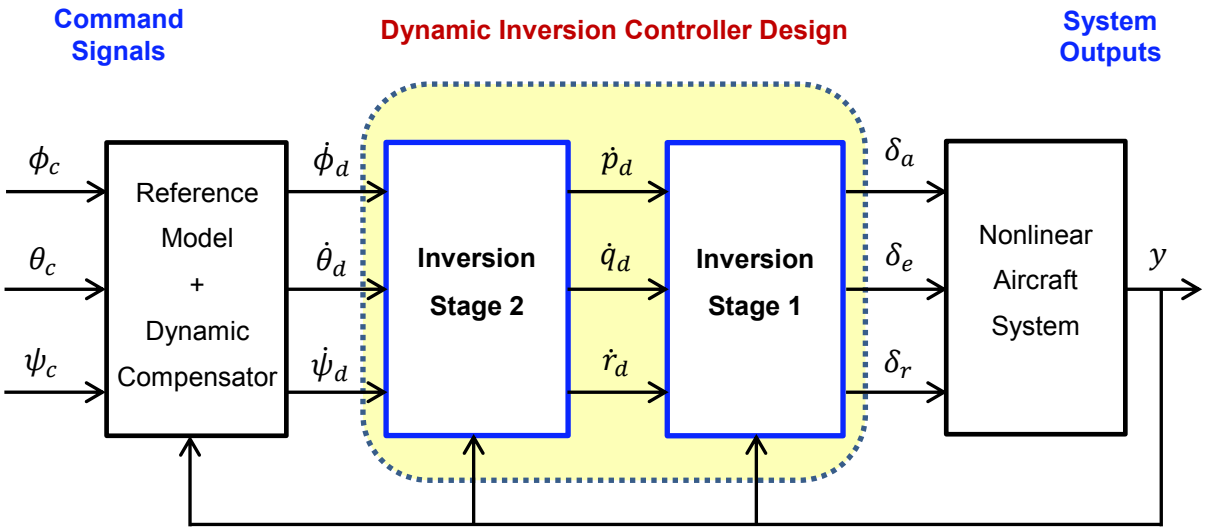

Figure 5-3 Two-stage dynamic inversion control structure for nonlinear aircraft

Assuming all the states and aerodynamic parameters are available, then the control variables for the Stage 1 dynamics are the effective actuator control displacement commands:

$$u_1 = [\delta_a \quad \delta_e \quad \delta_r]^T \tag{5-21}$$

The control variables for the Stage 2 dynamics are the angular rates of the roll, pitch and yaw as:

$$u_2 = [p \quad q \quad r]^T \tag{5-22}$$

So that the "inverting design" in each stage can be achieved based on the NDI law in (5-4) and (5-5) resulting in the regulated variables in each stage as:

$$\dot{y}_1 = [\dot{p} \quad \dot{q} \quad \dot{r}]^T = \nu_1$$
$$\dot{y}_2 = [\dot{\phi} \quad \dot{\theta} \quad \dot{\psi}]^T = \nu_2 \tag{5-23}$$

Note that the regulated variables of the stage 1 dynamics $[p \quad q \quad r]^T$ are related to the regulated variables $[\phi \quad \theta \quad \psi]^T$ according to the relative degree of each regulated variable as described in Section 4.4. The variables in Stage 1 have relative degree one, while the variables in Stage 2 have relative degree two (it is necessary to differentiate these variables twice before a control term appears). Thus y_1 and y_2 are defined as in (5-6) so that the control law appears in the first derivative of each of its element.

5.3.2 Reformulation of the model dynamics

Assuming all the system states are available, Figure 5-4 depicts a more compact and specific form of the adaptive NN based reconfigurable FTFC architecture for the two stage dynamics formulation described in Section 5.3.1. As shown in Figure 5-4, the command signal of $x_c = [\phi \quad \theta \quad \psi]^T$ is input to the command filters to generate reference signals, while employing a Proportional and Derivative (PD) controller to follow the reference commands. The control commands are obtained by the two-stage dynamic inversion with the adaptive NN signals (Johnson, 2000; Calise, Hovakimyan & Idan, 2001).

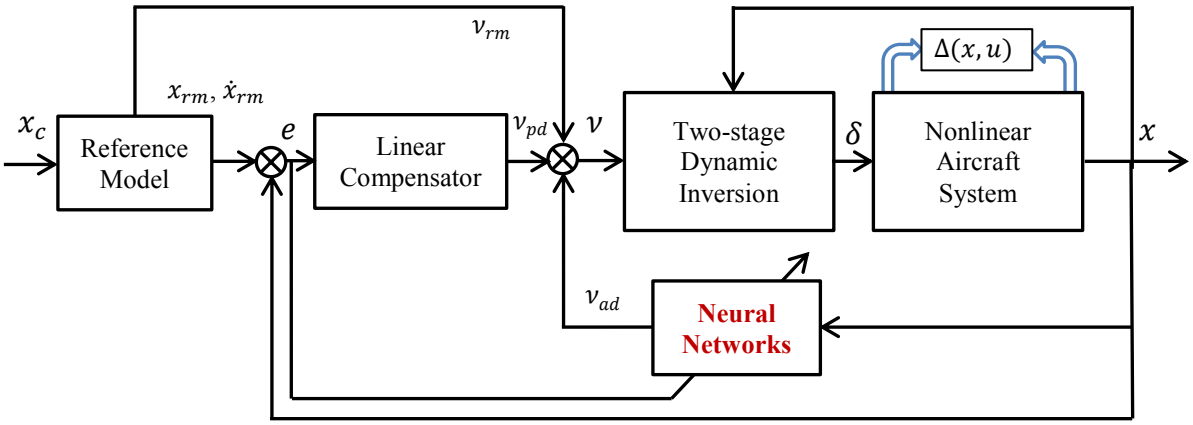

Figure 5-4 Reconfigurable FTFC scheme based on NDI and adaptive NN

Now reformulate the nonlinear aircraft system of (5-1) with consideration of (5-23) to the form as:

$$\ddot{x} = f(x, \dot{x}, \delta) \tag{5-24}$$

where $x, \dot{x}, \delta \in R^n$. The pseudo-control input ν which represents a desired $\ddot{x}$ and is expected to be approximately achieved by the actuating signal δ, in the following manner according to the NDI procedure of Section 5.2.1 (refer to (5-6)):

$$\ddot{x} = \nu \tag{5-25}$$

where

$$\nu = f(x, \dot{x}, \delta) \tag{5-26}$$

In a model dynamic inversion scheme the actual control input δ is found in the inverting form of (5-26). However since the function $f(x, \dot{x}, \delta)$ is usually not exactly known or hard to invert, an approximation is introduced as:

$$\nu = \hat{f}(x, \dot{x}, \delta) \tag{5-27}$$

This results in a modelling error $\Delta(x, \dot{x}, \delta)$ in the system dynamics as:

$$\ddot{x} = \nu + \Delta(x, \dot{x}, \delta) \tag{5-28}$$

where

$$\Delta(x, \dot{x}, \delta) = f(x, \dot{x}, \delta) - \hat{f}(x, \dot{x}, \delta) \tag{5-29}$$

The approximation $\hat{f}$ is chosen such that an inverse with respect to δ exists.

Based on the approximation in (5-27), the actuator command is determined by an approximate dynamic inversion of the form:

$$\delta_{cmd} = \hat{f}^{-1}(x, \dot{x}, \nu) \tag{5-30}$$

where ν is the pseudo-control and represents a desired $\ddot{x}$ that is expected to be approximately achieved by δ_{cmd}.

The reference model dynamics is given as:

$$\ddot{x}_{rm} = \nu_{rm}(x_{rm}, \dot{x}_{rm}, x_c, \dot{x}_c) \tag{5-31}$$

where x_c, $\dot{x}_c$ represent external commands. The instantaneous pseudo-control output of the reference model ν_{rm} in the feed-forward path is given as:

$$\nu_{rm} = f_{rm}(x_{rm}, \dot{x}_{rm}, x_c, \dot{x}_c) \tag{5-32}$$

Hence, in order to achieve the required MRAC performance at the flight regimes, an adaptive element ν_{ad} must be introduced which is the output of properly-trained NN for cancelling out the nonlinear uncertainties $\Delta(x, \dot{x}, \delta)$. Therefore the NN plays a key role in the adaptive control design for achieving reconfigurable performance against system internal errors/uncertainties and external faults and disturbances. The benefit of this approach is that no model structure needs to be assumed in order to estimate the error (Kim & Calise, 2008).

5.3.3 Model tracking error dynamics

According to Figure 5-4, it is easy to see that the ultimate control aim is to design a desirable control law such that the output tracking error:

$$e(t) = x_{rm}(t) - x(t) \tag{5-33}$$

tends to zero and all the signals in the system remain bounded as $t \to \infty$. For this purpose, the total pseudo-control signal ν for the system is usually constructed by three components as:

$$\nu = \nu_{rm} + \nu_{pd} - \nu_{ad} \tag{5-34}$$

where ν_{rm} is the control signal generated by the reference model in (5-32), ν_{ad} is the NN adaptation signal, and ν_{pd} is the output of the linear PD compensator as shown in Figure 5-4.

The parameters for the reference model to generate signal ν_{rm} must contain the requirements of the closed-loop system. In aerospace control problems, these parameters are chosen to ensure that handling quality specifications are met. In the thesis, a second order reference model is chosen as:

$$x_{rm} = \frac{\omega_n^2}{s^2 + 2\xi\omega_n s + \omega_n^2} x_c \tag{5-35}$$

where ω_n is the natural frequency and ξ is the damping ratio.

The linear compensator signal ν_{pd} can be designed using standard linear control design techniques which render the closed-loop system stable, which usually include PD compensation (Calise, Hovakimyan & Idan, 2001).

For the second order system PD compensation is expressed as:

$$\nu_{pd} = [K_p \quad K_d]e \tag{5-36}$$

where the reference model tracking error is defined as:

$$e = \begin{bmatrix} x_{rm} - x \\ \dot{x}_{rm} - \dot{x} \end{bmatrix} \tag{5-37}$$

The model tracking error dynamics $\dot{e}$ are then found by differentiating e in (5-37) and substituting (5-28) and (5-29) as:

$$\dot{e} = Ae + B\left[\nu_{ad}(x, \dot{x}, \delta) - f(x, \dot{x}, \delta) + \hat{f}(x, \dot{x}, \delta)\right] \tag{5-38}$$

where

$$A = \begin{bmatrix} 0 & I \\ -K_p & -K_d \end{bmatrix},\ B = \begin{bmatrix} 0 \\ I \end{bmatrix} \tag{5-39}$$

where both K_p and K_d are real positive matrices. With the above form, A is *Hurwitz*, i.e. has eigenvalues with negative real parts. Then the error dynamics can be represented as:

$$\dot{e} = Ae + B[\nu_{ad}(x, \dot{x}, \delta) - \Delta(x, \dot{x}, \delta)] \tag{5-40}$$

where

$$\Delta(x, \dot{x}, \delta) = f(x, \dot{x}, \delta) - \hat{f}(x, \dot{x}, \delta) \tag{5-41}$$

is regarded as the model error $\Delta(x, \dot{x}, \delta)$ to be approximated and cancelled by the adaptive NN output ν_{ad}.

5.3.4 NN-based adaptation for reconfigurable FTFC

For the reformulated model of the nonlinear FTFC system, the input-output map of the SHL NN can be expressed in a more compact matrix form as (Hovakimyan, Nardi, Calise & Kim, 2002; Hovakimyan, Calise & Kim, 2004):

$$\nu_{ad}(W, V, \bar{x}) = W^T \sigma(V^T \bar{x}) \in \mathcal{R}^{n_3 \times 1} \tag{5-42}$$

where the following definitions are used:

$$\bar{x} = \begin{bmatrix} b_v \\ x_{in} \end{bmatrix} = \begin{bmatrix} b_v \\ x_1 \\ x_2 \\ \vdots \\ x_n \end{bmatrix} \in \mathcal{R}^{(n_1+1)\times 1} \tag{5-43}$$

$$\sigma(z) = \begin{bmatrix} b_w \\ \sigma_1(z_1) \\ \sigma_2(z_2) \\ \vdots \\ \sigma_n(z_n) \end{bmatrix} \in \mathcal{R}^{(n_2+1)\times 1} \tag{5-44}$$

$$V = \begin{bmatrix} \theta_{w,1} & \cdots & \theta_{w,n_2} \\ v_{1,1} & \cdots & v_{1,n_2} \\ \vdots & \ddots & \vdots \\ v_{n_1,1} & \cdots & v_{n_1,n_2} \end{bmatrix} \in \mathcal{R}^{(n_1+1)\times n_2}, W = \begin{bmatrix} \theta_{w,1} & \cdots & \theta_{w,n_3} \\ w_{1,1} & \cdots & w_{1,n_3} \\ \vdots & \ddots & \vdots \\ w_{n_{2+1},1} & \cdots & w_{n_{2+1},n_3} \end{bmatrix} \in \mathcal{R}^{(n_2+1)\times n_3} \tag{5-45}$$

where, $\bar{x}$ is the input vector, σ is the sigmoidal activation function vector; V is a weight matrix representing the inter-connections between the input and the hidden layers; W is a weight matrix representing the inter-connections between the hidden and output layers; ν_{ad} is the NN output; $b_v \geq 0$ and $b_w \geq 0$ are input biases that allow the thresholds θ_V and θ_W to be included in the V and W; n_1, n_2, and n_3 represent the number of input, hidden and output layer modes respectively.

The input to the hidden layer neuron is:

$$z = V^T \bar{x} = \begin{bmatrix} z_1 \\ \vdots \\ z_{n_2} \end{bmatrix} \in \mathcal{R}^{n_2 \times 1} \tag{5-46}$$

The sigmoidal activation function used is:

$$\sigma_j(z_j) = \frac{1}{1+e^{-a_j z_j}} \tag{5-47}$$

The NN on-line adaptive learning law is:

$$\begin{aligned} \dot{W} &= -(\sigma - \sigma' V^T \bar{x}) r^T \Gamma_W - \kappa_w \|e\| W \\ \dot{V} &= -\Gamma_V \bar{x} r^T W^T \sigma'(V^T \bar{x}) - \kappa_v \|e\| V \end{aligned} \tag{5-48}$$

with the signal r defined as follows:

$$r = e^T P B \in \mathcal{R}^{n_3 \times 1} \tag{5-49}$$

where $P \in \mathcal{R}^{2n \times 2n}$ is the positive definite solution to the Lyapunov equation:

$$A^T P + P A + Q = 0 \tag{5-50}$$

5.4 Reconfigurable FTFC improved by Concurrent Learning NN

Chowdhary and Johnson (2008, 2009, 2010, 2011a, 2011b, 2012) focused on an aspect of *concurrent learning* NN and presented an improved NN adaptor learning structure based on the use of current (online) information as well as stored (background) information. This concurrent online adaptation is aiming to improve the system performance over repeated manoeuvres since the concurrent NN adaptor re-learns the underlying model error function every time the manoeuvre is performed, which results in a global parameterization of the tracking error of the reconfigurable FTFC system. These authors show that the flight controller is expected to have improved performance when the aircraft repeats a manoeuvre that has been previously performed.

This Section introduces the crucial concepts of the concurrent learning NN for simultaneously using enough online information to accomplish better FTFC performance, according to the control scheme outlined in Section 5.3. A more compact system derived from the concurrent learning law is studied further in the simplified application. The simulation results of the Machan UAV illustrate excellent performance of the reconfigurable FTFC scheme.

5.4.1 Improved on-line NN adaptor based on concurrent learning concept

As introduced in Section 5.3, a recursive update law based SHL NN function is used as the adaptive element, then the model uncertainties are parameterized by the NN and an adaptive law using the available information in order to adapt to the unknown model dynamics. By choosing the appropriate values for the NN training rate parameters, the model tracking error and the NN weights (W, V) are ultimately bounded uniformly.

The tracking error obtained from (5-40) shows that the NN adaptive element should be able to form an arbitrarily accurate map relating the input space to the model error, leading asymptotically to reduced bounds on the error dynamics. In a practical sense, this should thus lead to a global parameterization of the modelling error limited only by the input space that has been used for the training purpose. However, the current NN training laws only achieve a local parameterization of the model error. In Chowdhary and Johnson work (2008, 2009, 2010, 2011, 2012), the reasons for achieving only a local parameterization when using instantaneous data for training NN in adaptive control architectures is mainly summarized as:

(1) Lack of direct training information:

Direct training information (r_c=$\nu_{ad} - \Delta$) is not presented to the NN, instead a linear function of the tracking error is presented as training input ($r = e^T PB$). This information is not directly presented because the accurate model of the system is not normally available, hence it may not be possible to accurately calculate Δ online. Conceptually, a NN trained in this way could be thought to comprise an action similar to an integrator-like control action which cancels only the local steady-state tracking error.

(2) Use of only instantaneous data:

The sequential method of training is susceptible to local adaptation because weight updates occur only based on the instantaneous data.

Thus a novel long term learning NN weight adaption law is proposed based on the use of arbitrary stored data along with sequential instantaneous data. The weight adaption accounts for the local learning phenomena exhibited by current adaptive control algorithm while allows long term learning with semi-global adaptation. This is the so-called “Concurrent Learning Law” that incorporates a long-term learning by manipulating the stored and instantaneous data concurrently for computing the NN adaptation. The memory of the learning law consists of selected and stored input-output data pairs that can be further

processed in the *background* and can be used for NN training, which ensures that the adaptation based on stored data in the memory does not sacrifice the instantaneous adaptability of the NN. In this way, the Concurrent Learning Law overcomes the limitations of other NN training laws that are designed for improving NN model error parameterization. This new approach has been well tested and found to be robust for long-term learning architectures such as adaptive flight control that must guarantee boundedness of all system signals (Chowdhary & Johnson, 2008).

5.4.2 Concurrent learning training law

The *Concurrent Learning Law* for the online NN weight training updates of W, V is presented as (Chowdhary & Johnson, 2008):

$$\begin{aligned} \dot{W}(t) &= \dot{W}_t(t) + W_c(t)\dot{W}_b(t) \\ \dot{V}(t) &= \dot{V}_t(t) + V_c(t)\dot{V}_b(t) \end{aligned} \tag{5-51}$$

where $\dot{W}_t(t)$ and $\dot{V}_t(t)$ denote any generalized adaptive law framework in (5-48) to be evaluated using the current data; and $\dot{W}_b(t)$ and $\dot{V}_b(t)$ denote the adaptive laws evaluated using the stored data.

The orthogonal projection matrices W_c and V_c are dependent on the actual form of the NN training law in (5-48). The following projection matrices can be used:

$$W_c = \left(I - \frac{\Gamma_V \sigma^T \Gamma_V}{\sigma^T \sigma}\right), V_c = \left(I - \frac{\bar{x}\bar{x}^T}{\bar{x}^T \Gamma_V \Gamma_V \bar{x}}\right) \tag{5-52}$$

Hence, the complete training law is determined by combining (5-48) with (5-52) into (5-51), so that (5-51) can be simply expressed as a linear combination of the background and current learning laws as follows:

$$\begin{aligned} \dot{W} &= -(\sigma - \sigma' V^T \bar{x}) r^T \Gamma_W - k\|e\| W - W_c \textstyle\sum_{i=1}^{p} (\sigma_i - \sigma_i' V^T \bar{x}_i) r_{c_i}^T \Gamma_W \\ \dot{V} &= -\Gamma_V \bar{x} r^T W^T \sigma'(V^T \bar{x}) - k\|e\| V - V_c \textstyle\sum_{i=1}^{p} \Gamma_V \bar{x}_i r_{c_i}^T W^T \sigma'(V^T \bar{x}_i) \end{aligned} \tag{5-53}$$

where the background learning NN training signal is given by $r_{c_i} = v_{ad_i} - \Delta(\bar{x}_i, \delta_i)$ for every stored data point i, where σ, $\bar{x}$, r^T, Γ_W, Γ_V as defined in Section 5.3.

Following (5-51) the background data training are restricted to the subspace that is orthogonal to the linear combinations of the weight updates based on instantaneous data. It is important to note that the stored data can be used for concurrent adaptation to new data points, to improve further control performance without sacrificing the performance of the adaptive law to adapt.

Selection of the NN input data points for concurrent learning is given by satisfying the following criterion (Chowdhary & Johnson, 2008):

$$\frac{(\bar{x}-\bar{x}_p)^T(\bar{x}-\bar{x}_p)}{\bar{x}^T\bar{x}} > \varepsilon_{\bar{x}} \tag{5-54}$$

where the subscript p denotes the index of the last data point stored. The above method ascertains that only those data points are selected that are sufficiently different from the last data point stored. Since concurrent learning does not affect the performance of the primary learning law, it is possible to process the data point x_i further to extract information about the model error dynamics.

In the adaptive control framework given in (5-40) and (5-41), the model error Δ_i for the i^{th} data point is given by following (5-41) as:

$$\Delta_i(x_i, \dot{x}_i, \delta_i) = f_i(x_i, \dot{x}_i, \delta_i) - \hat{f}(x_i, \dot{x}_i, \delta_i) \tag{5-55}$$

By using (5-24) and (5-27), the above can be expressed as:

$$\Delta_i(x_i, \dot{x}_i, \delta_i) = \ddot{x}_i - \nu_i \tag{5-56}$$

In this way, the limitation on *lack of direct training information* mentioned in Section 5.4.1 can be alleviated for concurrent training. The residual signal that is used in the concurrent learning adaptation is (Chowdhary & Johnson, 2008):

$$r_{c_i} = W^T\sigma(V^T\bar{x}_i) - \Delta_i \tag{5-57}$$

Expressed in this form of (5-57) the function of the concurrent learning NN residual signal is to reduce the error between the current and stored model data. By incorporating r_{c_i}within a stable adaption law, the concurrent learning NN is forced to adapt the W and V weight matrices in such a way that the difference between the NN adaption and the model error for multiple data points are simultaneously reduced.

In summary, the underlying concept in the *Concurrent Learning Law* is to train the NN using stored and current data simultaneously in order to improve the NN global learning behaviour and guarantee long term adaptation. It is proposed that the total concurrent learning be found by simply summing the individual contributions of the stored (background) data point adaptation and then projecting the total contributions into the null-space of the current learning as in (5-51). Since the learning on stored (background) data takes place in the null-space of the learning based on instantaneous data, it does not affect the weight updates based on the instantaneous data.

5.4.3 Stability analysis using Lyapunov theorems

Chowdhary and Johnson (2008) derive the stability of the NN adaptor combined current and background learning law in the framework of control structure introduced in Section 5.4.2.

The *Proof* begins with the following assumptions:

- **Assumption 1**: The norms of the ideal weights W^*, V^* are bounded by a known positive values, according to:

$$0 < \|Z^*\|_F \leq \bar{Z} \tag{5-58}$$

  where $\|\cdot\|_F$ denotes the Frobenius norm and $Z = \begin{bmatrix} V & 0 \\ 0 & W \end{bmatrix}$.

- **Assumption 2**: The external commands x_c remain bounded.

- **Assumption 3**: The reference model is chosen such that the reference model states remain bounded, as:

$$\|e_r\| \leq \bar{e_r} \tag{5-59}$$

- **Assumption 4**: The NN approximation $\Delta(x, \dot{x}, \delta) = W^{*T}\bar{\sigma}\left(V^{*T}\bar{x}\right) + \bar{\varepsilon}(x)$ from (5-20), holds in a compact domain D, which is sufficiently large. Let the inputs to the NN be given by $\bar{x} = [b_v \quad x^T \quad \dot{x}^T]^T$, then $\|\bar{x}\| \leq b_v + x_c$ for some positive constant x_c, which is the inputs to the NN remain bounded.

Now consider the system in (5-24), with the inverting controller of (5-30) and the online NN training signal $r = e^T PB$, the background NN training signal given by (5-57) and the SHL NN output ν_{ad} given by (5-42). If the structure of the concurrent adaption law is characterized by (5-51), with W_c, V_c as given in (5-52), then the model-reference tracking error e, and the NN weight errors $\widetilde{W}$, $\tilde{V}$ are uniformly ultimately bounded.

Proof: The NN sigmoidal activation function given by (5-44) and its derivative can be bounded as follows (Chowdhary & Johnson, 2008):

$$\|\sigma(V^T\bar{x})\| \leq b_w + n_2 \tag{5-60}$$

$$\|\sigma'(V^T\bar{x})\| \leq \bar{a}(b_w + n_2)(1 + b_w + n_2) = 2k_1k_2 \tag{5-61}$$

where $\bar{a}$ is the maximum activation potential, and $k_1 = b_w + n_2$, $k_2 = 1 + b_w + n_2$ are constants defined for convenience. A further note can be added that due to **Assumption 4**, the input to the NN can be bounded as follows:

$$\|\bar{x}\| \leq b_v + x_c \tag{5-62}$$

The *Taylor series expansion* of the sigmoidal activation function about the ideal weight can be given by:

$$\sigma\left(V^{*T}\bar{x}\right) = \sigma(V^T\bar{x}) + \frac{\partial\sigma(Z)}{\partial z}\Big|_{z=V^T\bar{x}}\left(V^{*T}\bar{x} - V^T\bar{x}\right) + \Theta \tag{5-63}$$

where Θ represents the higher order terms of (5-63). A bound on Θ can be found by rearranging (5-63) as:

$$\|\Theta\| \leq \left\|\sigma\left(V^{*T}\bar{x}\right)\right\| + \|\sigma(V^T\bar{x})\| + \|\sigma'(V^T\bar{x})\|\left\|\tilde{V}\right\|\|\bar{x}\| \leq 2k_2 + \bar{a}k_1k_2(b_v + x_c)\left\|\tilde{Z}\right\|_F \tag{5-64}$$

where Z is defined as in **Assumption 1**, and $\tilde{Z} = Z - Z^*$, with $\tilde{V} \triangleq V - V^*$, $\widetilde{W} \triangleq W - W^*$ are the NN estimation update law errors as in (5-19). Then the error in the NN parameterization for a given state $(x, \dot{x})$ can be written as:

$$\nu_{ad}(x,\dot{x}) - \Delta(x,\dot{x}) = W^T\sigma(V^T\bar{x}) - W^{*T}\sigma\left(V^{*T}\bar{x}\right) + \varepsilon(x,\dot{x}) \tag{5-65}$$

Using the Taylor series expansion for the sigmoidal activation function from (5-63) this can be further expanded to:

$$\begin{aligned}\nu_{ad}(x,\dot{x}) - \Delta(x,\dot{x}) &= W^T\sigma(V^T\bar{x}) - W^{*T}\left(\sigma(V^T\bar{x}) + \sigma'(V^T\bar{x})\tilde{V}^T\bar{x} + \Theta\right) + \varepsilon(x,\dot{x}) \\ &= \widetilde{W}^T(\sigma(V^T\bar{x}) - \sigma'(V^T\bar{x})V^T\bar{x}) + W^T\sigma'(V^T\bar{x})\tilde{V}^T\bar{x} + w\end{aligned} \tag{5-66}$$

where w is given by:

$$w = \widetilde{W}^T\sigma'\left(V^{*T}\bar{x}\right)V^{*T} + W^{*T}(\Theta) + \varepsilon(x,\dot{x}) \tag{5-67}$$

Bounds on w can then be obtained from (5-67) combining (5-58), (5-61) and (5-64) as:

$$\begin{aligned}\|w\| &\leq \left\|\widetilde{W}^T\right\|\left\|\sigma'\left(V^{*T}\bar{x}\right)\right\|\|V^*\| + \|W^*\|\|\Theta\| + \bar{\varepsilon} \\ &\leq \bar{a}k_1k_2\bar{Z}\left\|\tilde{Z}\right\|_F + \bar{Z}\left(2k_1 + \bar{a}k_1k_2(b_v + x_c)\left\|\tilde{Z}\right\|_F + \bar{\varepsilon}\right)\end{aligned} \tag{5-68}$$

The elements c_0 and c_1 are then defined as:

$$\begin{aligned}c_0 &= \bar{\varepsilon} + 2\bar{Z}k_1 \\ c_1 &= \bar{a}k_1k_2\bar{Z} + \bar{Z}\bar{a}k_1k_2(b_v + x_c)\end{aligned} \tag{5-69}$$

Then from (5-68) it follows that:

$$\|w\| \leq c_0 + c_1\left\|\tilde{Z}\right\|_F \tag{5-70}$$

Based on the above Assumptions and analysis, the Lyapunov 2nd theorem can be used to show the boundedness of the reference model errors and the NN online adaptive weights.

A radially unbounded and positive definite Lyapunov candidate is chosen as (Chowdhary & Johnson, 2008):

$$L\left(e,\widetilde{W},\tilde{V}\right)=\frac{1}{2}e^{T}Pe+\frac{1}{2}tr\left(\widetilde{W}\Gamma_{w}^{-1}\widetilde{W}^{T}\right)+\frac{1}{2}tr\left(\tilde{V}^{T}\Gamma_{v}^{-1}\tilde{V}\right) \tag{5-71}$$

where $tr(\cdot)$ denotes the trace operator. Differentiating the Lyapunov candidate in (5-71) along the trajectory of system described by (5-38)-(5-41), results in:

$$\dot{L}\left(e,\widetilde{W},\tilde{V}\right)=-\frac{1}{2}e^{T}Qe+e^{T}PB(\nu_{ad}-\Delta)+tr\left(\dot{W}\Gamma_{w}^{-1}\widetilde{W}^{T}\right)+tr\left(\tilde{V}\Gamma_{v}^{-1}\dot{V}^{T}\right) \tag{5-72}$$

Expanding the NN model parameterization error using (5-66), and substituting (5-51) and adding and subtracting the following elements:

$$\begin{gathered}\sum_{i=1}^{P}\left(\nu_{ad}(x_i,\dot{x}_i)-\Delta(x_i,\dot{x}_i)\right)^{T}\left(\nu_{ad}(x_i,\dot{x}_i)-\Delta(x_i,\dot{x}_i)\right)\\ tr\left(k\|e\|W\widetilde{W}^{T}\right)\\ tr\left(k\|e\|V\tilde{V}^{T}\right)\end{gathered} \tag{5-73}$$

Resulting in:

$$\begin{aligned}\dot{L}\left(e,\widetilde{W},\tilde{V}\right)=&-\frac{1}{2}e^{T}Qe+e^{T}PB\left[\widetilde{W}^{T}(\sigma(V^{T}\bar{x})-\sigma'(V^{T}\bar{x})V^{T}\bar{x})+W^{T}\sigma'(V^{T}\bar{x})\tilde{V}^{T}\bar{x}+w\right]\\&+tr\left[\left(\dot{W}_t+W_c\dot{W}_b\right)\Gamma_{w}^{-1}\widetilde{W}^{T}\right]+tr\left[\tilde{V}\Gamma_{v}^{-1}\left(\dot{V}_t+V_c\dot{V}_b\right)^{T}\right]\\&+\sum_{i=1}^{P}\left(\nu_{ad}(x_i,\dot{x}_i)-\Delta(x_i,\dot{x}_i)\right)^{T}\left(\nu_{ad}(x_i,\dot{x}_i)-\Delta(x_i,\dot{x}_i)\right)\\&-\sum_{i=1}^{P}\left(\nu_{ad}(x_i,\dot{x}_i)-\Delta(x_i,\dot{x}_i)\right)^{T}\left(\nu_{ad}(x_i,\dot{x}_i)-\Delta(x_i,\dot{x}_i)\right)\\&+tr\left(k\|e\|W\widetilde{W}^{T}\right)-tr\left(k\|e\|W\widetilde{W}^{T}\right)+tr\left(k\|e\|V\tilde{V}^{T}\right)-tr\left(k\|e\|V\tilde{V}^{T}\right)\end{aligned} \tag{5-74}$$

Using (5-66) to expand $\nu_{ad}(x_i,\dot{x}_i)-\Delta(x_i,\dot{x}_i)$, collecting terms, and setting the following to zero:

$$\begin{gathered}tr\left\{\left[(\sigma(V^{T}\bar{x})-\sigma'(V^{T}\bar{x})V^{T}\bar{x})e^{T}PB+k\|e\|W+\dot{W}_t\Gamma_{w}^{-1}\right]\widetilde{W}^{T}\right\}=0\\ tr\left\{\tilde{V}^{T}\left[\bar{x}e^{T}PBW^{T}\sigma'(V^{T}\bar{x})+k\|e\|V^{T}+\Gamma_{v}^{-1}\dot{V}_t\right]\right\}=0\end{gathered} \tag{5-75}$$

$$\begin{gathered}tr\left\{\left[\sum_{i=1}^{P}\left((\sigma(V^{T}\bar{x}_i)-\sigma'(V^{T}\bar{x}_i)V^{T}\bar{x}_i)r_{b_i}^{T}+W_c\dot{W}_b\Gamma_{w}^{-1}\right)\right]\widetilde{W}^{T}\right\}=0\\ tr\left\{\tilde{V}^{T}\left[\sum_{i=1}^{P}\bar{x}_i r_{b_i}^{T}W^{T}\sigma'(V^{T}\bar{x}_i)+\Gamma_{v}^{-1}V_c\dot{V}_b\right]\right\}=0\end{gathered} \tag{5-76}$$

which leads to:

$$\begin{gathered}\dot{W}_t=-(\sigma(V^{T}\bar{x})-\sigma'(V^{T}\bar{x})V^{T}\bar{x})e^{T}PB\Gamma_w-k\|e\|\Gamma_w W\\ \dot{V}_t=-\Gamma_v\bar{x}e^{T}PBW^{T}\sigma'(V^{T}\bar{x})-k\|e\|\Gamma_v W\end{gathered} \tag{5-77}$$

and

$$W_c\dot{W}_b = -\sum_{i=1}^{P}\left((\sigma(V^T\bar{x}_i) - \sigma'(V^T\bar{x})V^T\bar{x}_i)r_{b_i}^T\Gamma_w\right)$$
$$V_c\dot{V}_b = -\sum_{i=1}^{P}\Gamma_v\bar{x}_i r_{b_i}^T W^T\sigma'(V^T\bar{x}_i) \tag{5-78}$$

Noting that the orthogonal projection operators are idempotent and hence multiplying both sides of (5-78) by W_c and V_c, respectively results in:

$$W_c\dot{W}_b = -W_c\sum_{i=1}^{P}\left((\sigma(V^T\bar{x}_i) - \sigma'(V^T\bar{x})V^T\bar{x}_i)r_{b_i}^T\Gamma_w^{-1}\right)$$
$$V_c\dot{V}_b = -V_c\sum_{i=1}^{P}\Gamma_v\bar{x}_i r_{b_i}^T W^T\sigma'(V^T\bar{x}_i) \tag{5-79}$$

The required concurrent training law of (5-53) follows by adding (5-77) and (5-79) results. The time derivative of the Lyapunov candidate (5-72) is now reduced to:

$$\dot{L}(e,\widetilde{W},\tilde{V}) = -\frac{1}{2}\lambda_{min}(Q)\|e\|^2 + \|e^TPB\|\|w\|$$
$$-\sum_{i=1}^{P}\|r_{b_i}\|^2 + \sum_{i=1}^{P}\|r_{b_i}\|\|w_i\| - k\|e\|\|\tilde{Z}\|_F^2 + k\|e\|\|\tilde{Z}\|_F\bar{Z} \tag{5-80}$$

By using previously computed bounds (5-70) then (5-80) is as:

$$\dot{L}(e,\widetilde{W},\tilde{V}) \le -\frac{1}{2}\lambda_{min}(Q)\|e\|^2 + \|e\|\|PB\|\left(c_0 + c_1\|\tilde{Z}\|_F\right)$$
$$-\sum_{i=1}^{P}\|r_{b_i}\|^2 + \sum_{i=1}^{P}\|r_{b_i}\|\left(c_0 + c_1\|\tilde{Z}\|_F\right) - k\|e\|\|\tilde{Z}\|_F^2 + k\|e\|\|\tilde{Z}\|_F\bar{Z} \tag{5-81}$$

Hence when $\lambda_{min}(Q)$ and k are sufficiently large, $\dot{L}(e,\widetilde{W},\tilde{V}) \le 0$ is everywhere outside of a compact set. Therefore, the system states are bounded. Specifically, $\dot{L}(e,\widetilde{W},\tilde{V}) \le 0$ when:

$$\|e\| \ge \frac{-a_0 + \sqrt{{a_0}^2 + 2\lambda_{min}(Q)\left(-\sum_{i=1}^{P}\|r_{b_i}\|^2 + \sum_{i=1}^{P}\|r_{b_i}\|\left(c_0 + c_1\|\tilde{Z}\|_F\right)\right)}}{\lambda_{min}(Q)}$$
$$= b_e\left(\|\tilde{Z}\|, \lambda_{min}(Q), \sum_{i=1}^{P}\|r_{b_i}\|\right) \tag{5-82}$$

where $a_0 = \|PB\|(c_0 + c_1\|\tilde{Z}\|) - k\|\tilde{Z}\|^2 + \|\tilde{Z}\|\bar{Z}$.

Condition 1: $\|e\| = 0$, $\|w_i\| = 0$, or $\|e\| \ne 0$, $\sum_{i=1}^{P}\|r_{b_i}\| \ne 0$, and

$$\|\tilde{Z}\| \ge \frac{-b_0 + \sqrt{{b_0}^2 + 4k\|e\|\left(-\frac{1}{2}\lambda_{min}(Q)\|e\|^2 + \|e\|\|PB\|c_0 - \sum_{i=1}^{P}\|r_{b_i}\|^2 + \sum_{i=1}^{P}\|r_{b_i}\|c_0\right)}}{\lambda_{min}(Q)}$$
$$= b_z\left(\|e\|, \sum_{i=1}^{P}\|r_{b_i}\|\right) \tag{5-83}$$

where $b_0 = \|e\|\|PB\|c_1 + \sum_{i=1}^{P}\|r_{b_i}\| c_1 + k\|e\|\bar{Z}$.

Condition 2: $\|e\| \neq 0$, $\|\tilde{Z}\| \neq 0$ and

$$\sum_{i=1}^{P}\|r_{b_i}\| \geq \frac{-(c_0+c_1\|\tilde{Z}\|_F)+\sqrt{(c_0+c_1\|\tilde{Z}\|_F)^2+4d_0}}{2} = b_{r_b}(\|e\|, \|\tilde{Z}\|) \tag{5-84}$$

where $d_0 = -\frac{1}{2}\lambda_{min}(Q)\|e\|^2 - k\|e\|\|\tilde{Z}\|_F + k\|e\|\|\tilde{Z}\|_F\bar{Z} + \|e\|\|PB\|\left(c_0 + c_1\|\tilde{Z}\|_F\right)$.

The curves represented by $b_e(\|\tilde{Z}\|, \lambda_{min}(Q), \sum_{i=1}^{P}\|r_{b_i}\|)$, $b_z(\|e\|, \sum_{i=1}^{P}\|r_{b_i}\|)$, $b_{r_b}(\|e\|, \|\tilde{Z}\|)$ are guaranteed to intersect, which means there is always a solution that satisfies the Lyapunov stability criterion. This completes the proof.

Thus, the system signals are all bounded in the sense of Lyapunov stability. With the incorporation of background learning, the bound on the time derivative of the Lyapunov function along the system trajectory is also a function of the NN adaption error for the data points. If no background points are stored, then the NN weight adaption law reduces to that of (5-48). This indicates that the purely online NN weight adaption method is a special case of the more general online and background weight adaption method of (5-51).

5.4.4 Change in concurrent learning training law for practice

Figure 5-5 shows that the schematic of the concurrent learning architecture requires that data points are processed in a sequential manner as they are presented to the NN. Data points that are found to be of particular interest for satisfying (5-54) are then stored in a particular history stack circle that simulates the long-term memory.

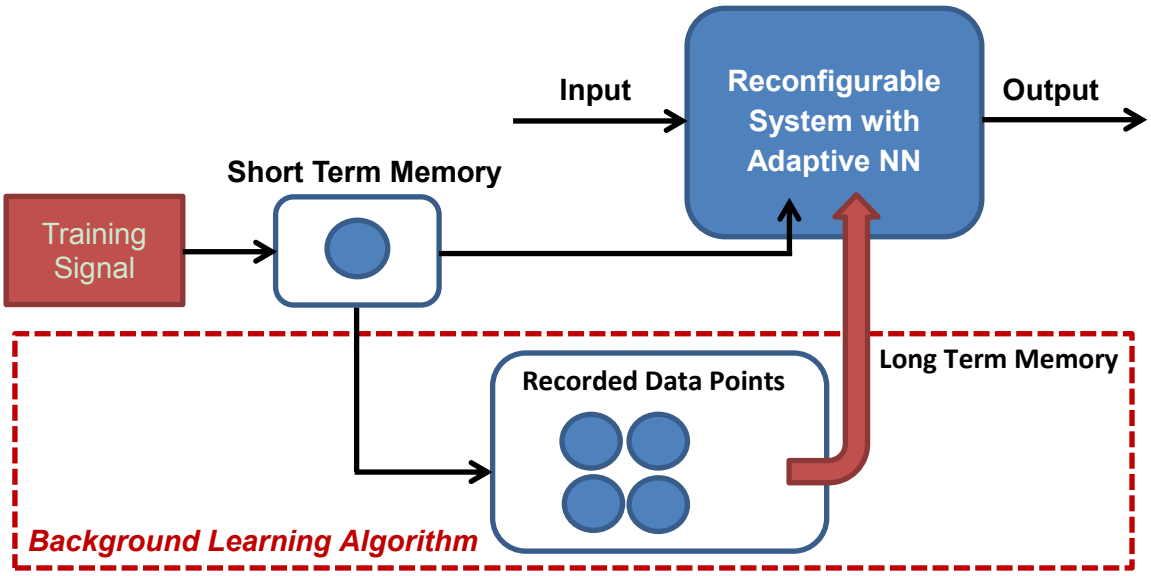

Figure 5-5 Schematic of the concurrent learning NN adaptor element

This strategy leads to a more complicated adaptive control architecture including an extra compute and store element for recording a sufficient number of points for concurrent training. Moreover, the superior reconfigurable performance is assumed to occur during repeated command signals that are already recorded in the memory stack for further NN adaptive training. The cost coming from the sophisticated system architecture may not be worthwhile considering the unpromising control performance and considering that the various uncertainties, faults and disturbances are always unknown and unexpected in practice. This performance should take into account practical on-line computation efficiency.

This online computation efficiency is taken into account here by simplifying the selection of the data for concurrent training by removing the history circle stack element described by (Chowdhury & Johnson, 2008) since the data chosen criteria are not involved in the stability analysis in Section 5.4.3. It should be noted that removal of the history circle stack may not lead to superior global approximation performance. However, repeated update sequences of the system input will not guarantee the improvement of the long-term compensation performance with respect to system uncertainties, unwanted faults and unexpected external disturbances. Hence, the assumption of repeated information for background training may also not be a good reason for building such a complicated system, not to mention that additional faults/disturbances may occur in the added elements.

For the purpose of simplifying the control scheme and to facilitate the application to a broad class of real problems without significantly compromising the adaptive performance, a simplified strategy for data handling is studied here and evaluated for the concurrent NN weight learning. The signal ($r_c = \nu_{ad} - \Delta$) is included in the training information for minimizing the tracking error and the history data are also presented online to the NN weight updating law. However, in this work a modified form of (5-51) is chosen for $\dot{W}_b$ and $\dot{V}_b$ as:

$$\begin{aligned} \dot{W}_b(t) &= \sum_{\tau=0}^{p-1}\left(\sigma - \sigma' V^T \bar{x}_{(t+\tau\cdot\Delta t)}\right) r_{c_{(t+\tau\cdot\Delta t)}}^T \Gamma_W \\ \dot{V}_b(t) &= \sum_{\tau=0}^{p-1} \Gamma_V \bar{x}_{(t+\tau\cdot\Delta t)} r_{c_{(t+\tau\cdot\Delta t)}}^T W^T \sigma'\left(V^T \bar{x}_{(t+\tau\cdot\Delta t)}\right) \end{aligned} \tag{5-85}$$

where p denotes the number of chosen data and Δt denotes the time interval for concurrent training. The advantage of this approach is that there is no need to involve either the data selection criterion of (5-54) or the history stack memory element in Figure 5-5. All the data recorded for concurrent learning are linear combinations of the current signal and its time delays at every recording time interval Δt. Figure 5-6 gives the new scheme of the modified concurrent NN learning method.

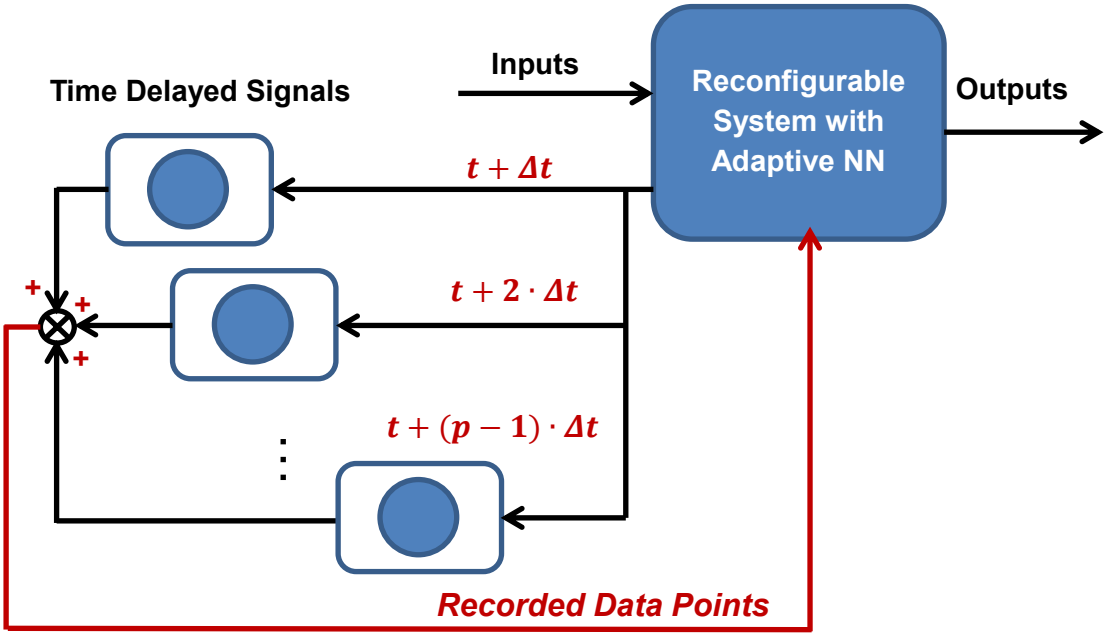

Figure 5-6 Reconfigurable FTFC scheme of the modified concurrent NN learning law

5.5 Simulation and Evaluation

This section shows that ultimate boundedness of all system signals can be guaranteed when the new scheme shown in Figure 5-6 is used in an MRAC framework with a SHL NN as the adaptive element. Simulation results for the Machan UAV model confirm the stability and improved performance as well as practical value of this approach.

5.5.1 Control parameters design

The Machan UAV modelled in Chapter 3 is used to illustrate the improved NN-based reconfigurable FTFC system designed in this chapter. The control design was carried out by assuming that the pilot command signals are used to control the three angles ϕ, θ, and ψ corresponding to appropriate subsystems that are linearized and decoupled by the dynamic inversion controller.

Consider the θ-channel control architecture design as an example, the structure of the linear PD compensator in (5-36) for stabilizing the tracking error dynamics with a second order reference model in (5-35) introduced to generate reference signals, is shown in Figure 5-7.

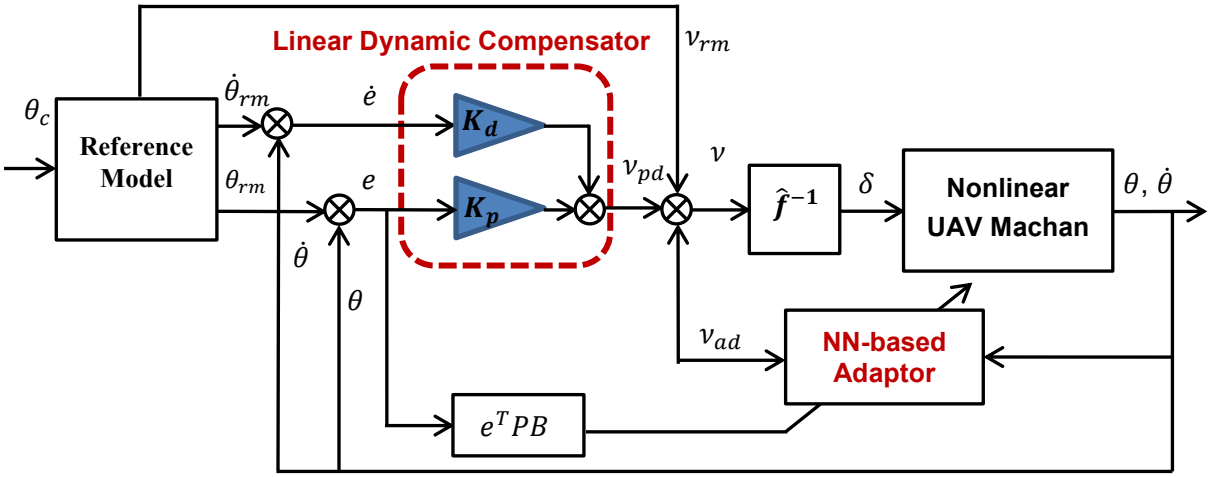

Figure 5-7 Linear PD compensator in the NN-based reconfigurable FTFC scheme

The second order reference models in (5-35) are chosen with $\omega_n = 3rad \cdot s^{-1}$ and $\xi = 1$. The PD compensator gains K_p and K_d are related to the natural frequency ω_n and damping ratio ξ of the reference model as:

$$K_p = \omega_n^2, \qquad K_d = 2\xi\omega_n$$

The state inputs for the NN adaptor defined in Section 5.3.4 are chosen as:

$$\bar{x} = [b_v \quad e_\theta \quad \dot{e}_\theta \quad \theta \quad \dot{\theta} \quad \ddot{\theta} \quad \nu_{ad} \quad \|Z\|]$$

The values selected for the NN adaptor, the number of hidden layer neurons n_2, and the number of inputs n_2, including input/output delays, to NN the update laws in (5-48) are given in Table 5-1.

Table 5-1 Adaptive NN parameters

Channel	Γ_V	Γ_W	κ_v	κ_w	n_1	n_2
θ	3.0	3.0	0.1	0.1	10	20

Following the suggested positive definite matrix solution to the Lyapunov equation (5-50), the matrix solution is taken as:

$$Q = \begin{bmatrix} 1 & 0 \\ 0 & 2 \end{bmatrix}.$$

The Machan UAV control surfaces are driven by the servo-controller actuators to produce the deflections commanded by the flight control system. The control surface actuators are modelled as first-order systems in (3-35) with known gains and time constants. The actuator signals have magnitude and deflection rate limits summarized in Table 5-2 according to a similar UAV study of Sonneveldt (2006).

Table 5-2 Aircraft control effectors and their dynamic constraints

Name	Symbol	Magnitude Limits (deg)	Rate Limits (deg/sec)
Aileron	δ_a	-20 to +20	-80 to +80
Elevator	δ_e	-25 to +25	-60 to +60
Rudder	δ_r	-30 to +30	-120 to +120

The Machan simulation model is constructed to implement the UAV's preliminary configuration data, mass properties and static wind tunnel data. The aircraft trim condition corresponds to: $V_T = 33m \cdot s^{-1}$, $h = 40m$. The trimmed throttle setting is chosen (fixed) to give a constant thrust of $X_e = 55N$ for ensuring that the rolling moment L_E $(m \cdot s^{-1})$ has non-zero value. All simulations begin from this trim condition.

5.5.2 Simulation and evaluation

In this Section some flight simulation results are given that characterize the benefits of using combined online and background learning adaptive control. For the FTFC system design of Machan, only simple static wind tunnel test data and mass properties were available. Its flight envelope includes low altitude and low speeds where air disturbances are common. The turbulence model is implemented in all the Machan control simulations and is modelled as Gaussian white noise signal shaped by a Dryden wind spectrum as described by (3-47). The command signal for the θ-channel is always chosen as: $\theta_c = 0.5rad$.

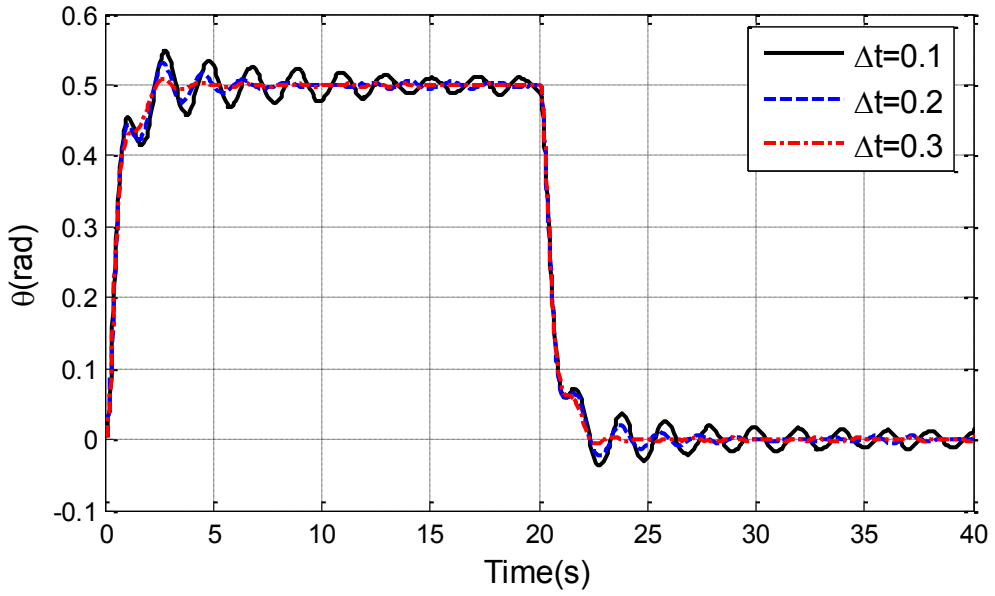

Figure 5-8 Concurrent NN-based system performances with various time delay intervals

Figure 5-8 shows the system tracking performances with the improved concurrent NN learning system under various values of time delay interval Δt in (5-85), demonstrating that the number of data samples and the sampling rate both affect the system responses. The following simulations use 5 data points and the sample time intervals are set as $\Delta t = 0.2\ s$.

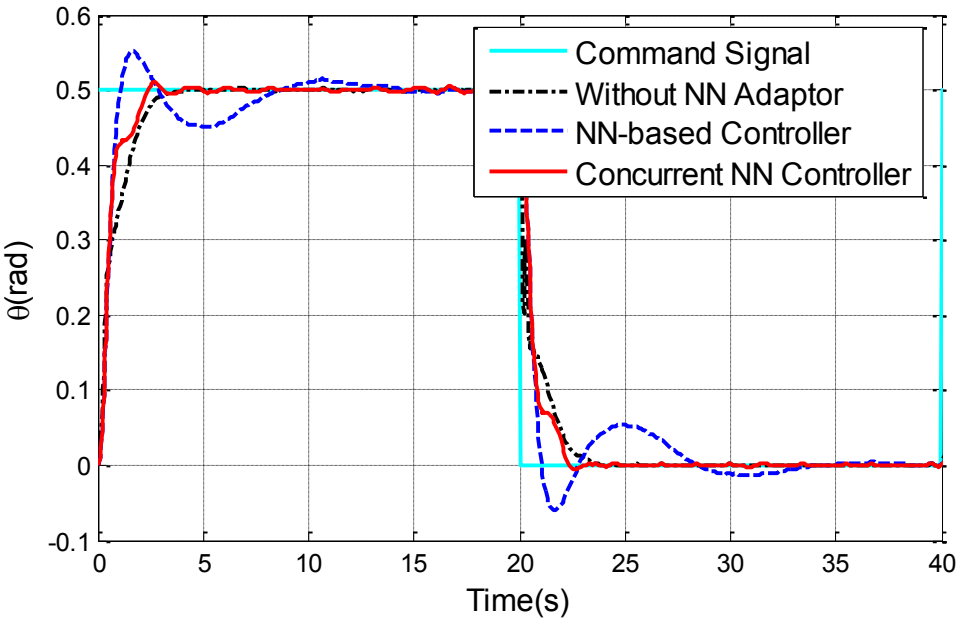

Figure 5-9 Reconfigured system performance (no fault or disturbance)

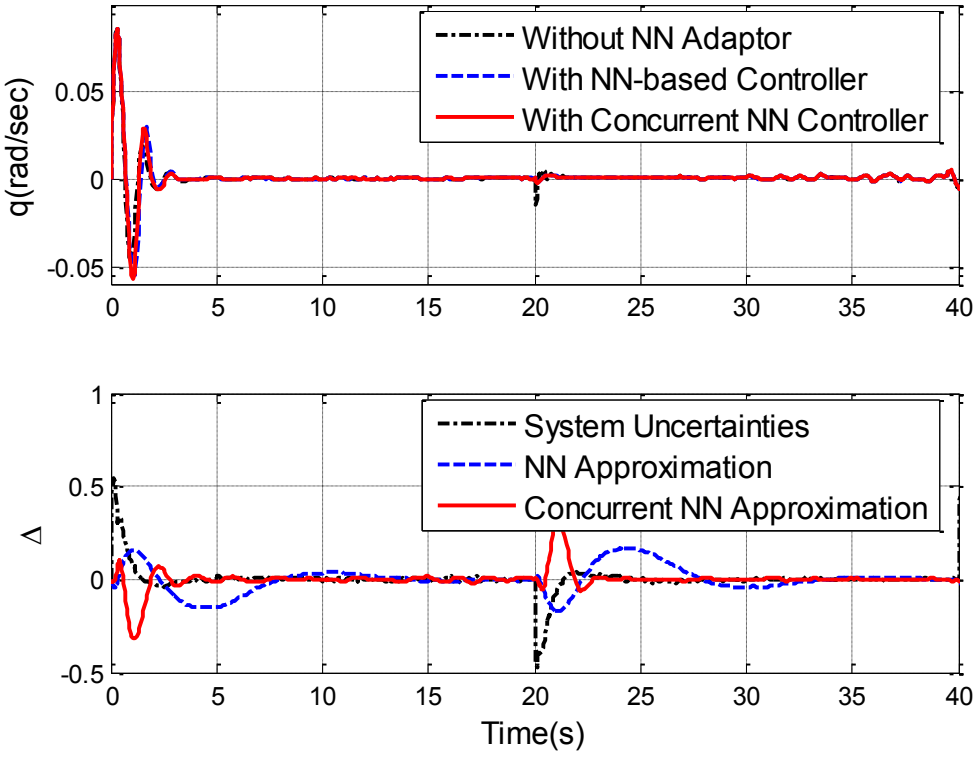

Figure 5-10 Pitch rate & uncertainty approximation (no fault or disturbance)

Figure 5-9 shows the tracking performance of the three controllers with no fault acting on the aircraft and Figure 5-10 shows the corresponding responses of the pitch rate q and the approximation values of the system uncertainty $\Delta(x,u)$. It is clear that the pitch angle θ of each controller follows successive step input command signals and there is considerable improvement between the classical NN adaptor and the improved concurrent NN adaptor.

For testing the robustness and reconfigurable performance of the three designed controllers, recall Section 3.4.2 for the modelled faults. The sensor bias fault of θ-channel is set as: $\theta_{out}(t) = \theta_{in}(t) + \Delta_{sensor}$, $(\Delta_{sensor} = 0.2)$ from continuous time $t = 0s$.

Figure 5-11 shows the system performances of three controllers with the pitch angle sensor bias and Figure 5-12 shows the corresponding responses of pitch rate and uncertainty approximation with sensor bias. The concurrent learning NN shows that a clear improvement in performance is seen characterized by the efficient tracking of the command signal.

Following this a pitch angle sensor calibration error fault is chosen as $\theta_{out}(t) = \beta \cdot \theta_{in}(t)$, $(\beta = 0.7)$ from continuous time $t = 0s$ to further validate the controller response. Figure 5-13 compares the system performances of the three controllers with the sensor calibration error and Figure 5-14 shows the corresponding responses of the angle rate and uncertainty approximation with this kind of sensor fault. The concurrent learning NN demonstrates that there is a clear improvement in the tracking performance of the command signal.

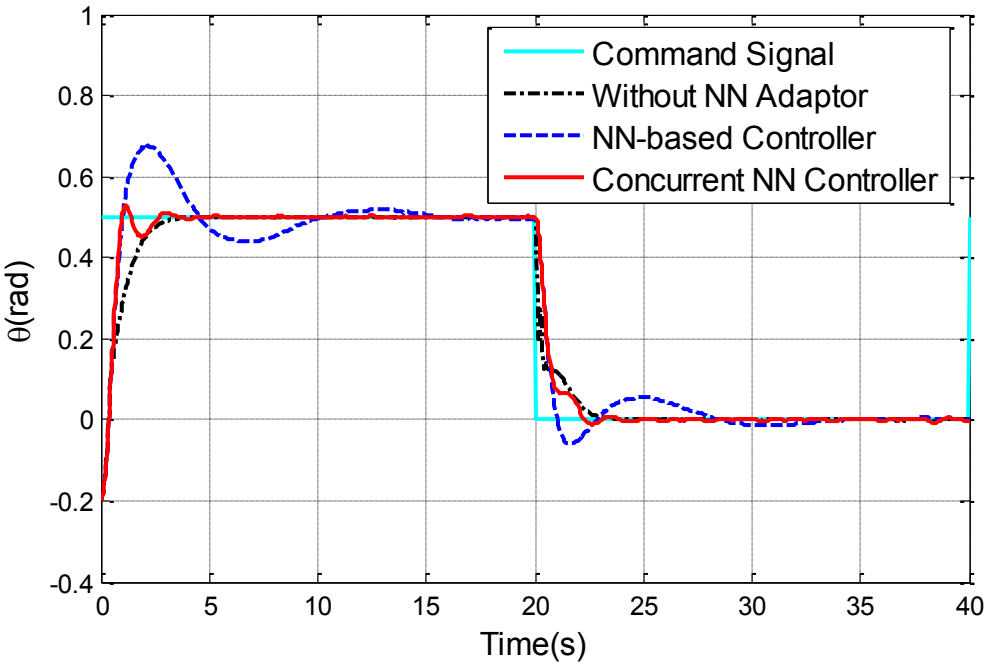

Figure 5-11 Reconfigured system performance with +0.2 sensor bias

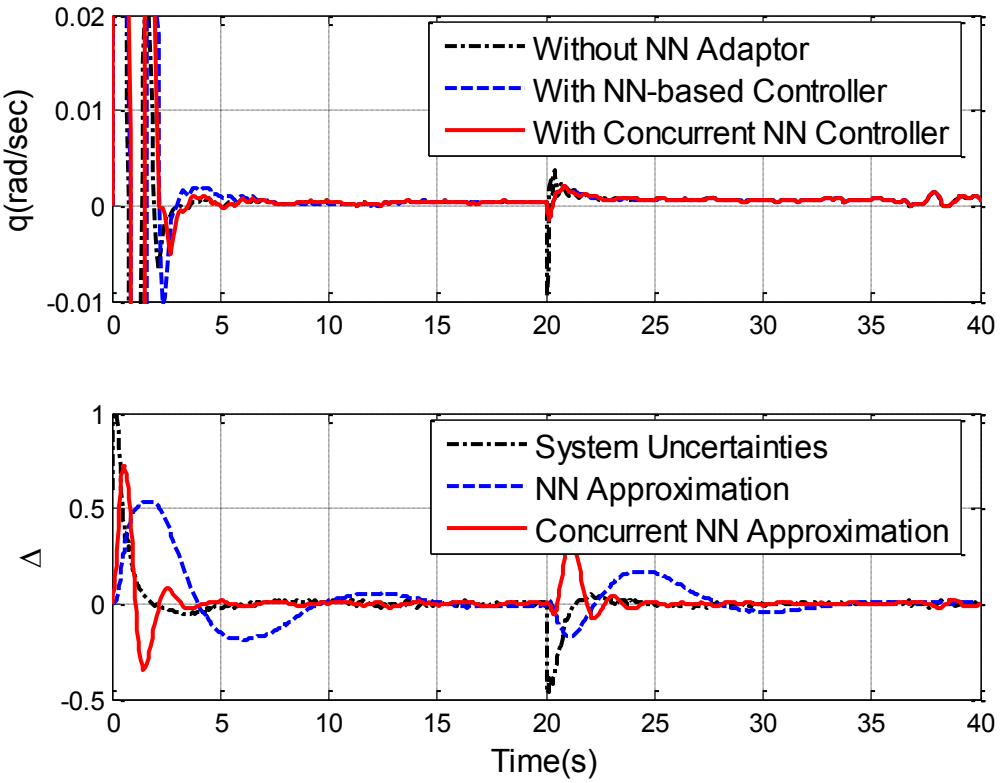

Figure 5-12 Pitch rate & uncertainty approximation with +0.2 sensor bias

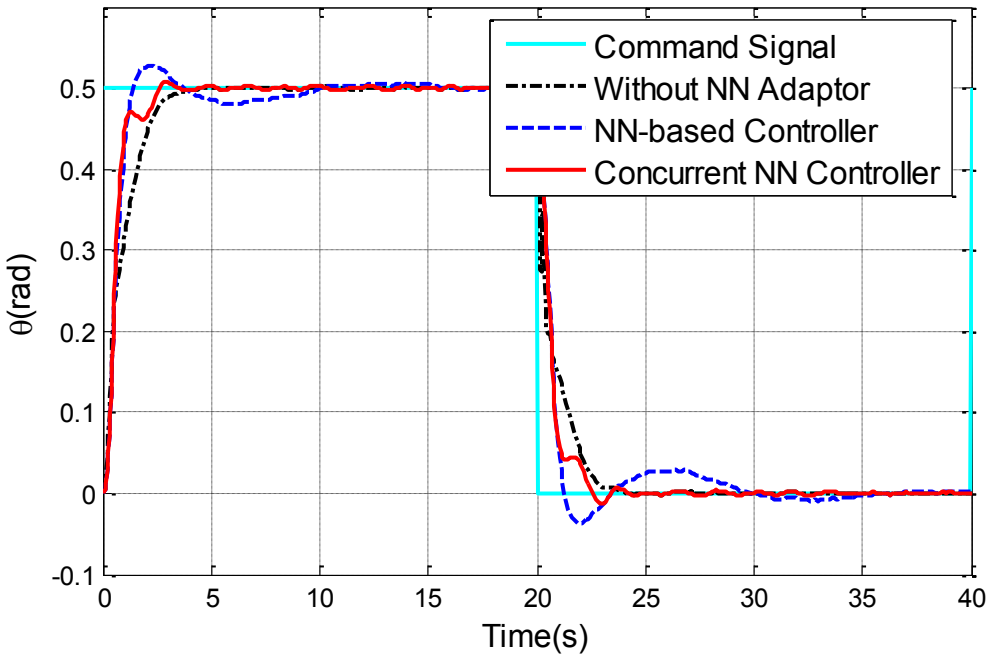

Figure 5-13 Reconfigured system performance with 30% sensor calibration error

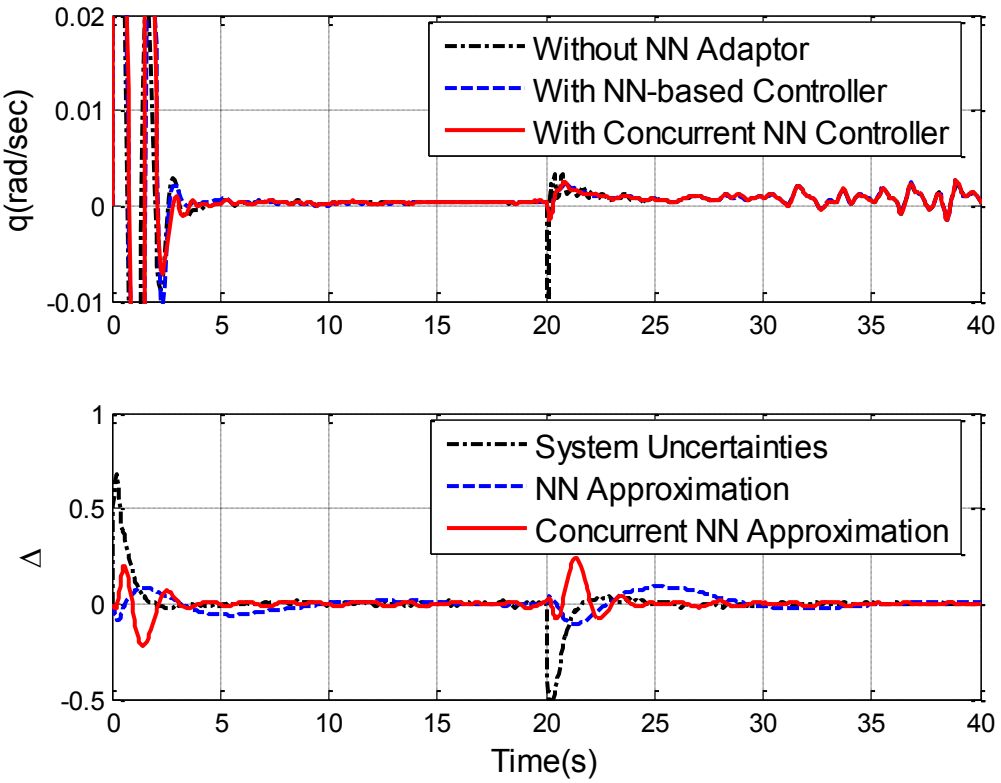

Figure 5-14 Pitch rate & uncertainty approximation with 30% sensor calibration error

Figure 5-13 and Figure 5-14 show that when the background learning is used along with the instantaneous learning the NN learns faster and retains the learning even when there is a lack of persistent excitation. This indicates that the combined instantaneous learning and background learning controller have better FTC performance. It should to be noted that the reconfigurable control system includes a linear PD compensator element for stabilizing the tracking error. Then the two types of faults, bias and calibration errors in the sensor feedback loop, can be considered as changes to the PD controller parameters. Thus in this simulation situation, the PD controller has a dominant effect on the FTFC performance whilst the NN adaptor may not show significant convergence to system uncertainties in Figure 5-14.

In the next simulation experiment the elevator input δ_e is used to replicate the loss of effectiveness considered as an actuator fault, modelled as $\delta_{eout} = \beta_e \cdot \delta_{ein}$, ($\beta_e = 0.9,0.7$). The fault is added to the model and the simulation is run from continuous time $t = 0s$. Figures 5-15 and 5-16 show the system responses when $\beta_e = 0.9$, Figures 5-17 and 5-18 show the system responses when $\beta_e = 0.7$.

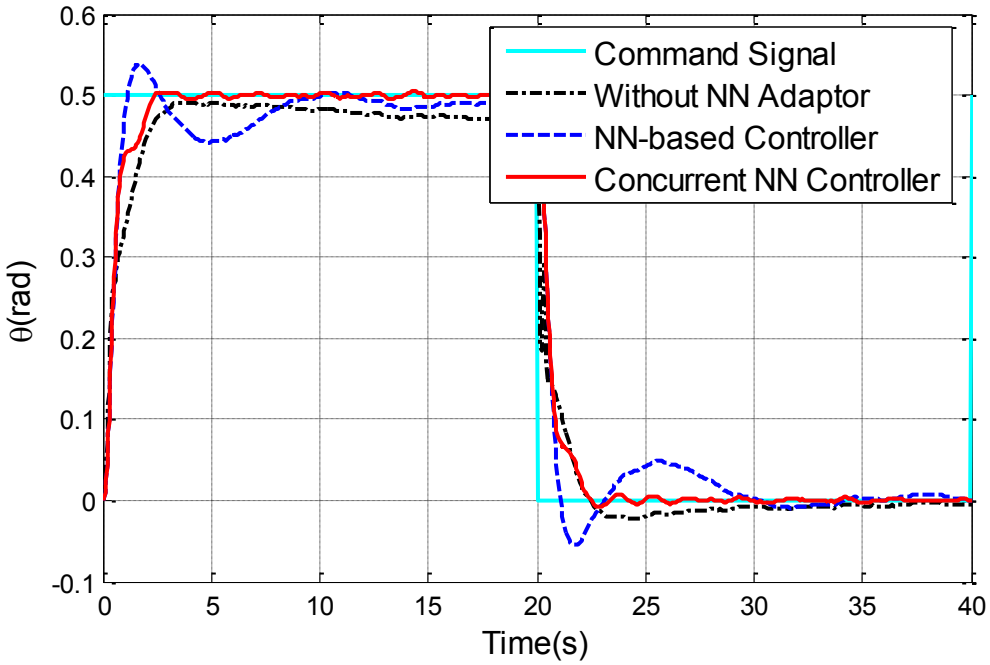

Figure 5-15 Reconfigured system performance with 10% actuator loss

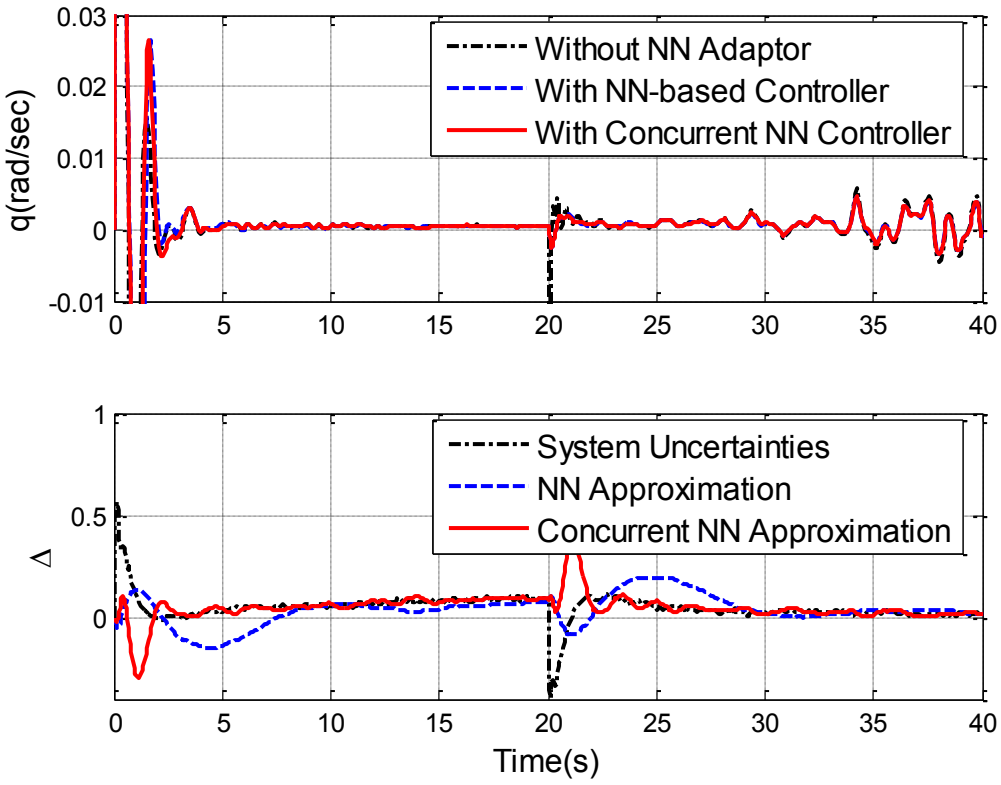

Figure 5-16 Pitch rate & uncertainty approximation with 10% actuator loss

These results indicate a modest but noticeable improvement of the reconfiguration ability for the designed system using the concurrent learning NN as well as asserting better stability and robustness of the combined background and online learning approach during severe actuator

faults. In Figures 5-15 and 5-17, it is seen that the UAV tends not to track each successive step accurately after the fault occurs. Only the concurrent learning NN adaptive scheme achieves the desired reconfiguration and FTC performances.

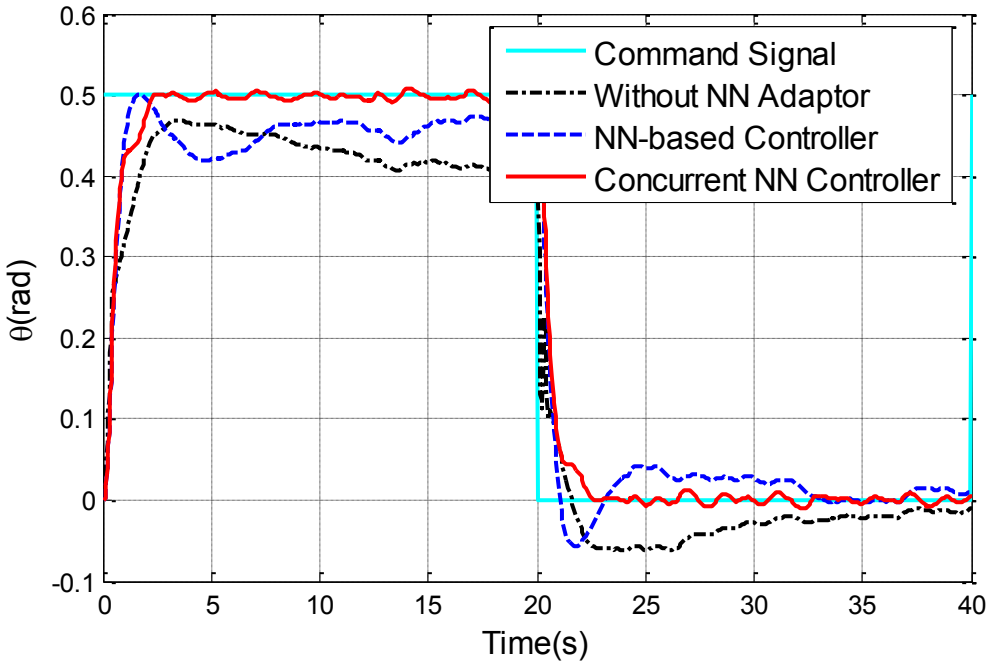

Figure 5-17 Reconfigured system performance with 30% actuator loss

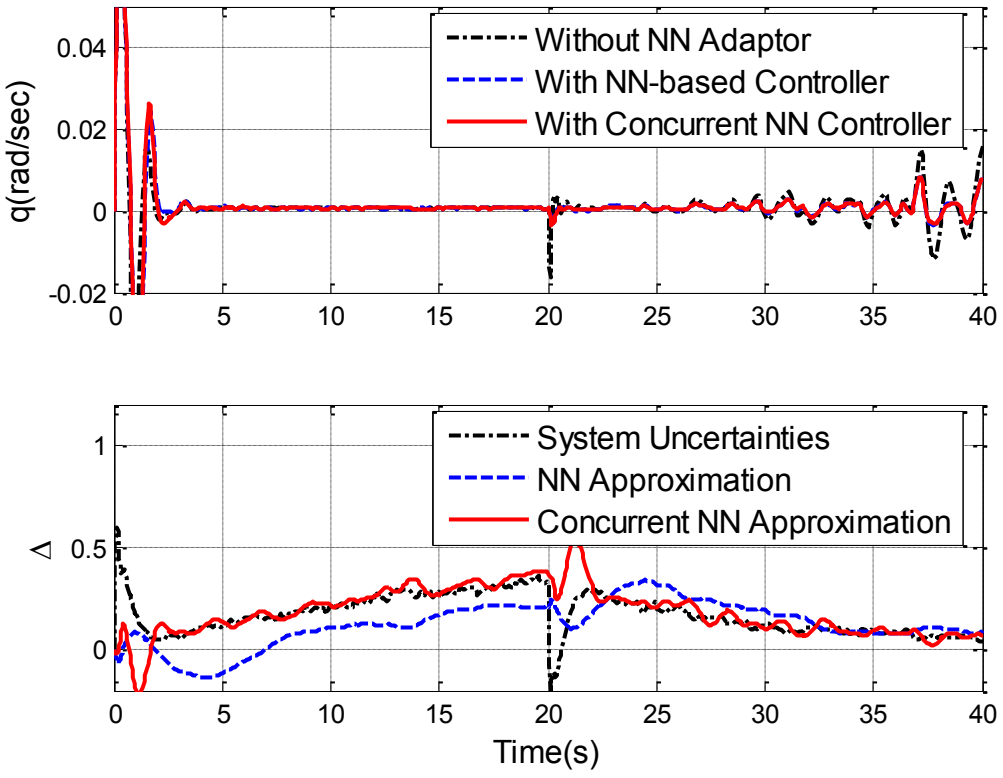

Figure 5-18 Pitch rate & uncertainty approximation with 30% actuator loss

This is also seen in Figures 5-16 and 5-18 where it can be noted that the actuator fault is considered to be represented within the system uncertainty itself. It is shown that for cases of both 10% and 30% loss of actuator effectiveness the normal controller has unstable performance. On the other hand the classical NN adaptor yields inaccurate but stable responses. Once again only the concurrent learning NN adaptor achieves the required reconfiguration performance. These effects in combination indicate that the combined online and background learning system is able to improve performance over the baseline controller and PD compensator, indicating improved reconfigurable control system.

The next simulation experiment considers the inclusion of the Dryden Spectrum wind turbulence model as described in (3-47) together with a multi-step up-step down signal (rad) to represent the actuator faults. The latter is chosen to test the effect as this fault is an excitation signal on the system nonlinearity. The disturbances and fault model responses are depicted in Figure 5-19.

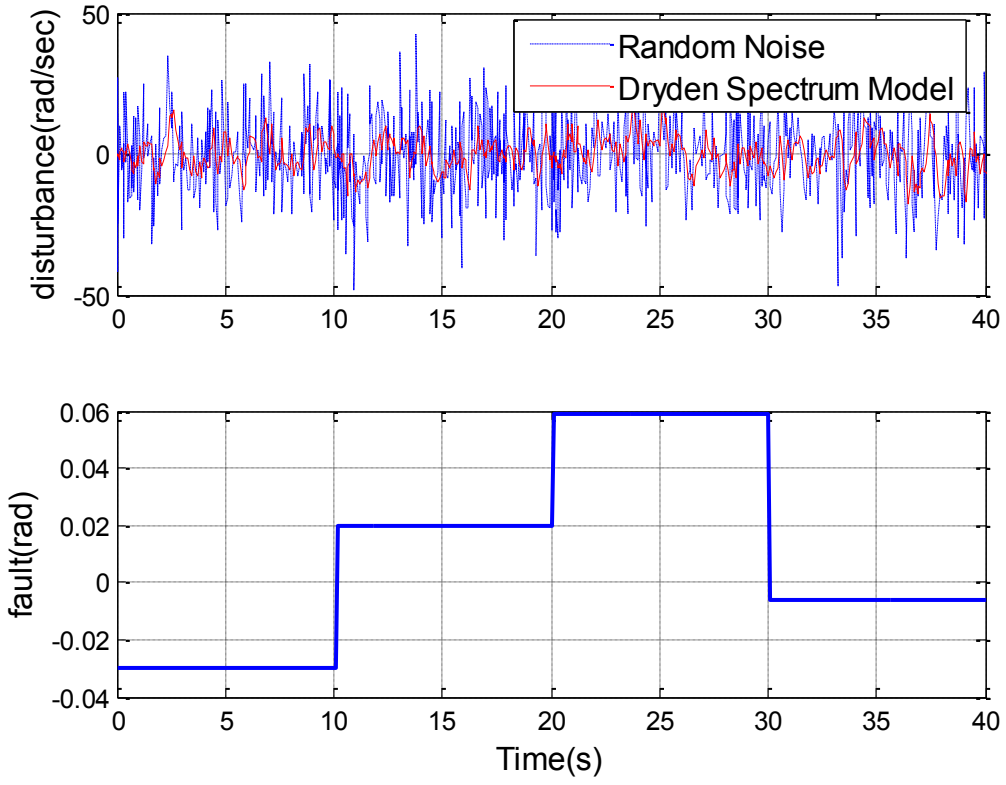

Figure 5-19 Disturbance & multi-step elevator fault

Corresponding to the fault signal the time histories of the θ-channel aerodynamics for cases with and without adaptation are depicted in Figures 5-20. The two kinds of NN adaptation signal are compared in Figure 5-21, which shows clearly that the NN adaptation is able to

compensate for the system error and the concurrent learning NN has better approximation performance with respect to the system uncertainty. In all cases, the concurrent learning NN based on instantaneous and background information shows correct adaptation and improved reconfigurable control achievements.

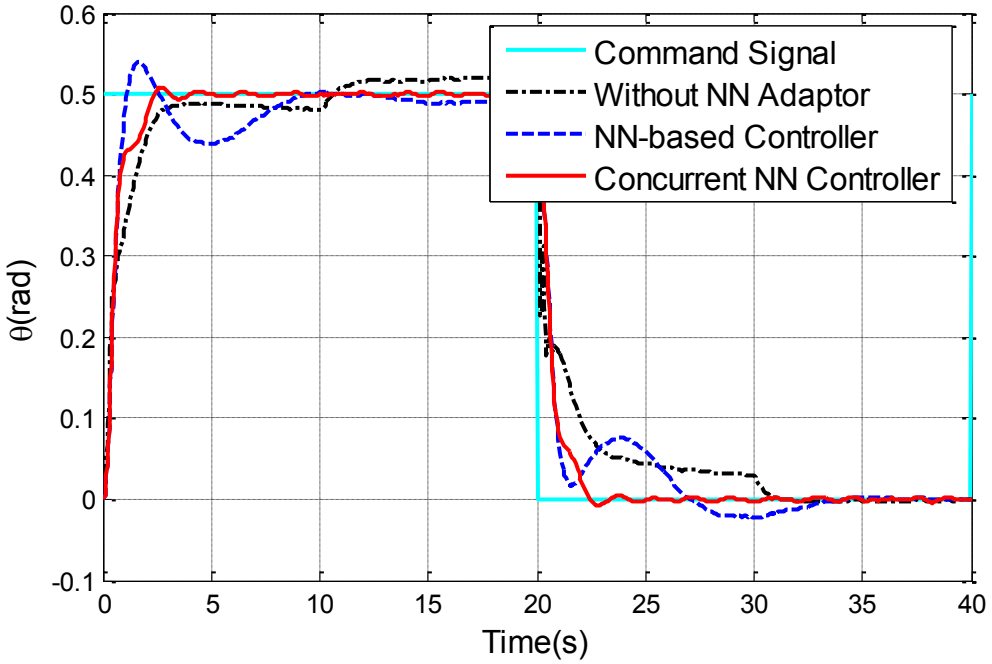

Figure 5-20 Reconfigured system performance with elevator fault & wind disturbance

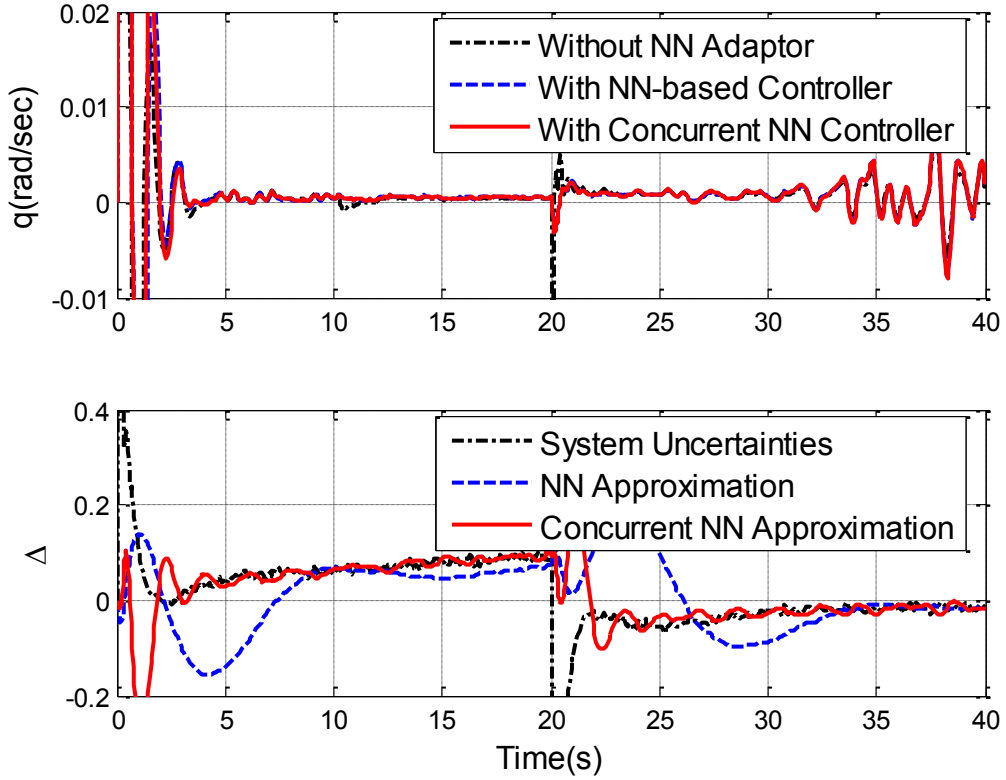

Figure 5-21 Pitch rate & uncertainty approximation with elevator fault & wind disturbance

It is also instructive to notice that the concurrent learning NN shows significant sensitivity to disturbances. Although improved trajectory tracking performance has been seen, when combined online and the background learning is included, the system responses tend to be more oscillatory than when only the online learning is included. The reason for this phenomenon is caused by the use of the multiple history data points in the concurrent leaning NN scheme. This means that the disturbance information acting on the aircraft has been passed to each data point and linearly added by the concurrent learning NN adaptive law, which eventually leads to an amplified effect on the overall tracking performance.

5.6 Conclusion

This chapter illustrates the use of a NN-based adaptive element in a FTFC reconfiguration scheme. Designs based on this approach have been tested on the nonlinear Machan UAV system simulation introduced in Chapter 3. The main objective is to enhance the flight system stability and robustness to model uncertainty due to incomplete modelling, faults, with or without disturbance in the form of wind turbulence. An improved NN-based reconfigurable controller has been designed for the Machan system to deal with the modelling and disturbance uncertainties without sacrificing performance. A recently proposed concurrent NN adaptive learning algorithm has been modified in this chapter to achieve better reconfigurable FTFC performance. The NN adaptive element of this approach is improved by including system background information (historical data points) for adaptively training the NN weights. The stability analysis of this improved SHL NN is given by means of appropriate Lyapunov results to provide boundedness conditions of all the errors of the closed-loop system. The FTFC performance of the Machan system is validated through simulations under various faults and disturbance conditions. The adaptive responses are robust to both parametric uncertainty and unmodelled dynamics. The modified concurrent learning NN adaptor is shown to achieve improved reconfigurable FTFC performance.

Chapter 6 Reconfigurable FTFC for Nonlinear Aircraft based on SMC-NN Adaptor

For improving system performance and to enhance the disturbance rejection capability, Sliding Mode Control (SMC) is a popular systematic approach to the problem of maintaining robust stability and robust performance. In this chapter, an expanded reconfigurable FTFC strategy using a SMC training concurrent learning NN strategy is developed based on the adaptive flight control scheme described in Chapter 5. Implemented as a learning algorithm, SMC treats the NN as a controlled system and allows a stable, dynamic calculation of the learning rates. While considering the system's stability, this robust online learning method therefore offers a higher speed of convergence. The SMC-based reconfigurable FTFC system is tested on the Machan UAV and compared with the NN adaptor achieved in Section 5.5, in the presence of fault and disturbance scenarios. The results show that the flight controller achieves better adaptive performance by using the SMC in the on-line NN learning law.

6.1 Introduction

In recent years, the control problem of dynamical systems uncertainties has attracted great interest in the research community for improved control performance during application (Corless & Leitmann, 1981; Francis, 1987; Young, Utkin & Ozguner, 1996; Zhou, Doyle & Glover, 1996; Serrani, Isidori & Marconi, 2001; Ioannou & Sun, 2012). Among existing methodologies, the SMC technique (Zinober, 1990; Slotine & Li, 1991; Utkin, 1992; Edwards & Spurgeon, 1998; Utkin, Guldner & Shi, 2009) based on Variable Structure Control (VSC) theory turns out to be characterized by high simplicity and robustness.

SMC was first described in the Soviet Union by Emelyanov (1959) in Russia in the early 1960s (Emelyanov, 1959; Itkis, 1976; Utkin, 1977; Fernandez & Hedrick, 1987; Young, Utkin & Ozguner, 1996). It quickly attracted great interest because of its robustness property (Zinober, 1990; Edwards & Spurgeon, 1998). Later research and development continue to apply SMC to a wide variety of engineering application systems such as in automotive systems (Yoshimura, Kume, Kurimoto & Hino, 2001), general mechanical systems (Bartolini, Pisano, Punta & Usai, 2003), robotics (Zhihong, Paplinski & Wu, 1994), in process control (Camacho & Smith, 2000; Castillo, Edgar & Fernández, 2012), in aerospace applications

(Young, 1993; Xu, Mirmirani & Ioannou, 2004), and for power systems (Carpita & Marchesoni, 1996).

The primary characteristic of an SMC system is that the feedback signal is discontinuous, switching on one or more manifolds in state space. When the state crosses each discontinuity surface, the structure of the feedback system is altered. Under certain circumstances, all motions in the neighborhood of the manifold are directed toward the manifold. Hence, a sliding motion on a predefined subspace of the state space is established in which the system state repeatedly crosses the switching surface (Zinober, 1990; Bartolini, Ferrara & Utkin, 1995; Edwards & Spurgeon, 1998). Once the sliding surface design is achieved, the controlled system trajectories must belong to the sliding manifold in which the behaviour of the system is the expected one. In order to obtain the control aim, a controller with a sufficient authority is necessary for dominating the uncertainties and the disturbances acting on the system. The control promptly reacts to any deviation from the prescribed behaviour steering the system back to the sliding manifold. An advantage of this approach is that the sliding behaviour is insensitive to model uncertainties and disturbances which do not steer the system outside from the chosen manifold. Thus this mode has useful invariance properties in the face of uncertainties in the plant model and, therefore, is a good candidate for tracking control of uncertain nonlinear systems. It should be noted that the SMC theory is well developed especially for Single-Input and Single-Output (SISO) systems in controller canonical form (White, 1986).

In spite of the claimed robustness properties, the implementation of SMC techniques for real systems presents some drawbacks, due to the finite switching frequency of real control devices and the presence of the high frequency chattering. The high-frequency components of the control could excite parasitic resonant modes so that the system trajectories can differ from the ideal ones. This is particularly true when simplified model representations are used, for example using a lumped representation of a distributed parameter system as for a flexible solar panel or bridge structure (Orlov & Utkin, 1987). Similarly, unmodelled parasitic dynamics in measurement devices and actuators may lead to higher-order sliding modes which can be either stable or unstable (Fridman & Levant, 1996; Fridman, 2002). Generally speaking, the system and the non-ideal behaviour of the actuators can produce the so-called chattering phenomenon, which is a high frequency motion that makes the state trajectories rapidly oscillating out the sliding manifold brought about by the high-speed (ideally, at infinite frequency) switching necessary for the establishment of a sliding mode. Chattering

and the need for discontinuous control constitute two of the main criticisms of SMC. These drawbacks are much more evident when dealing with distributed parameter and some mechanical systems. Furthermore, rapidly changing control actions induce fatigue in mechanical parts and the system could be damaged in a short time.

Several methods have been proposed to remove or reduce the effects of chartering in SMC (Slotine & Sastry, 1983; Zinober, 1990; Rundell, Drakunov & DeCarlo, 1996; Bartolini, Ferrara & Usani, 1998; Bartoszewicz, 1998; Allen, Bernelli-Zazzera & Scattolini, 2000; Levant, Pridor, Gitizadeh, Yaesh & Ben-Asher, 2000; Wang & Stengel, 2000, 2005; Utkin, Guldner & Shi, 2009). Most of these methods use a straightforward approach to avoid chattering, and often the sign function of the discontinuous control is approximated by a saturation function. As a result, the system motion is confined within a boundary layer of the sliding manifold. A different approach to avoid chattering is to augment the controlled system dynamics, by adding integrators at the input side, so as to obtain a higher-order system in which the actual control signal and its derivatives appear explicitly. If the discontinuous signal coincides with the highest derivative of the actual plant control, the latter results are continuous with a smoothness degree depending on the considered derivative order (Bartolini, Ferrara & Usani, 1998).

It is now feasible to combine SMC strategies with computational intelligence methods such as Fuzzy Logic (FL), Neural Networks (NN) or evolutionary computing, e.g. using Genetic Algorithms (GA). These methodologies associated with SMC provide an extensive freedom for control design to deal with problems of fault, uncertainty, or imprecision and disturbances (Kaynak, Erbatur & Ertugnrl, 2001; Yu, 2009).

This chapter makes use of some ideas from SMC methodology combined with computational intelligence applied to a reconfigurable FTFC problem for the nonlinear Machan UAV system described in Chapter 5. The work involves the use of a base-line controller (as outlined in Section 4.4) to decouple and linearize the aircraft system. The SMC concept is then constructed around the existing controller to maintain further robustness against uncertainties, faults and disturbances. This is achieved by using SMC to improve the robustness of the NN learning performance. Analysis of the performance of the sliding mode learning within the reconfigurable FTFC scheme with the goal of achieving a high degree of fault tolerance to bounded actuator faults. Simulated results of the reconfigurable FTFC scheme applied to the nonlinear Machan UAV demonstrates the improvement that is gained by including the SMC for training the parameters of the on-line concurrent learning NN adaptor.

6.2 SMC Theory and Application with Computational Intelligence

6.2.1 Description of the general SMC dynamics

Consider a nonlinear MIMO dynamical system of the form:

$$x_i^{(n_i)} = \frac{d^{(n_i)}x_i}{dt^{(n_i)}} = f_i(x) + \sum_{j=1}^{m} g_{ij}(x)u_j\,,\ (\ i = 1, \dots, m, j = 1, \dots, m) \tag{6-1}$$

where $u = [u_1 \quad \cdots \quad u_m]^T$ and the state vector x with components x_i are functions of time t. The x_i and their first $n_i - 1$ time derivatives are expressible in simplified form as:

$$\dot{x}(t) = f(x) + g(x)u(t) \tag{6-2}$$

where state vector $x \in \mathcal{R}^m$, control input vector $u \in \mathcal{R}^m$; nonlinear vector fields $f(x) \in \mathcal{R}^m$, and $g(x) \in \mathcal{R}^{m\times m}$.

It is assumed that the additive and multiplicative errors $\Delta_f(x)$ and $\Delta_g(x)$, respectively in $f(x)$ and $g(x)$ of (6-2) are bounded but unknown. By defining their nominal values as $\hat{f}(x) \in \mathcal{R}^m$ and $\hat{g}(x) \in \mathcal{R}^{m\times m}$, respectively, the functions of $f(x)$ and $g(x)$ can be modelled as (Slotine & Sastry, 1983):

$$f(x) = \hat{f}(x) + \Delta_f(x), \left\|\Delta_f(x)\right\|_\infty \le C_f, and\ C_f > 0 \tag{6-3}$$

$$g(x) = \left(I + \Delta_g(x)\right)\hat{g}(x), \left\|\Delta_g(x)\right\|_\infty \le C_g, and\ C_g > 0 \tag{6-4}$$

where $\hat{g}(x)$ is everywhere an invertible square matrix of functions continuously dependent on parametric uncertainty, so that $\hat{g}(x) = g(x)$ in the absence of uncertainty makes the system have as many control inputs as outputs x_i $(i = 1,2 \dots m)$ to be controlled. $\|\cdot\|_\infty$ denotes the infinity norm.

The design purpose is to force the state x to track a desired trajectory: $x_d(t) = [x_{1d}(t), \dots, x_{md}(t)]^T$. This can be done by defining a sliding surface: $S(x;t) = \{x \in \mathcal{R}^m || s_i(x;t) = 0|, \forall i = 1, \dots, m\}$, such that if $x \in S(x;t)$ then $x(t) = x_d(t)$. The dynamic behaviour of the system can be split into two phases: the reaching and sliding dynamic regimes, respectively. During the reaching phase $s_i(x;t) \neq 0$ so that a stabilizing control law is required so that the state reaches the sliding surface asymptotically, i.e. such that $lim_{t\to\infty}\ s_i(x;t) = 0, (i = 1,2 \dots m)$.

The tracking error is set as:

$$e(t) = x_d(t) - x(t) \tag{6-5}$$

By introducing a variable of interest $\int_0^t e(r)dr$, a general form of sliding surface function can be defined as a third-order relative to this variable as (Slotine & Li, 1991; Zinober, 1994):

$$s_i(x;t) = \left(\frac{d}{dt} + \lambda\right)^{n_i-1} \int_0^t e_i \, dr \tag{6-6}$$

where $s_i(x;t) = [s_1(x;t), \dots, s_m(x;t)]^T$ and λ is a selected positive constant. For example, if $n = 3$, the sliding surface would be a Proportional Integral Derivative (PID) format of e_i as:

$$\begin{aligned} s_i(x;t) &= \frac{d^2 \int_0^t e_i \, dr}{dt^2} + 2\lambda \frac{d \int_0^t e_i \, dr}{dt} + \lambda^2 \int_0^t e_i \, dr \\ &= \dot{e}_i + 2\lambda e_i + \lambda^2 \int_0^t e_i \, dr \end{aligned} \tag{6-7}$$

For convenience of notation the time subscript for e_i has been omitted and in the following the time subscript for x is also omitted.

The objective of the resulting SMC is to force the system states to reach the sliding surface $s_i(x;t)$. Once the states are on the sliding surface, the design target becomes one of keeping the state on the surface. For achieving this, a control law is needed which makes $S(t)$ an invariant set by selecting a control law such that $s_i(x;t) = 0, \forall x \in S(t), (i = 1,2 \dots m)$.

Define that $e_r = [e_{1r}, \dots, e_{mr}]^T$, $e_{ir} = C_i^1 e_i^{(n_i-1)} + \cdots + C_i^{n_i} e_i - x_{id}^{(n_i)}$, where C_j^i are appropriate constants computed from (6-6), which then becomes:

$$\begin{aligned} \dot{s}_i(x;t) &= x_i^{(n_i)} - x_{id}^{(n_i)} + C_i^1 e_i^{(n_i-1)} + \cdots + C_i^{n_i} e_i \\ &= x_i^{(n_i)} + e_{ir} \\ &= f_i(x) + \sum_{j=1}^m g_{ij}(x) u_j + e_{ir} \end{aligned} \tag{6-8}$$

For $\dot{s}_i(x;t) = 0$, the best estimate for the so-called *equivalent control* which is the ideal control law that would give perfect sliding (Slotine & Li, 1991, Chapter 7, pp285), from (6-8) it leads to:

$$\dot{s}_i(x;t) = f_i(x) + \sum_{j=1}^m g_{ij}(x) u_j + e_{ir} = 0 \tag{6-9}$$

which then leads to:

$$\sum_{j=1}^m \hat{g}_{ij}(x) \hat{u}_j = -\hat{f}_i(x) - \hat{e}_{ir} \tag{6-10}$$

By using (6-10), the *equivalent control* law $\hat{u}$ of system in (6-2) with nominal values in (6-3) and (6-4) is obtained as:

$$\hat{u} = -\hat{g}(x)^{-1}\left[\hat{f}(x) + \hat{e}_r\right] \tag{6-11}$$

The method described above is based on the selection of a Lyapunov function. To ensure that the control law $s(x;t) \to 0$ in finite time for all x, the control should be chosen such that the candidate Lyapunov function satisfies the Lyapunov stability criterion.

The Lyapunov function is usually selected as (Slotine & Li, 1991; Edwards & Spurgeon, 1998):

$$V(s) = \frac{1}{2}\, s(x;t)^T s(x;t) > 0 \tag{6-12}$$

It is aimed that the time derivative $\dot{V}$ of the Lyapunov function of V, is negative everywhere outside of $S(t)$, while still maintaining the property $\dot{s}_i(x;t) = 0, \forall x \in S(t)$. If this can be assured, the Lyaunov Theorem (Slotine & Li, 1991) can be used to show that $S(t)$ is globally asymptotically stable.

In order to keep the error system motion close to the sliding domain by switching action, despite the uncertainty of the system dynamics, a discontinuous control signal $K \cdot sgn(s)$ is required and added to the SMC *equivalent control* as follows:

$$u = \hat{u} + \begin{bmatrix} k_1 sgn(s_1) \\ \vdots \\ k_m sgn(s_m) \end{bmatrix} = \hat{u} + K \cdot sgn(s) \tag{6-13}$$

where the function $sign(s_i)$ is defined as:

$$sign(s_i) = \begin{cases} +1 & s_i > 0 \\ 0 & s_i = 0 \\ -1 & s_i < 0 \end{cases} \tag{6-14}$$

From (6-8) and (6-11) it leads to (by dropping the notation of dependency on x, t):

$$\dot{V} = s^T \dot{s} = \sum_{i=1}^{m} s_i \dot{s}_i \leq 0 \quad if \quad s_i \dot{s}_i \leq 0, \forall i \tag{6-15}$$

$$\begin{aligned} s_i \dot{s}_i &= s_i\left(f_i + \sum_{j=1}^{m} g_{ij} u_j + e_{ir}\right) \\ &= s_i\left(\hat{f}_i + \Delta_{f_i} - \sum_{j=1}^{m}\left(1 + \Delta_{g_{ij}}\right)\left(\hat{f}_{ij} + e_{r_{ij}} + k_i sgn(s_i)\right) + e_{ir}\right) \\ &= s_i\left(\Delta_{f_i} - \sum_{j=1}^{m} \Delta_{g_{ij}}\left(\hat{f}_{ij} + e_{r_{ij}} + k_i sgn(s_i)\right) - k_i sgn(s_i)\right) \\ &= |s_i|\left(sgn(s_i)\left(\Delta_{f_i} - \sum_{j=1}^{m} \Delta_{g_{ij}}\left(\hat{f}_{ij} + e_{r_{ij}} + k_i sgn(s_i)\right) - k_i\right)\right) \end{aligned} \tag{6-16}$$

Therefore for $\dot{V} \leq 0$ the system is globally asymptotically stable if K is chosen such that:

$$k_i \geq \frac{C_f + C_g\|\hat{f}_i + e_{ir}\|}{1 + C_g msgn(s_i)} \tag{6-17}$$

This control law will cause a large amount of chattering due to the $sgn(\cdot)$ term. This problem can be removed by introducing a so-called *boundary layer* around the switching surface, so that the motion is maintained with a small distance Υ from the surface:

$$S(t) = \{x||s(x;t) \leq \Upsilon|\}, \Upsilon > 0 \tag{6-18}$$

To maintain the properties of the Lyapunov function but minimize the chattering effects (using the boundary layer), the sign function $sgn(\cdot)$ term can be changed to a saturation function as:

$$sat(y) = y, \quad if\ |y| \leq 1 \tag{6-19}$$

$$sat(y) = sgn(y), otherwise \tag{6-20}$$

The control law then becomes:

$$u = \hat{u} + K \cdot sat\left(\frac{s}{\Upsilon}\right) \tag{6-21}$$

As a summary, SMC is kind of nonlinear control method which allows an intuitive tradeoff between tracking performance and parametric uncertainty. This tradeoff can be adjusted online by modifying the boundary layer. As a result, it can be used to adaptively reduce tracking performance, while simultaneously increasing insensitivity to uncertainty during the action of faults. It should be noticed that SMC with a sliding mode is usually based on the argument that the control of first-order systems (i.e., systems described by first-order differential equations) is much easier than the control of general n^{th}-order systems, even when they are nonlinear or uncertain (Slotine & Li, 1991; Edwards & Spurgeon, 1998; Ioannou & Sun, 2012).

Since the work in this chapter is mainly based on the linearized and decoupled aircraft system (arising from the feedback linearization), the SMC scheme derived above will be used and discussed with reference to first order tracking error system for training the NN updating law of the reconfigurable FTFC scheme, as developed in Section 6.3.

6.2.2 SMC combined with computational intelligence

To overcome the drawbacks of using SMC, computational intelligence algorithms can be combined with the SMC structure to facilitate the handling of the modelling uncertainty and disturbance. This general approach is often considered for application of SMC methods to

complex real world systems. In the control systems developed by these intelligence algorithms, the tolerance for imprecision and uncertainty is exploited to achieve an acceptable solution at a low cost, tractability, and high machine intelligence (Kaynak, Erbatur & Ertugnrl, 2001).

The principal examples of computational methods mainly include: 1) Fuzzy Logic (FL); 2) Artificial NN; 3) Genetic Algorithms (GA); 4) Chaos Theory; etc. It is seen that the approaches are complementary rather than competitive, and there can be much to be gained by using a combination of these computational intelligence algorithms with the SMC. What is required is a combination that leads to a good use of the advantages of both the SMC and the specific computational intelligence method (Kaynak, Erbatur & Ertugnrl, 2001).

It is expected that the fusion of a computing intelligence methodologies within an SMC framework will have the main objective of dealing with modelling uncertainty problems arising from the modelling and control of a physical system. Conversely, the use of SMC theory in systems based on computational intelligence techniques may have a further goal of rigorous design and stability analysis. For example, when a NN is used, a sliding-mode approach can ensure convergence and stability of the NN learning algorithm.

The most popular strategies integrating SMC and intelligent algorithms together include:

- **FL and SMC**

  The integration of FL theory in an SMC system is seen in many examples attempting to relieve the implementation difficulties of the SMC. Although the basic design and implementation philosophy of SMC is followed to a great extent, but the FL systems are usually implemented: I) in a smoothing filter, II) for tuning of the SMC parameters; III) for modelling uncertainties or IV) as controller complementary to improve performance or eliminate chattering (Bekit, Whidborne, & Seneviratne, 1997; Lin & Chen, 1997; Wang, Rad & Chan, 2001; Tong & Li, 2003).

- **NN with SMC**

  The integration of an NN with an SMC can be classified into two main categories: I) use of NN in feedback (or feed-forward) control-loop with a SMC, either in parallel or to compute the equivalent control part; II) use of NN for online adaptation of the SMC parameters. For the first category, *equivalent control* computation requires exact knowledge of the system dynamics and parameters. However, for real application

problems only approximate values can be determined for partly known or uncertain systems. For example, computation of the SMC *equivalent control* by means of a NN can be a promising solution for such systems since the NN has been widely used and has already gained successful results for modelling, or inverse modelling, of dynamic systems. As an another example, considering the case of SMC parameter adaptation, the NN is used to progressively update the slope of the sliding surface and the controller gain (Shakev, Topalov & Kaynak, 2003; Nied, Seleme, Parma & Menezes, 2007; Kruger, Mossner, Kuhn, Axmann & Vorsmann, 2010).

- **Tuning of Sliding-Mode Parameters Using GA**

  The integration of GA and SMC is of an indirect nature in that the former tunes the control parameters of the latter. A number of reports have appeared in the literature in this respect. For example, Li, Ng, Murray-Smith, Gray & Sharman (1996) describes the difficulties in SMC design and gives guidelines on the use of the GA. These authors give two detailed but quite practical and illustrative examples on the use of GA in SMC construction. A combined fuzzy SMC structure in which the antecedents are fuzzy sets on the sliding variable and the consequents are control outputs is considered in (Lin & Chen, 1997), two types of GA-based fuzzy SMC design methods are studied.

- **Use of SMC Theory for Robustness in NN Learning**

  As described above, NN is used to improve the performance of the SMC system. Conversely, the theory of SMC can also be used to improve the performance of the NN, which could be used in: I) a sliding mode strategy for robust adaptive NN learning (Sira-Ramirez & Colina-Morles, 1995); II) a generic sliding mode algorithm for online training NN multilayer (Sun, Sun & Woo, 1998; Topalov, Cascella, Giordano, Cupertino & Kaynak, 2007); III) stabilization and robustness of a learning procedure in computational intelligence for alleviating system noise (internal/external), or reducing the effects of modelling uncertainty (Elmali & Olgac, 1992).

6.3 Reconfigurable FTFC Scheme based on SMC Learning NN Adaptor

As introduced in Chapter 5, the NN has a well-known property of representing complex nonlinear mappings. In the parameter tuning of NN structures the back-propagation (BP)

error technique is often used based on Newton methods such as the Levenberg–Marquardt optimization algorithm (Hornik, Stinchcombe & White, 1989; Yu & Efe, 2002; Melin & Castillo, 2003; Kruger, Schnetter, Placzek & Vorsmann, 2011). However, the use of such approaches in noisy environments and under the existence of abruptly changing system dynamics requires more attention. The reason for this is that the noise effects may excite the high-frequency dynamics of the chosen training strategy. These dynamics are generally nonlinear, and the desired behaviour can be controlled only for slowly changing stimuli. Thus, the idea of designing a training strategy based on SMC theory can ensure robustness of the training mechanism and handle the uncertainty, impreciseness and disturbance problems.

6.3.1 The SMC learning approach for NN

The most significant property of a dynamic system with SMC is its robustness against external disturbances and parameter changes (Bartolini, Ferrara & Utkin, 1995; Kaynak, Erbatur & Ertugnrl, 2001; Utkin, Guldner & Shi, 2009). Several studies utilizing SMC theory in the training of computationally intelligent structures are reported in the literature (Venelinov Topalov, 2001; Yu, 2009; Kruger, Mossner, Kuhn, Axmann & Vorsmann, 2010). Implementations on several FL and NN inference system models have appeared in the literature (Jang, Sun & Mizutani, 1997; Melin & Castillo, 2003; Chao, Cao & Chen, 2007; Kurnaz, Cetin & Kaynak, 2010), showing very promising properties and proving to be faster and more robust than the traditional techniques. One of the first studies on adaptive learning in simple network architectures known as adaptive linear elements (ADALINEs) is due to Sira-Ramirez & Colina-Morles (1995), in which the inverse dynamics of a Kapitsa pendulum is identified by assuming constant bounds for uncertainties. There is a computational speed improvement available by using the proposed NN algorithm. On the other hand, SMC has the potential of improving the convergence and stability of the NN training. Hence, a combination of both is a desirable goal in this work for application to a nonlinear reconfigurable FTFC problem.

In order to transfer the SMC training approach to the adaptive NN compensator scheme described in Chapter 5, the network training and its adaptive computational process are considered as a dynamical system. The SMC system is then applied to this structure as a control system to enhance the training and tracking performance in the presence of the system uncertainties arising from modelling errors and disturbances. The resulting scheme

combining the NN with the SMC is shown in Figure 6-1 (Kruger, Schnetter, Placzek & Vorsmann, 2012).

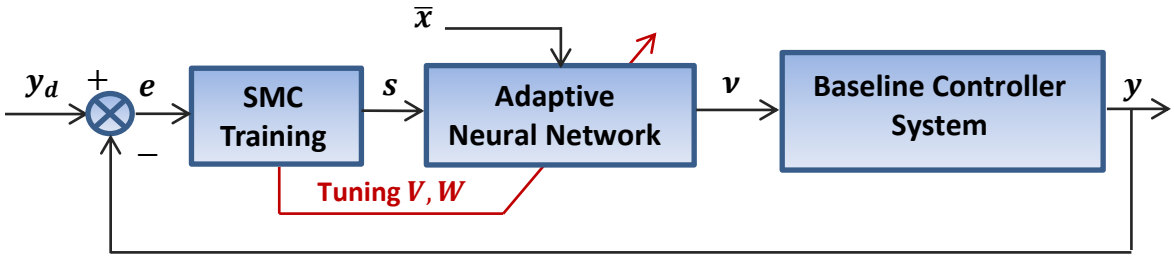

Figure 6-1 Training of a NN considered as control process

In Figure 6-1, the NN propagates an output signal v to adaptively compensate the tracking error e caused by the system uncertainty, faults and disturbances. The input signals $\bar{x}$ and the weights V, W are as defined in Chapter 5 and are also summarized in the following Section 6.3.2. The tracking error e, i.e. the difference between the desired system outputs y_d and the actual outputs y, is involved in designing the sliding surface for tuning the online NN law. The off-line designed sliding surface is used as a network training parameter training law which is then fed into the training block generating a control signal composed of the weight changes of the NN (Yu & Efe, 2002; Nied, Seleme, Parma & Menezes, 2007).

There are different approaches to combine NN with SMC, especially regarding possible definitions of the sliding surface functions $S(x;t)$ defined in Section 6.2.1. To achieve a network training structure consistent with Figure 6-1 the change of the connection weights can be defined in a general way as (Kruger, Schnetter, Placzek & Vorsmann, 2012):

$$\Delta V, \Delta W = \left(\frac{\partial v(V,W,\bar{x})}{\partial V,W}\right) \cdot \mu \cdot (sign(s)) \cdot |e| \tag{6-22}$$

where μ is an adjustable convergence parameter. This is an expansion of the standard gradient descent method by including the sign function $sign(s)$ defined in (6-14) of the sliding surface function S. This adaptive BP weight change can be used within the adaptive learning law (see (5-48) of Section 5.3.4) and (6-34) of Section 6.3.2) by calculating the learning rates dynamically (Kruger, Schnetter, Placzek & Vorsmann, 2012). Recall that the purpose of the work in this chapter is to apply the above learning strategy to the concurrent NN on-line learning law introduced and simplified in Section 5.4, as well as the simulation study on the Machan UAV for better FTFC performance compared with the purely NN-based adaptor.

6.3.2 Reconfigurable FTFC Scheme based on SMC-NN adaptor

In this study, the SHL Perceptron NN described in Section 5.3.4 is employed with a first order PD controller to guarantee asymptotic stability in compact space and as an inverse reference model of the response of the system under control. The further developed reconfigurable FTFC scheme based on Figure 5-4 includes the SMC learning element for the concurrent NN online adaptor is developed as shown in Figure 6-2.

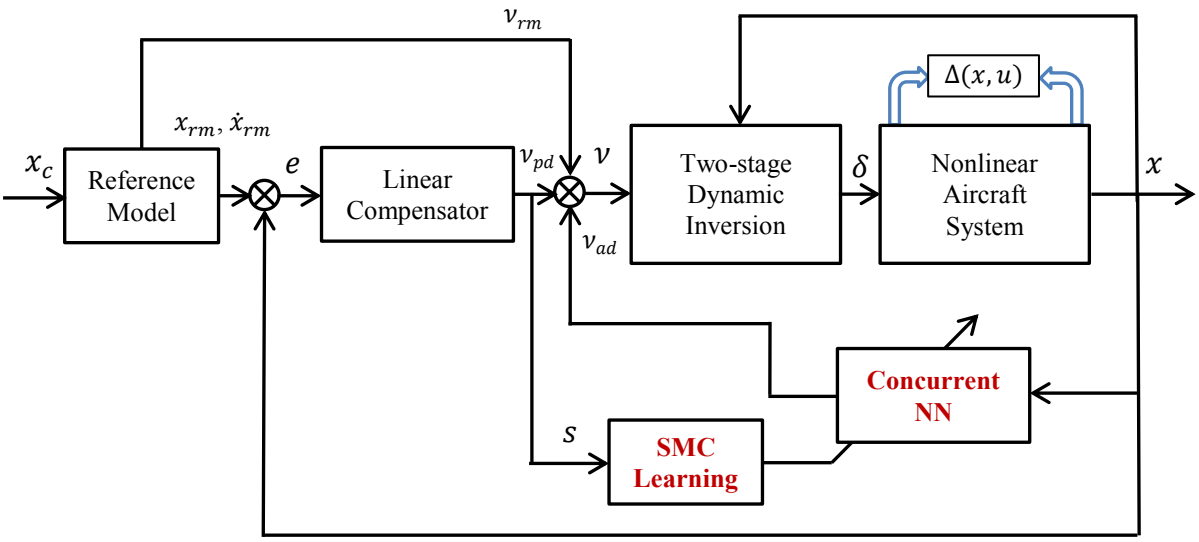

Figure 6-2 Reconfigurable FTFC scheme based on inversion dynamics and SMC training NN

Recall that (5-42) to (5-45) in Section 5.3.4, the SHL NN used as the online adaptive compensator is expressed in the compact matrix form as:

$$v_{ad}(W,V,\bar{x}) = W^T\sigma(V^T\bar{x}) \in R^{n_3\times 1} \tag{6-23}$$

with the definitions for $\bar{x}$, $\sigma(t)$, V and W are given as:

$$\bar{x} = \begin{bmatrix} x_1(t) \\ \vdots \\ x_n(t) \end{bmatrix} \in R^{(n_1+1)\times 1} \tag{6-24}$$

$$\sigma(t) = \begin{bmatrix} \sigma_1(t) \\ \vdots \\ \sigma_n(t) \end{bmatrix} \in R^{(n_2+1)\times 1} \tag{6-25}$$

$$V = \begin{bmatrix} v_{1,1} & \cdots & v_{1,n_2} \\ \vdots & \ddots & \vdots \\ v_{(n_1+1),1} & \cdots & v_{(n_1+1),n_2} \end{bmatrix} \in R^{(n_1+1)\times n_2} \tag{6-26}$$

$$W = \begin{bmatrix} w_{1,1} & \cdots & w_{1,n_3} \\ \vdots & \ddots & \vdots \\ w_{(n_2+1),1} & \cdots & w_{(n_2+1),n_3} \end{bmatrix} \in R^{(n_2+1)\times n_3} \tag{6-27}$$

To prove the stability and robustness of the sliding mode training NN adaptor, certain parameters within the online training law in (6-23) to (6-27) are bounded as follows.

The time derivative of the activation function $\sigma(\cdot)$ in the single hidden layer is expressed as $\dot{\sigma}(\cdot)$, where:

$$0 < \dot{\sigma}(t), = \frac{d}{dt}[\sigma(V^T\bar{x})] \leq B_M \quad \forall t \tag{6-28}$$

where B_M corresponds to the maximum value (as an upper bound).

The input vector and its time derivative are assumed to be bounded as:

$$\|\bar{x}(t)\| = \sqrt{x_1^2(t) + \cdots + x_n^2(t)} \leq B_{\bar{x}} \quad \forall t \tag{6-29}$$

$$\|\dot{\bar{x}}(t)\| = \sqrt{\dot{x}_1^2(t) + \cdots + \dot{x}_n^2(t)} \leq B_{\dot{\bar{x}}} \quad \forall t \tag{6-30}$$

where $B_{\bar{x}}$ and $B_{\dot{\bar{x}}}$ known positive constants.

Due to the physical constraints, it is also assumed that the magnitude of all elements in the i^{th} row $V_i(t)$ of the matrix $V(t)$ and the elements of the vector $W(t)$ are bounded as (Nied, Seleme, Parma & Menezes, 2007), so that:

$$\|V_i(t)\| = \sqrt{v_{i,1}^2(t) + v_{i,2}^2(t) + \cdots + v_{i,n_2}^2(t)} \leq B_V \quad \forall t \tag{6-31}$$

$$|W_i(t)| \leq B_W \quad \forall t \tag{6-32}$$

For the known constants B_V and B_W, where $i = 1,2,\ldots,n_1 + 1$, the error $\varepsilon(t)$ of the NN adaptor and its time derivative $\dot{\varepsilon}(t)$ are also considered to be bounded as:

$$|\varepsilon(t)| \leq B_\varepsilon, |\dot{\varepsilon}(t)| \leq B_{\dot{\varepsilon}} \quad \forall t \tag{6-33}$$

where B_ε and $B_{\dot{\varepsilon}}$ are positive constants.

Based on these defined bounds for the parameters and signals, the SMC training design is divided into two phases. Firstly, a sliding surface to produce the input/output behaviour is designed. Secondly, the weights are updated in order to satisfy the conditions for tracking and sliding on the designed surface (Topalov & Aydin, 2007).

In the BP error-learning approach studied in Chapter 5, the NN adaptive learning law is given as:

$$\begin{aligned} \dot{W} &= -(\sigma - \sigma' V^T\bar{x})r^T\Gamma_W - \kappa_w\|e\|W \\ \dot{V} &= -\Gamma_V\bar{x}r^T W^T\sigma'(V^T\bar{x}) - \kappa_v\|e\|V \end{aligned} \tag{6-34}$$

The tracking error signal e, is used as a learning error for the NN training. An SMC-based on-line learning algorithm is applied to replace the gradient-based algorithm in (6-34). This leads to the establishment of an inner sliding motion in terms for the NN adaptor parameters, which is designed to provide enhanced learning error convergence towards zero.

The first order sliding surface for the adaptive learning element is defined as:

$$s(e, \dot{e}) = \dot{e} + \lambda e \tag{6-35}$$

where λ is a constant determining the *slope* of the sliding surface.

This means that the system error e and $\dot{e}$ are states of the SMC training NN adaptor as shown in Figure 6-1. Thus for $s = 0$, the system is directly on the sliding surface, where the control error tends to 0 asymptotically. The learning algorithm for the NN adaptor weights V and W must then be derived in such a way that the sliding mode condition $s = 0$ is enforced.

To enable $s = 0$ to be reached, the following adaption law for the NN weights V and W is introduced as (Topalov & Aydin, 2007):

$$\begin{aligned} \dot{V} &= -\left(\frac{W\bar{x}}{\bar{x}^T\bar{x}}\right)\alpha \cdot sign(s) \\ \dot{W} &= -\left(\frac{\sigma}{\sigma^T\sigma}\right)\alpha \cdot sign(s) \end{aligned} \tag{6-36}$$

where the sign function $sign(s)$ is defined as:

$$sign(s) = \begin{cases} +1 & s > 0 \\ 0 & s = 0 \\ -1 & s < 0 \end{cases} \tag{6-37}$$

and α is chosen as a sufficiently large positive constant satisfying:

$$\alpha > n_2 B_M B_v B_{\bar{x}} B_w + B_{\dot{\varepsilon}} \tag{6-38}$$

Since the linear PD compensation in Figure 6-2 is expressed as (refer to Section 5.3.3):

$$v_{pd} = [K_p \quad K_d]e \tag{6-39}$$

where K_p and K_d are the gains of the PD controller.

The *slope* constant λ in (6-35) is usually taken as (Topalov & Aydin, 2007):

$$\lambda = \frac{K_p}{K_d} \tag{6-40}$$

By substituting (6-40) to (6-35) which then leads the sliding surface to become:

$$s(e, \dot{e}) = K_d\left(\dot{e} + \frac{K_p}{K_d}e\right) = K_d\dot{e} + K_p e = v_{ad} + \varepsilon \tag{6-41}$$

where ε is the NN network adaptive error being bounded as in (6-33).

Proof: A general approach to prove existence as well as reachability of the sliding mode and therefore stability is to choose a Lyapunov candidate function for the sliding surface as (Topalov, Cascella, Giordano, Cupertino & Kaynak, 2007):

$$V = \frac{1}{2} s^T s \tag{6-42}$$

Then differentiating V with respect to time yields:

$$\begin{aligned}
\dot{V} = s\dot{s} &= s(\dot{v}_{ad} + \dot{\varepsilon}) = s\left\{\frac{d}{dt}[W^T\sigma(V^T\bar{x})] + \dot{\varepsilon}\right\} \\
&= s\left[\sum_{i=1}^{n_2} \dot{w}_i\sigma_i + \sum_{i=1}^{n_2} w_i\,\dot{\sigma}_i \sum_{j=1}^{n_1}\left(\dot{v}_{i,j}\bar{x}_j + v_{i,j}\dot{\bar{x}}_j\right) + \dot{\varepsilon}\right] \\
&= s\left[-\sum_{i=1}^{n_2}\left(\frac{\sigma}{\sigma^T\sigma}\right)\alpha sign(s)\,\sigma_i + \sum_{i=1}^{n_2}\dot{\sigma}_i\sum_{j=1}^{n_1}\left(-\left(\frac{w_i\bar{x}}{\bar{x}^T\bar{x}}\right)\alpha sign(s)\bar{x}_j w_i + v_{i,j}\dot{\bar{x}}_j w_i\right) + \dot{\varepsilon}\right] \\
&= s\left[-\sum_{i=1}^{n_2}\alpha sign(s) - \sum_{i=1}^{n_2}\dot{\sigma}_i\alpha w_i^2 sign(s) + \sum_{i=1}^{n_2}\dot{\sigma}_i w_i\sum_{j=1}^{n_1} v_{i,j}\dot{\bar{x}}_j + \dot{\varepsilon}\right] \\
&= -\left(\alpha + \alpha\sum_{i=1}^{n_2}\dot{\sigma}_i w_i^2\right)|s| + \left(\sum_{i=1}^{n_2}\dot{\sigma}_i w_i\sum_{j=1}^{n_1} v_{i,j}\dot{x}_j + \dot{\varepsilon}\right)s \\
&\le -\alpha|s| + (n_2 B_M B_w B_v B_{\dot{\bar{x}}} + B_{\dot{\varepsilon}})|s| \\
&= |s|(-\alpha + n_2 B_M B_w B_v B_{\dot{\bar{x}}} + B_{\dot{\varepsilon}}) < 0 \;\; \forall s \neq 0
\end{aligned} \tag{6-43}$$

This means that by applying the SMC-based adaptation law for the NN weights, the achieved reconfigurable control trajectories will converge in a stable manner since the negative definiteness of the time derivative $\dot{V}$ is ensured for a continuous system.

6.3.3 Controller parameters design

The effectiveness of the proposed SMC-NN adaptive approach for reconfigurable FTFC has been tested by implementing the control scheme in a continuous-time simulation for the nonlinear Machan UAV introduced in Chapter 3. The nonlinear Machan model is linearized and decoupled online through the NDI strategy used in Section 5.2.1.

It should to be noted that, for the three outer-loop control channels of the aircraft, the control scheme in Figure 6-2 is run after selecting the tracking commands x_c and the control inputs δ as:

$$\begin{aligned}
x_c &= [\phi_c \quad \theta_c \quad \beta_c]^T \\
x &= [\phi \quad \theta \quad \beta]^T \\
\delta &= [\delta_a \quad \delta_e \quad \delta_r]^T
\end{aligned} \tag{6-44}$$

The multiple control loop of feedback linearization for aircraft proposed in Section 4.4 is not unique, thus in this study using designed SMC-NN adaptor, the sideslip angle β is used as one of the control states instead of the yaw angle ψ for further trajectory control-loop design in modern flight control application (Lombaerts, Chu, Mulder & Stroosma, 2010). The initial value and command signal of β is set to be zero during simulation study for maintaining symmetrical stability for the UAV Machan case.

Recall that all the parameters of the basic reconfigurable control elements within the NN adaptor are based on a second order reference model. The linear PD compensator, the two-stage NDI structure for feedback linearization of the nonlinear aircraft model and the concurrent online adaptive NN, as well as the Machan UAV control surface saturation, are as described in Section 5.5.1.

It is well-known that SMC suffers from high-frequency oscillations in the control input, which are called "chattering" (see brief discussion of the concept of chattering in Section 6.1). Chattering is undesired because it may excite any high-frequency modes of a system. The common method to eliminate the chattering is using a saturation or the sigmoid function to replace the sign function (see Section 6.2.1), so that system motion is kept within a boundary layer that is infinitesimally close to the sliding or switching surface. In this study the function in (6-45) has been used in this investigation instead of the sign function in the dynamic strategy described in (6-36) to reduce the effect of the chattering:

$$sign(x) \approx \frac{x}{|x|+0.05} \tag{6-45}$$

To apply the simplified concurrent learning law in the SMC training NN, the direct training information (r_c=$v_{ad} - \Delta$) is also included in the training information to minimize the tracking error. The historical training data are also presented for updating the NN weights by using the SMC learning law in (6-36). Then the concurrent NN learning law in (5-85) is modified by involving the designed sliding surface in function $sign(s)$ as:

$$\begin{aligned} \dot{W}_b &= \alpha \cdot \sum_{\tau=0}^{p-1} \left(\frac{\sigma}{\sigma^T \sigma} \right)_{(t+\tau \cdot \Delta t)} \cdot sign(s) \\ \dot{V}_b &= \alpha \cdot \sum_{\tau=0}^{p-1} \left(\frac{W \bar{x}_{(t+\tau \cdot \Delta t)}}{\bar{x}^T_{(t+\tau \cdot \Delta t)} \cdot \bar{x}_{(t+\tau \cdot \Delta t)}} \right) \cdot sign(s) \end{aligned} \tag{6-46}$$

where p denotes the number of chosen data and Δt denotes the sampling interval for the concurrent training and the constant parameter α of the sliding mode learning algorithm has been selected as $\alpha = 0.1$. All the data recorded for the concurrent learning are linear

combinations of the current signal and its time delays at every recording time interval Δt as defined in Section 5.4.4.

6.4. Simulation and Evaluation

The simulation model was constructed implementing the Machan UAV preliminary configuration data: the mass properties and static wind tunnel data. The aircraft trim conditions are: $V_T = 33m \cdot s^{-1}$, $h = 40m$. The trimmed throttle setting is $X_e = 55N$ and is held constant to ensure that the rolling moment L_E has non-zero value. All simulations begin from this trim condition.

The system command reference signals to be followed by the system tracking response are chosen as square wave functions. These reference signals are smoothed using a filter consisting of two consecutively connected blocks each with a transfer function in the reference model. The controller architecture using the two different learning approaches (the concurrent NN learning and the concurrent SMC-NN learning) is tested and validated in simulations with multi-step up and down signal (rad) as elevator fault and wind turbulence modelled in (3-47). The disturbance acts on the vertical motion of the aircraft via the normal velocity w_b. The disturbances and fault model responses are depicted in Figure 6-3.

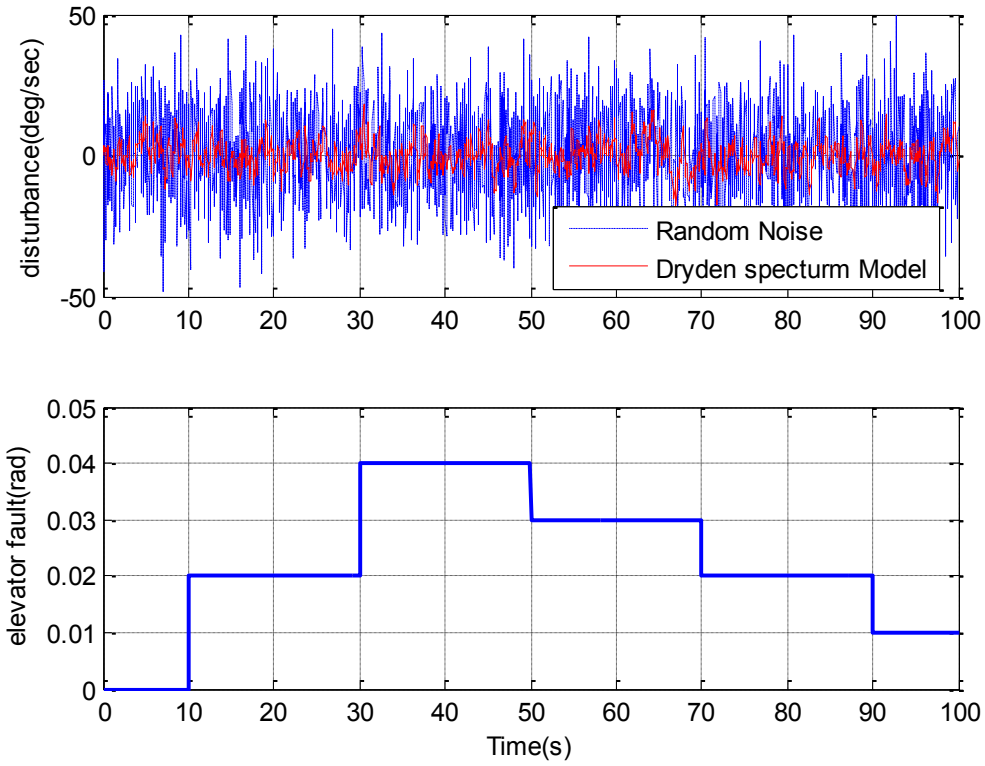

Figure 6-3 Disturbance and elevator faults simulating on the Machan UAV aircraft

The command signals for the three-channel are chosen as: $\phi_c = 0.1\,rad \cdot s^{-1}$, $\theta_c = 0.5rad \cdot s^{-1}$, $\beta_c = 0\,rad \cdot s^{-1}$. The system tracking performances of the flight angle control used for the comparison of the concurrent NN learning (marked as "Con NN") adaptor and the concurrent SMC-NN adaptor (marked as "Con SMC&NN") are depicted in Figure 6-4, and the two kinds of adaptation signals are compared in Figure 6-5.

Both learning approaches show nearly identical behaviour and cancel the network error completely after a few seconds. Besides, it can be clearly seen in Figures 6-4 and 6-5, that the SMC-based NN learning adaptation is not only able to compensate for system error and uncertainty, but also ensures the smooth tracking performance with considerably reduced tuning time. This indicates that the SMC-based NN training approach has better adaptation and improved reconfigurable control achievements. The oscillation caused by the simulated wind disturbance also has an acceptable value.

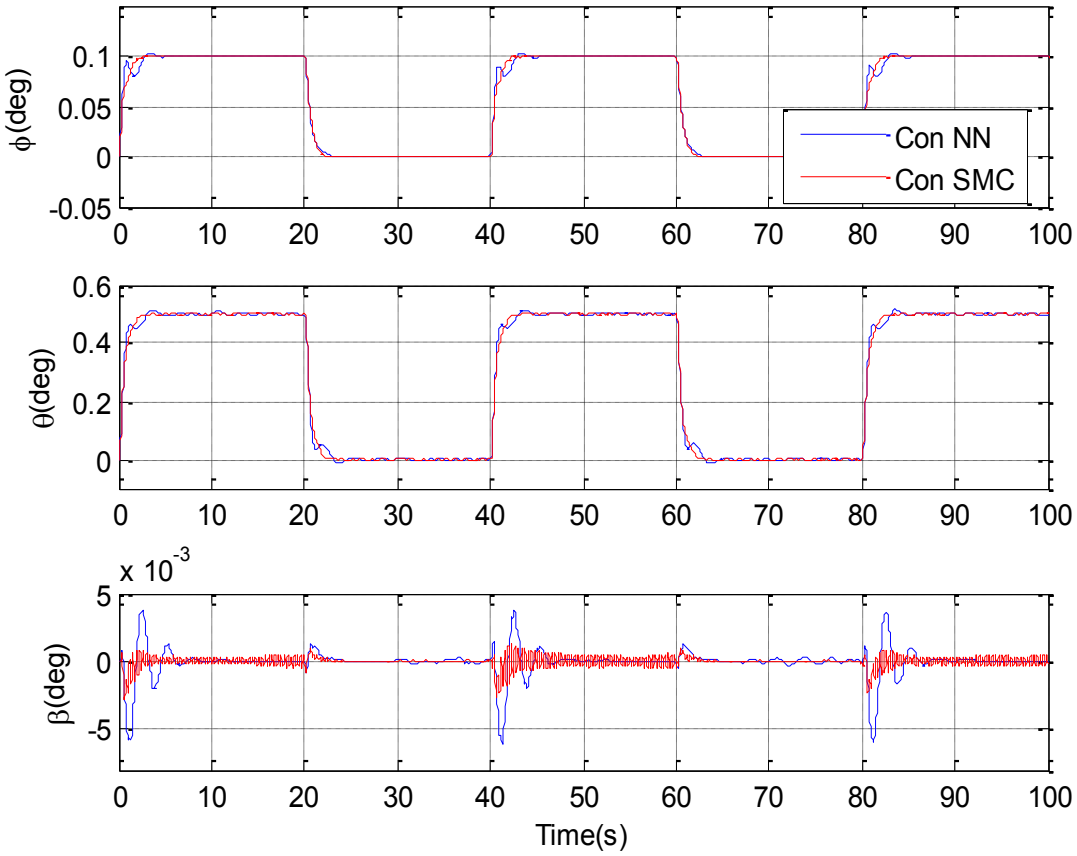

Figure 6-4 System performance with elevator fault and wind disturbance

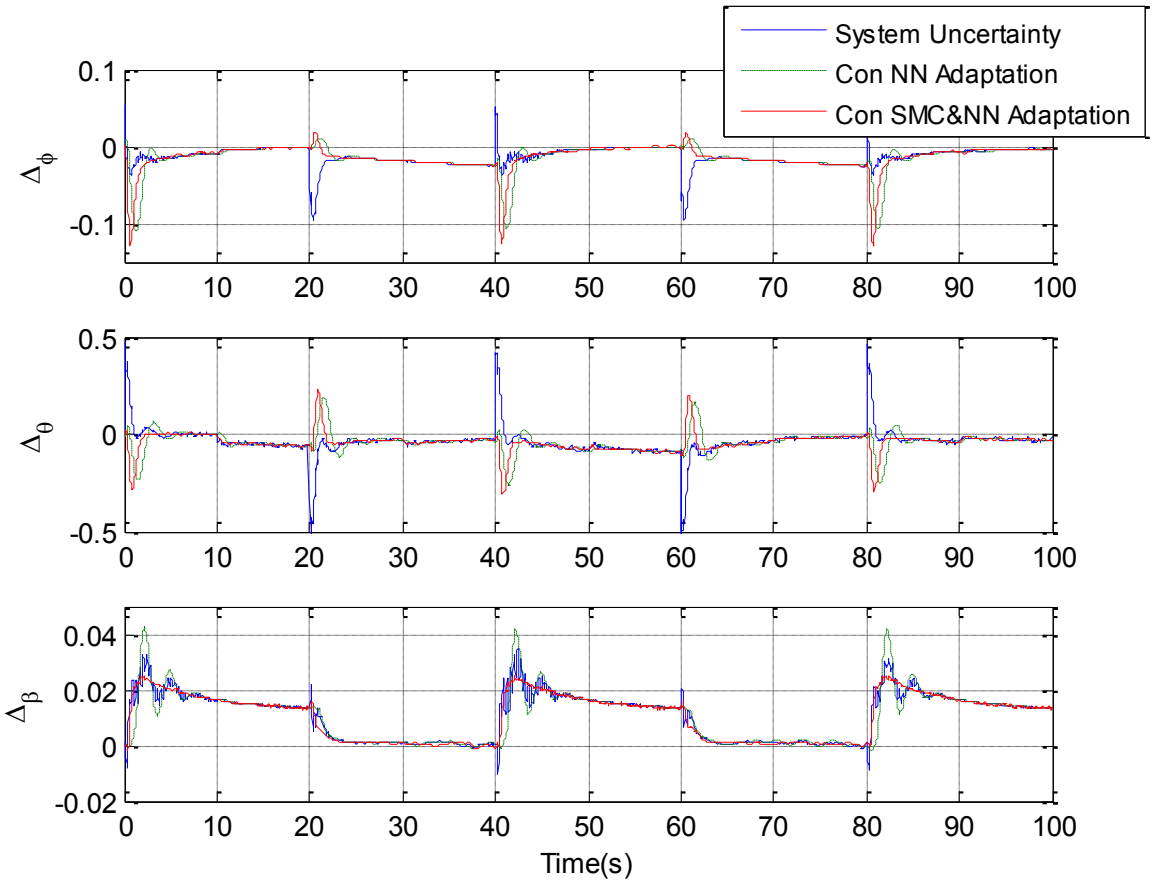

Figure 6-5 System uncertainty approximation with elevator fault and wind disturbance

To further demonstrate the FTFC quality of the SMC-NN training algorithms for the controlled aircraft system during the fault scenario described above, the full-state aircraft responses of the two adaption strategies are shown below in Figure 6-6 (with concurrent NN learning adaptor) and Figure 6-7 (with concurrent SMC-NN learning adaptor).

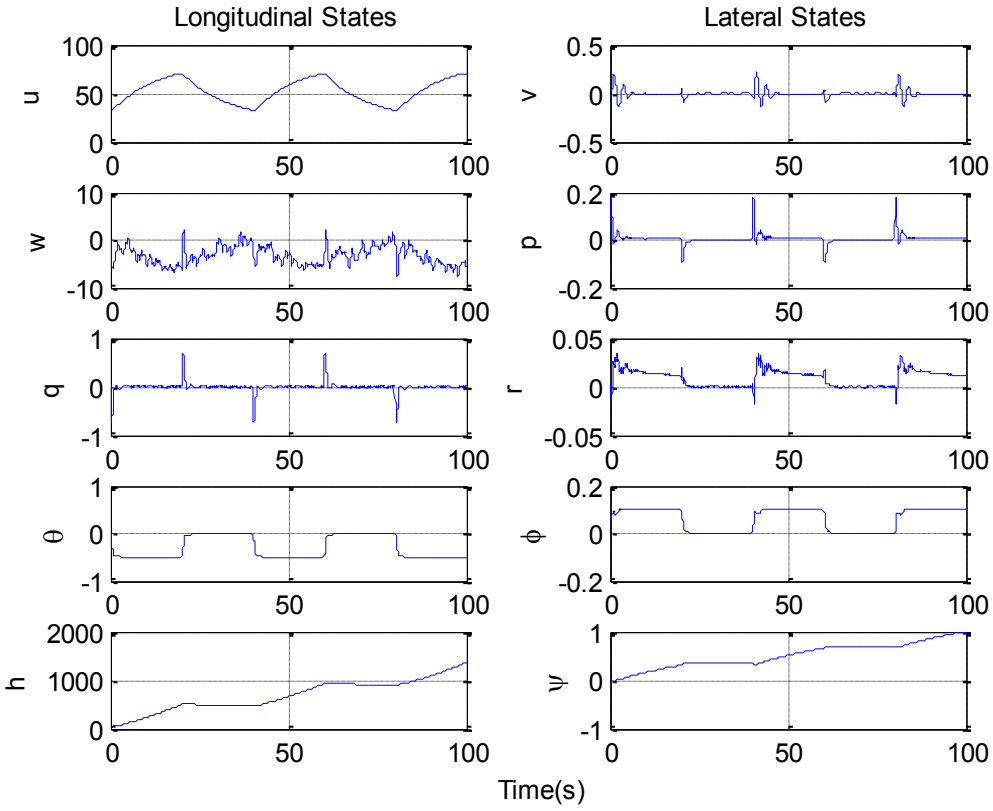

Figure 6-6 Full-state responses of Machan with concurrent NN adaptor

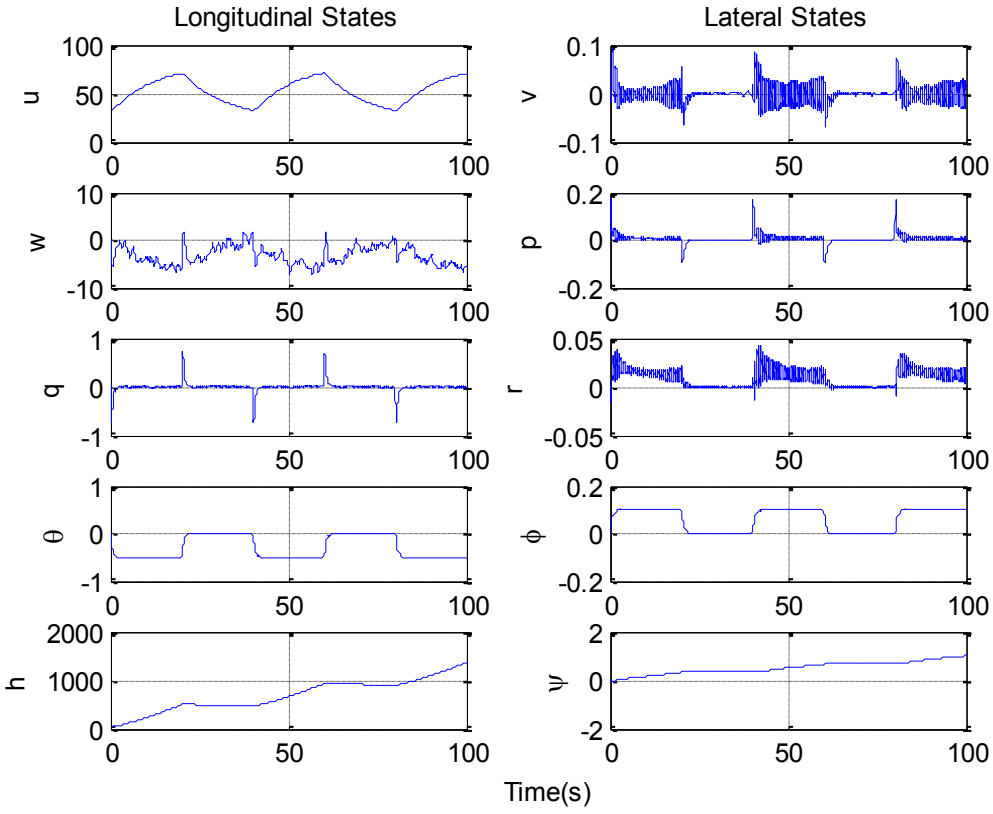

Figure 6-7 Full-state responses of Machan with concurrent SMC-NN adaptor

Both control architectures perform similarly over a longer time running of 100s. Figure 6-6 and Figure 6-7 underline two main aspects: (i) The noisy characteristics of the aircraft motion (caused by the wind turbulence) are seen in the inversion error and cannot be completely compensated by both the NN and SMC-NN algorithm. This leads to increased oscillation of the network; (ii) For the controlled states, the SMC learning offers improved robustness and a higher speed of convergence in the presence of actuator fault and turbulence scenarios. Hence, it has been demonstrated that the concept of SMC learning can improve the established reconfigurable FTFC strategy based on NDI combined with adaptive NN compensator.

6.5 Conclusion

In this chapter, the concept of SMC is described in view to combining together SMC with a concurrent NN scheme. The proposal is that the NN training mechanism behaves as a dynamic system so that the learning convergence and robustness can be improved by suitable SMC design. The reconfigurable FTFC strategy presented in Chapter 5 based on feedback linearization together with a concurrent NN adaptor is further developed in this chapter. It is shown that the reconfigurable FTFC scheme with on-line NN adaptor is improved by using the SMC as an online training law for the NN learning process. This chapter elaborates more accurately the differences between the conventional NN adaptor and the SMC-NN training approaches in fault situations. The effectiveness of the proposed approach has been experimentally tested on the Machan UAV described in Chapter 3 as a nonlinear simulation model. The simulation results show that the SMC algorithm allows dynamic calculation of the learning rates of a NN adaptive processing and increases the robustness against external disturbances while assuring system output stability.

Chapter 7 Active FTFC for Nonlinear Aircraft based on NDI and Robust Estimation

As outlined in Chapter 2 research into FDI/FDD for dynamic systems has long been recognized as one of the important aspects in accomplishing effective solutions to improve reliability of practical control systems. For modern aircraft, the model-based approach to FDI/FDD (based on analytical redundancy) has also long been emphasized for achieving robust and prompt detection of faults in the presence of modelling uncertainty for ensuring high reliability during flight mission. Some approaches to FDI/FDD are based on fault estimation as an alternative to the use of residual-based methods. As stated in Section 2.2, one of the goals of robust fault estimation is that the estimated fault can be used in fault compensation to achieve a form of active FTC system scheme. This chapter considers the development of active FTFC strategies for nonlinear flight control based on robust fault estimation.

The NDI controller based on feedback linearization processing is used to set the base-line controller for on-line approximately linearizing and decoupling the nonlinear aircraft as used in Chapters 5 & 6. A novel simultaneous state/fault estimator presented by Gao & Ding (2007) is combined with the base-line controller to compensate for the faults acting on the control system. For the linearized system with bounded input disturbance, a robust state-space observer is designed to simultaneously estimate system states and actuator faults by solving a Lyapunov equation. By introducing the estimated states and faults into the control loop, an FTC scheme is then achieved via a Linear Matrix Inequality (LMI) approach, which ensures stable operation of the controlled system when a suitably bounded fault occurs. The simulation results on the Machan UAV model demonstrate the efficiency and robustness of the proposed design under the scenario of different faults acting on three actuators and with wind turbulence assumed to disturb the aircraft motion affecting the normal velocity.

7.1 Introduction

The FDI/FDD schemes have received very significant attention in the literature since the 1980s, as demonstrated by the books (Patton, Frank & Clark, 1989; Gertler, 1998; Mangoubi, 1998; Chen & Patton, 1999; Patton, Frank & Clark, 2000; Simani, Fantuzzi & Patton, 2003;

Blanke, Kinnaert, Lunze & Staroswiecki, 2006, Isermann, 2006; Ding, 2008). However, most of these studies are developed for monitoring or diagnostic purposes, rather than for FTC applications. Even bearing this in mind the systematic study of the role of FDI/FDD in the overall framework for active FTC systems and reconfigurable control has also been of considerable interest, particular for FTFC (Patton, 1997).

Considering wider application problem, during the 2000s and more recently there has been a steady up-surge in interest in this subject. Many of the studies show the value of using state estimation-based FTFC schemes as this approach obviates the time-delay problem that is a major challenge in the use of reconfiguration based on real-time residual-based fault decision-making. Furthermore, since 2000 there has been a strong interest in the development of fast and robust fault estimation methods, e.g. using SMC (Edwards, Spurgeon & Patton, 2000), unknown input fault estimation (Koenig, 2005), finite time derivative fault estimation (Gao, Ding & Ma, 2007), fast adaptive fault estimation (Zhang, Jiang & Cocquempot, 2008). All of these methods involve joint state and fault estimation strategies that are important for application to FTC schemes, with the potential of robust estimation and fast fault compensation. The estimation of faults and states is needed to achieve a reliable control strategy, so that the system can continue to operate with reasonable performance in the presence of bounded faults and disturbances. A seamless integration of a fault estimation scheme within the appropriate reconfigurable control structure still poses significant challenges for theoretical development, realism in design towards real application studies (Zhang & Jiang, 2008).

The literature of the development of fault estimation within active FTC systems is well summarized in a Lipschitz non-linear descriptor system study by Gao and Ho (2006). These authors consider nonlinear systems with bounded input disturbances and bounded faults. A robust state-space observer is developed to simultaneously estimate the descriptor system states, actuator faults, their finite times derivatives, and attenuate input disturbances within any desired accuracy based on a Lyapunov approach. The descriptor states and faults are estimated and an FTC scheme is worked via a LMI technique to handle the actuator faults and disturbances. Gao and Ding (2007) extended this study to an actuator fault estimation approach for nonlinear descriptor systems as a strategy within a robust FTC scheme incorporating both state and fault estimation and fault compensation. They demonstrated an FTC design approach which ensures the closed-loop system to be stable using a suitable H_∞ performance index in the presence of bounded faults.

Considering advanced aircraft with high nonlinearity, MIMO control requirements, joint state, the fault estimation schemes have been shown to be important for FTFC systems involving flight reconfiguration when severe failures and structural damage occur (Banda, 1999; Boskovic, Bergström & Mehra, 2005; Cieslak, Henry, Zolghadri & Goupil, 2008). For FTFC the joint state and fault estimation ensures fast fault decision speed, accuracy and robustness in fault compensation.

For the purpose of efficiency and simplification, the procedure of feedback linearization as outlined in Chapter 4 has been proposed as a feasible design tool for nonlinear aircraft flight control systems (Isidori, 1995; Chang, 2009; Ducard, 2009) as discussed in the NDI controller form in Chapters 5 & 6. Feedback linearization seeks to remove nonlinear features from the system dynamics and provide a linearized and decoupled closed-loop form as a "base-line" start for developing good flight control structures. The use of NDI control has an advantage of simplicity in physical realization (Enns, Bugajski, Hendrick & Stein, 1994; Calise, Lee & Sharma, 2000). By using results from the NDI control strategy, an inner-loop/base-line controller design may ensure the stability of the nonlinear aircraft system.

In the light of the above background the contribution of this chapter lies in the application of the combined NDI controller with a robust estimator & active fault compensation FTC approach to the nonlinear aircraft system with wind turbulence and actuator faults. The proposed estimator and FTC scheme is efficient and reliable for real-time application on the Machan UAV test.

7.2 The Baseline Controller of Nonlinear Aircraft

The concept of feedback linearization introduced in Chapter 4 is further studied and incorporated with the dynamic inversion controller to the nonlinear aircraft for making use of the principle of transforming a smooth non-linear dynamical system into linear input-output form via feedback control, as illustrated and simulated in Chapter 5 & 6.

7.2.1 NDI controller based on feedback linearization theory

For the FTC control scheme in this chapter, the baseline control loop is also considered as the inner loop for online linearizing the system. The further outer-loop would be the FTC loop based on the information obtained from an estimator. Refer to the feedback linearization theory in Chapter 4 and the application in Chapter 5 & 6, for the MIMO affine nonlinear system as:

$$\begin{aligned} \dot{x} &= f(x) + g(x)u_{in} \\ y &= h(x) \end{aligned} \tag{7-1}$$

where state vector $x \in \mathcal{R}^n$, inner-loop control input vector $u_{in} \in \mathcal{R}^m$; controlled output vector $y \in \mathcal{R}^m$; nonlinear vector fields $f(x) \in \mathcal{R}^n$, $g(x) \in \mathcal{R}^{n\times m}$, and $h(x) \in \mathcal{R}^m$.

Following Section 5.2.1 define γ_i to be the smallest integer such that at least one of the inputs appears in ${y_i}^{(\gamma_i)}$using Lie derivatives as:

$${y_i}^{(\gamma_i)} = L_f^{\gamma_i} h_i + \sum_{j=1}^{m} \left(L_{g_i} L_f^{\gamma_i - 1} h_i u_{in_j} \right) \tag{7-2}$$

with at least one of the $L_{g_i} L_f^{\gamma_i - 1} h_i \neq 0 \forall x$, and u_{in_j} is the j^{th} row of u_{in}. The input-output relation can then be defined as:

$$[{y_1}^{(\gamma_1)} \quad {y_2}^{(\gamma_2)} \quad \dots \quad {y_m}^{(\gamma_m)}]^T = \alpha(x) + \beta(x) u_{in} \tag{7-3}$$

$$\alpha(x) = \begin{bmatrix} L_f^{\gamma_1} h_1(x) \\ \vdots \\ L_f^{\gamma_m} h_m(x) \end{bmatrix}, \beta(x) = \begin{bmatrix} L_{g_1} L_f^{\gamma_1 - 1} h_1 & \cdots & L_{g_m} L_f^{\gamma_1 - 1} h_1 \\ \vdots & \ddots & \vdots \\ L_{g_1} L_f^{\gamma_m - 1} h_m & \cdots & L_{g_m} L_f^{\gamma_m - 1} h_m \end{bmatrix} \tag{7-4}$$

The new system and input functions $\alpha(x)$ and $\beta(x)$ are introduced in (7-3) to achieve linear dependence between the inputs and outputs. If the matrix $\beta(x) \in \mathcal{R}^{m\times m}$ is invertible, then the system can be linearized by decoupling the non-linear terms in (7-3) by choosing u_{in} as:

$$u_{in} = \beta^{-1}(x)[-\alpha(x) + \nu] \tag{7-5}$$

Thus, if the feedback signal u_{in} in (7-5) is substituted into (7-3) the result is a closed-loop decoupled linear system as:

$$[{y_1}^{(\gamma_1)} \quad {y_2}^{(\gamma_2)} \quad \dots \quad {y_m}^{(\gamma_m)}]^T = [\nu_1 \quad \nu_2 \quad \dots \quad \nu_m]^T \tag{7-6}$$

By assuming that all the states of the system are measured as a special case in (7-1) as $y = x$, it then follows that:

$$\dot{y} = f(x) + g(x)u_{in} \tag{7-7}$$

which means $\dot{y}$ is determined by (7-4) in the case that $\alpha(x) = f(x), \beta(x) = g(x)$. If $g(x)$ is invertible, the control input u_{in} can be obtained as:

$$u_{in} = g^{-1}(x)[-f(x) + \nu] \tag{7-8}$$

As a result, the output of the closed-loop system is given by the solution to the following linear system:

$$\dot{y} = v \tag{7-9}$$

Since the system dynamics are used to obtain the inverse function $\beta^{-1}(x)$ of $\beta(x)$ for approximately cancelling the nonlinearity, this control approach is also known as NDI as described in Chapters 5 & 6. Once such kind of linearization has been achieved and the linearized system in (7-9) is achieved, any further control objectives may be easily met. In this case, a further simultaneous state/fault estimator and FTC scheme are concerned for the nonlinear aircraft.

7.2.2 Inner control loop of nonlinear aircraft

In Section 3.2 & 3.3, the essential details of the dynamics of the Machan UAV are described.

The *Euler equations* relating the forces X, Y, Z and moments L, M, N in the aircraft body axes to the angular and linear velocities in the inertial axes are given as [refer to (3-18) & (3-19)]:

$$\begin{aligned} m(\dot{u} + qw - rv) &= X \\ m(\dot{v} + ur - pw) &= Y \\ m(\dot{w} + vp - qu) &= Z \\ I_x\dot{p} + (I_z - I_y)rq &= L \\ I_y\dot{q} + (I_x - I_z)pr &= M \\ I_z\dot{r} + (I_y - I_z)pq &= N \end{aligned} \tag{7-10}$$

where, m is the mass of the aircraft. I_x, I_y, I_z are the moments of inertia about the axes through the centre of gravity parallel to the aircraft body axes. u, v and w are the forward, side and vertical velocity of the aircraft respectively. p, q and r are the roll, pitch and yaw rates, respectively.

The aerodynamic force and moment equations of the Machan UAV are given as [refer to (3-23) & (3-24)]:

$$\begin{aligned} X &= X_E - Dcos\alpha + (L_w + L_T)sin\alpha - mgsin\theta \\ Y &= Y_a + mgcos\theta sin\varphi \\ Z &= -(L_W + L_T)cos\alpha - Dsin\alpha + mgcos\theta cos\varphi \\ L &= L_a + L_E \\ M &= M_a + L_w(cg - 0.25)\bar{c} - L_q(l_t + 0.25 - cg) \\ N &= N_a \end{aligned} \tag{7-11}$$

where α (degree) is the incidence angle, θ and φ (degree) are the pitch angle and roll angle respectively, Y_a (N) is the side force, cg (%) is the position of the aircraft centre of gravity, X_E (N) is the thrust force due to the engine, l_t (N/m) is the tail moment, D (N) is the force

acting on the airframe, L_w, L_T and L_q (N) represent the wing lift, total tail lift and tail lift due to the pitch rate respectively, M_a, N_a and L_a (N/m) are the pitching moment, yawing moment and rolling moment component respectively, $\bar{c}$ (m) is the mean aerodynamic chord and L_E (N/m) is the rolling moment due to the engine.

The first order non-linear engine dynamic is given as [refer to Section 3.3.1]:

$$\dot{X}_E = (P_{max} T_c \eta_t - X_E U_2)/K_e \tag{7-12}$$

where, P_{max}, T_c, η_t, K_e and U_2 represent the maximum engine power, the throttle demand, the propeller efficiency, the engine rises rate and the air flow rate respectively (Aslin, 1985).

The open-loop Machan UAV is unstable as shown in Section 3.5, thus to achieve a stable fault estimator and FTC system, a closed-loop "base-line" control system must be configured before the FTC system can be developed. To achieve an inner-loop controller using the NDI control strategy in Section 7.2.1, the system variables are chosen to form a square and invertible matrix. To simplify the system and just to illustrate the methodology, only the rate variables $[p \quad q \quad r]^T$ are involved in this chapter, based on a relative degree requirement outlined in Section 4.4.

Thus the nonlinear model system state and input vectors are as:

$$\begin{gathered} x = [x_1 \quad x_2 \quad x_3]^T = [p \quad q \quad r]^T \\ u_{in} = [\delta_a \quad \delta_e \quad \delta_r]^T \end{gathered} \tag{7-13}$$

where δ_a, δ_e, δ_r are the control surface aileron, elevator and rudder, respectively.

To express the aircraft model in affine nonlinear functional form in (7-1), combine (7-10) to (7-12), the simplified (reduced order) nonlinear Machan equations can then be expressed in terms of:

$$f(x) = [f_p(x) \quad f_q(x) \quad f_r(x)]^T \tag{7-14}$$

with

$$\begin{aligned} f_p(x) &= (I_y - I_z) qr/I_x + l_p/I_x \\ f_q(x) &= (I_z - I_x) pr/I_y + l_q/I_y \\ f_r(x) &= (I_x - I_y) pq/I_z + l_r/I_z \end{aligned} \tag{7-15}$$

where the parameters l_p, l_q, l_r calculated from the aerodynamic coefficients have no relation to the inputs u_{in}.

The control distribution matrix of (7-1) is determined as:

$$g(x) = \begin{bmatrix} l_{\delta_a}/I_x & 0 & 0 \\ 0 & l_{\delta_e}/I_y & 0 \\ 0 & 0 & l_{\delta_r}/I_z \end{bmatrix} \tag{7-16}$$

The parameters l_{δ_a}, l_{δ_e}, l_{δ_r} are calculated from the aerodynamic coefficients related to control input u_{in}. Some of the model parameters are non-zero, so that the $g^{-1}(x)$ exists and hence the dynamic inversion controller can be achieved.

Commonly, v can be chosen as $v = \omega \cdot (x_d - x)$, where x_d is the desired output required by the outer-loop control law u_{out}; ω is the bandwidth described in Section 4.4. In this study, the bandwidth can be chosen as $\omega_p = \omega_q = \omega_r = 10rad \cdot s^{-1}$. The desired fast variable states can be defined as:

$$\begin{aligned} \dot{p}_d &= \omega_p \cdot (u_{outp} - p) \\ \dot{q}_d &= \omega_q \cdot (u_{outq} - q) \\ \dot{r}_d &= \omega_r \cdot (u_{outr} - r) \end{aligned} \tag{7-17}$$

where the suffices c and d represent the command signals and the desired values, respectively. Thus the inner-loop control law is derived from the NDI strategy above as:

$$u_{in} = g^{-1}(x)\left\{\begin{bmatrix} \dot{p}_d \\ \dot{q}_d \\ \dot{r}_d \end{bmatrix} - \begin{bmatrix} f_p(x) \\ f_q(x) \\ f_r(x) \end{bmatrix}\right\} \tag{7-18}$$

For the Machan UAV study the trimmed thrust is set as a constant value to ensure that the rolling moment has non-zero value. The resulting inner-loop NDI controller, shown in Figure 7-1, will be further represented in Figure 7-2 as "linearized system" block.

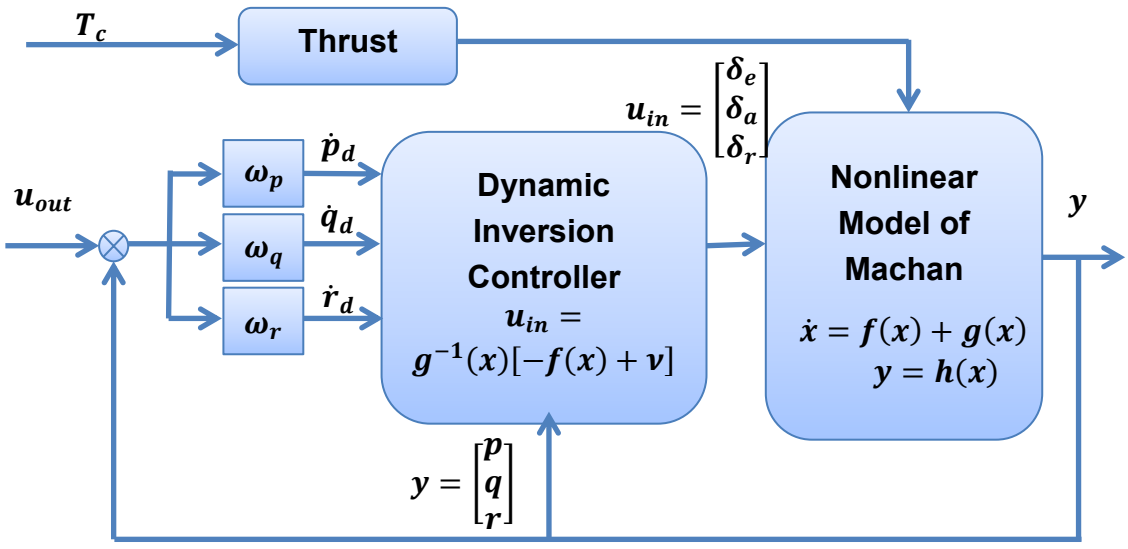

Figure 7-1 Inner loop NDI controller for nonlinear aircraft

7.3 Robust Estimator and Active FTC system

After feedback linearization by the NDI controller, the system model can be simplified to a classical linear state-space system introduced in Section 3.3.3 as:

$$\begin{aligned} \dot{x} &= Ax + Bu_{out} \\ y &= Cx \end{aligned} \tag{7-19}$$

where $x \in \mathcal{R}^n$; $u_{out} \in \mathcal{R}^m$ and $y \in \mathcal{R}^n$; u_{out} refers to the input vector for the linearized system derived from the outer-loop FTC controller.

A computational error is inevitable in solving the dynamic inversion matrix, thus the linearized system also needs on-line compensation to achieve a satisfactory degree of accuracy. By including a model description of the action of both actuator faults and random disturbances, the system described in (7-19) can be broadened to encompass systems (Gao & Ding, 2007) of the form:

$$\left.\begin{aligned} E\dot{x} &= Ax + Bu_{out} + \Phi(t, x, u_{out}) + B_d d + B_f f \\ y &= Cx \end{aligned}\right\} \tag{7-20}$$

where $d \in \mathcal{R}^l$ is the unknown bounded process disturbance vector; $f \in \mathcal{R}^k$ is the unknown actuator fault vector; $E \in \mathcal{R}^{n \times n}$ may be singular; B_d, B_f are constant real matrices of appropriate dimensions; $\Phi(t, x, u_{out}) \in \mathcal{R}^n$ is a smooth nonlinear vector function for compensating the inversion error and the unmodelled uncertainty. It is assumed that the actuator fault vector f has unknown fault components, but its q^{th} derivative $f^{(q)}$, is assumed to be bounded.

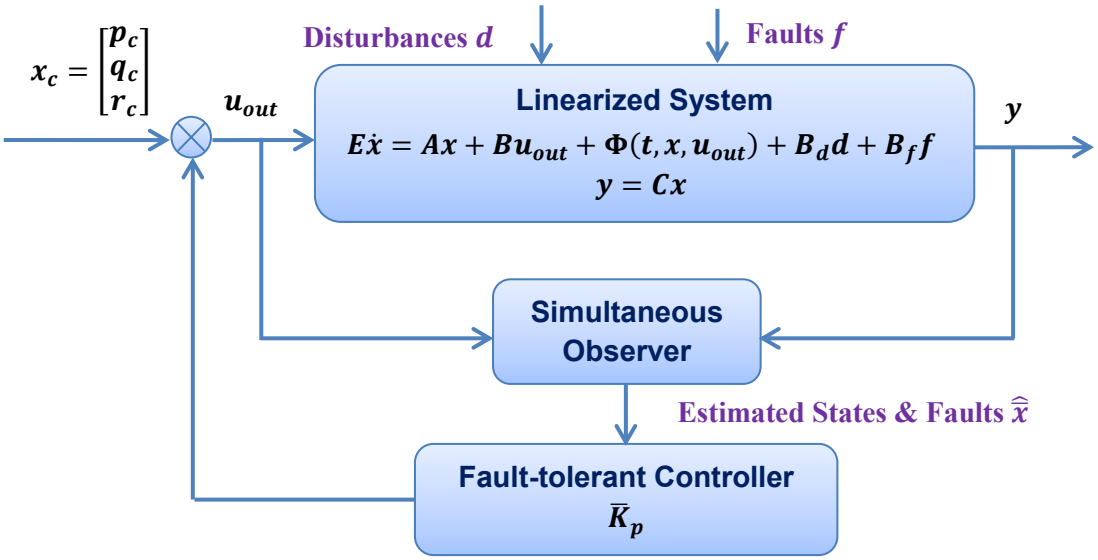

Figure 7-2 Fault estimation and FTC system

From the work of Gao and Ding (2007), the first step is to develop a robust state-space observer to estimate both the system states x and the fault signal f simultaneously by using the known input u_{out} and the measurement output y. The second step is to develop an efficient FTC scheme by using estimated information of states and faults. The complete design strategy is achieved by combining the above estimator with the dynamic inversion linearization procedure as illustrated in Figure 7-2.

7.3.1 Robust state and fault estimator

To simplify the notation in the determination of the robust estimation scheme let:

$$\xi_i = f^{(q-i)}(i = 1,2, \dots q) \tag{7-21}$$

and by using (7-20), an augmented descriptor process can be constructed as follows (Gao & Ding, 2007):

$$\left.\begin{array}{c} \bar{E}\dot{\bar{x}} = \bar{A}\bar{x} + \bar{B}u_{out} + \bar{B}_d d + \bar{G}f^{(q)} + \bar{\Phi}(t, x, u_{out}) \\ y = \bar{C}\bar{x} \end{array}\right\} \tag{7-22}$$

where

$$\begin{aligned} &\bar{n} = n + kq \\ &\bar{x} = \left[x^T, \xi_1^T, \xi_2^T, \dots, \xi_q^T\right]^T \in \mathcal{R}^{\bar{n}} \\ &\bar{\Phi}(t, x, u_{out}) = [\bar{\Phi}^T(t, x, u_{out}), 0, \dots, 0]^T \in \mathcal{R}^{\bar{n}} \\ &\bar{E} = blockdiag(E, I, \dots, I, I) \in \mathcal{R}^{\bar{n}\times\bar{n}} \\ &\bar{B} = [B^T, 0, 0, \dots, 0]^T \epsilon \mathcal{R}^{\bar{n}\times m} \\ &\bar{B}_d = [B_d^T, 0, 0, \dots, 0]^T \epsilon \mathcal{R}^{\bar{n}\times l} \\ &\bar{G} = [0, I_k, 0, \dots, 0]^T \epsilon \mathcal{R}^{\bar{n}\times k} \\ &\bar{C} = [C, 0, 0, \dots, 0, 0]^T \epsilon \mathcal{R}^{p\times\bar{n}} \\ &\bar{A} = \begin{bmatrix} A & 0 & & 0 & B_f \\ 0 & 0 & \cdots & 0 & 0 \\ 0 & I & & 0 & 0 \\ \vdots & & \ddots & \vdots & \\ 0 & 0 & \cdots & I & 0 \end{bmatrix} \epsilon \mathcal{R}^{\bar{n}\times\bar{n}} \end{aligned} \tag{7-23}$$

Consider a state-space dynamic system as follows:

$$\left.\begin{array}{c} \dot{\hat{z}} = \bar{A}\hat{\bar{x}} + \bar{B}u_{out} + (1 + \alpha_0)\bar{L}_p(y - \bar{C}\hat{\bar{x}}) + \bar{\Phi}(t, \hat{\bar{x}}, u_{out}) \\ \hat{\bar{x}} = (\bar{E} + \bar{L}_D\bar{C})^{-1}(\bar{z} + \bar{L}_D y) \end{array}\right\} \tag{7-24}$$

where $\hat{\bar{x}}\epsilon\mathcal{R}^{\bar{n}}$ is the estimate of the augmented state$\bar{x}\epsilon\mathcal{R}^{\bar{n}}$; proportional gains $\bar{L}_p$ and $\bar{L}_D$ are to be designed the following forms:

$$\bar{L}_D = [L_D^T \quad 0 \quad 0 \quad \dots \quad 0]^T \epsilon \mathcal{R}^{\bar{n}\times p} \tag{7-25}$$

$$\bar{L}_p = \begin{bmatrix} L_p^T & (L_I^1)^T & (L_I^2)^T & \dots & (L_I^q)^T \end{bmatrix}^T \epsilon \mathcal{R}^{\bar{n} \times p} \tag{7-26}$$

and α_0 is a positive scalar to be designed. $\bar{x} = \left[x^T, \xi_1^T, \xi_2^T, \dots, \xi_q^T\right]^T$ includes the estimated states $\hat{x}$, the fault derivative estimates $\hat{\xi}_i (i = 1,2, \dots q-1)$ and the fault estimates $\hat{\xi}_q = \hat{f}$, which enable the observer (7-22) to be a simultaneous state and fault estimator.

Then there exists a robust observer in the form of (7-22) for the plant (7-20) to make the steady estimator error dynamics as small as any desired accuracy, if the derivative gain $\bar{L}_D$ is well selected such that $\bar{S} = \bar{E} + \bar{L}_D \bar{C}$ is non-singular.

The proportional gain $\bar{L}_p$ is computed as:

$$\bar{L}_p = \bar{S}\bar{P}^{-1}C^T \tag{7-27}$$

where $\bar{P}$ can be solved from the Lyapunov equation:

$$-(\mu I + \bar{S}^{-1}\bar{A})^T \bar{P} - \bar{P}(\mu I + \bar{S}^{-1}\bar{A}) = -\bar{C}^T\bar{C} \tag{7-28}$$

with $\mu > 0$ satisfying $R_e[\lambda_i(\bar{S}^{-1}\bar{A})] > -\mu \forall i \epsilon \{1,2, \dots, \bar{n}\}$; the scalar α_0 is chosen with a positive scalar θ_0 as:

$$\alpha_0 = \theta_0^2 \left\| \bar{P}^{1/2}\bar{S}^{-1} \right\|^2 \tag{7-29}$$

with a reasonably large μ, the designed estimator can reduce the effects of the disturbance d and the fault model error $f^{(q)}$, as desired. The proof is given in Gao and Ding (2007).

7.3.2 Active FTC system based on estimated information

Consider system (7-20) and its augmented system (7-22). An observer-based controller can be constructed as (Gao & Ding, 2007):

$$\left.\begin{array}{c} \dot{\bar{z}} = \left[\bar{A} - (1+\alpha_0)\bar{L}_p\bar{C}\right]\hat{\bar{x}} + \bar{B}u_{out} + (1+\alpha_0)\bar{L}_p y + \bar{\Phi}(t, \hat{x}, u_{out}) \\ \hat{\bar{x}} = (\bar{E} + \bar{L}_D\bar{C})^{-1}(\bar{z} + \bar{L}_D y) \\ u = \bar{K}_p \hat{\bar{x}} \end{array}\right\} \tag{7-30}$$

where it is assumed that the observer gains $\bar{L}_D$, $\bar{L}_p$ and the scalar parameter α_0 are designed according to the procedure given in Section 7.3.1.

Let $\bar{K}_p = (K_p, K_f^1, K_f^2, \dots, K_f^q)$, with $K_p \epsilon \mathcal{R}^{m \times m}$ and $K_f^i \epsilon \mathcal{R}^{m \times k} (i = 1,2, \dots, q)$. By choosing:

$$K_f^q = -B^{\dagger}B_f \tag{7-31}$$

Then it is clear that: $B_f + BK_f^q = 0$. Furthermore, choose:

$$K_f^i = 0, i = 1,2, \dots, q-1 \tag{7-32}$$

The effect of the fault f on the plant can thus be removed since in this case the effect of the matrix B_f is absent in the descriptor system matrix $\bar{A}$ of (7-22) and (7-23).

If there exist a positive definite matrix $W \epsilon \mathcal{R}^{n \times n}$, and matrices $Q \epsilon \mathcal{R}^{(n-r) \times n}$, $Y \epsilon \mathcal{R}^{m \times n}$ such that:

$$\begin{bmatrix} \Gamma_{a11} & (\Gamma_{a12})^T & (\Gamma_{a13})^T & B_d \\ \Gamma_{a12} & -I & 0 & 0 \\ \Gamma_{a13} & 0 & -I & 0 \\ B_d^T & 0 & 0 & -\gamma^2 I \end{bmatrix} < 0 \tag{7-33}$$

where $\Gamma_{a11} = (AWE^T + AE_r^{\perp}Q + BY)^T + AWE^T + AE_r^{\perp}Q + BY + \theta^2 I$, $\Gamma_{a12} = WE^T + E_r^{\perp}Q$, $\Gamma_{a13} = CWE^T + CE_r^{\perp}Q$, $E_r^{\perp} \epsilon \mathcal{R}^{n \times (n-r)}$ is a matrix with the conditions that $EE_r^{\perp} = 0$ and rank $rank(E_r^{\perp}) = n - rank(E) = n - r$. Furthermore, if a feasible solution (W, Q, Y) exists in the LMI (7-33), the state-feedback gain can be computed as:

$$K_p = Y(WE^T + E_r^{\perp}Q)^{-1} \tag{7-34}$$

In this case, the normal dynamical output feedback controller (7-34) can perform a FTC operation by ensuring the closed-loop plant to be internally proper stable and attenuate the bounded input disturbance d with prescribed H_∞ performance.

7.4 Simulation and Evaluation

To achieve the robust estimator (7-20), construct an augmented model in the form of (7-22) with derivative order $q = 2$. Choose $\bar{L}_D = 0_{3\times9}$, $\mu = 15.8$, $\theta_0 = 0.5650$. From (7-29) one can compute $\alpha_0 = 0.1995$. By solving the Lyapunov function (7-28) and using (7-27), the observer gain can be determined as:

$$\bar{L}_p = 1 \times 10^6 \times \begin{bmatrix} 0.0001 & 0 & 0 \\ 0 & 0.0001 & 0 \\ 0 & 0 & 0.0001 \\ 0 & -1.7298 & 0 \\ 0 & 0 & -0.8201 \\ -4.8308 & 0 & 0 \\ 0 & -0.1896 & 0 \\ 0 & 0 & -0.0899 \\ -0.4195 & 0 & 0 \end{bmatrix} \tag{7-35}$$

This Gao and Ding (2007) estimator has a high gain, which may lead to an unrealizable range of gain magnitudes. However, the condition number of the gain matrix $\bar{L}_p$ is calculated as

$cond(\bar{L}_p) = 5.8449$, which is acceptable from a practical standpoint and is suitable for eliminating the effect of nonlinearity.

To achieve the robust FTC system, the choice of $\gamma = 0.5668$, and the solution of (7-33) & (7-34) lead to the following:

$$K_p = \begin{bmatrix} 0.7302 & 0 & 0 \\ 0 & 0.7302 & 0 \\ 0 & 0 & 1.2699 \end{bmatrix} \tag{7-36}$$

Choose $K_f^1 = 0_{3\times3}$ as in (7-32), K_f^2 is then defined as (7-31).

Therefore, the FTC gain matrix can be obtained as:

$$\bar{K}_p = \begin{bmatrix} K_p & K_f^1 & K_f^2 \end{bmatrix} \tag{7-37}$$

The simulation model was constructed implementing the UAV's preliminary configuration data, inertia and mass properties and static wind tunnel data. The aircraft trim conditions are: $V_T = 33m \cdot s^{-1}$, $h = 40m$. The trimmed throttle setting is $X_e = 55N$ and is held constant for ensuring the rolling moment L_E has non-zero value. All simulations begin from the trim condition.

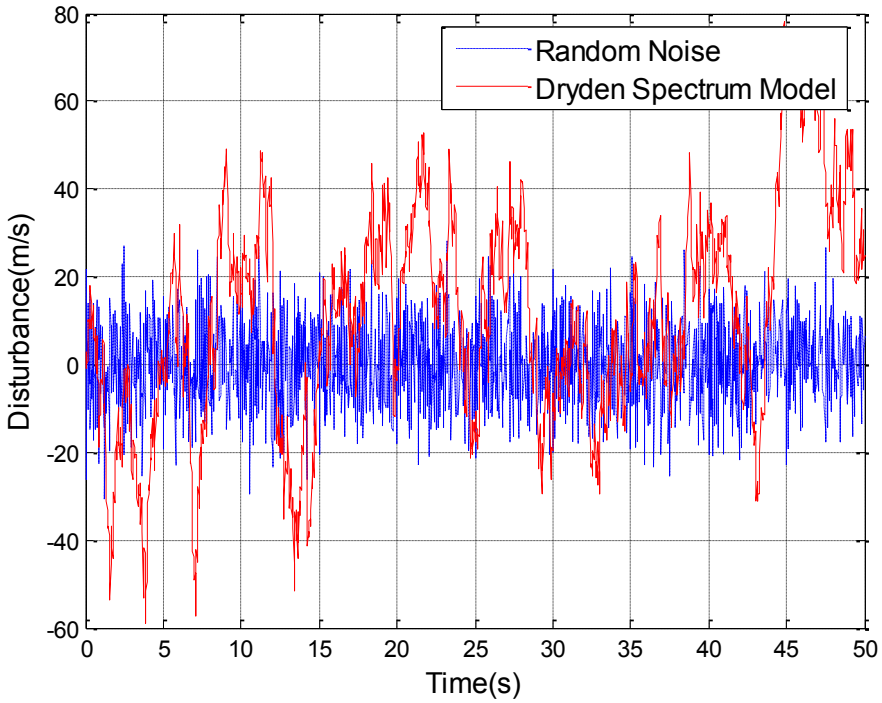

Figure 7-3 Wind disturbance model affecting normal velocity

The fault test signals acting on the elevator, aileron and rudder are depicted as a multi-step up-step down signal (rad), which is useful for exciting non-linearity and testing for fault detectability properties. The input command signals are chosen as: $[p_c \quad q_c \quad r_c] = [0 \quad 0 \quad 0]$, and the disturbance model affecting the normal velocity is according to the Dryden wind turbulence spectrum described in Section 3.4.3. The disturbances model responses are depicted in Figure 7-3.

The estimation results corresponding to the three actuator faults during wind disturbance are shown in Figure 7-4. The errors between the estimated states and real states are shown in Figure 7-5. Figure 7-6 shows the output responses resulting from the FTC system with wind turbulence acting on the normal velocity. From Figures 7-4 to 7-6, the efficient and accurate control performance demonstrates the robustness of this FTC strategy based on the estimation information of states and faults.

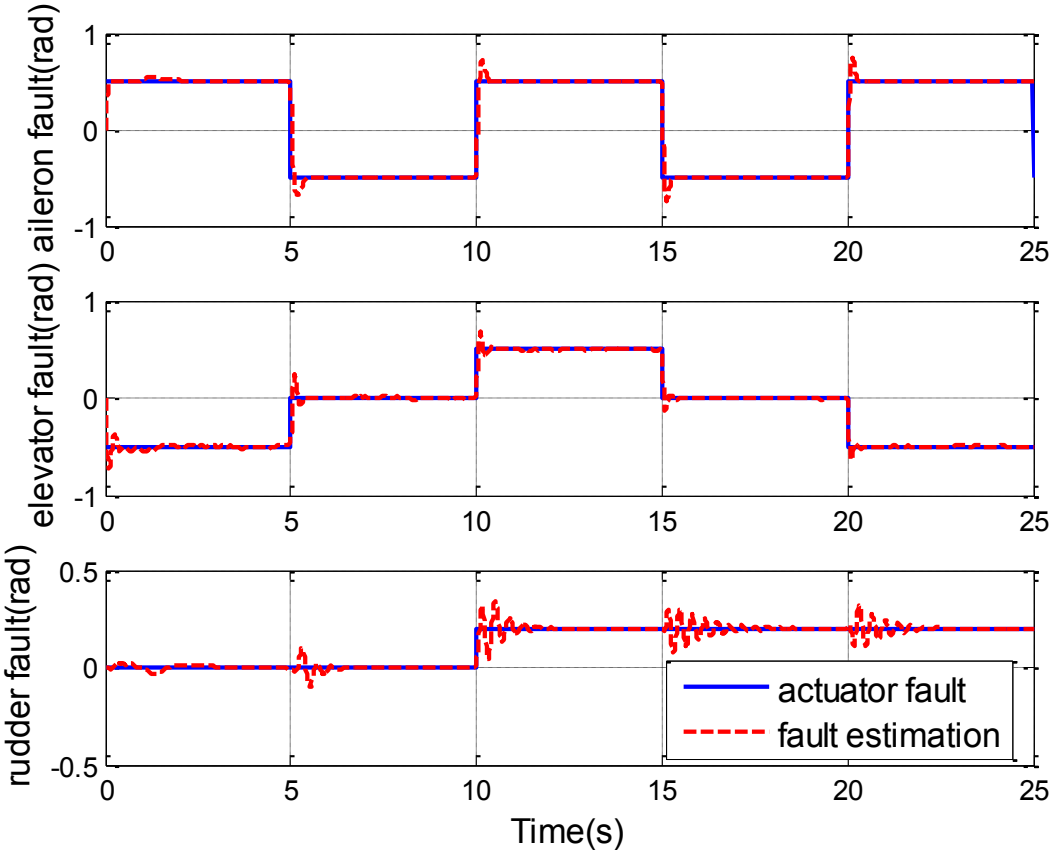

Figure 7-4 Faults and their estimation

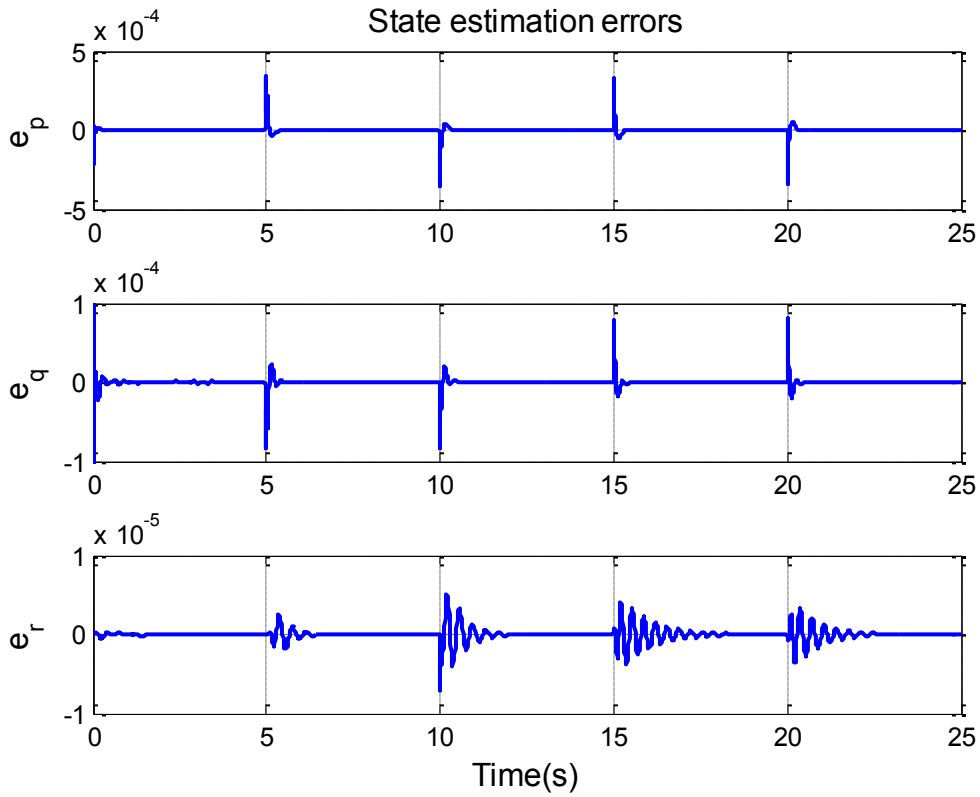

Figure 7-5 Errors between estimated and real states

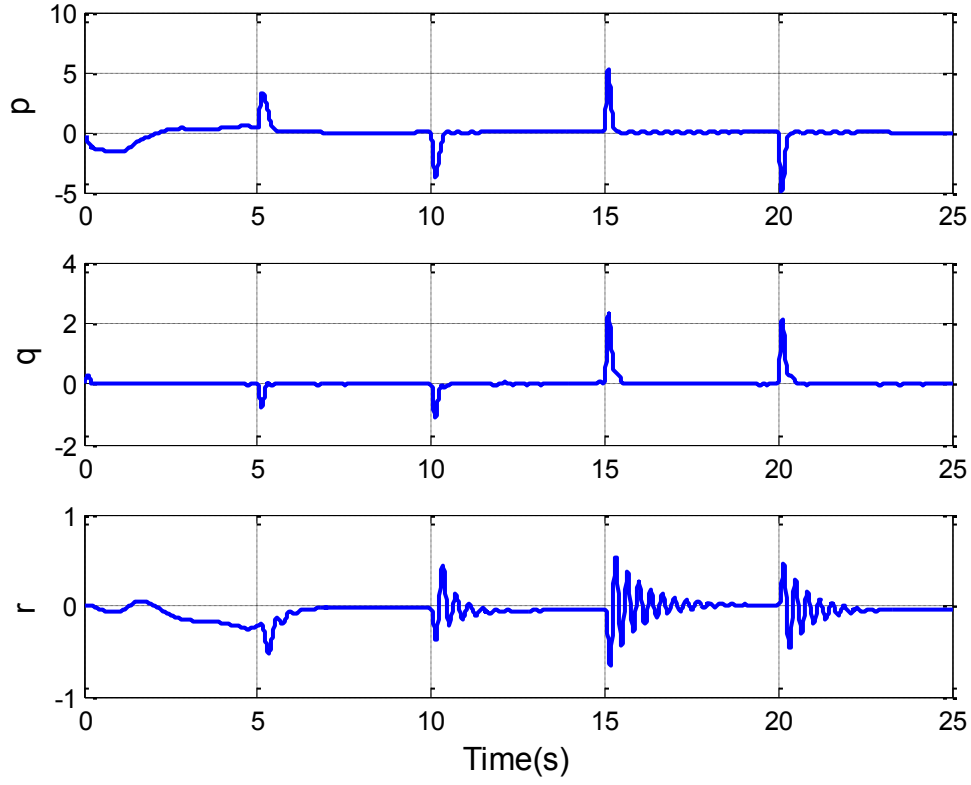

Figure 7-6 FTC system responses with faults and disturbance

7.5 Conclusion

In this chapter, the principle of NDI control design for nonlinear systems has been outlined through the use of feedback linearization. A robust estimator for simultaneous fault and state estimation is designed for the on-line linearized model by solving a Lyapunov equation. Based on the estimated vectors, the robust FTC loop is accomplished by using an LMI technique to ensure that the flight system satisfies robust performance. Both the estimator and the FTC are expressed in state-space form and are based on the original system matrices making them preferable for real control application. The full force and moment nonlinear UAV Machan has been used as an example of a system with highly nonlinear dynamics which are difficult to control. The simulation results demonstrate the robustness of the active FTC with fault estimation, corresponding to disturbances and faults. The results are very promising and demonstrate the ability of the vehicle to have reliable FTFC performance in the presence of some significant faults/failures and wind gust disturbance.

Chapter 8 A Boeing 747 Benchmark Study

This chapter focuses on the study of a large transport aircraft simulation benchmark developed by the European GARTEUR Flight Mechanics Action Group 16 (FM-AG 16) on "Fault Tolerant Flight Control" (FTFC) for the integrated evaluation of FDI/FDD and reconfigurable FTFC systems. The benchmark includes a suitable set of assessment criteria and failure cases, based on reconstructed accident scenarios, to assess the potential of new adaptive control strategies to improve aircraft survivability. The application of reconstruction and modelling techniques, using accident flight data for validation, has resulted in high fidelity non-linear aircraft and fault models to evaluate new FTFC concepts for the aircraft and their real-time performance to accommodate flight failures (Edwards, Lombaerts & Smaili, 2010).

The GARTEUR RECOVER Benchmark, validated with accident flight data and used during the GARTEUR FM-AG 16 project of FTFC is generally described in this chapter to outline the need for reliable flight control systems design. The proposed reconfigurable FTFC system described in Chapter 6 is applied in this chapter to the Boeing 747 RECOVER Benchmark that was used in the FM-AG 16 project. This control system is used as one of the feedback controllers during simulation of the benchmark. Since in this study only a few aerodynamic parameters from the benchmark system are known, the selected state variables of the benchmark are used to close the NDI control loop. The adaptive SMC-NN compensator is involved for tuning the total moments acting on the nonlinear aircraft model for mitigating the potentially failures. The simulation results demonstrate that the nonlinear FTFC using the adaptive compensator (based on advanced algorithms) shows considerable promise in terms of good reconfigurability and stability performance.

8.1 Introduction

8.1.1 Flight 1862 aircraft accident case

On October 4th, 1992, a Boeing 747-200F freighter aircraft, Flight El Al 1862 (refer to Chapter 1, as shown in Figure 1-3), went down near Amsterdam Schiphol Airport after the separation of both right-wing engines. In an attempt to return to the airport for an emergency landing, the aircraft flew several right-hand circuits in order to lose altitude and to line up

with the runway as intended by the crew. During the second line-up, the aircraft went out of the control and crashed into an eleven-floor apartment building in the Bijlmermeer, a suburb of Amsterdam, 13km east of the airport.

The accident investigation results, conducted by several organizations including the Netherlands Accident Investigation Bureau and the aircraft manufacturer Boeing, were hampered by the fact that the actual extent of the structural damage to the right-wing, due to the loss of both engines, was unknown. The analysis from this investigation concluded that given the performance and controllability of the aircraft after the separation of the engines, a successful landing was highly improbable (Smaili & Mulder, 2000).

In 1997, the division of Control and Simulation of the Faculty of Aerospace Engineering of the Delft University of Technology, in collaboration with the Netherlands National Aerospace Laboratory NLR, performed an independent analysis of the accident (Smaili & Mulder, 2000). The purpose of the analysis was to acquire an estimate of the actual flying capabilities of the aircraft and to study alternative control strategies for a successful flight recovery and landing safely. The application of this technique resulted in a simulation model of the impaired aircraft that could reasonably predict the performance, controllability effects and control surface deflections.

From 2004-2008, a research group on “Fault Tolerant Flight Control”, comprising a collaboration of thirteen European partners from industry, universities and research institutions, was established within the framework of the Group for Aeronautical Research and Technology in Europe (GARTEUR) co-operation program as shown in Table 8-1. The aim of the research group, FM-AG 16, is to demonstrate the capability and potential of innovative reconfigurable flight control algorithms to improve aircraft survivability. Despite that the faults of modern aircraft have been accommodated by hardware design using duplex, triplex or even quadruplex redundancy of critical components, the approach of the GARTEUR FM-AG 16 research still tried to focus on providing analytical redundancy by means of advanced adaptive control law to accommodate unanticipated faults that dramatically change the configuration of the aircraft. These methods take into account a novel combination of robustness, reconfiguration and adaptation of the FTFC system design (Lombaerts, Joosten, Breeman, Smaili, van den Boom, Chu & Verhaegen, 2006; Edwards, Lombaerts & Smaili, 2010; Lombaerts, Chu, Mulder & Joosten, 2011).

Table 8-1 GARTEUR FM-AG 16

Country	Member of FM-AG 16	Contact
France	Airbus France University of Bordeaux University of Lille	P. Goupil A. Zolghadri; D. Henry; J. Cieslak M. Staroswiecki
Germany	German Aerospace Center (DLR)	A. Varga
Netherland	Delft University of Technology NLR, National Aerospace Laboratory	J.A. Mulder; J. van den Boom J. Breeman, M H Smaili
Italy	CIRA, Flight Systems Department	A. Sollazzo
Great Britain	QinetQ DSTL University of Leicester University of Hull University of Cambridge	J. King J. Keirl C.Edwards, A. Alwi R. Patton J. Maciejowski
Denmark	University of Aalborg	Y. Zhang

The GARTEUR group addressed the need for high-fidelity nonlinear simulation models relying on accurate failure modelling to improve the prediction of reconfigurable system performance. As part of this research, the analysis of the reconstructed model of the Flight 1862 case was developed into the GARTEUR FM-AG 16 benchmark (available via the website of the project after registration: www.faulttolerantcontrol.nl) for the assessment of novel FTFC methods (Lombaerts, Joosten, Breeman, Smaili, van den Boom, Chu & Verhaegen, 2006).

The Flight 1862 failure mode configuration after the separation of both right-wing engines is modelled and studied in the GARTEUR FM-AG 16 program. An analysis of the engine separation dynamics concluded that the sequence was initiated by the detachment of the right inboard engine and pylon from the main wing due to a combination of structural overload and metal fatigue in the pylon-wing joint. Following detachment, the right inboard engine struck the right outboard engine in its trajectory also rupturing the right-wing leading edge up to the front spar. The associated loss of hydraulic systems resulted in limited control capabilities due to unavailable control surfaces aggravated by aerodynamic disturbances caused by the right-wing structural damage. The above analysis means that the crew of Flight 1862 was confronted with a flight condition that was very different from what they expected based on

training. The Flight 1862 failure mode configuration resulted in degraded flying qualities and performance that required adaptive and unconventional control strategies. The further simulation study on GARTEUR FM-AG 16 benchmark indicated that from a flight mechanics point of view, the Flight 1862 accident aircraft was recoverable if unconventional control strategies were used (Maciejowski & Jones, 2003; Lombaerts, Joosten, Breeman, Smaili, van den Boom, Chu & Verhaegen, 2006; Smaili, Breeman, Lombaerts & Stroosma, 2008; Lombaerts, Chu, Mulder & Joosten, 2011).

8.1.2 GARTEUR RECOVER benchmark

The GARTEUR benchmark simulation environment is based on the Delft University Aircraft Simulation and Analysis Tool DASMAT. The DASMAT tool was further enhanced with a full nonlinear simulation of the Boeing 747-100/200 aircraft, including flight control system architecture for the Flight 1862 accident study (Edwards, Lombaerts & Smaili, 2010). The original version of the Boeing 747-100/200 aircraft was developed, without the Flight 1862 accident details, at the University of Minnesota (Marcos & Balas, 2001). After the FM-AG 16 project the RECOVER simulation environment was subsequently further enhanced as a realistic tool for evaluation of FDI/FDD and FTC schemes within other research program and currently available at www.faulttolerantcontrol.nl.

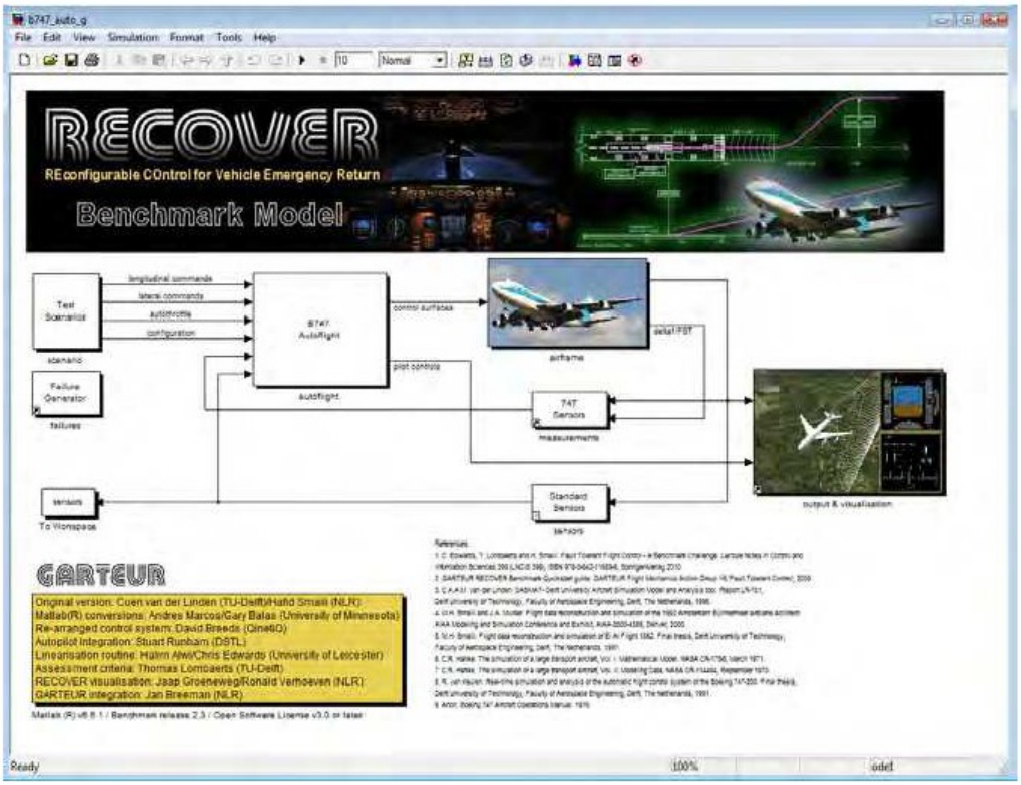

Figure 8-1 GARTEUR RECOVER Benchmark model components for closed-loop simulation

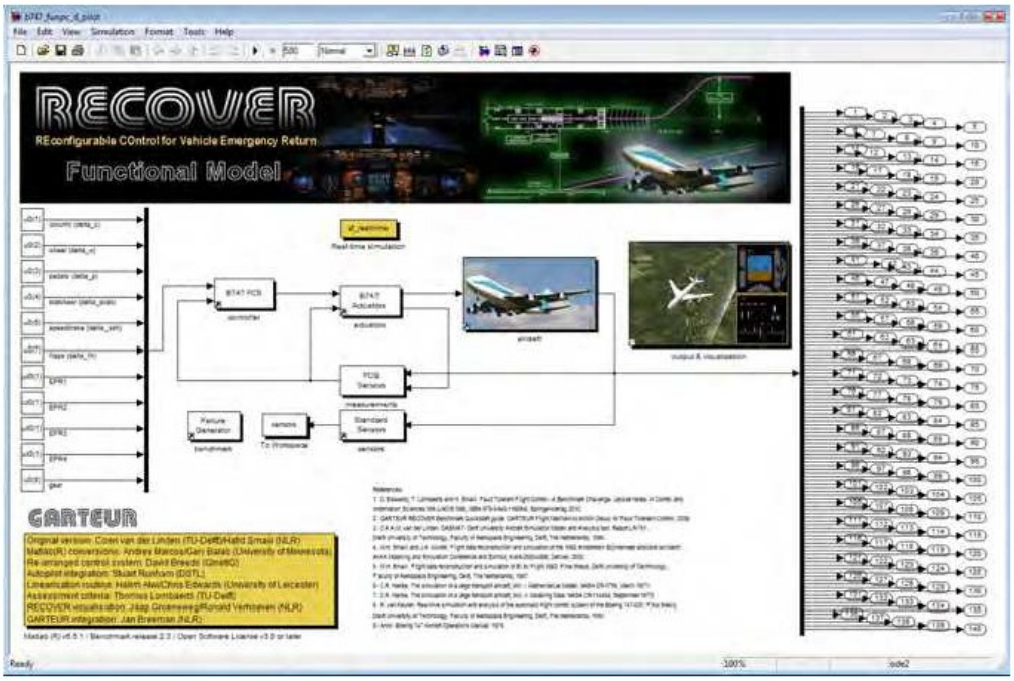

Figure 8-2 GARTEUR RECOVER Benchmark functional model for open-loop simulation

This benchmark has been developed as a Matlab/Simulink platform for the design and real-time evaluation of FTC techniques as shown in Figure 8-1 and Figure 8-2. The benchmark consists of a set of high fidelity simulation and flight control design tools including aircraft fault scenarios. For a representative simulation of damaged aircraft handling qualities and performances, the benchmark aircraft model has been validated against data from the Digital Flight Data Recorder of the Flight 1862 Boeing 747-200 accident aircraft (Smaili, Breeman & Lombaerts, 2012).

The GARTEUR FM-AG 16 RECOVER benchmark software package is equipped with several simulation and analysis tools, all centred around a generic nonlinear model for a 6DoF aircraft simulation. The tools of the GARTEUR FM-AG 16 RECOVER benchmark include trimming and linearization for flight control law design, nonlinear off-line simulation, simulation data analysis and flight trajectory. The test scenarios that are an integral part of the benchmark were selected to provide operational assessment criteria, as specifications for reconfigurable control, to evaluate the effectiveness and potential of the FTC methods. The benchmark also provides accurate aerodynamic and flight control failure models, realistic scenarios and assessment criteria for a civil large transport aircraft with fault conditions ranging in severity from major to catastrophic (Smaili, Breeman & Lombaerts, 2012). Figure 8-3 illustrates a schematic overview of the GARTEUR RECOVER benchmark including relationships between the different model components of the benchmark (Breeman, 2006).

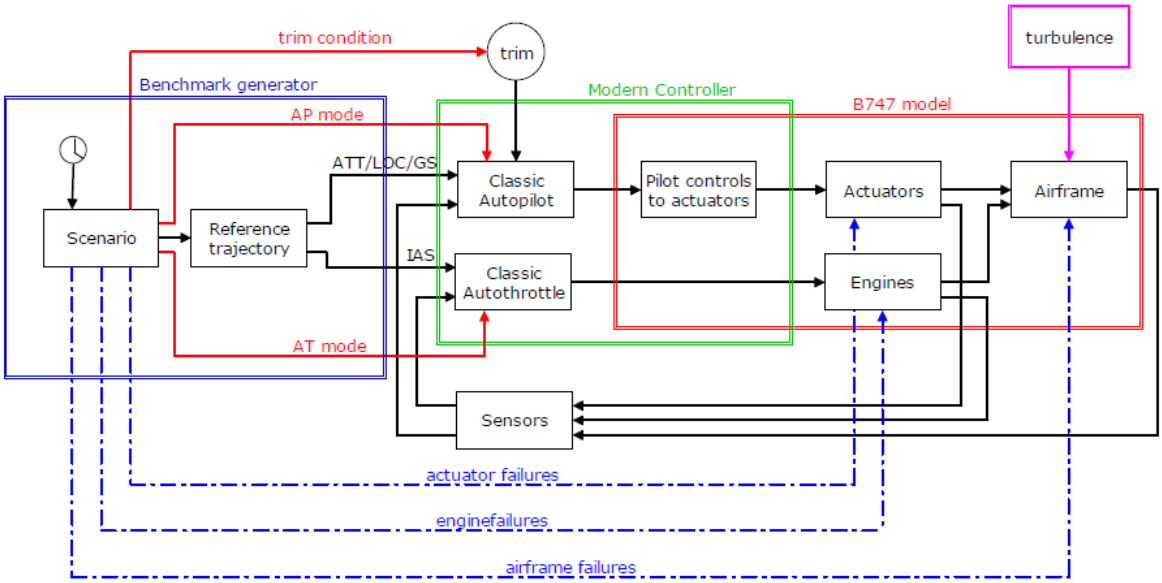

Figure 8-3 Detailed schematic of the GARTEUR benchmark model

As shown in Figure 8-3, the basic aircraft model of the benchmark contains airframe, actuator, engines and turbulence models and is represented by the red outline in the diagram. It was also desired to have a basic classical controller available in the benchmark, based on the Boeing 747 autopilot including auto-throttle, to serve as a reference for the new FTC controller developments. In order to operate the benchmark, a scenario and failure generator was added. The scenario consists of commands into the auto-pilot and auto-throttle, while the failures are directly introduced into the airframe and system models as indicated by the broken lines.

The data used for the Flight 1862 reconstruction, as part of the study conducted by Delft University, was obtained from the Netherlands National Aerospace Laboratory NLR. All fault scenarios, selected for the GARTEUR benchmark, have proven to be critical in recent aircraft accident and incident cases. The benchmark failure scenarios are listed in Table 8-2 (Breeman, 2006; Smaili, Breeman, Lombaerts & Stroosma, 2008).

As a flight integration simulator, the SIMONA (Simulation, Motion and Navigation) Research Simulator, built by the Delft University of Technology, represents a full 6DoF motion flight simulator, with a high performance motion system, wide field of view outside visual system, a programmable glass cockpit, hydraulically loaded flight controls and a flexible computer and software architecture as shown in Figure 8-4 (Smaili, Breeman, Lombaerts & Stroosma, 2008; Cieslak, Henry & Zolghadri, 2010).

Table 8-2 GARTEUR benchmark fault scenarios

Mode	Name	Description
0.	No failure	
1.	Stuck	All elevator surfaces are stuck in a faulty position with an offset from trim.
2.	Stuck aileron	All aileron surfaces are stuck in a faulty position with an offset form trim.
3.	Stabiliser runaway	The stabiliser surface moves quickly to an extreme position.
4.	Stuck rudder	All rudder surfaces move quickly to an extreme position.
5.	Stuck elevators (with turbulence)	The turbulence and wind can also be selected independently in the current benchmark.
6.	Stuck aileron (with turbulence)	
7.	Elevator runaway (with turbulence)	
8.	Stuck rudder (with turbulence)	
9.	Loss of vertical tail	The loss of the vertical tail leads to the loss of all rudder control surfaces as well as the loss of all damping in the roll and yaw axes.
10.	El Al failure case (dynamic method)	This implementation allows the introduction of the Flight 1862 failures within the benchmark run as required by scenario #1.
11.	El Al failure case (static method)	This failure mode is left to allow comparison with an earlier version of the Flight 1862 failure model. Since it is implemented using values in mask entries, it cannot be used for scenario #1, which requires a failure to occur at t=5s. Otherwise this should work the same as failure mode 10.

(a) Boeing 747 cockpit configuration (b) visual system dome

Figure 8-4 SIMONA research simulator for GARTEUR benchmark in the Delft University

For the piloted FTFC performance assessment, the SIMONA cockpit was configured to represent the Boeing747 aircraft type. For pilot workload measurements, the cockpit control wheel, column and pedal forces were recorded as a measure of pilot workload. The validation steps were performed to assure the benchmark model was implemented correctly. This included proof of match validation and piloted checkout of the baseline aircraft, control feel system and Flight 1862 controllability and performance characteristics (Smaili, Breeman & Lombaerts, 2012).

Several developed FTFC schemes for the GARTEUR benchmark model have been evaluated in a piloted simulator assessment using the SIMONA research simulation facility in a real-time integration, including reconstructed accident scenarios. In most cases, following slight failure transients, the pilot could continue to control the aircraft's stability, while the control algorithms successfully recover the damaged aircraft (Stroosma, Smaili & Mulder, 2009; Edwards, Lombaerts & Smaili, 2010; Smaili, Breeman & Lombaerts, 2012).

8.2 The Reconfigurable FTFC based on Moment Compensation

For the Flight 1862 case study, the flight control strategies, presented by the GARTEUR FM-AG 16 partners in Table 8-1, as an alternative controller scheme for maintaining stability during severe faults scenarios are (Smaili, 2006):

- **Robust control**: same controller deals with range of conditions.
- **Adaptive control**: controller structure fixed and parameters respond to tracking changes in aircraft.
- **Fault-tolerant/reconfigurable control**: FDI; actuator/sensor status feedback and on-line controller redesign.

The detailed study topic of FM-AG 16 is shown in Table 8-3 (Smaili, 2006). Referring to the methods listed in Table 8-3, it is noticed that that computational intelligent algorithms for accomplishing or improving flight reconfiguration ability had more emphasis in the project.

The Cambridge University team proposed Model Predictive Control (MPC) as a method for flight reconfiguration due to its ability to handle constraints and changing model dynamics systematically (Maciejowski & Jones, 2003). The jammed actuator and structural failures, within the Flight 1862 case, can be handled naturally in a an MPC framework via changes in the input constraints and internal model, which is used to make prediction in either an adaptive fashion with a multi-model switching scheme or by assuming an FDI/FDD scheme

which provides a fault model. The MPC simulation results show that it is possible to recover enough of the nominal performance that a pilot could continue to manoeuvre the aircraft after the damage sustained during Flight 1862.

Table 8-3 FTC methods of the FM-AG 16 partners

Partners of FM-AG 16	Fault tolerant control methods
• **Hull**	Analytical redundancy
• **Lille**	Analytical redundancy; Control re-allocation
• **Leicester**	Sliding modes control
• **Aalborg**	Interacting multiple models
• **Cambridge**	Model predictive control
• **Delft/NLR**	Model predictive control; Nonlinear dynamic inversion
• **QinetiQ**	Nonlinear dynamic inversion
• **DLR**	Least-order filter design
• **CIRA**	Trim analysis of nonlinear model (previous presentation)

The Leicester University team concerns the actuator and sensor FTFC schemes development and implementation based on SMC theory for this Boeing 747 benchmark (Alwi, 2008; Alwi, Edwards, Stroosma & Mulder, 2010). The SMC allocation schemes for FTFC based on integral action and model reference framework is proposed, which shows that faults and even certain total actuator failures can be handled directly without reconfiguring the controller. An adaptive gain for the nonlinear component of the SMC system is also included for compensating faults. The schemes have been evaluated by experienced pilots on the SIMONA flight simulator at Delft University of Technology and the test results have shown good performance in both nominal and failure scenarios.

The Bordeaux University team together with Airbus in Toulouse (Cieslak, Henry, Zolghadri & Goupil, 2007), proposed an FTFC strategy to provide a highly reliable “self-repairing” reconfigurable control scheme for the RECOVER benchmark system. Their work was based on the use of an FDI/FDD unit to detect and isolate the faults and incorporated a fault compensation loop. The key idea is that the design of FTC loop is done independently of the nominal autopilot and the nominal flight control system in place. Nonlinear simulation results demonstrate the capability and viability of the proposed FTFC scheme.

The Delft University of Technology/NLR team (Lombaerts, Chu, Mulder & Joosten, 2011) proposed a reconfiguring flight control algorithm for the damaged aircraft based upon a “two step method”, which combines real time physical model identification with adaptive NDI. In failure situations, the damaged aircraft model is identified and updated to the model-based adaptive NDI routine, which could reconfigure the aircraft system for the faults in real time. Reconfiguration test results for damaged aircraft models indicate good FTFC capabilities of this strategy. The analysis of the manual control in the SIMONA research simulator has demonstrated good handling qualities.

As a summary, for the model-based reconfigurable flight control strategies achieved with GARTEUR program, an on-line aerodynamic estimator is normally needed before the controller design to identify real-time performance and integration issues of the FTC during simulating integration of the Boeing 747 case. Since the NDI-based reconfigurable FTFC approach (original proposed by Calise, as introduced in Chapter 5) has been successfully simulated on this RECOVER benchmark (Lombaerts, Chu, Mulder & Joosten, 2011), the study in this chapter is aiming to testify the application performance on the Flight 1862 scenario by using the improved adaptive SMC-NN based on NDI reconfigurable FTFC scheme introduced in Chapter 6.

The Boeing 747 RECOVER benchmark model is complex and it is difficult to use the benchmark to analyze the effects of the failures. The model is constructed from recorded flight data and as a result, there are a large number of lookup tables. The aerodynamic parameter identification have not been available from the benchmark itself and they are not estimated in this study, thus some simplification for the aircraft model has to be used to obtain the FTFC results. The simplifications given in this Section are appropriate for the simulations described in Section 8.3.

The complete GARTEUR benchmark model was with 12 system states and based on a “fly-by-wire” version of the Boeing 747-100/200 aircraft, where all 30 aerodynamic control surfaces can be controlled individually, as shown in Table 8-4.

Table 8-4 States and control surfaces of the Boeing 747 benchmark

	No.	variable	symbol	unit
States x	1	body roll rate	*p*	rad/s
	2	body pitch rate	*q*	rad/s
	3	body yaw rate	*r*	rad/s
	4	true air speed	*V*	m/s
	5	angle of attack	*alpha* (α)	rad
	6	angle of sideslip	*beta* (β)	rad
	7	angle of roll	*phi* (ϕ)	rad
	8	angle of pitch	*theta* (θ)	rad
	9	angle of yaw	*psi* (ψ)	rad
	10	altitude	*h*	m
	11	distance in Xe-direction	*xe*	m
	12	distance in Ye-direction	*ye*	m
Control surfaces u	1	right inner aileron	*delta_air*	rad
	2	left inner aileron	*delta_ail*	rad
	3	right outer aileron	*delta_aor*	rad
	4	left outer aileron	*delta_aol*	rad
	5	spoiler aileron #1	*delta_sp1*	rad
	6	spoiler aileron #2	*delta_sp2*	rad
	7	spoiler aileron #3	*delta_sp3*	rad
	8	spoiler aileron #4	*delta_sp4*	rad
	9	spoiler aileron #5	*delta_sp5*	rad
	10	spoiler aileron #6	*delta_sp6*	rad
	11	spoiler aileron #7	*delta_sp7*	rad
	12	spoiler aileron #8	*delta_sp8*	rad
	13	spoiler aileron #9	*delta_sp9*	rad
	14	spoiler aileron #10	*delta_sp10*	rad
	15	spoiler aileron #11	*delta_sp11*	rad
	16	spoiler aileron #12	*delta_sp12*	rad
	17	right inner elevator	*delta_eir*	rad
	18	left inner elevator	*delta_eil*	rad
	19	right outer elevator	*delta_eor*	rad
	20	left outer elevator	*delta_eol*	rad
	21	stabiliser trim angle	*ih*	rad
	22	upper rudder surface	*delta_ru*	rad
	23	lower rudder surface	*delta_rl*	rad
	24	outer flaps	*delta_fo*	rad
	25	inner flaps	*delta_fi*	rad
Other controls u_t	1	thrust engine #1	*EPR1*	rad
	2	thrust engine #2	*EPR2*	rad
	3	thrust engine #3	*EPR3*	rad
	4	thrust engine #4	*EPR4*	rad
	5	gear position (up/down)	*gear*	0/1

As introduced in Section 3.2.3, the complete *Euler equations* relate the forces X, Y, Z and the moments L, M, N are shown as [refer to (3-17)]:

$$\begin{aligned} &I_x\dot{p} + \left(I_z - I_y\right)rq - I_{yz}(q^2 - r^2) - I_{xz}(\dot{r} + pq) - I_{xy}(\dot{q} - pr) = L + Ya_z - Za_y \\ &I_y\dot{q} + (I_x - I_z)pr - I_{yz}(\dot{r} - pq) - I_{xz}(r^2 - p^2) - I_{xy}(\dot{p} + qr) = M + Za_x - Xa_z \\ &I_z\dot{r} + (I_y - I_x)qr - I_{yz}(\dot{q} + pr) - I_{xz}(\dot{p} - rq) - I_{xy}(p^2 - q^2) = N + Xa_y - Ya_x \end{aligned} \quad (8\text{-}1)$$

where, m is the mass of the aircraft; I_x, I_y, I_z, I_{xy}, I_{yz}, I_{xz} are the moments of inertia about the axes through the centre of gravity but parallel to the aircraft body axes OX_B, OY_B, OZ_B; a_x, a_y, a_z are the co-ordinates of the centre of gravity with respect to the origin of the axes OX_B, OY_B, OZ_B; p, q and r are the roll, pitch and yaw rates, respectively.

Assuming that the origin of the inertial axis system, O, is at the vehicle's centre of gravity, leads to: $a_x = a_y = a_z = 0$.

However, in contrast to the simpler Machan UAV system, the Boeing 747 RECOVER benchmark is asymmetric, which leads to the moment of inertia $I_{xz} \neq 0$, although $I_{xy} = I_{yz} = 0$. Then the state variables p, q, r in (8-1) are expressed as:

$$\begin{aligned} \dot{p} &= \frac{I_y - I_z}{I_x}rq + \frac{(pq + \dot{r})I_{xz}}{I_x} + \frac{L}{I_x} \\ \dot{q} &= \frac{I_z - I_x}{I_y}pr + \frac{(r^2 - p^2)I_{xz}}{I_y} + \frac{M}{I_y} \\ \dot{r} &= \frac{I_x - I_y}{I_z}pq + \frac{(\dot{p} - qr)I_{xz}}{I_z} + \frac{N}{I_z} \end{aligned} \quad (8\text{-}2)$$

Additionally, the roll, pitch and yaw angles ϕ, θ and ψ are expressed in the terms of the rates p, q and r as [refer to (3-5)]:

$$\begin{aligned} \dot{\phi} &= p + qsin\phi tan\theta + r\,cos\phi tan\theta \\ \dot{\theta} &= qcos\phi - r\,sin\phi \\ \dot{\psi} &= qsin\phi sec\theta + rcos\phi sec\theta \end{aligned} \quad (8\text{-}3)$$

Since the detailed information of the aerodynamic parameters are not completely available in this case, the input vector u comprising the combined feedback linearization and decoupling control components are chosen following (8-2) as:

$$u = [u_1 \quad u_2 \quad u_3]^T = \left[\frac{L}{I_x} \quad \frac{M}{I_y} \quad \frac{N}{I_z}\right]^T \quad (8\text{-}4)$$

Then u_{real} can be calculated as follows as:

$$u_{real} = [\delta_a \quad \delta_e \quad \delta_r]^T = [l_{\delta_a} \quad l_{\delta_e} \quad l_{\delta_r}]^T u \quad (8\text{-}5)$$

where l_{δ_a}, l_{δ_e}, l_{δ_r} are all the linear parameters which can be estimated on-line in a complete FDI/FDD & FTC scheme according to the lookup tables of the benchmark model within the Matlab/Simulink environment.

Thus the vector expression of the affine system introduced in (5-1) for this Boeing 747 benchmark is chosen to be simplified as:

$$f(x) = \begin{bmatrix} p + qsin\phi tan\theta + r\,cos\phi tan\theta \\ qcos\phi - r\,sin\phi \\ qsin\phi sec\theta + rcos\phi sec\theta \\ \frac{(I_y - I_z)}{I_x} rq + \frac{(pq + \dot{r})I_{xz}}{I_x} \\ \frac{(I_z - I_x)}{I_y} pr + \frac{(r^2 - p^2)I_{xz}}{I_y} \\ \frac{(I_x - I_y)}{I_z} pq + \frac{(\dot{p} - qr)I_{xz}}{I_z} \end{bmatrix}$$

$$g(x) = \begin{bmatrix} 0_{3\times3} \\ I_{3\times3} \end{bmatrix}$$

$$h(x) = [I_{3\times3} \quad 0_{3\times3}] \tag{8-6}$$

The Two-stage closed-loop control design (refer to Section 5.3.1) using the NDI control method is used and the further SMC-NN based adaptor is added on the control input in the outer control loop for compensating the moment change caused by the fault actuators or structure damage.

8.3 Simulation and Evaluation

Simulations on the Boeing 747 benchmark were carried out on both the failed aircraft model with and without using the SMC-NN based reconfigurable controller.

First, the failed model is used in simulation to demonstrate the investigation of the basic aircraft behaviour without the control reconfiguration, during the failure event scenario. All the command line scripts in the Boeing 747 benchmark are set up to give reasonable defaults.

For the simulation the failure mode is selected as No. 10 referring to Flight 1862 failure case in Table 8-2. This kind of failure model is achieved by using *Boolean Function* to operate logic performance for simulating the aerodynamic change of the aircraft during Flight 1862 failure scenario. The related aerodynamic effect of this failure model is implemented as logic functions acting on the aircraft system, as shown in Table 8-5.

Table 8-5 Aerodynamics and their logic implement of Flight 1862 failure model

Aerodynamics	Physical Meaning	Logical Operation	
sys3	Hydraulic system no.3 pressure	On=1	Off=0
sys3	Hydraulic system no.4 pressure	On=1	Off=0
eng34	Engine no.3 & 4 separation	Operation=1	Separation=0
wd	Wind damage due to engine separation	No damage=1	Damage=0
m34	Account for engine separation 3&4 weight loss	No=1	Yes=0
ycg34	Lateral cg displacement due to engine 3 & 4 separation	No=1	Yes=0
eff	Degraded lateral control effects due to wing damage	No=1	Yes=0
eng4	Engine failure no.4	No=1	Yes=0

The fault signal is set to act at $t = 5s$ during the simulation by using a step-up time signal. The turbulence test scenario is also selected. The three angle mode is selected with constant reference values as: $[\phi_r \quad \theta_r \quad \psi_r] = [0 \quad 0 \quad 0]$. The simulation results are shown in Figures 8-5, 8-6, 8-7 & 8-8.

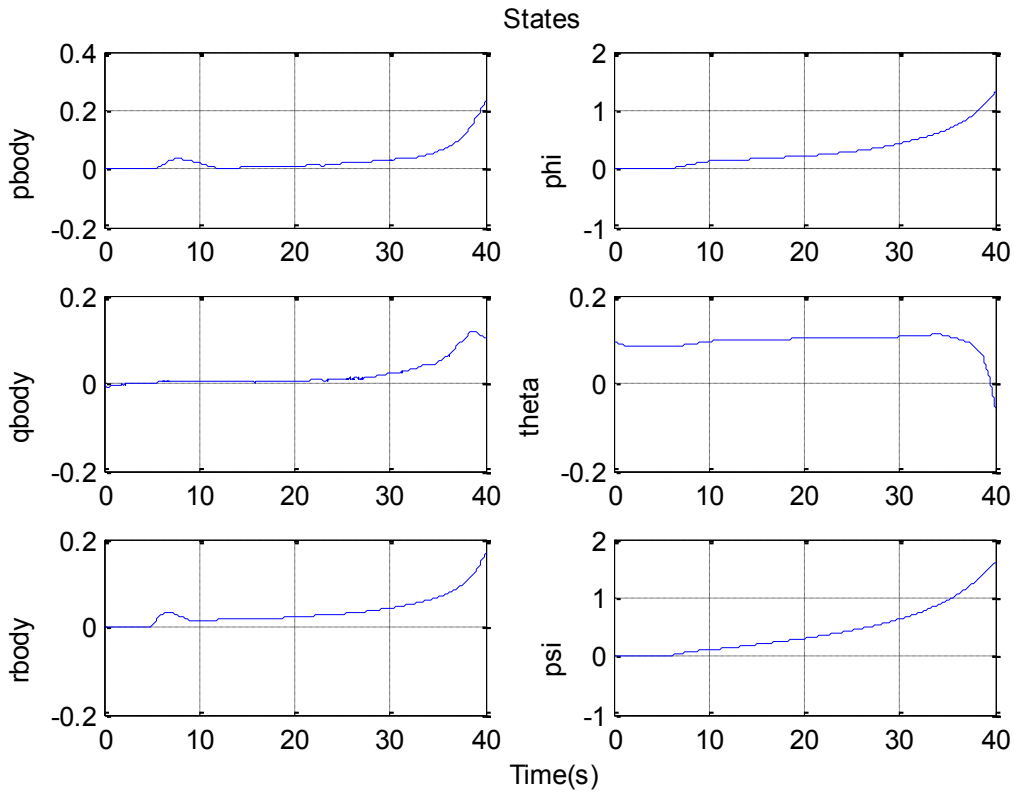

Figure 8-5 States response of Flight 1862 failure case without reconfigurable control

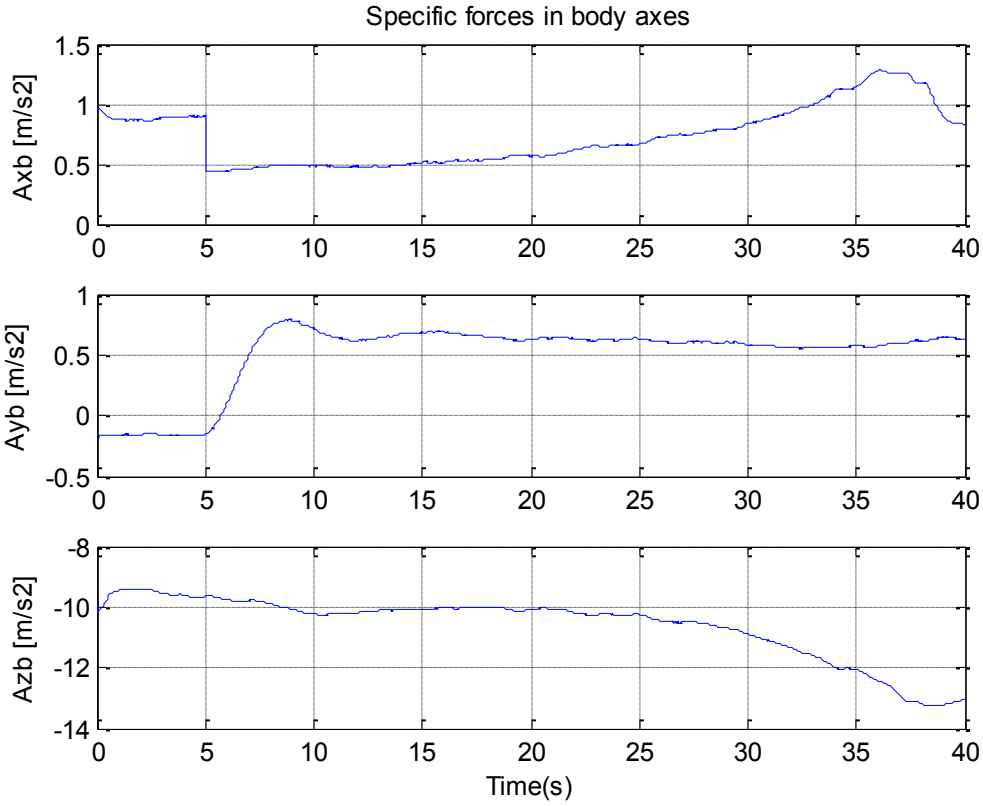

Figure 8-6 Specific forces response of Flight 1862 failure case without reconfigurable control

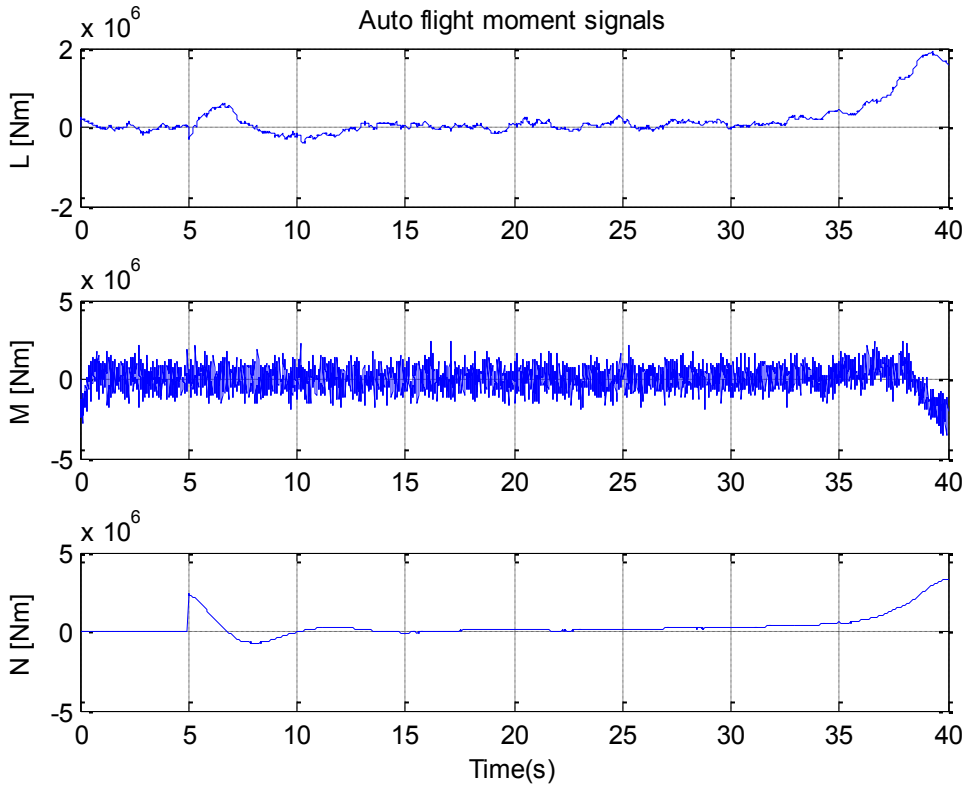

Figure 8-7 Moments response of Flight 1862 failure case without reconfigurable control

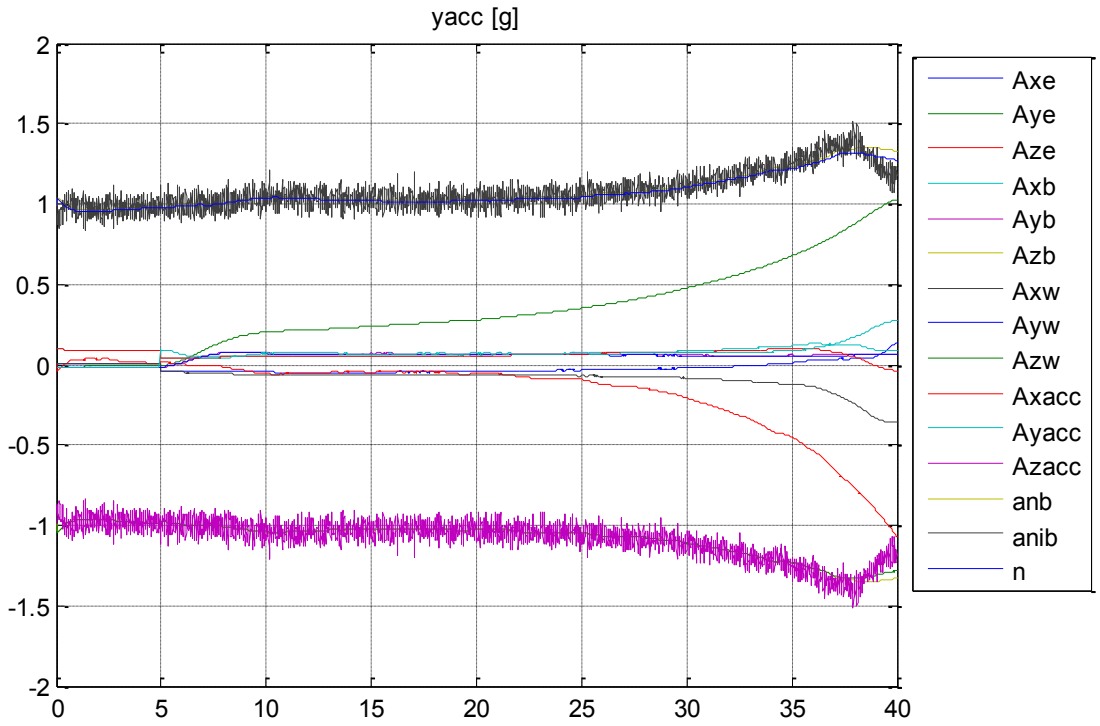

Figure 8-8 Aerodynamics response of Flight 1862 failure case without reconfigurable control

In Figures 8-5, 8-6, 8-7 & 8-8, the system response trajectories show the effect of the fault occurrence after 5 seconds of flight. Up to $t = 5s$ the flight is normal, but after that the flight parameters begin to diverge. The autopilot block shown in Figure 8-3 is an attempt to handle the faults during the simulation run until the failure occurs due to the exceeded value of the model validity.

Then adding the designed reconfigurable controller with SMC-NN based adaptor to the benchmark model, the simulation results under the same simulation scenario with failure event and turbulence are shown in Figures 8-9, 8-10, 8-11, 8-12 & 8-13.

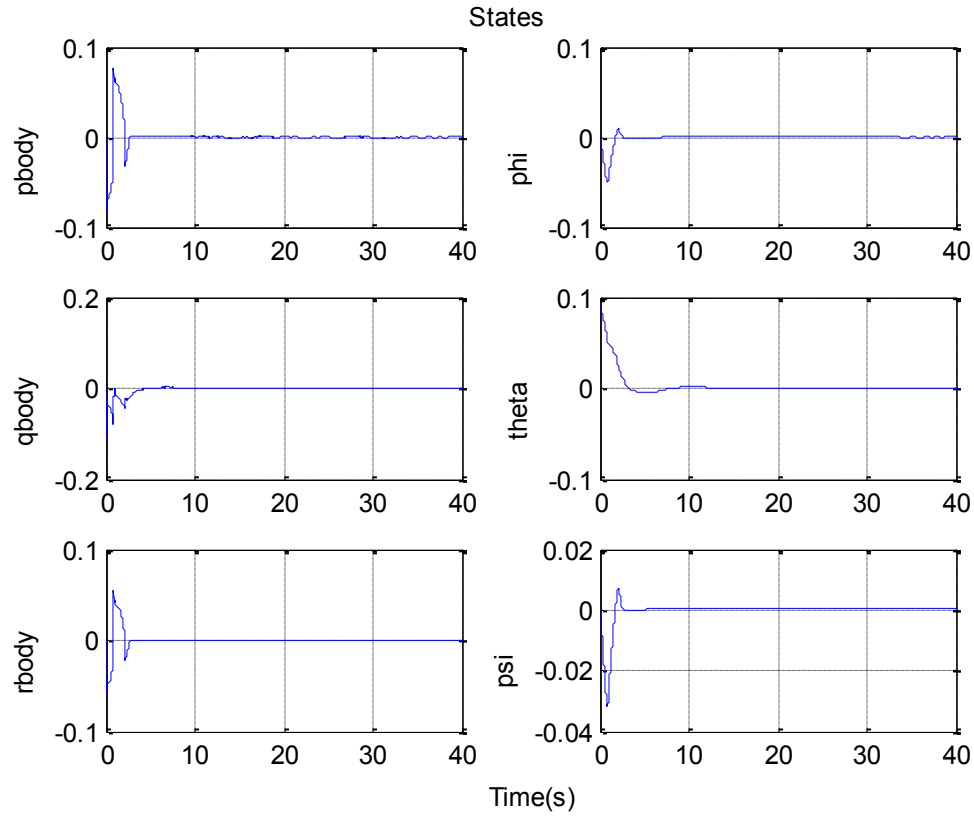

Figure 8-9 State responses of Flight 1862 failure case with reconfigurable control

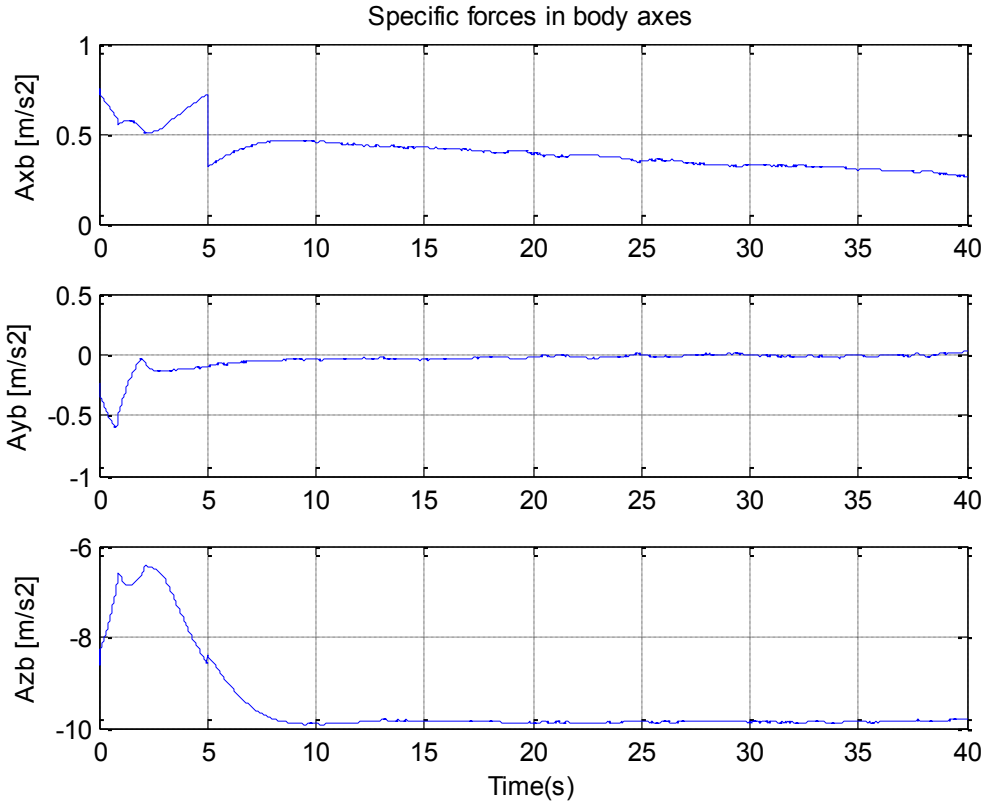

Figure 8-10 Specific forces response of Flight 1862 failure case with reconfigurable control

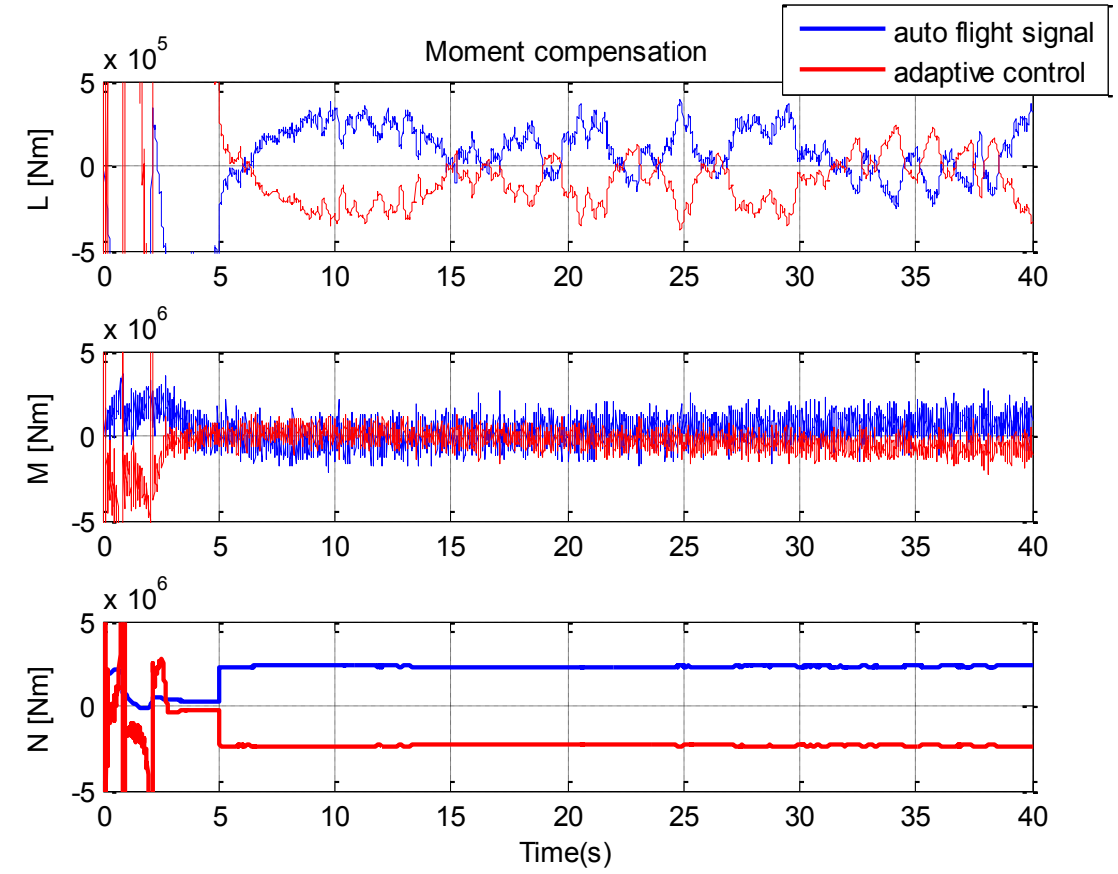

Figure 8-11 Moments response of Flight 1862 failure case with reconfigurable control

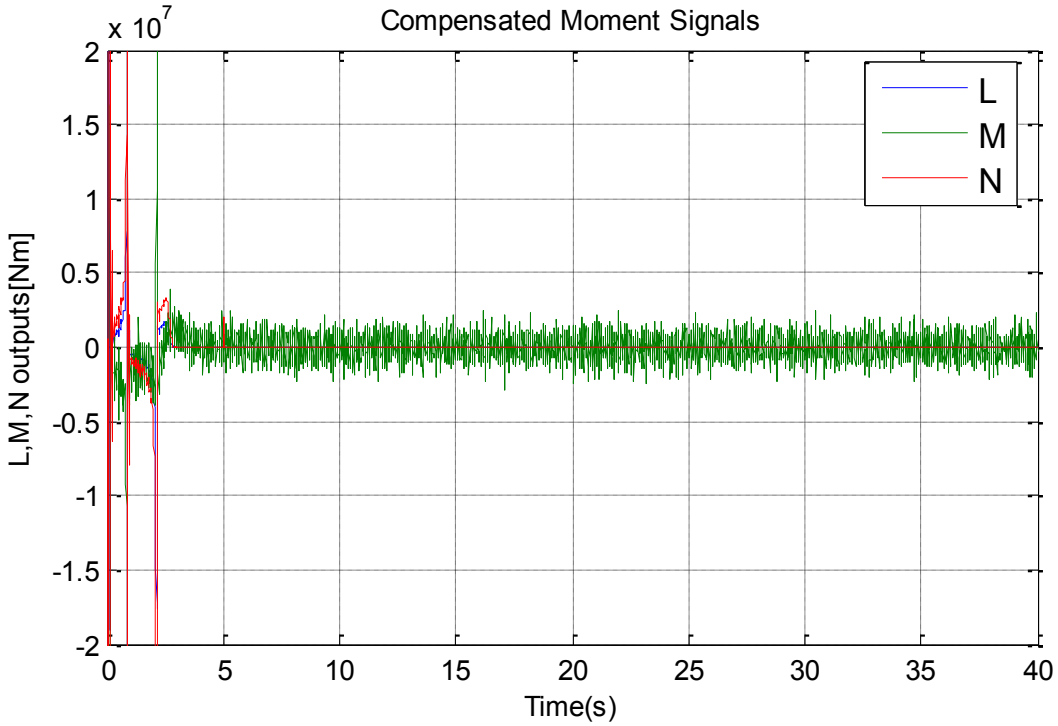

Figure 8-12 Compensated moments of Flight 1862 failure case with reconfigurable control

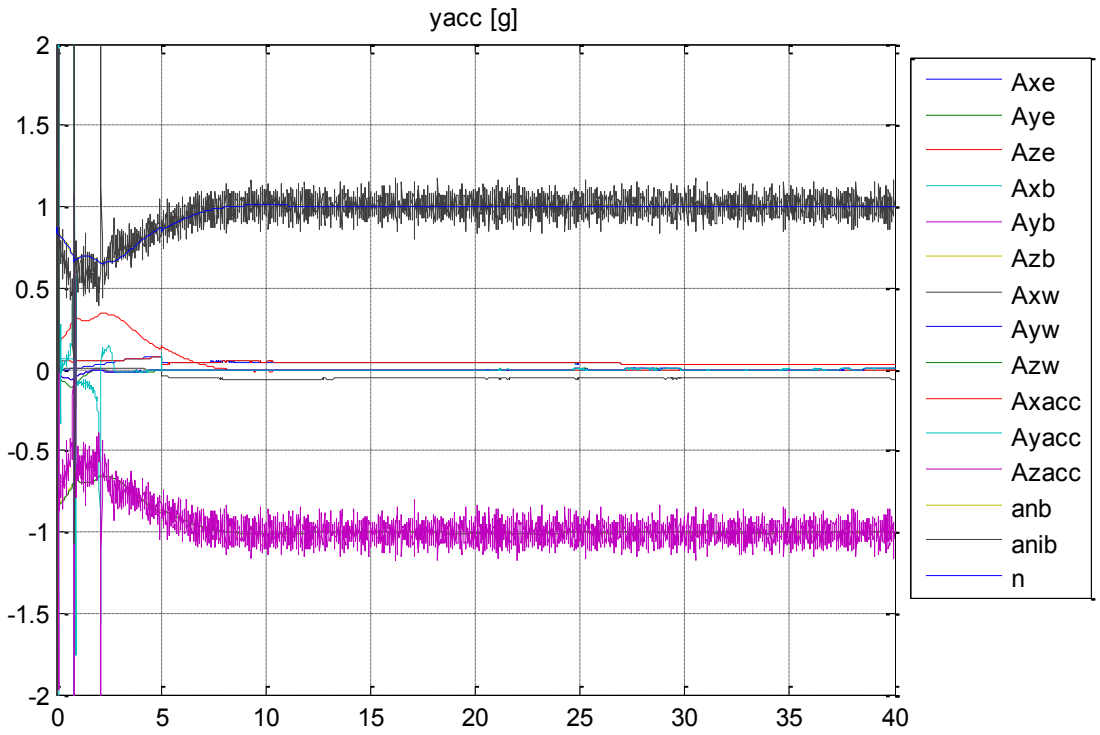

Figure 8-13 Aerodynamics response of Flight 1862 failure case with reconfigurable control

Again the sudden occurrence of the chosen fault test scenario is at $t = 5s$. Figure 8-9 to Figure 8-13 show that the damaged aircraft is still able to be controlled in a manner offset through the same manoeuvres. This indicates that the reference model was being successfully tracked by the reconfigurable FTFC element by compensating for the damage to the aircraft. It should be emphasized that Figure 8-11 shows that during the flight on the damaged aircraft the SMC-NN compensator has been used to adapt and compensate the drastically different moment responses after the structural failure occurs. The approximate value of the system tracking error is then used to counteract the real moment errors. Figure 8-12 gives the compensated moment outputs, which is the input to control the nonlinear aircraft motions. As a result, the stability of the simulated aircraft is maintained.

Thus, the system response comparisons between the control scheme with and without the proposed reconfigurable strategy shows that, starting from the same initial flight conditions and failure event scenario, the SMC-NN based reconfigurable FTFC system performs suitable control actions to compensate for the effects of the failure occurring on the simulated aircraft, avoiding the unstable condition which led to the fatal crash.

8.4 Conclusion

A Boeing 747 benchmark for the integrated evaluation of new FDI/FDD and reconfigurable FTFC techniques, developed within the framework of the European GARTEUR FM-AG 16 program on “Fault Tolerant Flight Control”, is introduced in this chapter. The chapter also provides the details of the Flight 1862 accident case within the RECOVER benchmark model architecture, including an outline of the mathematical models, tabulated fault scenarios and proposed control strategies. The use of the benchmark model is simplified for the simulation study due to the unavailability of the aerodynamic and control derivative parameters (as these have not been estimated on-line). The application of the concurrent SMC-NN based reconfigurable FTFC system presented in Chapter 6 to on-line compensation of the system tracking error is tested on the Boeing 747 RECOVER model. The simulation results of the benchmark obtained in Section 8.3 show a promising reconfiguration performance. Future study for complete flight control scheme will be encouraged by using this advanced algorithm in preventing and mitigating the problem of flight loss-of-control.

Chapter 9 Conclusions and Future Work

This chapter provides conclusions based on the work achieved in this thesis especially the successful combination of the concurrent NN with SMC in order to compensate system tracking error for a nonlinear aircraft reconfigurable FTFC problem subject to disturbance and faults. The limitation of this work and possible future research topics are also discussed, keeping in mind the application focus on modern nonlinear aircraft control design and application.

9.1 Conclusions

Following a brief definition of FTC in **Chapter 1** and a general overview of the main strategies behind the development of FTFC schemes in the literature in **Chapter 2**, this thesis provides the relevant background and preliminary knowledge for establishing a flight control system from the full force and moment equations of an aircraft. The goal of control is: (a) to provide inner-loop de-coupling of the aircraft dynamics into simple linearized subsystems and (b) develop a NN-based adaption mechanism for providing robust flight performance to (i) modelling uncertainties (e.g. arising from "system uncertainty") arising from a procedure of feedback linearization, (ii) bounded faults (e.g. actuator faults), in a reconfigurable FTFC scheme, and (iii) suitable wind gust alleviation. The flight dynamics of a nonlinear Machan UAV system are introduced in **Chapter 3**, via a suitable open-loop simulation study.

An approach of feedback linearization based on differential geometry is introduced in **Chapter 4** as a powerful method of developing a "baseline" controller for a fault-free aircraft system with the required linearization and de-coupling properties, bearing in mind the need to develop an FTFC scheme capable of having fault reconfiguration and gust alleviation properties. A study of the feasibility and validity of using a feedback linearization approach for a MIMO aircraft system based on a cascaded control strategy is considered by separating the aircraft system states into multiple closed-loops.

Based on the on-line linearizing and decoupling strategy for the nonlinear aircraft, the following FTFC control strategies are studied and tested via simulation using the nonlinear Machan UAV system in:

Chapter 5: As a development of feedback linearization the NDI strategy for nonlinear control is combined with a simplified concurrent NN learning adaptor to compensate for the aircraft system tracking error caused by faults, disturbance and system uncertainty. The combined NN learning adaptor and NDI scheme goal is required to have good reconfigurable FTFC properties.

Chapter 6: An improved approach to FTFC involving a combination of SMC theory for on-line training of a NN adaptive law within a simplified concurrent NN scheme is introduced.

Chapter 7: The NDI on-line linearization approach of Chapter 5 is extended further to include simultaneous state and fault estimation within an active FTC system made "active" by using on-line estimation and compensation of actuator fault.

The simulation results obtained from a tracking control demonstrate the improved FTFC performance for all the presented control schemes above, validated under various faults and disturbance scenarios.

A Boeing 747 nonlinear benchmark model, developed within the framework of the GARTEUR FM-AG 16 to study the EL AL flight 1862 failure scenario, is introduced and discussed in **Chapter 8** for simulation study and further testing. The application of the previously presented and studied concurrent SMC-NN based FTFC scheme is tested on this Boeing 747 RECOVER benchmark under certain model simplifications. The simulation results under the actual Flight 1862 failure scenario show a promising reconfiguration performance and future study for a complete flight control scheme using this compensation scheme is encouraged to further explore the reconfigurability and stability performance of this approach.

In general, the results show that the developed FTFC strategies based on feedback linearization combined with computational intelligence are able to handle faults that are potentially catastrophic. Suitable tolerance of faults before they become serious can avoid failures which may dramatically change the aircraft configuration.

9.2 Future Work

The first observation to be made is that in the proposed reconfigurable FTFC approaches, an adaptive NN element is used to recursively train some form of sequentially processed input-output data pairs. The purpose of training is to develop a parameterized mapping of the input data to the output data within a nonlinear system. The attractive universal approximation

properties of the NN form the leading basis for selecting the NN as an adaptive element. However, in the main body of the literature only local parameterization approaches have ever been achieved. If a global parameterization of the error were to be achieved, then an improvement in the performance of the adaptive control algorithm should follow.

Another important issue of the reconfigurable FTFC system based on NDI base-line controller and NN adaptor is that the *safe flight envelope* is determined by the saturation limits of the control inputs. The dynamic inversion process is only successful without control input saturation. Therefore, a method of so-called "pseudo control hedging" studied (Shin, Johnson & Calise, 2003; Lombaerts, Chu, Mulder & Joosten, 2011) could be used to scale back the reference signals such that control input saturation is prevented. In this context, this signal hedging sometimes can be considered as safe flight envelope enforcement. However, a more elaborate investigation of on-line safe flight envelope enforcement is a crucial point for future research.

Furthermore, little attention has been paid to the analysis and design with the overall system structure and interaction between FDI/FDD and Reconfigurable FTFC. However, from the viewpoint of FTFC design, the information provided by the existing FDI/FDD techniques for overall FTFC system design is crucial to systematically analyze the interaction between the FDI/FDD and FTFC functions for on-line applications.

Extensive study of the appropriate literature shows that real-world applications have so far been limited to very simple system examples, dealing with simple fault representations. It is a fact that the more advanced adaptive and intelligent approaches are not used in practice. One reason for this is due to a difficulty of certifying these approaches for flight safety for anything more advanced than simple switching approaches similar to redundancy management techniques. The need for approaches to enable rapid re-certification following any changes made to a previously cleared control law render the use of anything other than very simple approaches to flight control particularly difficult to verify and certify for air worthiness. A good example is the joint program by the USAF, USN, NASA and Boeing for demonstrating the NN adaptive approach on UAV control systems in 1999 (Steinberg, 2005). Although investigators claim that they continue to study this topic, nevertheless the program ended with the Boeing decision to not incorporate the adaptive approach on the aircraft. The value of using this approach has long been debated since the addition of a baseline control law may be a key to successful implementation of an adaptive approach. Thus, there is still

much progress that needs to be made before computational intelligence-based reconfigurable FTFC approaches can be regularly used.

Many other challenging issues still remain open for further research and development:

- The effects of sensor faults, which are considered minor in the presence of sensor redundancy and sensor loss detection.
- A complete proof of stability for the design of the sliding surface whilst including the effect of uncertainty should be an important research subject.
- The certification for the proposed FTFC strategies with Monte-Carlo test should be important (this has not been possible in the current study).
- Alternative design strategies to obtain better robustness and FTC performance for the flight control system, with strong robustness properties, including the effects of system uncertainty, handling of incipient faults (before they become serious), as well as very good wind gust alleviation.

As a final conclusion, the topics of "Fault Tolerant Control for Nonlinear Aircraft" are discussed briefly in this thesis. Although certain promising results can be provided to demonstrate the effect of the chosen control strategies, a more extensive comparative analysis of alternative methods should be an interesting recommendation for future research. Meanwhile, this subject awaits important stimulus from potential aerospace industrial collaborators, with a view to realistic in-house industrial evaluation studies.

References

ACARE (2012). "Horizon 2020", Advisory Council Aviation Research and Innovation in Europe, http://www.acare4europe.org/ (accessed 13th May 2013).

ADDSAFE (2009). EU FP7 project "Advanced Fault Diagnosis for Sustainable Flight Control", http://addsafe.deimos-space.com (accessed 4th April 2013).

Agrachev, A. A., & Sachkov, Y. (2004). *Control theory from the geometric viewpoint* (Vol. 2). Springer, New York.

Allen, M., Bernelli-Zazzera, F., & Scattolini, R. (2000). Sliding mode control of a large flexible space structure. *Control Engineering Practice*, 8(8), 861-871.

Alwi, H. (2008). Fault tolerant sliding mode control schemes with aerospace applications (Doctoral dissertation). University of Leicester.

Alwi, H., & Edwards, C. (2010). Fault tolerant control using sliding modes with on-line control allocation. Chapter 8 in *Fault Tolerant Flight Control*, Edwards, C., Lombaerts, T. and Smaili, H. M. (eds), 247-272. Springer, Berlin.

Alwi, H., Edwards, C., & Hamayun, M. T. (2011). Nonlinear integral sliding mode fault tolerant longitudinal aircraft control. IEEE International Conference on Control Applications, 970-975.

Alwi, H., Edwards, C., & Tan, C. P. (2011). *Fault detection and fault-tolerant control using sliding modes*. Springer.

Alwi, H., Edwards, C., Stroosma, O., & Mulder, J. A. (2010). Evaluation of a sliding mode fault-tolerant controller for the El Al incident. *Journal of Guidance, Control, and Dynamics*, 33(3), 677-694.

Aslin, P. (1985). Aircraft simulation and robust flight control system design. PhD thesis, Department of Electronics, University of York, UK.

Aström, K. J., & Wittenmark, B. (2008). *Adaptive control*. Dover Publications.

Banda, S. (Ed.). (1999). Special issue on reconfigurable flight control system design. *International Journal of Robust and Nonlinear Control*, 9(14), 997–1115.

Bartolini, G., Ferrara, A., & Utkin, V. I. (1995). Adaptive sliding mode control in discrete-time systems. *Automatica*, 31(5), 769-773.

Bartolini, G., Ferrara, A., & Usani, E. (1998). Chattering avoidance by second-order sliding mode control. *IEEE Trans. on Automatic Control*, 43(2), 241-246.

Bartolini, G., Pisano, A., Punta, E., & Usai, E. (2003). A survey of applications of second-order sliding mode control to mechanical systems. *International Journal of Control*, 76, 875-892.

Bartoszewicz, A. (1998). On the robustness of variable structure systems in the presence of measurement noise. In Proceedings of the 24th Annual Conference of the IEEE in Industrial Electronics Society (IECON'98), 3, 1733-1736.

Beard, H. E. (1994). Intelligent fault diagnosis and control reconfiguration. *IEEE Control Systems Magazine*, 14(3), 6–12.

Bedrossian, N. S. (1991). Nonlinear control using linearizing transformations. PhD thesis, the Department of Mechanical Engineering, Massachusetts Institute of Technology.

Bekit, B. W., Whidborne, J. F., & Seneviratne, L. D. (1997). Fuzzy sliding mode control for a robot manipulator. In Proceedings of the 1997 IEEE International Symposium on Computational Intelligence in Robotics and Automation, 320-325.

Belcastro, C. M., & Belcastro, C. M. (2001). Application of fault detection, identification, and accommodation methods for improved aircraft safety. In Proceedings of the 2001 American Control Conference, 2623–2624.

Belkharraz, A. I., & Sobel, K. (2000). Fault tolerant flight control for a class of control surface failures. In Proceedings of the 2000 IEEE American Control Conference, 6, 4209-4213.

Benosman, M. (2009). A survey of some recent results on nonlinear fault tolerant control. Mathematical Problems in Engineering, vol. 2009.

Blanke, M., Frei, C., Kraus, F., Patton, R. J., & Staroswiecki, M. (2000). What is fault-tolerant control. In Proceedings of the 4th IFAC Symposium on Fault Detection, Supervision and Safety for Technical Process, 40–51.

Blanke, M., Kinnaert, M., Lunze, J., Staroswiecki M., & Schröder J. (2006). *Diagnosis and Fault-Tolerant Control*. Springer-Verlag, New York.

Blanke, M., Staroswiecki, M., &Wu, N. E. (2001). Concepts and methods in fault-tolerant control. In Proceedings of the 2001 American Control Conference, 2606–2620.

Bodson, M. (2003). Reconfigurable nonlinear autopilot. *Journal of Guidance, Control, and Dynamics*, 26(5): 719-727.

Bodson, M., & Groszkiewicz, J. E. (1997). Multivariable adaptive algorithms for reconfigurable flight control. *IEEE Trans. on Control Systems Technology*, 5(2), 217-229.

Boskovic, J. D. & Mehra, R. K. (2001). A hybrid fault-tolerant scheme for flight control applications. In Proceedings of the AIAA Guidance, Navigation, and Control Conference and Exhibit.

Boskovic, J. D., Bergström, S. E., & Mehra, R. K. (2005). Robust integrated flight control design under failures, damage, and state-dependent disturbances. *Journal of Guidance, Control, and Dynamics*, 28(5), 902–917.

Boskovic, J. D., Prasanth, R., & Mehra, R. K. (2007). Retrofit fault-tolerant flight control design under control effector damage. *Journal of Guidance, Control, and Dynamics*, 30(3), 703–712.

Breeman, J. (2006). Quick start guide to AG 16 benchmark model. National Aerospace Lab. (The Netherlands) Technical Rept.

Brian, L. S., & Frank, L. L. (2003). *Aircraft control and simulation*. John Wiley & Sons, New York.

Brinker, J. S., & Wise, K. A. (1996). Stability and flying qualities robustness of a dynamic inversion aircraft control law. Journal of Guidance, Control, and Dynamics, 19(6), 1270-1277.

Brockett, R. W., Millman, R. S., & Sussmann, H. J. (Eds.). (1983). *Differential geometric control theory*. In Proceedings of the conference held at Michigan Technological University, June 28-July 2, (Vol. 27). Birkhauser.

Brunovský, P. (1970). A classification of linear controllable systems. Kybernetika, 6(3), 173-188.

Bryan, G. H. (1911). *Stability in aviation: an introduction to dynamic stability as applied to the motions of aeroplanes*. Macmillan, London.

Bullo, F., & Lewis, A. D. (2004). *Geometric control of mechanical systems* (Vol. 49). Springer.

Buonanno, A., & Cook, M. V. (2005). An aerodynamic simulation model of the Eclipse UAV. Internal Report FLAV-A01-002.

Burcham F. W., Fullerton, C. G., & Maine, T. A. (2004). Manual manipulation of engine throttles for emergency flight control. NASA Dryden Flight Research Center, Technical Report NASA/TM, 212045.

Burcham, F. W., Burken, J. J., Maine, T. A., & Fullerton, C. G. (1997). Development and flight test of an emergency flight control system using only engine thrust on an MD-11 transport airplane. National Aeronautics and Space Administration, Dryden Flight Research Center.

Byrnes, C. I., & Isidori, A. (2000). Output regulation for nonlinear systems: an overview. *International Journal of Robust and Nonlinear Control*, 10(5), 323-337.

Byrnes, C. I., Isidori, A., & Willems, J. C. (1991). Passivity, feedback equivalence, and the global stabilization of minimum phase nonlinear systems. *IEEE Trans. on Automatic Control*, 36(11), 1228-1240.

Byrnes, C. I., Priscoli, F. D., & Isidori, A. (1997). *Output regulation of uncertain nonlinear systems*. Birkhauser.

Byushgens, G. S. & Studnev, R. V. (1988). *Aircraft Dynamics. Spatial Motion*. Mashinostroenie.

Calise, A. J., Lee, S., & Sharma, M. (1998a). Direct adaptive reconfigurable control of a tailless fighter aircraft. In AIAA Guidance, Navigation and Control Conference, 1, 88-97.

Calise, A. J., & Rysdyk, R. T. (1998b). Nonlinear adaptive flight control using neural networks. *Control Systems*, 18(6), 14-25.

Calise, A. J., Hovakimyan, N., & Idan, M. (2001). Adaptive output feedback control of nonlinear systems using neural networks. *Automatica*, 37(8), 1201-1211.

Calise, A. J., Lee, S., & Sharma, M. (2000). Development of a reconfigurable flight control law for the X-36 tailless fighter aircraft. In AIAA Guidance, Navigation, and Control Conference.

Camacho, O., & Smith, C. A. (2000). Sliding mode control: an approach to regulate nonlinear chemical processes. *ISA transactions*, 39(2), 205-218.

Carpita, M., & Marchesoni, M. (1996). Experimental study of a power conditioning system using sliding mode control. *IEEE Trans. on Power Electronics*, 11(5), 731-742.

Castillo, I., Edgar, T. F., & Fernández, B. R. (2012). Robust model-based fault detection and isolation for nonlinear processes using sliding modes. *International Journal of Robust and Nonlinear Control*, 22(1), 89-104.

Chandler, P. R. (1984). Self-repairing flight control system reliability a maintainability program—Executive overview. In IEE National Aerospace and Electronics Conference, 586–590.

Chang, Y. (2009). Adaptive sliding mode control of multi-input nonlinear systems with perturbations to achieve asymptotical stability. *IEEE Trans. on Automatic Control*, 54(12):2863–2869.

Chao, H., Cao, Y., & Chen, Y. (2007). Autopilots for small fixed-wing unmanned air vehicles: A survey. IEEE International Conference on Mechatronics and Automation (ICMA), 3144-3149.

Charlet, B., Lévine, J., & Marino, R. (1989). *On dynamic feedback linearization*. Systems & Control Letters, 13(2), 143-151.

Chen, J., & Patton, R. J. (1999). *Robust model-based fault diagnosis for dynamic systems*. Kluwer Academic Publishers.

Chen, L. & Patton, R. J. (2011). Polytope LPV estimation for non-linear flight control. In Proceedings of IFAC World Congress, 6680-6685.

Chowdhary, G., & Johnson, E. N. (2008). Theory and flight test validation of long term learning adaptive flight controller. In Proceedings of the AIAA Guidance Navigation and Control Conference, Honolulu, HI.

Chowdhary, G., & Johnson, E. N. (2009). Flight test validation of a neural network based long term learning adaptive flight controller. In AIAA Guidance, Navigation and Control Conference, Chicago, Illinois.

Chowdhary, G. V (2010, December) Concurrent learning for convergence in adaptive control without persistency of excitation, PhD Thesis, School of Aerospace Engineering, Georgia Institute of Technology.

Chowdhary, G., & Johnson, E. (2010). Concurrent learning for convergence in adaptive control without persistency of excitation. In IEEE Conference on Decision and Control, 3674-3679.

Chowdhary, G. V., & Johnson, E. N. (2011a). Theory and flight-test validation of a concurrent-learning adaptive controller. *Journal of Guidance, Control, and Dynamics*, 34(2), 592-607.

Chowdhary, G., & Johnson, E. (2011b). A singular value maximizing data recording algorithm for concurrent learning. In IEEE American Control Conference, 3547-3552.

Chowdhary, G., Yucelen, T., Mühlegg, M., & Johnson, E. N. (2012). Concurrent learning adaptive control of linear systems with exponentially convergent bounds. *International Journal of Adaptive Control and Signal Processing*.

Cieslak, J., Henry, D., Zolghadri, A., & Goupil, P. (2007). Development of an on-board fault tolerant control strategy with application to the Garteur AG16 benchmark. In Proceeding of the IFAC Symposium, Automatic Control in Aerospace, Toulouse, France, June 25-29, 17(1), 97-102.

Cieslak, J., Henry, D., Zolghadri, A., & Goupil, P. (2008). Development of an active fault-tolerant flight control strategy. *Journal of Guidance, Control, and Dynamics*, 31(1), 135-147.

Cieslak, J., Henry, D., & Zolghadri, A. (2010). Fault tolerant flight control: from theory to piloted flight simulator experiments. *IET Control Theory & Applications*, 4(8), 1451-1464.

Cook, M. V. (1997). *Flight dynamics principles*. John Wiley & Sons, New York.

Cook, M. V. (2012). *Flight dynamics principles: a linear systems approach to aircraft stability and contro*l. Butterworth-Heinemann.

Corless, M., & Leitmann, G. (1981). Continuous state feedback guaranteeing uniform ultimate boundedness for uncertain dynamic systems. *IEEE Trans. on Automatic Control*, 26(5), 1139-1144.

Ding, S. X. (2008). *Model-based fault diagnosis techniques: design schemes, algorithms, and tools*. Springer.

Ding, S. X. (2009). Integrated design of feedback controllers and fault detectors. Annual Reviews in Control, 33(2), 124-135.

Ducard, G. J. J. (2009). *Fault-tolerant flight control and guidance systems*. Springer.

Ducard, G. J. J. (2007). Fault tolerant flight control and guidance systems for a small unmanned aerial vehicle. PhD Thesis of ETH Zurich.

Durham, W. C. (1997). *Aircraft dynamics &control*. Virginia Polytechnic Institute.

Edwards, C., & Spurgeon, S. K. (1998). *Sliding Mode Control: Theory and Applictions* (Vol. 7). CRC Press.

Edwards, C., Lombaerts, T., & Smaili, H. (Eds.). (2010). *Fault tolerant flight control: A benchmark challenge* (Vol. 399). Springer-Verlag.

Edwards, C., Spurgeon, S. K., & Patton, R. J. (2000). Sliding mode observers for fault detection and isolation. *Automatica*, 36(4), 541-553.

Elmali, H., & Olgac, N. (1992). Robust output tracking control of nonlinear MIMO systems via sliding mode technique. *Automatica*, 28(1), 145-151.

Emelyanov, S. V. (1959). Control of first order delay systems by means of an astatic controller and nonlinear correction. *Autom. Remote Control*, 8, 983-991.

Enns, D., Bugajski, D., Hendrick, R., & Stein, G. (1994). Dynamic inversion: an evolving methodology for flight control design. *International Journal of Control*, 59(1), 71-91.

Eterno, J. S., Weiss, J. L., Looze, D. P., & Willsky, A. S. (1985) Design issues for fault tolerant restructurable aircraft control. In IEEE Conference on Decision and Control, 900-905.

Etkin, B. & Reid, L D. (1996). *Dynamics of flight-stability and control*. John Wiley & Sons.

Fernandez R, B., & Hedrick, J. K. (1987). Control of multivariable non-linear systems by the sliding mode method. *International Journal of Control*, 46(3), 1019-1040.

Fliess, M. (1990). Generalized controller canonical form for linear and nonlinear dynamics. *IEEE Trans. on Automatic Control*, 35(9), 994-1001.

Fliess, M., Lévine, J., Martin, P., & Rouchon, P. (1995). Flatness and defect of non-linear systems: introductory theory and examples. *International Journal of Control*, 61(6), 1327-1361.

Francis, B. A. (1987). A course in H_∞ control theory. Lecture notes in control and information sciences, no. 88. Springer-Verlag.

Fridman, L. M. (2002). Sliding mode control for systems with fast actuators: singularly perturbed approach. In Variable Structure Systems: Towards the 21st Century (pp. 391-415). Springer Berlin Heidelberg.

Fridman, L., & Levant, A. (1996). Higher order sliding modes as a natural phenomenon in control theory. In Robust Control via Variable Structure and Lyapunov Techniques (pp. 107-133). Springer Berlin Heidelberg.

Ganguli, S., Marcos, A., & Balas, G. (2002). Reconfigurable LPV control design for Boeing 747-100/200 longitudinal axis. In Proceedings of the American Control Conference, 3612–3617.

Gao, Z., & Antsaklis, P. J. (1991). Stability of the pseudo-inverse method for reconfigurable control systems. *International Journal of Control*, 53(3), 717-729.

Gao, Z., & Ding, S. X. (2007). Actuator fault robust estimation and fault-tolerant control for a class of nonlinear descriptor systems. *Automatica*, 43(5), 912-920.

Gao, Z., & Ho, D. W. (2006). State/noise estimator for descriptor systems with application to sensor fault diagnosis. *IEEE Trans. on Signal Processing*, 54(4), 1316-1326.

Gao, Z., Ding, S. X., & Ma, Y. (2007). Robust fault estimation approach and its application in vehicle lateral dynamic systems. *Optimal Control Applications and Methods*, 28(3), 143-156.

Gertler, J. (1988). Survey of model-based failure detection and isolation in complex plants. *IEEE Control Systems Magazine*, 8(6), 3–11.

Gertler, J. (1998). *Fault detection and diagnosis in engineering systems*. NY: Marcel Dekker Inc.

Goman, M. G. & Khramtsovsky, A. V. (1997). Global stability analysis of nonlinear aircraft dynamics. AIAA Paper: 97-3721.

Gross, J., Hansford, N., Phillips, K., Waldie, B., & Perhinschi, M. (2008). Flight Simulation of WVU YF-22 Aircraft.

Guckenheimer, J., & Holmes, P. (1983). *Nonlinear oscillations, dynamical systems, and bifurcations of vector fields*. Springer.

Hauser, J., Sastry, S. & Meyer, G. (1992). Nonlinear control design for slightly non-minimum phase systems: application to V/STOL aircraft. *Automatica*, 28(4): 665-679.

Hedrick J. K. & Girard A., (2005). Control of nonlinear dynamic systems: theory and applications. Available on: http://www.me.berkeley.edu/ME237/8_feedback_lin.pdf

Henry, D., Simani, S., & Patton, R. J. (2010). *Fault detection and diagnosis for aeronautic and aerospace missions*. In Fault Tolerant Flight Control (pp. 91-128). Springer Berlin Heidelberg.

Henson, M. A. (1992). Feedback linearization strategies for nonlinear process control. PhD thesis, University of California, Santa Barbara, CA.

Henson, M. A., & Seborg, D. E. (1997). *Nonlinear process control*. Prentice-Hall.

Hess, R. A. (Ed.). (2005). Special issue on reconfigurable flight control system design. Proceedings of IMechE, Part G: *Journal of Aerospace Engineering*, 219(4), 263–361.

Hornik, K., Stinchcombe, M., & White, H. (1989). Multilayer feed-forward networks are universal approximators. *Neural Networks*, 2(5), 359-366.

Hovakimyan, N., Calise, A. J., & Kim, N. (2004). Adaptive output feedback control of a class of multi-input multi-output systems using neural networks. *International Journal of Control*, 77(15), 1318-1329.

Hovakimyan, N., Nardi, F., Calise, A., & Kim, N. (2002). Adaptive output feedback control of uncertain nonlinear systems using single-hidden-layer neural networks. *IEEE Trans. on Neural Networks*, 13(6), 1420-1431.

Hsieh, C. S. (2002). Performance gain margins of the two-stage LQ reliable control. *Automatica*, 38(11), 1985–1990.

Hunt, L. R., Su, R., & Meyer, G. (1983). Design for multi-input nonlinear systems. *Differential Geometric Control Theory*, 27, 268-298.

Idan, M., Johnson, M., & Calise, A. J. (2002). Hierarchical approach to adaptive control for improved flight safety. *Journal of Guidance, Control, and Dynamics*, 25(6), 1012-1020.

Idan, M., Johnson, M., Calise, A. J., & Kaneshige, J. (2001). Intelligent aerodynamic/propulsion flight control for flight safety: a nonlinear adaptive approach. In American Control Conference, 4, 2918-2923.

Ioannou, P. A., & Sun, J. (2012). *Robust adaptive control*. Courier Dover Publications.

Isermann, R. (1993). Fault diagnosis of machines via parameter estimation and knowledge processing—Tutorial paper. *Automatica*, 29(4), 815–835.

Isermann, R. (2006). *Fault-diagnosis systems: An introduction from fault detection to fault tolerance*. Berlin, Germany: Springer.

Isermann, R., & Balle, P. (1997). Trends in the application of model based fault detection and diagnosis of technical processes. *Control Engineering Practice*, 5(5), 709–719.

Isidori, A. (1995). *Nonlinear control systems*. Communications and control engineering series., Springer-Verlag, Berlin.

Itkis, U. (1976). *Control systems of variable structure* (pp. 168-178). New York: Wiley.

Jakubczyk, B. (2001). Introduction to geometric nonlinear control; controllability and Lie bracket. *Mathematical Control Theory*, 1(2), 107-168.

Jang, J. S. R., Sun, C. T., & Mizutani, E. (1997). Neuro-fuzzy and soft computing-a computational approach to learning and machine intelligence [Book Review]. *IEEE Trans. on Automatic Control*, 42(10), 1482-1484.

Jankovic, M., Sepulchre, R., & Kokotovic, P. V. (1996). Constructive Lyapunov stabilization of nonlinear cascade systems. *IEEE Trans. on Automatic Control*, 41(12), 1723-1735.

Johnson, E. N. (2000). Limited authority adaptive flight control. Doctoral dissertation, Georgia Institute of Technology.

Johnson, E. N., & Calise, A. J. (2001). Neural network adaptive control of systems with input saturation. In American Control Conference, 5, 3527-3532.

Johnson, E. N., & Kannan, S. K. (2005). Adaptive trajectory control for autonomous helicopters. *Journal of Guidance, Control, and Dynamics*, 28(3), 524-538.

Joosten, D., & Maciejowski, J. (2009). MPC design for fault-tolerant flight control purposes based upon an existing output feedback controller. *In Fault Detection, Supervision and Safety of Technical Processes*, 253-258.

Kaynak, O., Erbatur, K., & Ertugnrl, M. (2001). The fusion of computationally intelligent methodologies and sliding-mode control-a survey. *IEEE Trans. on Industrial Electronics*, 48(1), 4-17.

Khalil, H. K. (1996). Adaptive output feedback control of nonlinear systems represented by input-output models. *IEEE Trans. on Automatic Control*, 41(2), 177-188.

Khalil, H. K., & Grizzle, J. W. (2002). *Nonlinear systems* (Vol. 3). Upper Saddle River: Prentice hall.

Kim, B. S., & Calise, A. J. (1997). Nonlinear flight control using neural networks. *Journal of Guidance, Control, and Dynamics*, 20(1), 26-33.

Kim, N., & Calise, A. J. (2007). Several extensions in methods for adaptive output feedback control. *IEEE Trans. on Neural Networks*, 18(2), 482-494.

Kim, N., & Calise, A. J. (2008). Neural network based adaptive output feedback augmentation of existing controllers. *Aerospace Science and Technology*, 12(3), 248-255.

Koenig, D. (2005). Unknown input proportional multiple-integral observer design for linear descriptor systems: application to state and fault estimation. *IEEE Trans. on Automatic Control*, 50(2), 212-217.

Krener, A. J. (1984). Approximate linearization by state feedback and coordinate change. *Systems & Control Letters*, 5(3), 181-185.

Kruger, T., Mossner, M., Kuhn, A., Axmann, J., & Vorsmann, P. (2010). Sliding mode online learning for flight control applications in unmanned aerial systems. The IEEE International Joint Conference on Neural Networks (IJCNN), 1-8.

Kruger, T., Schnetter, P., Placzek, R., & Vorsmann, P. (2011). Nonlinear adaptive flight control using sliding mode online learning. The IEEE International Joint Conference on Neural Networks (IJCNN), 2897-2904.

Kruger, T., Schnetter, P., Placzek, R., & Vorsmann, P. (2012). Fault-tolerant nonlinear adaptive flight control using sliding mode online learning. *Neural Networks*, 32, 267-274.

Kurnaz, S., Cetin, O., & Kaynak, O. (2010). Adaptive neuro-fuzzy inference system based autonomous flight control of unmanned air vehicles. *Expert Systems with Applications*, 37(2), 1229-1234.

Lanchester, F. W. (1907). *Aerodonetics*. Constable, London.

Lane, S. H. & Stengel, R. F. (1988). Flight control design using non-linear inverse dynamics. *Automatica*, 24(4): 471-483.

LaSalle, J. P. (1968). Stability theory for ordinary differential equations. *Journal of Differential Equation*s, 4, 57-65.

Lavretsky, E., & Wise, K. A. (2005). Adaptive flight control for manned/unmanned military aircraft. In Proceedings of the American Control Conference.

Lee, T., & Kim, Y. (2001). Nonlinear adaptive flight control using backstepping and neural networks controller. *Journal of Guidance, Control, and Dynamics*, 24(4), 675-682.

Levant, A., Pridor, A., Gitizadeh, R., Yaesh, I., & Ben-Asher, J. Z. (2000). Aircraft pitch control via second-order sliding technique. *Journal of Guidance, Control, and Dynamics*, 23(4), 586-594.

Lewis, F. L. (1999). Nonlinear network structures for feedback control. *Asian Journal of Control*, 1(4), 205-228.

Li, Y., Ng, K. C., Murray-Smith, D. J., Gray, G. J., & Sharman, K. C. (1996). Genetic algorithm automated approach to the design of sliding mode control systems. *International Journal of Control*, 63(4), 721-739.

Liang, Y. W., Liaw, D. C., & Lee, T. C. (2000). Reliable control of nonlinear systems. *IEEE Trans. on Automatic Control*, 45(4), 706–710.

Lin, S. C., & Chen, Y. Y. (1997). Design of self-learning fuzzy sliding mode controllers based on genetic algorithms. *Fuzzy Sets and Systems*, 86(2), 139-153.

Lombaerts, T. J. J., Chu, P., Mulder, J. A. & Joosten, D. A. (2011). Modular flight control reconfiguration design and simulation. *Control Engineering Practice*, 19(6), 540–554.

Lombaerts, T. J. J., Chu, P., Mulder, J. A. B., & Stroosma, O. (2010). *Fault Tolerant Flight Control: A Physical Model Approach*. Wöhrmann Print.

Lombaerts, T. J. J., Joosten, D. A., Breeman, J., Smaili, M. H., van den Boom, A. J. J., Chu, Q. P., & Verhaegen, M. (2006). Assessment criteria as specifications for reconfiguring control. In Proceedings of the AIAA Guidance, Navigation, and Control Conference and Exhibit. Keystone, Colorado, August 21-24.

Lombaerts, T., Huisman, H., Chu, P., Mulder, J. A., & Joosten, D. (2009). Nonlinear reconfiguring flight control based on online physical model identification. *Journal of Guidance, Control, and Dynamics*, 32(3), 727-748.

Maciejowski, J. M., & Jones, C. N. (2003). MPC fault-tolerant flight control case study: Flight 1862. In Proceeding of the IFAC SAFEPROCESS Conference, Washington, D. C., USA, June 9-11, 121-126.

Mackall, D., Nelson, S., & Schumann, J. M. (2002). Verification and validation of neural networks for aerospace systems. National Aeronautics and Space Administration, Ames Research Center.

Mangoubi, R. S. (1998). *Robust estimation and fault detection: A concise treatment*. London, UK: Springer.

Marcos, A., & Balas, G. J. (2001). Linear Parameter Varying Modelling of the Boeing 747-100/200 Longitudinal Motion, Proceedings of AIAA Guidance, Navigation and Control Conference, AIAA-2001-4347, Montreal, August.

Marino, R., & Tomei, P. (1993). Robust stabilization of feedback linearizable time-varying uncertain nonlinear systems. *Automatica*, 29(1), 181-189.

Maybeck, P. S. (1999). Multiple model adaptive algorithms for detecting and compensating sensor and actuator/surface failures in aircraft flight control systems. *International Journal of Robust and Nonlinear Control*, 9(14), 1051-1070.

Maybeck, P. S., & Stevens, R. D. (1991). Reconfigurable flight control via multiple model adaptive control methods. *IEEE Trans. on Aerospace and Electronic Systems*, 27(3), 470–479.

McMahan, J. (1978, July). Flight 1080. Air Line Pilot.

McRuer, D. T., Graham, D., & Ashkenas, I. (1972). *Aircraft dynamics and automatic control*. Princeton University Press.

Melin, P., & Castillo, O. (2003). Adaptive intelligent control of aircraft systems with a hybrid approach combining neural networks, fuzzy logic and fractal theory. *Applied Soft Computing*, 3(4), 353-362.

Möckli, M. R., (2006). Guidance and control for aerobatic maneuvers of an unmanned airplane. PhD thesis of ETH Zurich, Dissertation No. 16586.

Moerder, D. D., Halyo, N., Broussard, J. R., & Caglayan, A. K. (1989). Application of precomputed control laws in a reconfigurable aircraft flight control system. *Journal of Guidance, Control, and Dynamics*, 12(3), 325–333.

Monaco, J., Ward, D., Barron, R., & Bird, R. (1997). Implementation and flight test assessment of an adaptive, reconfigurable flight control system. In Proceedings of the AIAA Guidance Navigation and Control Conference, AIAA Paper, 3738).

Montoya, R. J., Howell, W. E., Bundick, W. T., Ostroff, A. J., Hueschen, R. M., & Belcastro, C. M. (1983). Restructurable controls. Tech. Rep. NASA CP-2277. Proceedings of a workshop held at NASA Langley Research Center, Hampton, VA, USA, September 21-22, 1982.

Napolitano, M. R., An, Y., & Seanor, B. A. (2000). A fault tolerant flight control system for sensor and actuator failures using neural networks. *Aircraft Design*, 3(2), 103-128.

Napolitano, M. R., Neppach, C., Casdorph, V., & Naylor, S. (1995). Neural network based scheme for sensor failure detection, identification, and accommodation. *Journal of Guidance, Control, and Dynamics*, 18(6), 1280–1286.

Nied, A., Seleme Jr, S. I., Parma, G. G., & Menezes, B. R. (2007). On-line neural training algorithm with sliding mode control and adaptive learning rate. *Neuro-computing*, 70(16), 2687-2691.

Orlov, Y. V., & Utkin, V. I. (1987). Sliding mode control in indefinite-dimensional systems. *Automatica*, 23(6), 753-757.

Ozdemir, U. & Kavsaoglu, M. S. (2008). Linear and nonlinear simulations of aircraft dynamics using body axis system. *Aircraft Engineering and Aerospace Technology*, 80(6): 638-648.

Patton, R. J. (1991). Fault detection and diagnosis in aerospace systems using analytical redundancy. *Computing and Control Engineering Journal*, 2(3), 127–136.

Patton, R. J. (1993). Robustness issues in fault-tolerant control. In Proceedings of the IEE Colloquium on Fault Diagnosis and Control System Reconfiguration, 9, 1–25.

Patton, R. J. (1997). Fault-tolerant control: The 1997 situation. In Proceedings of the 3rd IFAC Symposium on Fault Detection, Supervision and Safety for Technical Processes, 1033–1055.

Patton, R. J., Frank, P. M., & Clark, R. N. (2000). *Issues of fault diagnosis for dynamic systems*. *London*, UK: Springer.

Patton, R. J., Frank, P. M., & Clarke, R. N. (1989). *Fault diagnosis in dynamic systems: theory and application*. Prentice-Hall.

Polycarpou, M. M., & Vemuri, A. T. (1995). Learning methodology for failure detection and accommodation. *IEEE Control Systems Magazine*, 15(3), 16–24.

Rauch, H. E. (1995). Autonomous control reconfiguration. *IEEE Control Systems Magazine*, 15(6), 37–48.

Rundell, A. E., Drakunov, S. V., & DeCarlo, R. A. (1996). A sliding mode observer and controller for stabilization of rotational motion of a vertical shaft magnetic bearing. *IEEE Trans. on Control Systems Technology*, 4(5), 598-608.

Sadraey, M. & Colgren, R. (2005). UAV flight simulation: credibility of linear decoupled vs. nonlinear coupled equations of motion. AIAA Modelling and Simulation Technologies Conference and Exhibit.

Sadraey, M. & Colgren, R. (2009). *Robust nonlinear controller design for a complete UAV mission*. VDM Publishing.

Sastry, S. (1999). *Nonlinear systems: analysis, stability, and control* (Vol. 10). New York: Springer.

Serrani, A., Isidori, A., & Marconi, L. (2001). Semi-global nonlinear output regulation with adaptive internal model. *IEEE Trans. on Automatic Control*, 46(8), 1178-1194.

Shakev, N. G., Topalov, A. V., & Kaynak, O. (2003). Sliding mode algorithm for online learning in analog multilayer feedforward neural networks. Lecture Notes in Computer Science, 2714, 1064–1072.

Shearer, C. M. & Cesnik, C. E. S. (2007). Nonlinear flight dynamics of very flexible aircraft. *Journal of Aircraft*, 44(5): 1528-1545.

Shin, D. H., & Kim, Y. (2004). Reconfigurable flight control system design using adaptive neural networks. *IEEE Trans. on Control Systems Technology*, 12(1), 87-100.

Shin, Y. (2005). Neural network based adaptive control for nonlinear dynamic regimes. PhD Thesis, School of Mechanical Engineering, Georgia Institute of Technology.

Shin, Y., Johnson, M., & Calise, A. J. (2003). Neural network-based adaptive control for nonlinear flight regimes. In AIAA Guidance, Navigation and Control Conference, (Austin, TX), AIAA-2003-5717.

Shore, D. & Bodson, M. (2005). Flight testing of a reconfigurable control system on an unmanned aircraft. *Journal of Guidance, Control, and Dynamics*, 28(4): 698-707.

Siljak, D. D. (1980). Reliable control using multiple control systems. *International Journal of Control*, 31(2), 303–329.

Simani, S., Fantuzzi, C., & Patton, R. J. (2003). *Model-based fault diagnosis in dynamic systems using identification techniques*. New York, NY: Springer.

Sira-Ramirez, H., & Colina-Morles, E. (1995). A sliding mode strategy for adaptive learning in adalines. Circuits and Systems I: Fundamental Theory and Applications, 42(12), 1001-1012.

Slotine, J. J. E., & Li, W. (1991). *Applied nonlinear control* (Vol. 199, No. 1). New Jersey: Prentice hall (Chapter 7, pp. 285).

Slotine, J., & Sastry, S. S. (1983). Tracking control of non-linear systems using sliding surfaces, with application to robot manipulators. *International Journal of Control*, 38(2), 465-492.

Smaili, H. M., (2006). Research on Fault Tolerant Controls within GARTEUR. Aeronautics Days, Vienna, Austria, June 19. Available from: http://www.aerodays2006.org/sessions/F_Sessions/F1/F14.pdf

Smaili, H. M., Breeman, J., Lombaerts, T. J. J., & Stroosma, O. (2008). A simulation benchmark for aircraft survivability assessment. In Proceedings of the International Congress of Aeronautical Sciences, 9(2).

Smaili, H., Breeman, J., & Lombaerts, T. (2012). Tool-based design and evaluation of resilient flight control systems, Automatic Flight Control Systems - Latest Developments, Dr. Thomas Lombaerts (Ed.), ISBN: 978-953-307-816-8, InTech, Available from: http://www.intechopen.com/books/automatic-flightcontrol-systems-latest developments/tool-based-design-and-evaluation-of-resilient-flight-control-systems

Smaili, M. H. & Mulder, J. A. (2000). Flight data reconstruction and simulation of the 1992 Amsterdam Bijlmermeer airplane accident. In Proceedings of AIAA Modelling and Simulation Conference, AIAA-2000-4586, Denver, Colorado, August.

Smaili, M. H., Breeman, J., Lombaerts, T. J. J., & Joosten, D. A. (2006). A simulation benchmark for integrated fault tolerant flight control evaluation. In AIAA Modelling and Simulation Technologies Conference and Exhibit, 21-24.

Snell, S. A., Enns, D. F. & Garrard, W. L. (1992). Nonlinear inversion flight control for a super-maneuverable aircraft. *Journal of Guidance, Control, and Dynamics*, 15(4): 976-984.

Sonneveldt, L. (2006). Nonlinear F-16 model description. Software manual. The Netherlands: Delft University of Technology.

Srichander, R., & Walker, B. K. (1993). Stochastic stability analysis for continuous-time fault tolerant control systems. *International Journal of Control*, 57(2), 433-452.

Staroswiecki, M. & Gehin, A. L. (2001). From control to supervision. Annual Reviews in Control, 25, 1–11.

Steffen, T. (2005). *Control reconfiguration of dynamic systems: Linear approaches and structural tests.* Lecture notes in control and information sciences (Vol. 320). Berlin, Germany: Springer.

Steinberg, M. (2005). Historical overview of research in reconfigurable flight control. Proceedings of the Institution of Mechanical Engineers, Part G: *Journal of Aerospace Engineering*, 219(4), 263-275.

Stengel, R. F. (1991). Intelligent failure-tolerant control. *IEEE Control Systems Magazine*, 11(4), 14–23.

Stengel, R. F. (2005). Flight dynamics. *Aircraft Engineering and Aerospace Technology*, 77(3).

Stroosma, O., Smaili, M. H. & Mulder, J. A. (2009). Pilot-in-the-Loop evaluation of fault tolerant flight control systems. In Proceedings of the IFAC SAFEPROCESS Conference, Barcelona, June 30-July 03.

Sun, F., Sun, Z., & Woo, P. Y. (1998). Stable neural-network-based adaptive control for sampled-data nonlinear systems. *IEEE Trans. on Neural Networks*, 9(5), 956-968.

Sussmann, H. J. (1983). Lie brackets, real analyticity and geometric control. *Differential Geometric Control Theory*, 27, 1-116.

Theilliol, D., Noura, H., & Ponsart, J. C. (2002). Fault diagnosis and accommodation of a three-tank system based on analytical redundancy. *ISA Transactions*, 41(3), 365–382

Tong, S., & Li, H. X. (2003). Fuzzy adaptive sliding-mode control for MIMO nonlinear systems. *IEEE Trans. on Fuzzy Systems*, 11(3), 354-360.

Topalov, A. V., & Aydin, G. (2007). Neuro-adaptive sliding-mode tracking control of robot manipulators. *International Journal of Adaptive Control and Signal Processing*, 21(8-9), 674-691.

Topalov, A. V., Cascella, G. L., Giordano, V., Cupertino, F., & Kaynak, O. (2007). Sliding mode neuro-adaptive control of electric drives. *IEEE Trans. on Industrial Electronics*, 54(1), 671-679.

Utkin, V. (1977). Variable structure systems with sliding modes. *IEEE Trans. on Automatic Control*, 22(2), 212-222.

Utkin, V. I. (1992). *Sliding modes in control and optimization* (Vol. 116). Berlin: Springer-Verlag.

Utkin, V., Guldner, J., & Shi, J. (2009). *Sliding mode control in electro-mechanical systems*. Taylor & Francis, London

Veillette, R. J. (1995). Reliable linear-quadratic state-feedback control. *Automatica*, 31(1), 137–143.

Veillette, R. J., Medanic, J. V., & Perkins, W. R. (1992). Design of reliable control systems. *IEEE Trans. on Automatic Control*, 37(3), 290–300.

Venelinov Topalov, A. (2001). Online learning in adaptive neuro control schemes with a sliding mode algorithm. Systems, Man, and Cybernetics, Part B: Cybernetics, 31(3), 445-450.

Vincent, T. L., & Grantham, W. J. (1999). Nonlinear and optimal control systems. John Wiley & Sons.

Wang, J., Rad, A. B., & Chan, P. T. (2001). Indirect adaptive fuzzy sliding mode control: Part I: fuzzy switching. *Fuzzy Sets and Systems*, 122(1), 21-30.

Wang, Q., & Stengel, R. F. (2000). Robust nonlinear control of a hypersonic aircraft. *Journal of Guidance, Control, and Dynamics*, 23(4), 577-585.

Wang, Q., & Stengel, R. F. (2005). Robust nonlinear flight control of a high-performance aircraft. *IEEE Trans. on Control Systems Technology*, 13(1), 15-26.

Weingarten, N. C., & Rynaski, E. G. (1972). Flight Control Principles for Control Configured Vehicles. Final report of Cornell Aeronautical Lab Inc. Buffalo, New York.

White, B. A. (1986). Range-space dynamics of scalar-variable-structure control systems. In Proceeding of IEE Control Theory and Applications Conference, 133(1), 35-41.

White, B. A., & Zinober, A. S. I. (1990). Applications of output feedback in variable structure control. *Deterministic Control of Uncertain Systems*, Peregrinus Ltd, Stevenage, UK, 144-169.

Wigdorowitz, B. (1992). Application of linearization analysis to aircraft dynamics. *Journal of Guidance, Control, and Dynamics*, 15(3): 746-750.

Willsky, A., Chow, E., Gershwin, S., Greene, C., Houpt, P., & Kurkjian, A. (1980). Dynamic model based techniques for the detection of incidents on freeways. *IEEE Trans. on Automatic Control*, 25(3), 347-360.

Xu, H., Mirmirani, M. D., & Ioannou, P. A. (2004). Adaptive sliding mode control design for a hypersonic flight vehicle. *Journal of Guidance, Control, and Dynamics*, 27(5), 829-838.

Yang, G. H., Wang, J. L., & Soh, Y. C. (2000). Reliable LQG control with sensor failures. In Proceedings of IEE Control Theory and Applications, 147(4), 433–439.

Yang, G. H., Zhang, S. Y., Lam, J., & Wang, J. L. (1998). Reliable control using redundant controllers. *IEEE Trans. on Automatic Control*, 43(11), 1588–1593.

Yoshimura, T., Kume, A., Kurimoto, M., & Hino, J. (2001). Construction of an active suspension system of a quarter car model using the concept of sliding mode control. *Journal of Sound and Vibration*, 239(2), 187-199.

Young, K. D., Utkin, V. I., & Ozguner, U. (1996). A control engineer's guide to sliding mode control. IEEE International Workshop on Variable Structure Systems, 1-14.

Young, K. K. (1993). *Variable structure control for robotics and aerospace systems*. Studies in Automation and Control, vol. 10.

Yu, X. (2009). Sliding-mode control with soft computing: A survey. *IEEE Trans. on Industrial Electronics*, 56(9), 3275-3285.

Yu, X., & Efe, M. O. (2002). A general backpropagation algorithm for feedforward neural networks learning. *IEEE Trans. on Neural Networks*, 13(1), 251-254.

Zemlyakov, S. D., Rutkovskii, V. Y., & Silaev, A. V. (1996). Reconfiguring aircraft control systems in case of failures. *Automation and Remote Control*, 57(1), 1–13.

Zhang, K., Jiang, B., & Cocquempot, V. (2008). Adaptive observer-based fast fault estimation. *International Journal of Control Automation and Systems*, 6(3), 320.

Zhang, Y. M., & Jiang, J. (2001a). Integrated active fault tolerant control using IMM approach. *IEEE Trans. on Aerospace and Electronic Systems*, 37(4), 1221–1235.

Zhang, Y. M., & Jiang, J. (2003). Fault tolerant control system design with explicit consideration of performance degradation. *IEEE Trans. on Aerospace and Electronic Systems*, 39(3), 838–848.

Zhang, Y., & Jiang, J. (2001b). Integrated design of reconfigurable fault-tolerant control systems. *Journal of Guidance, Control, and Dynamics*, 24(1), 133-136.

Zhang, Y., & Jiang, J. (2002). An active fault tolerant control system against partial actuator failures. In Proceedings of IEE Control Theory and Applications Conference, 149(1), 95–104.

Zhang, Y., & Jiang, J. (2008). Bibliographical review on reconfigurable fault-tolerant control systems. Annual Reviews in Control, 32(2), 229-252.

Zhao, Q., & Jiang, J. (1998). Reliable state feedback control systems design against actuator failures. *Automatica*, 34(10), 1267–1272.

Zhihong, M., Paplinski, A. P., & Wu, H. R. (1994). A robust MIMO terminal sliding mode control scheme for rigid robotic manipulators. *IEEE Trans. on Automatic Control*, 39(12), 2464-2469.

Zhou, K., Doyle, J. C., & Glover, K. (1996). *Robust and optimal control* (Vol. 40). Prentice Hall.

Zinober, A. S. (1994). An introduction to sliding mode variable structure control. In *Variable Structure and Lyapunov Control* (pp. 1-22). Springer Berlin Heidelberg.

Zinober, A. S. (Ed.). (1990). *Deterministic nonlinear nontrol of uncertain systems* (Vol. 40). IET.

Zolghadri, A. (2012). Advanced model-based FDIR techniques for aerospace systems: Today challenges and opportunities. *Progress in Aerospace Sciences*, 53, 18-29.